INSIGHTS INTO DEEP STRUCTURE AND EVOLUTION OF ALASKA BASED ON A DECADE OF OBSERVATIONS OF SHEAR WAVE SPLITTING AND MANTLE FLOW

By

Anna K. Bellesiles

RECOMMENDED:

Advisory Committee Chair

Chair Department of Geology and Geophysics

APPROVED:

Dean, College of Natural Science and Mathematics

Dean of the Graduate School

Apr 4, 2011

Date

INSIGHTS INTO DEEP STRUCTURE AND EVOLUTION OF ALASKA BASED ON A DECADE OF OBSERVATIONS OF SHEAR WAVE SPLITTING AND MANTLE FLOW

A

THESIS

Presented by the Faulty

Of the University of Alaska Fairbanks

In Partial Fulfillment of the Requirements

For the Degree of

MASTERS OF SCIENCE

By

Anna K. Bellesiles, B.S.

Fairbanks, Alaska

May 2011

Abstract

This thesis covers shear wave splitting results from a decade of temporary networks deployed throughout Alaska. The analysis and interpretation of data from the MOOS (Multidiscipline Observations Of Subduction) and ARCTIC (Alaska Receiving Cross Transect for the Inner Core) PASSCAL (Program for Array Seismic Studies of the Continental Lithosphere) deployments, combined with the previously published BEAAR (Broadband Experiment Across the Alaska Range) results provide anisotropy and flow observations across the state.

In south central Alaska, a region dominated by the subduction of the Pacific plate under the North American plate, fast directions are dominantly in the direction of convergence (NNW-SSE), or trench-normal. This is either due to entrained flow below the subducting portion of the Yakutat block, or anisotropy within the block itself. Farther north above the mantle wedge the shear wave splitting results are dominated by fast directions along the strike of the subducting slab (NE-SW), due to along strike flow within the mantle wedge. North of the mantle wedge, fast directions transition into a more NNE to SSW orientation which is the Brooks Range and North slope are in the direction of absolute plate motion.

Table of Contents

List of Figures

Page

List of Tables

Page

List of Appendices

Page

Acknowledgments

This thesis would not have been possible without my advisor Dr. Doug Christensen. Thank you for giving me the opportunity to work with a network named MOOS, and for wonderful field experiences in Alaska and Bolivia. I would also like to thank my committee members Dr. Mike West and Dr. Wesley Wallace for all their guidance.

I would also like to show my gratitude to the numerous other colleagues that have worked on this project, especially Dr. Geoffrey Abers, Mairi Litherland, Lizzie Entwistle, and everyone assisted in various ways with the project. I would also like to thank my colleagues at the University of Alaska Fairbanks in the Geology and Geophysics department for challenging classes, expanding my education beyond books and helping me truly experience Alaska.

Finally I would like to thank Brian Perttu and my family for being there and supporting me. I cannot thank them enough for all the help they have given me.

1. Introduction

This thesis uses data from three temporary IRIS (Incorporated Research Institutions for Seismology)/PASSCAL (Program for Array Seismic Studies of the Continental Lithosphere) experiments, as well as part of the Alaska permanent seismic network, to explore mantle dynamics below Alaska. These networks provide a transect across Alaska, from the active subduction of the Pacific plate and the Yakutat block in the south, to the passive margin in the north. The deployment of the networks occurred over a decade from 1999 to 2009. The results of shear wave splitting analysis, completed using SKS waves, are presented in the following chapters.

1.1 Shear Wave Splitting and Mantle Anisotropy

Shear wave splitting is the result of the interaction of a shear wave with an anisotropic medium. Seismic anisotropy is a material property that describes the directional variability in seismic velocity within a specific medium. As the shear wave travels through the anisotropic medium, the component of particle motion in the fast direction is faster than the component of particle motion in the slow direction (perpendicular to the fast direction). This in effect splits the wave into a fast and slow component. Anisotropy is measured by determination of two splitting parameters; the fast direction and the delay time. The fast direction is the orientation of the fast particle motion and the delay time is the amount of time between the fast and slow components (Savage, 1999).

Mantle anisotropy is the result of alignment of anisotropic minerals. The alignment is caused by deformation resulting from solid state shear flow in the mantle. The anisotropy measured by shear waves is caused by the lattice preferred orientation (LPO) of olivine (the most dominant mineral by volume) and other anisotropic minerals through dislocation creep (Nicholas and Christensen, 1987; Ismail and Mainprice, 1998; Savage, 1999; Zhang et al., 2000). Olivine has a single crystal anisotropy of ~18% (Mainprice, 2007), and the fast direction or "a-axis" of the olivine crystals aligns through dislocation creep, creating the dominant "a-type" LPO fabric seen in most shear wave splitting studies. Only 16% of natural samples found are not "a-type" fabric, however, other fabrics do exist in the upper mantle. The most notable is the "b-type" fabric, which aligns the "b-axis" in the direction of flow, making the fast direction perpendicular to the flow direction. "B-type" fabric occurs in a wet mantle that deforms in a high stress and relatively low temperature environment (Jung and Karato, 2001). Experiments on natural samples and geodynamic modeling indicate that "b-type" fabric is restricted to the forearc corner of some subduction zone mantle wedges, often referred to as a "cold nose" where water is present (Jung and Karato, 2001; Mizukami et al., 2004; Katayama and Karato, 2006; Karato et al., 2008; Kneller et al., 2005, 2008). Along with a- and b- type fabric, c-, d-, and e-, fabrics also exist under specific conditions, however, the only fabric to significantly change the relationship between fast direction and flow direction is "b-type" (Long and Silver, 2009). This study considers only "a-type" and "b-type" fabrics for interpretation.

This study uses SKS waves from teleseismic events to study mantle anisotropy along a transect across Alaska. SKS waves are shear waves that leave the source as an S-wave, convert to a P-wave at the core-mantle boundary (CMB), and back to an S-wave when leaving the outer core (figure 1.1). SKS and SKKS (one bounce in the outer core) polarization is controlled by the P-S conversion at the CMB; therefore splitting must occur on the receiver side of the ray path, between the CMB and the station (Long and Silver, 2009). SKS and SKKS pairs were used by Niu and Perez (2004) and Restivo and Helffrich (2006) to help constrain the location of this splitting. A similar study was conducted with SKS and deep S waves by Meade et al. (1995). These pairs are used because of the similarity of the ray paths in the upper mantle and differences in the lower mantle. In general, these studies show that splitting occurs in the upper mantle due to similarity in results for SKS and SKKS waves. SKS and SKKS waves that arrive at the same station have similar ray paths in the upper mantle but different ray paths in the lower mantle. The only notable exception is the study by Long et al. (2009), which showed significant discrepancies between SKS and SKKS pairs in the western United States indicating a contribution to the splitting due to lower mantle anisotropy.

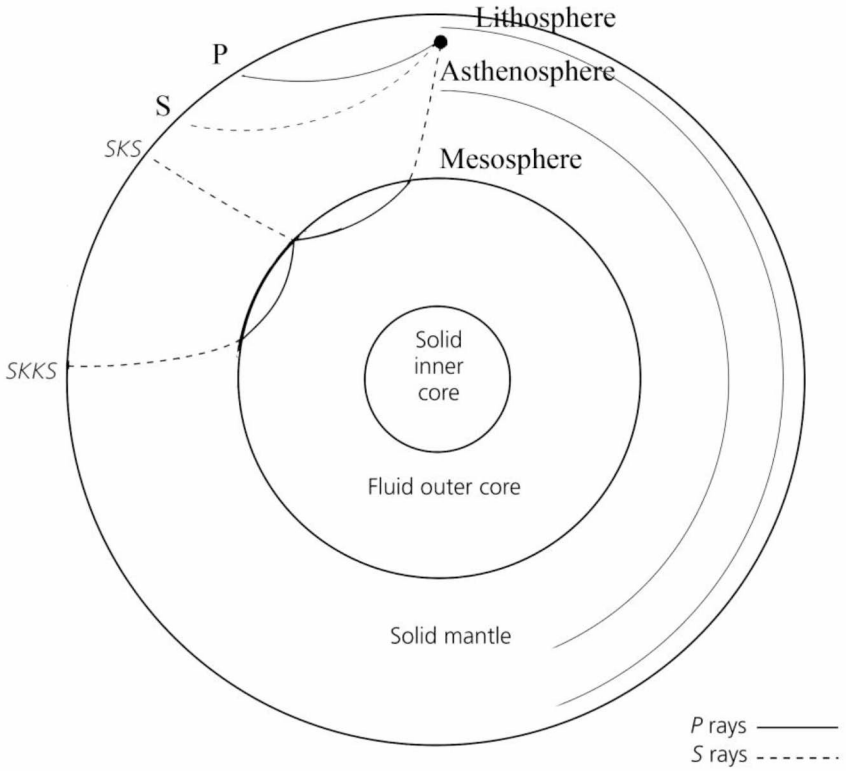

Figure 1.1: **Ray paths in the earth**.
Modified from figure 3.5-5 in Stein and Wysession (2003). Note the SKS wave leaves the source as an S wave, goes through the outer core as a P wave, and converts back to the S wave at the core-mantle boundary. An SKKS wave bounces in the outer core before traveling to the stations as an S wave. Boundaries in the earth are also plotted. On the right are the rheologic boundaries of lithosphere (crust and mantle lithosphere), asthenosphere, and mesosphere.

Measurements from SKS wave splitting are generally attributed to the upper mantle or the crust. The crustal contribution is thought to be on the order of ~0.1 seconds (e.g., Savage, 1999) while the upper mantle is capable of contributing up to 1.0 second or more of splitting (Silver, 1996; Fouch and Rondenay, 2006). The low (and sometimes lack of) splitting in continental crust is due to the heterogeneous nature of the crust and the short path length through the crust when compared to other sources, like the upper mantle.

Shear wave splitting measurements in continental areas can be attributed to two possible sources; first, the asthenosphere, and second, the lithosphere. Anisotropy in the asthenosphere is produced by the alignment of olivine in the flow direction, often occurring in the direction of absolute plate motion. In the lithosphere, vertically coherent deformation is thought to "lock-in" or "freeze-in" anisotropy from past or current tectonic processes (Long and Silver, 2009).

Subduction zones are more complicated. In a subduction zone there are four possible locations for anisotropy. These are the overriding lithosphere, the mantle wedge asthenosphere, the subducting slab and the sub-slab asthenosphere (figure 1.2). These different sources can have varying influences on results depending on where in the subduction regime the stations are located. When the overriding plate is a continental plate, anisotropy in the overriding crust tends to be small, and the plate is considered to be too heterogeneous to produce a coherent splitting measurement.

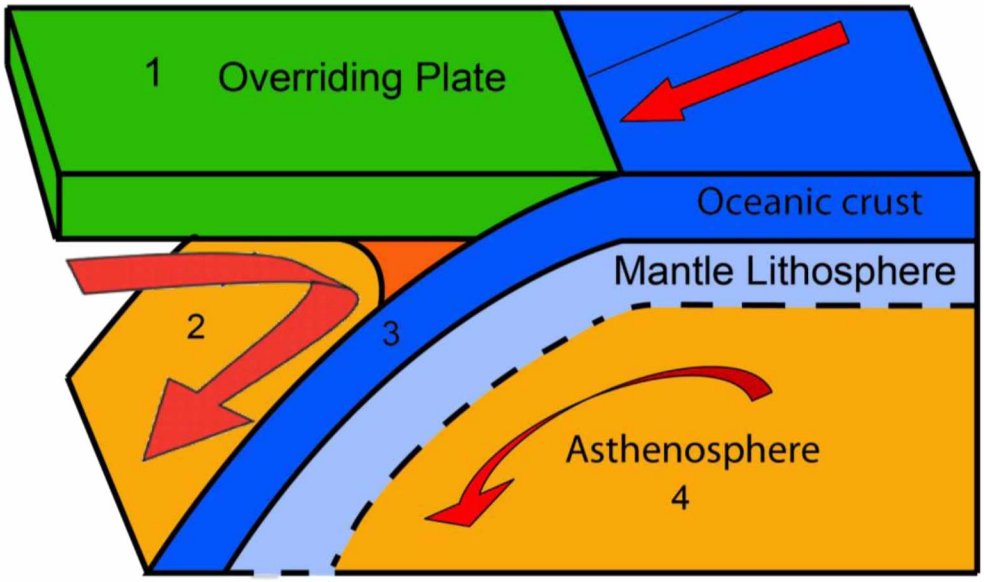

Figure 1.2: Four anisotropy sources in a subduction zone.
There are four possible anisotropy sources in a subduction zone system. The first source is the overriding plate or lithosphere (green), the second is the mantle wedge asthenosphere (light orange with dark orange "cold nose"), the third is the slab (blue), and the fourth is the sub-slab asthenosphere (light orange). The 2D corner flow model for the mantle wedge is shown along with entrained flow below the slab, and fast directions parallel to fracture zones in the slab lithosphere.

In the classic model of plate tectonics, asthenospheric mantle wedge is entrained by the slab and produces a 2D corner flow (figure 1.2). This model would predict trench-normal fast directions for stations sampling the mantle wedge. Corner flow has been invoked for the Tonga subduction zone, where flow is thought to be driven by differential movements of the two plates (Fischer et al., 2000, Hall et al., 2000). World wide, numerous subduction zone shear wave splitting studies have shown no consistent correlation between mantle wedge properties and trench-normal fast directions. Trench-parallel fast directions, as seen in some mantle wedges, have been explained in several

ways. One of these explanations is a change from "a-type" fabric to "b-type" in the cold nose of the mantle wedge. The conditions in the nose of the mantle wedge match the relatively low temperature, high pressure and wet conditions required to generate "b-type" olivine fabric. This produces fast directions that are perpendicular to the flow direction, and would explain trench-parallel fast directions in the nose while still assuming a corner flow regime. This model has been used to explain the complex pattern of splitting observations seen in Japan and the Ryukyu subduction system (Long et al., 2007; Kneller et al., 2008). The other possible explanation for splitting in the mantle wedge is 3D flow around slab edges and trench-parallel flow induced by trench migration (Long and Silver, 2009). Kneller and Van Keken (2007) state that three-dimensional flow may be caused by small-scale convection, oblique subduction, differential slab rollback, trench-parallel motion of the overriding plate, and variations in slab geometry. Both explanations have been used in different subduction systems, and the existence of corner flow (or more complicated flow patterns) in the mantle wedge is likely controlled by the specific geometry of each individual subduction system and will be discussed further in chapter 4.

The source of anisotropy in the subducting slab is due to "frozen" anisotropy from formation of the oceanic plate at the mid-ocean ridge and thickening of the mantle lithosphere as the plate cools. Anisotropy in oceanic plates results in fast directions that are parallel to fracture zones and the spreading direction of the ridge at the time of formation (Silver and Chan, 1988). Walker et al. (2001) in a study of the flow around the Hawaii plume, interpreted data from two regional stations: one ocean bottom

seismometer (ENE of Hawaii) and one on Johnston Atoll. They expected to find fast directions aligning to the direction of absolute plate motion, indicating flow in the asthenosphere. However, the resulting fast directions were parallel to the fracture zones and were therefore interpreted as fossil anisotropy in the lithosphere. The authors then used a single layer model and calculated 5-8% anisotropy in the Pacific Plate (Walker et. al., 2001).

In the sub-slab mantle, a simple model would suggest that asthenospheric mantle is entrained in the direction of plate motion. This model would predict fast directions that are parallel to the plate motion of the subducting slab. However, in practice this does not fit with the majority of observations. Long and Silver (2008) compiled sub-slab splitting measurements for many subduction zones, and only Cascadia had trench-normal fast directions. The other subduction zones had trench-parallel fast directions in the sub-slab mantle. In general, splitting in the sub-slab mantle is caused by trench-parallel flow and not, as expected, material being entrained by the slab (figure 1.3).

In summary, in subduction zone systems there are, in practice, three sources for anisotropy. First, mantle wedge anisotropy is usually interpreted as the result of two-dimensional corner flow, three-dimensional flow or a transition from a- to b- type fabric (figure 1.3). Next, splitting in the subducting slab is due to fossil anisotropy, is parallel to fracture zones in the plate and is due to anisotropy formed at the mid-ocean ridge during creation of the plate. Finally, splitting in the sub-slab mantle was originally expected to reflect entrained flow below the slab, but in practice, observed trench-parallel flow may be related to trench migration (Long and Silver, 2008).

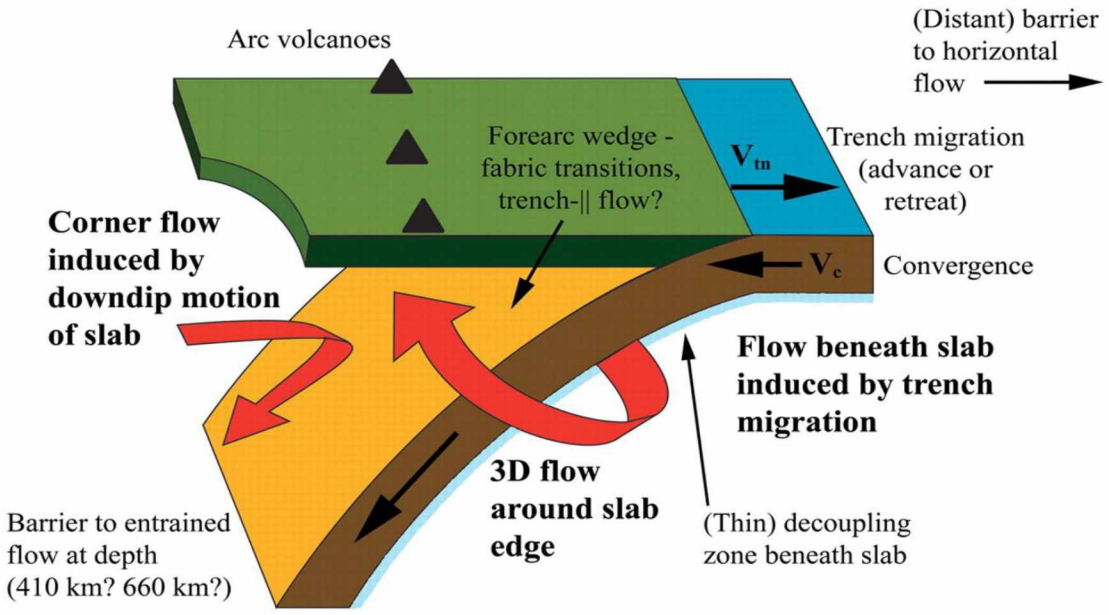

Figure 1.3: Global model of flow in a subduction zone system, from Long and Silver (2008). In this model anisotropy in the overriding plate is considered negligible. Anisotropy in the mantle wedge is considered to be either corner flow or 3D flow around the slab edge, depending on whether the system is dominated by convergence or trench migration. Anisotropy in the subducted slab is considered relict from plate formation, and anisotropy in the sub-slab mantle is expected to be trench-parallel.

1.2 Networks

Shear wave splitting observations were processed and interpreted from data collected by two temporary networks as well as several permanent stations that lie within those networks (figure 1.4). These networks cover the south central Alaska region, in particular, Prince William Sound and the Kenai Peninsula, and the interior, Brooks Range, and North Slope regions of Alaska.

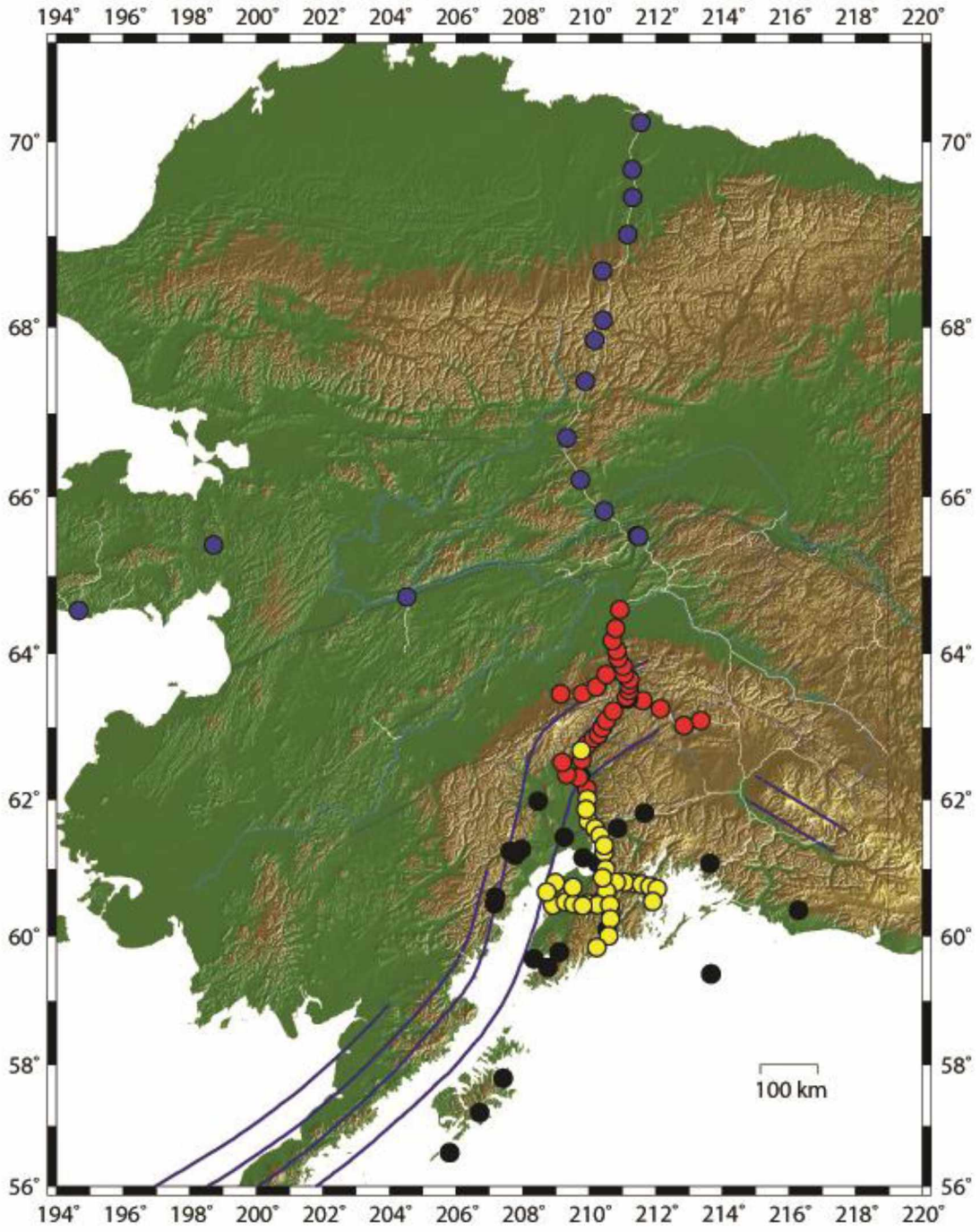

Figure.1.4: **Map of station locations.**
All broadband stations in the state that were used in this analysis are shown. Stations in yellow are from the MOOS network, the red stations are the BEAAR network (Christensen and Abers, 2010), and the blue stations are the ARCTIC network (Litherland et al., 2007). The black stations are permanent broadband stations operated by AEIC and AVO.

1.2.1 Multidisciplinary Observations Of Subduction

Multidisciplinary Observations Of Subduction (MOOS) was an IRIS (Incorporated Research Institutions for Seismology)/PASSCAL (Program for Array Seismic Studies of the Continental Lithosphere) experiment on the Kenai Peninsula in South central Alaska. MOOS was designed to study the subduction of the Pacific plate and the accretion and subduction of the Yakutat block in the region, which ruptured in the 1964 earthquake. The network consisted of 34 three-component broadband seismometers, deployed for a three year period. Four stations were deployed in the summer of 2006 (BING, HOPJ, NANC, PORT), and the remaining 30 stations were deployed in the summer of 2007. In the summer of 2008 seventeen stations were removed, while the remaining seventeen stations were removed in the summer of 2009. MOOS extended from Byers Lake (BYR) in the north to the Kenai Peninsula and Prince William Sound in the south (figure 1.5).

Each station consisted of a Guralp 3T or ESP three-component broadband seismometer in a vault, a buried instrumentation package with a Q330 Digitizer, Baler data recorder, breakout box , 6 air-cell batteries, and a GPS antenna for a clock (figure 1.6). Vaults were designed to minimize the chance of water damage. However, several stations did suffer varying amounts of water damage. Several stations also suffered minor bear damage, and one GPS antenna was stolen during the course of the experiment (table 1-1). Holgate Glacier station (HOLG) had significant water issues and the least data were recovered from this site.

In order to extend the area covered by the MOOS network and fill in a few gaps, several permanent stations were also used in this analysis. The permanent stations used in this study are a combination of AEIC (Alaska Earthquake Information Center) and AVO (Alaska Volcano Observatory) maintained stations. From this network, 14 of the broadband stations yielded results used in this study (figure 1.7). These stations were chosen to expand the coverage across the Cook Inlet, through the rest of Kenai Peninsula, and to Kodiak Island (table 1-1).

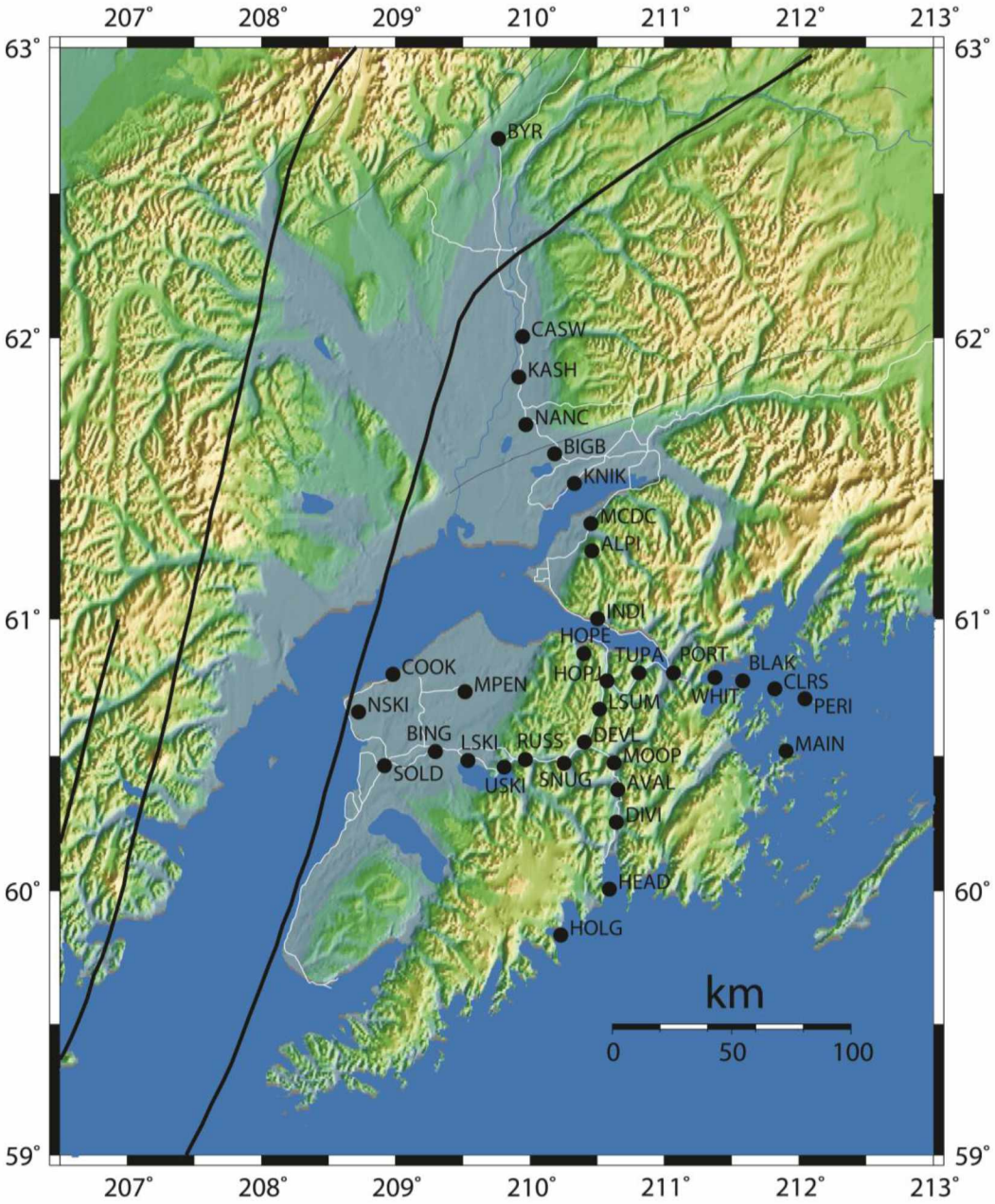

Figure 1.5: Map of MOOS station locations.
Station Locations for the MOOS deployment. Byers Lake (BYR) in the north is a station that overlaps with the BEAAR network. Contours are the 50, 100 and 150 km contours of the Wadati-Benioff zone.

Figure 1.6: **Station set up.**
Station set up for the MOOS network. In 1.6a the GPS antenna is to the left, the action packer is buried in the foreground and the drum with the seismometer is buried in the background. Logs and sticks were used to try to dissuade moose from walking across the instrumentation. 1.6b shows the instrument package in the action packer. The Q330 digitizer is in the front of the action packer and the Baler is in the upper right hand corner next to the breakout box. This instrumentation package is situated on a piece of plywood, with the 6 air cell batteries beneath. 1.6c is a shot of the vault for the seismometer. This particular station did not have water issues, so no drain was installed. The vault is pictured with the inner inverted 20 gallon barrel removed. The seismometer can be seen situated on a concrete pad. Photo credit: Lizzie Entwistle and Anna Bellesiles.

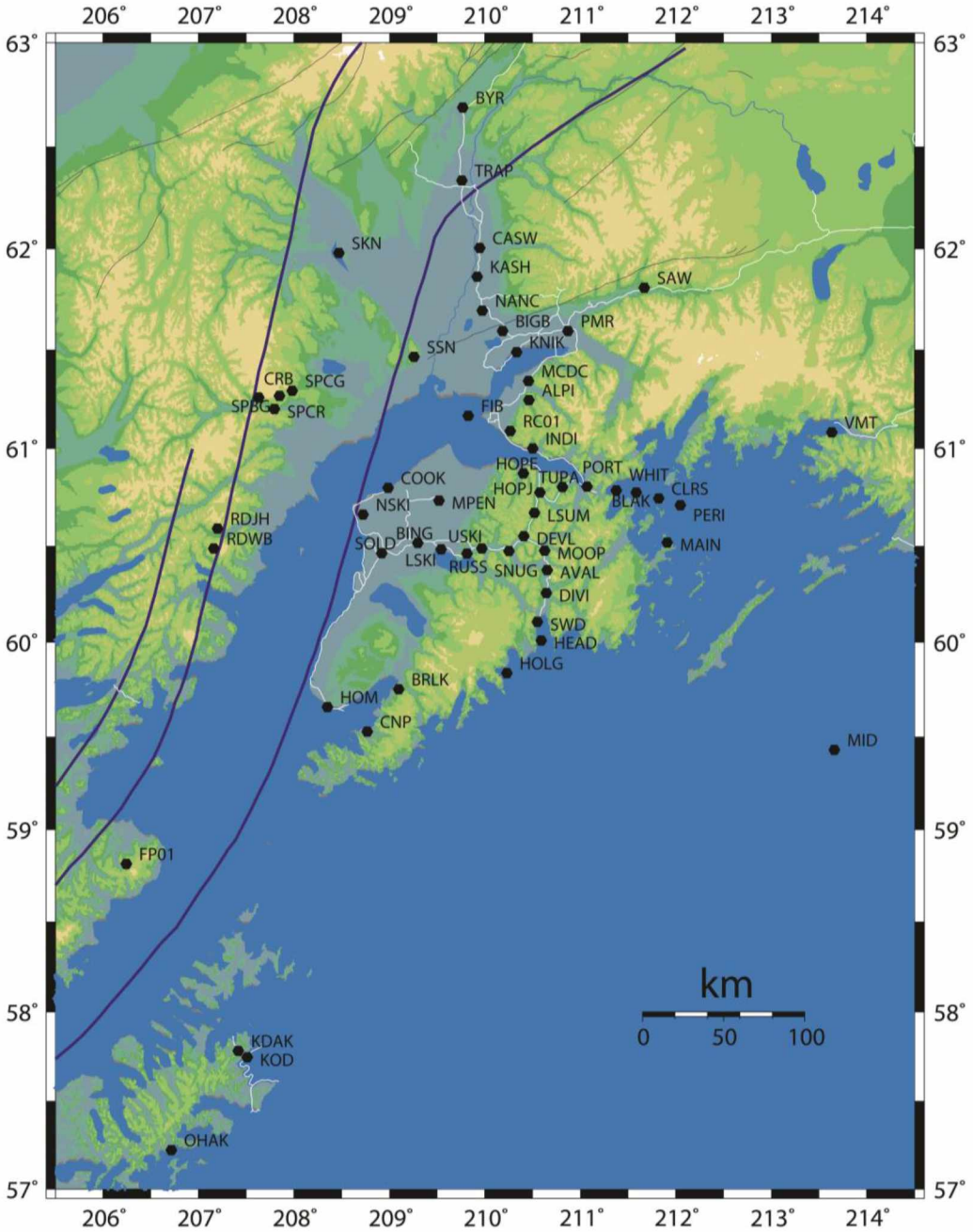

Figure 1.7: Map of MOOS and permanent station locations.
Locations of the permanent stations from AEIC and AVO plotted with the locations of the stations in the MOOS network. Wadati-Benioff zone contours are plotted at 50, 100 and 150 km.

1.2.2 Alaska Receiving Cross-Transect for the Inner Core

The ARCTIC (Alaska Receiving Cross-Transect for the Inner Core) network was also an IRIS/PASSCAL network. ARCTIC was originally designed and deployed to study inner core anisotropy and rotation. However, data from this network were also processed for shear wave splitting. This network consisted of 16 three-component broadband seismometers (table 1-1). The network was deployed from the summer of 2004 through the end of summer, 2007. This network covered a 550 km transect, north from the Fairbanks area to the Arctic Ocean along the Dalton Highway. There was also a sparse line west from Fairbanks to the Bering Sea (figure 1.8). Three stations (CHS, PRB and LVG) were installed in 2004, with the remaining 12 stations installed in 2005. The only difference in experimental set up in ARCTIC from MOOS was that ARCTIC had solar panels to power the instruments in the summer, as well as batteries for power in the winter. The data were initially processed as part of a summer internship program (Litherland et al., 2007). The data were revisited for the purpose of this thesis to complete an Alaska transect.

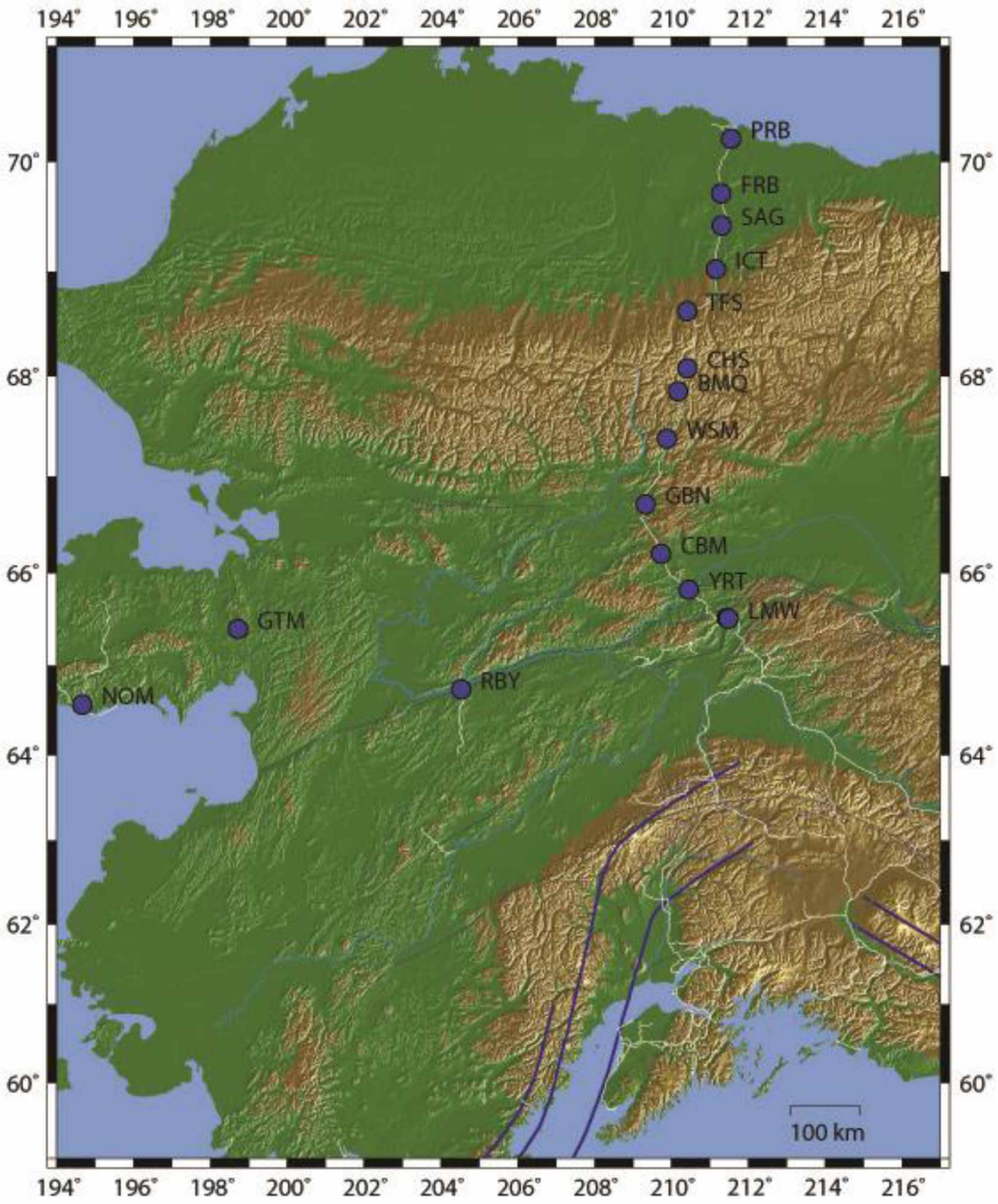

Figure 1.8: Map of ARCTIC station locations.
The locations of the ARCTIC network stations in northern Alaska. Wadati-Benioff zone contours are plotted at 50, 100 and 150 km.

1.3 Tectonic setting

Alaska has a varied and complex tectonic setting. It is important to understand these complexities in order to interpret shear wave splitting observations and determine anisotropic sources.

1.3.1 MOOS tectonic setting

South central Alaska is dominated by the subduction of the Pacific plate under the North American plate. This region includes the eastern end of the Aleutian-Alaskan arc and is bounded on the east by the transition from convergent plate boundary to transform plate boundary (Fairweather and Queen Charlotte faults) and the accretion and partial subduction of the Yakutat block. The Wadati-Benioff Zone (WBZ) reaches 300 km depth in the central Aleutians, but in south central Alaska it reaches only 100-150 km (Page et al., 1989; Taber et al., 1991). The WBZ is abruptly truncated east of 148°W longitude beneath the Alaska Range, either because the subducted plate is torn or contorts sharply (Gutscher and Peacock, 2003).

The MOOS network is located in the "Denali" segment of the subduction zone, which is characterized by shallow subduction or "flat slab" subduction (Gutscher and Peacock, 2003). The Pacific plate is being subducted at a very low dip of $< 5°$ which can be seen in the contours of the slab (Ratchkovski and Hansen, 2002). The dip angle increases below 50 km to 22°, and seismicity continues to 130 km (Ratchkovski and Hansen, 2002). This segment is also characterized by a drastic change in volcanic character. Arc volcanism is absent in this segment except for one small maar, which is

above the easternmost intermediate depth seismicity. Volcanism returns in the Wrangell segment to the east.

The convergence of the Pacific plate with the North American plate takes place at a rate of 5.5 cm/yr (DeMets et al., 1990). The subducting crust is Eocene in age and the magnetic anomalies adjacent to the Yakutat block are 25-35 Ma (Naugler and Wageman, 1973). The southern margin of Alaska is comprised of several major exotic terranes that have been accreted in an ongoing process that continues today with the accretion and partial subduction of the Yakutat block. The subduction of thick, buoyant crust has led to the shallowing of the subduction zone over the last 5-10 Ma (Bruns, 1983; Ferris et al., 2003; Fletcher and Freymueller, 1999). The mantle wedge for this segment of the subduction zone is located north of the MOOS network and does not influence the MOOS results except for the northernmost station.

The Yakutat block is composed of a combination of oceanic plateau and continental material (Lahr and Plafker, 1980; Christeson et al., 2010). It is believed that the Yakutat block has been moving with the Pacific plate since the Pliocene, and is currently coupled, but moving at a slightly lower velocity relative to North America (Fletcher and Freymueller, 1999). The Yakutat block is bounded on the east by the Fairweather and Queen Charlotte fault systems, on the north by the Chugach-Saint Elias thrust system, and on the south by the Transition fault and the base of the continental slope, as illustrated in figure 1.9. Recent studies have shown that the eastern half of Kenai Peninsula and Prince William Sound are underlain by subducted Yakutat terrane crust, which continues deeper into the subduction zone back to the Alaska Range (Ferris et al.,

2003; Eberhart-Phillips et al., 2006). The location of the subducted Yakutat block under Kenai Peninsula and Prince William Sound is coincident with the site of major moment release during the Great Alaska Earthquake of 1964 (Doser and Veilleaux, 2009).

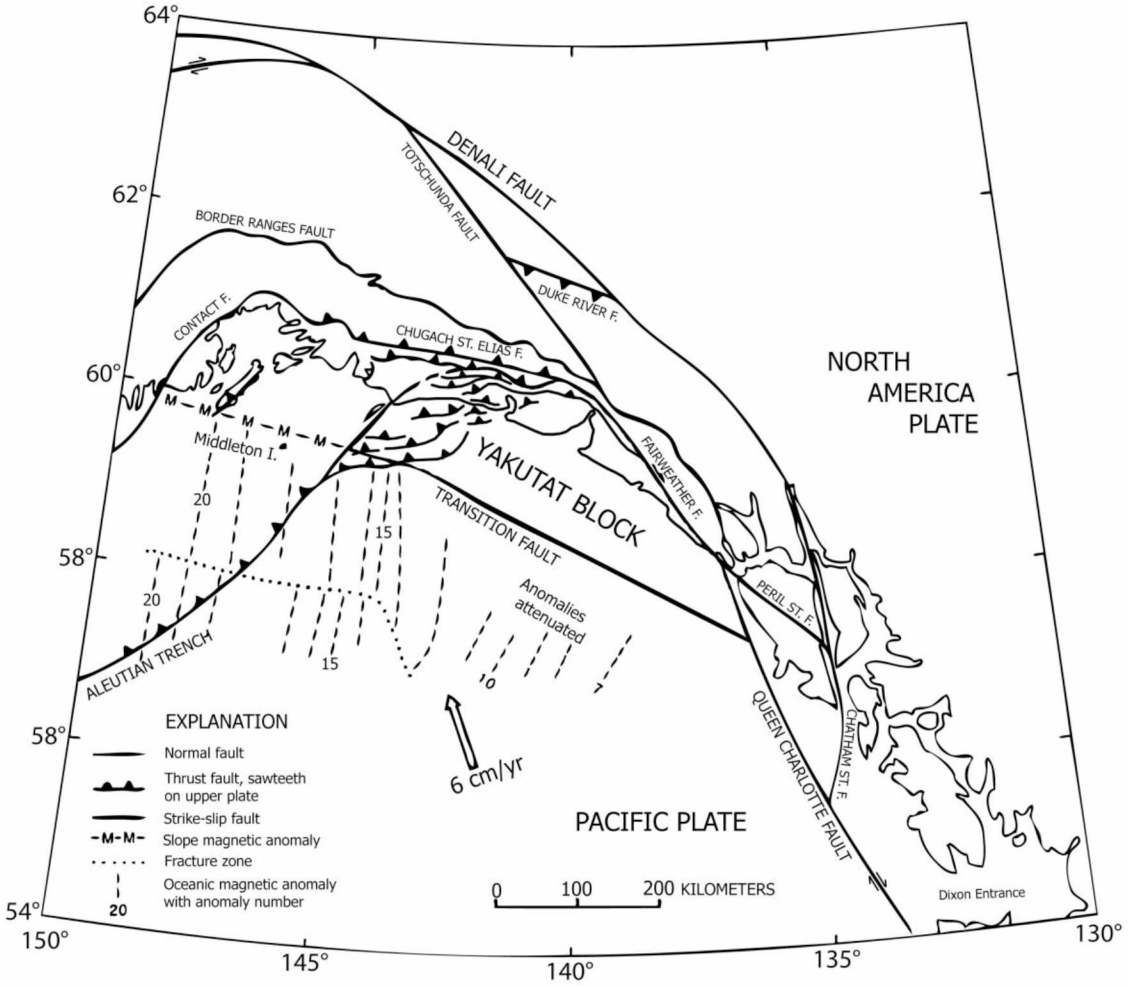

Figure 1.9: Yakutat block and Alaska subduction zone geology.
Location of the Yakutat block in relation to the subduction zone and other prominent geologic features in south central Alaska. Modified from Bruns (1983).

1.3.2 1964 Prince William Sound Earthquake

On March 28, 1964, the Great Prince William Sound Earthquake (Mw=9.2) occurred in the study region. This earthquake was caused by the underthrusting of the Pacific plate under the North American plate. The epicenter was located in Prince William Sound, and the rupture extends southwest approximately 800 km to a point past Kodiak Island. It is the second largest earthquake ever recorded, surpassed only by the 1960 Chile earthquake (Mw=9.5). The MOOS network and permanent stations used for this study cover the rupture area of this event.

The 1964 earthquake was a complicated event with two major asperities and resulted in displacements as large as 25 meters. The first and largest asperity was located near the epicenter in Prince William Sound and extended southwest to the central Kenai Peninsula. The second asperity was located in the Kodiak Island region. The main asperity in Prince William Sound and the Kenai Peninsula appears to be coincident with the subducting Yakutat block, which may act as the asperity in this region.

Zweck et al. (2002) examined the GPS data from the Kenai Peninsula, Prince William Sound, and Kodiak regions. There is currently a large locked patch of the subduction zone coincident with the large asperity from the 1964 earthquake (figure 1.10). The locked zone extends down dip to a depth of around 30 km, and the depth of maximum locking is at 20 km. This is shallow for subduction zones world wide, but is consistent with the estimated depth for the 1964 hypocenter, which was calculated by Oleskovich et al. (1999) to be 25 ± 10km. The western end of the locked patch matches the western end of the Prince William Sound asperity as determined by Johnson et al.

(1996). Zweck et al. (2002) used GPS data to show that the areas of greatest slip in the 1964 earthquake, known as the Prince William Sound and Kodiak asperities, are currently locked (figure 1.11). The asperities from the 1964 event are therefore likely to be persistent features of the subduction zone system and not ephemeral features.

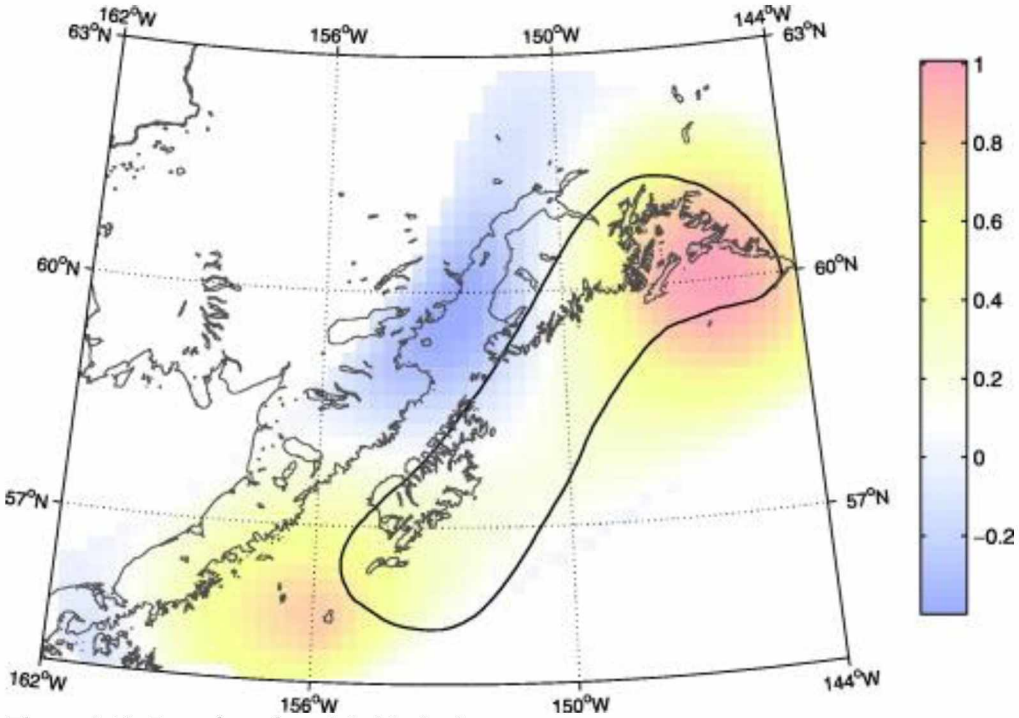

Figure 1.10: Location of modeled locked zone.
This figure shows the modeled locked zone from Zweck et al. (2002) for the 1964 Great Alaska Earthquake. Colors are a range of locking that is given in a coupling ratio that is in units of fraction of Pacific-North American plate rate. The outlined region in this figure shows the aftershock distribution for the 1964 event.

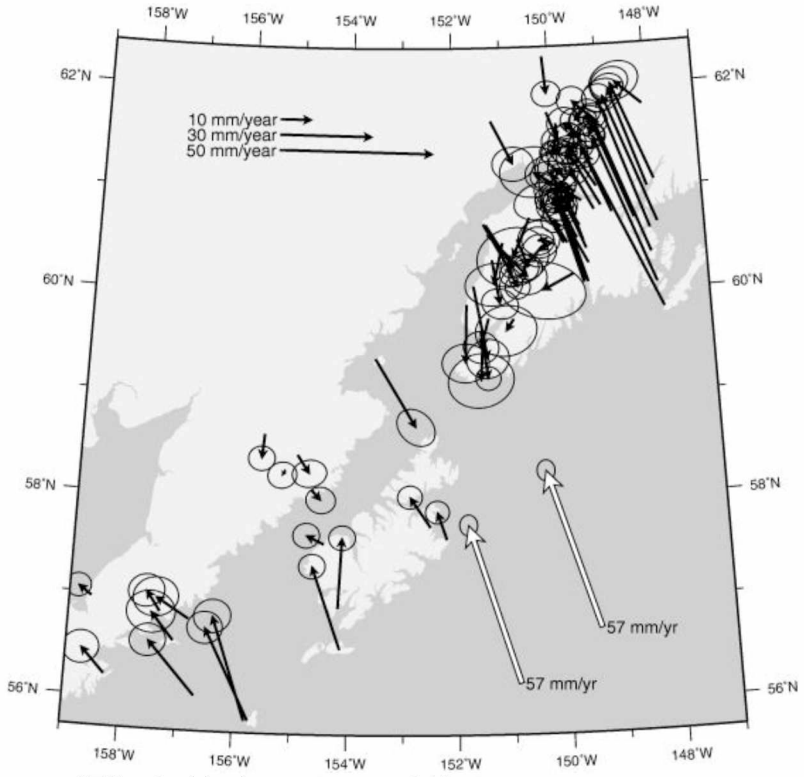

Figure 1.11: Current GPS velocities in south central Alaska.
This figure shows the current GPS data showing locked vs. creeping zones in the rupture zone of the 1964 earthquake. From Zweck et al. (2002).

1.3.3 ARCTIC tectonic setting

The ARCTIC network extends from central Alaska just north of Fairbanks, to the Arctic Ocean at Prudhoe Bay (figure 1.12). The southern half of this line is in the interior of Alaska while the northern half crosses the Brooks Range and the North Slope. Interior Alaska is characterized by rolling hills underlain by various terranes; the largest more or less coherent terrane is the polymetamorphic Yukon-Tanana terrane (Stone and Wallace, 1987; Plafker and Berg, 1994).

Stretching from the western edge of Alaska into Canada, the Brooks Range is dominated by east to west trending fold and thrust structures. The southern edge of the Brooks Range and the Ruby terrane to the southeast are both polymetamorphic

assemblages (Plafker and Berg, 1994). The Brooks Range is an extension of the Rocky Mountains (Moore et al., 1994), the western end of which has undergone hundreds of kilometers of shortening, and the stacking of at least seven major thrust sheets (Moore et al., 1994).

The far north of Alaska, the North Slope, is characterized by low rolling hills and a wide coastal plain. It is bounded on the north by the Arctic Ocean and on the south by the Brooks Range. The northern passive continental margin was formed with the opening of the Arctic Ocean in the Early to Late Cretaceous. The tectonic origin of this region is complicated and still not well understood. The most widely recognized model suggests that northern Alaska rotated counter-clockwise away from Canadian North America (Moore et al., 1994). The basin that underlies the North Slope formed on the displaced Arctic Alaska continental fragment (Bird and Molenaar, 1992).

The North Slope contains the Colville Trough, an elongate foreland basin adjacent to the Brooks Range (Bird and Molenaar, 1992). The northern margin of the Colville Trough is defined by the Barrow Arch. The Barrow Arch is a composite structure that formed as the northern edge of the Colville foreland basin and the rift shoulder on the southern margin of the Arctic Ocean, and it is now a passive subsurface high. The northern margin of the Barrow Arch extends beneath the Beaufort Sea (Moore et al., 1994, Bird and Molenaar, 1992). The southern part of the Colville basin is folded at the surface, and the basin ends at the range front of the Brooks Range (Moore et al., 1994). The basin narrows to the east, where the Brooks Range extends almost to the coast line (Bird and Molenaar, 1992).

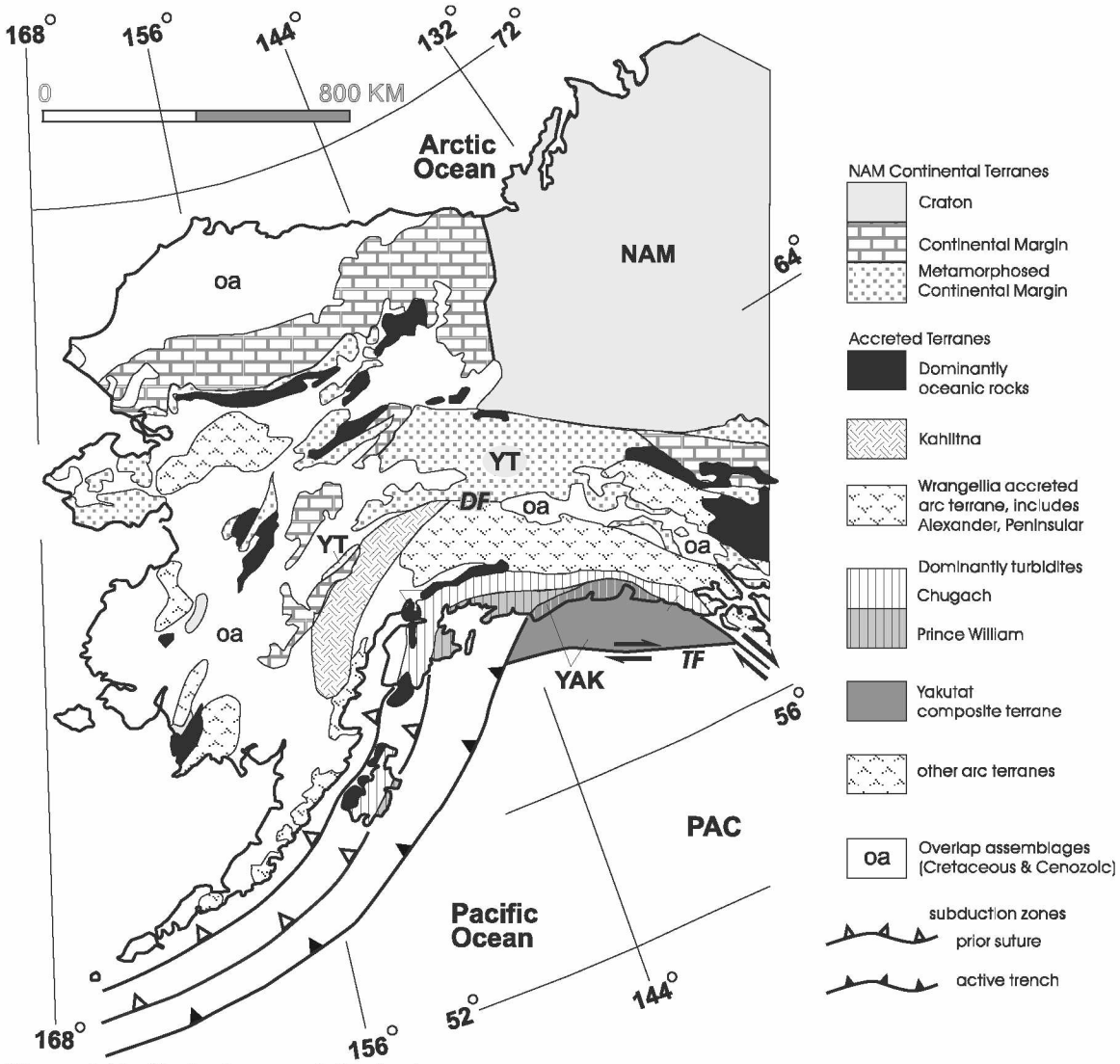

Figure 1.12: Geologic map of Alaska terranes.
This map shows the geology of Alaska. NAM stands for North American craton, YT stands for the Yukon-Tanana terrane, DF stands for the Denali fault, YAK stands for the Yakutat block, TF stands for the transition fault and PAC stands for Pacific plate crust. This figure is modified from Eberhart-Philips et al., (2006).

Table 1-1: Station information.
This table shows the name, on and off dates, locations, network, number of results and any known issues for all the stations used in this thesis. Networks denote if they are from MOOS, ARCTIC, BEAAR, AVO or AEIC. The AVO and AEIC stations are permanent broadband stations managed and maintained by either AVO or AEIC.

Station	On date	Off date	Latitude (degrees)	Longitude (degrees)	Elevation (Km)	Station full name	Network	Number of results	Issues
ALPI	8/11/2007	8/13/2009	61.2448	-149.54	0.811	Alpenglow	MOOS	11	
AVAL	6/9/2007	8/17/2009	60.3755	-149.347	0.222	Avalanche	MOOS	7	
BIGB	8/11/2007	8/12/2009	61.5919	-149.817	0.091	Big Beaver Lake	MOOS	5	
BING	6/26/2006	8/1/2008	60.5169	-150.704	0.089	Bing's Landing	MOOS	2	
BLAK	8/13/2007	8/15/2009	60.7746	-148.417	0.046	Blackstone	MOOS	7	
BYR	8/15/2007	8/1/2008	62.6892	-150.232	0.402	Byers Lake	MOOS	11	
CASW	6/20/2007	8/1/2008	62.0056	-150.054	0.106	Caswell	MOOS	7	
CLRS	6/14/2007	8/1/2008	60.7458	-148.178	0.05	Cullross Island	MOOS	0	
COOK	8/10/2007	8/1/2008	60.799	-151.018	0.04	Captain Cook Rec.	MOOS	0	
DEVL	6/17/2007	8/17/2009	60.5508	-149.594	0.306	Devils Pass Trail	MOOS	15	bear
DIVI	8/6/2007	8/1/2008	60.2564	-149.356	0.273	Divide	MOOS	4	
HEAD	6/15/2007	8/18/2009	60.0084	-149.41	0.055	Caines Head	MOOS	5	
HOLG	6/13/2007	6/11/2009	59.8351	-149.77	0.046	Holgate Glacier	MOOS	6	water
HOPE	6/12/2007	8/15/1009	60.8738	-149.598	0.498	Hope	MOOS	13	
HOPJ	6/28/2006	8/1/2008	60.776	-149.426	0.221	Hope Junction	MOOS	5	
INDI	6/16/2007	8/1/2008	61.001	-149.498	0.127	Indian Creek	MOOS	7	
KASH	8/12/2007	8/12/2009	61.8636	-150.082	0.1	Kashwitna	MOOS	2	
KNIK	8/15/2007	8/1/2008	61.4859	-149.669	0.065	Knik	MOOS	8	
LSKI	8/5/2007	8/14/2009	60.4832	-150.462	0.116	Lower Skilak Lake	MOOS	2	data recorder
LSUM	8/4/2007	8/15/2009	60.6717	-149.481	0.446	Lower Summit Lake	MOOS	10	mining
MAIN	6/14/2007	8/1/2008	60.5183	-148.091	0.044	Main Bay	MOOS	1	
MCDC	6/16/2007	8/1/2008	61.3427	-149.545	0.162	McDonald Center	MOOS	0	
MOOP	8/6/2007	8/1/2008	60.4754	-149.374	0.242	Moose Pass	MOOS	7	
MPEN	8/10/2007	8/14/2009	60.7352	-150.482	0.13	Moose Pens	MOOS	0	
NANC	6/29/2006	8/1/2008	61.6954	-150.029	0.125	Nancy Lake	MOOS	9	
NSKI	8/10/2007	8/17/2009	60.6622	-151.277	0.06	Nikilski	MOOS	1	

Table 1-1 continued…

PERI	6/14/2007	8/15/2009	60.7098	-147.953	0.065	Perry Island	MOOS	2	
PORT	6/28/2006	8/1/2008	60.8049	-148.932	0.043	Portage	MOOS	1	
RUSS	8/5/2007	8/14/2009	60.4881	-150.032	0.15	Russian River	MOOS	7	
SNUG	8/4/2007	8/1/2008	60.4731	-149.747	0.191	Snug Harbor	MOOS	1	
SOLD	6/9/2007	8/17/2009	60.4641	-151.082	0.116	Soldotna	MOOS	1	
TUPA	8/4/2007	8/13/2009	60.8045	-149.187	0.344	Turnagin Pass	MOOS	5	GPS stolen
USKI	6/9/2007	8/1/2008	60.4601	-150.19	0.127	Upper Skilak Lake	MOOS	6	
WHIT	6/11/2007	8/1/2008	60.7866	-148.624	0.081	Whittier	MOOS	3	
BERG	7/15/2005	NA	60.3928	-143.702	0.474	Berg Lake	AEIC	1	
BRLK	7/1/2008	NA	59.751	-150.906	0.409	Bradley Lake	AEIC	5	
CNP	7/24/2008	NA	59.5259	-151.235	0.572	China Poot	AEIC	2	
FIB	1/4/1996	NA	61.1662	-150.175	0.062	Fire Island Broadband	AEIC	6	
HOM	6/18/2009	NA	59.6578	-151.649	0.221	Homer Trailer	AEIC	1	
KDAK	6/9/1997	NA	57.7828	-152.584	0.152	Kodiak Island	AEIC	9	
MID	10/18/2007	NA	59.4278	-146.339	0.037	Middleton Island	AEIC	2	
OHAK	6/23/2006	NA	57.2225	-153.288	0.0775	Old Harbor, Alaska	AEIC	6	
PMR	9/1/1967	NA	61.5922	-149.131	0.1	Palmer, AK, USA	AEIC	10	
RC01	8/7/1998	NA	61.0896	-149.737	0.383	Rabbit Creek	AEIC	28	
RDJH	2/3/2009	NA	60.5911	-152.804	1.414	Redoubt Juergen Hut	AVO	1	
RDWB	2/21/2009	NA	60.4881	-152.84	1.546	Redoubt W. Broadband	AVO	1	
SAW	11/7/1999	NA	61.8076	-148.33	0.782	Sawmill	AEIC	4	
SKN	5/15/2006	NA	61.9806	-151.529	0.603	Skwentna	AEIC	4	
SPBG	9/9/2004	NA	61.2597	-152.37	1.087	Spurr Blockage Glacier	AVO	4	
SPCG	9/8/2004	NA	61.2919	-152.021	1.329	Spurr Capps Glacier	AVO	1	
SPCR	9/8/2004	NA	61.2009	-152.207	0.984	Spurr Chakachatna Riv.	AVO	2	
SSN	8/15/2008	NA	61.464	-150.744	1.293	Susitna	AEIC	5	

Table 1-1 continued…

SWD	6/4/2001	NA	60.1049	-149.451	0.0677	Seward broadband	AEIC	15	
BMQ	6/2/2005	8/1/2007	67.8516	-149.824	0.59	Black Marble Quarry	ARCTIC	18	
CBM	6/21/2005	8/1/2007	66.2066	-150.264	0.57	Caribou Mountain	ARCTIC	10	
CHS	7/30/2004	8/1/2007	68.0789	-149.582	1.025	Chandalar Shelf	ARCTIC	15	
FRB	6/4/2005	8/1/2007	69.7162	-148.699	0.146	Franklin Bluff	ARCTIC	13	
GBN	6/2/2005	8/1/2007	66.7192	-150.671	0.349	Gobbler's Knob	ARCTIC	12	
GTM	7/31/2005	8/1/2007	65.4015	-161.278	0.409	Granite Mountain	ARCTIC	2	
ICT	6/4/2005	8/1/2007	69.0223	-148.836	0.418	Ice Cut	ARCTIC	16	
LMW	6/24/2005	8/1/2007	65.5114	-148.511	0.59	Livengood Microwave	ARCTIC	18	
LVG	8/3/2004	8/1/2007	65.522	-148.551	0.222	Livengood DOT	ARCTIC	0	
NOM	7/29/2005	8/1/2007	64.5695	-165.338	0.211	Nome	ARCTIC	4	
PRB	7/31/2004	8/1/2007	70.2036	-148.446	0.0465	Prudhoe Bay	ARCTIC	41	
RBY	7/31/2005	8/1/2007	64.74	-155.466	0.221	Ruby	ARCTIC	3	
SAG	6/4/2005	8/1/2007	69.424	-148.694	0.342	Sag River	ARCTIC	16	
TFS	6/5/2005	8/1/2007	68.6274	-149.59	0.759	Toolik Field Station	ARCTIC	16	
WSM	6/2/2005	8/1/2007	67.3812	-150.11	0.422	Wiseman	ARCTIC	13	
YRT	6/24/2005	8/1/2007	65.825	-149.543	0.645	Yukon Radio Tower	ARCTIC	8	
AND	5/22/2000	12/31/2001	64.3306	-149.2	0.178	Anderson	BEAAR	4	
ANT	6/4/2000	12/31/2001	63.0992	-149.483	0.614	Antimony	BEAAR	10	
BSH	6/6/1999	12/31/2001	64.1713	-149.295	0.284	Browne	BEAAR	0	
BYR	6/1/1999	12/31/2001	62.6893	-150.232	0.384	Byers Microwave	BEAAR	48	
CAR	5/25/2000	12/31/2001	63.5831	-148.802	0.662	Carlo	BEAAR	6	
CZN	6/1/2000	12/31/2001	63.1033	-146.644	1.021	Crazy Notch	BEAAR	3	
DH1	5/27/2000	12/31/2001	63.3734	-148.383	0.756	Denali Highway 1	BEAAR	16	
DH2	5/30/2000	12/31/2001	63.2652	-147.855	0.943	Denali Highway 2	BEAAR	3	
DH3	5/29/2000	12/31/2001	63.0345	-147.144	1.028	Denali Highway 3	BEAAR	6	
EFS	6/11/2000	12/31/2001	63.5581	-149.781	0.964	East Fork / Sable	BEAAR	9	

Table 1-1 continued…

FID	5/28/2000	12/31/2001	62.7622	-150.069	0.308	Fiddlehead	BEAAR	4	
GNR	5/20/2000	12/31/2001	63.8345	-148.978	0.581	Garner	BEAAR	9	
GOO	6/4/2000	12/31/2001	63.2286	-149.271	0.7	Igloo	BEAAR	16	
HURN	5/30/1999	12/31/2001	62.9991	-149.606	0.607	Hurricane N	BEAAR	36	
MCK	5/31/1999	12/31/2001	63.7323	-148.937	0.643	McKinley	BEAAR	14	
MHR	5/31/2000	12/31/2001	62.8603	-149.865	0.378	Moosehead Rock	BEAAR	15	
NNA	5/29/1999	12/31/2001	64.5797	-149.079	0.383	Nenana	BEAAR	20	
PVE	5/28/2000	12/31/2001	62.3551	-150.664	0.347	Petersville East	BEAAR	2	
PVW	6/16/2000	12/31/2001	62.5277	-150.804	0.646	Petersville West	BEAAR	14	
PYY	5/26/2000	12/31/2001	62.9094	-149.712	0.43	Parrott Yesteryear	BEAAR	4	
RCK	11/7/1999	12/31/2001	64.0412	-149.166	0.385	Rock Creek	BEAAR	11	
RND	6/25/1999	12/31/2001	63.4057	-148.86	0.984	Reindeer	BEAAR	23	
RND5	6/16/2000	12/31/2001	63.4015	-148.855	0.987	Reindeer Tower 5	BEAAR	0	
RNDE	6/15/2000	12/31/2001	63.4003	-148.815	1.109	Reindeer East	BEAAR	0	
RNDN	6/11/2000	12/31/2001	63.4157	-148.878	0.699	Reindeer North	BEAAR	0	
RNDR	6/10/2000	12/31/2001	63.4014	-148.867	0.928	Reindeer Rock	BEAAR	0	
RNDS	6/11/2000	12/31/2001	63.3896	-148.868	0.817	Reindeer South	BEAAR	0	
SAN	6/12/2000	12/31/2001	63.7231	-149.478	0.78	Sanctuary	BEAAR	14	
SBL	6/11/2000	12/31/2001	63.4686	-150.2	1.099	Stony / Bergh Lake	BEAAR	6	
SLM	5/28/2000	12/31/2001	63.5067	-148.805	0.661	Slime Creek	BEAAR	8	
SLT	5/26/2000	12/31/2001	63.9391	-149.121	0.465	Slate Creek	BEAAR	2	
SOB	6/10/2000	12/31/2001	64.1702	-149.299	0.36	Son of Browne	BEAAR	8	
TCE	5/21/2000	12/31/2001	62.3147	-150.314	0.159	Trapper Creek Elem.	BEAAR	6	
TLKY	6/3/1999	12/31/2001	62.15	-150.061	0.129	Talkeetna Y	BEAAR	25	
WOLF	5/22/2000	12/31/2001	62.5604	-150.204	0.34	Wolf	BEAAR	5	
WON	6/14/2000	12/31/2001	63.4621	-150.854	0.66	Wonder Lake	BEAAR	16	
YAN	6/28/1999	12/31/2001	63.6559	-148.775	0.781	Yanert	BEAAR	18	

2. Methods

In this study, the method of Silver and Chan (1991), as implemented by Fischer et al. (1998) and Christensen and Abers (2010), was used. There were two primary reasons that SKS waves were used. First SKS waves have a predictable polarization controlled by the conversion from P to S at the core mantle boundary (CMB). Second, due to the specific ray path of SKS waves and the effects of the conversation at the CMB, the anisotropy measured is constrained to the receiver side of the ray path. Earthquakes with epicentral distances between 85 to 145 degrees and a magnitude between 5.5 and 7.9 were chosen for analysis due to the SKS waves being isolated from other phases and reliably recorded. There were 301 events extracted for analysis of the MOOS network data. Of these, 37 events yielded results (plotted in figure 2.1a and 2.1b). For the ARCTIC data set, 49 events yielded results (figure 2.1c). For the permanent stations, 55 events were used (figure 2.1d).

The SKS arrival for each event was first identified, and examined manually to ensure a sufficient signal-to-noise ratio, and separation from other arrivals. Events where the SKS arrival was distinguishable from the background were used. Next, the signal was isolated in a 30 second window. The horizontal components of the waveform were then extracted for analysis and processing. The data was then bandpass filtered at 0.01 to 1.0Hz.

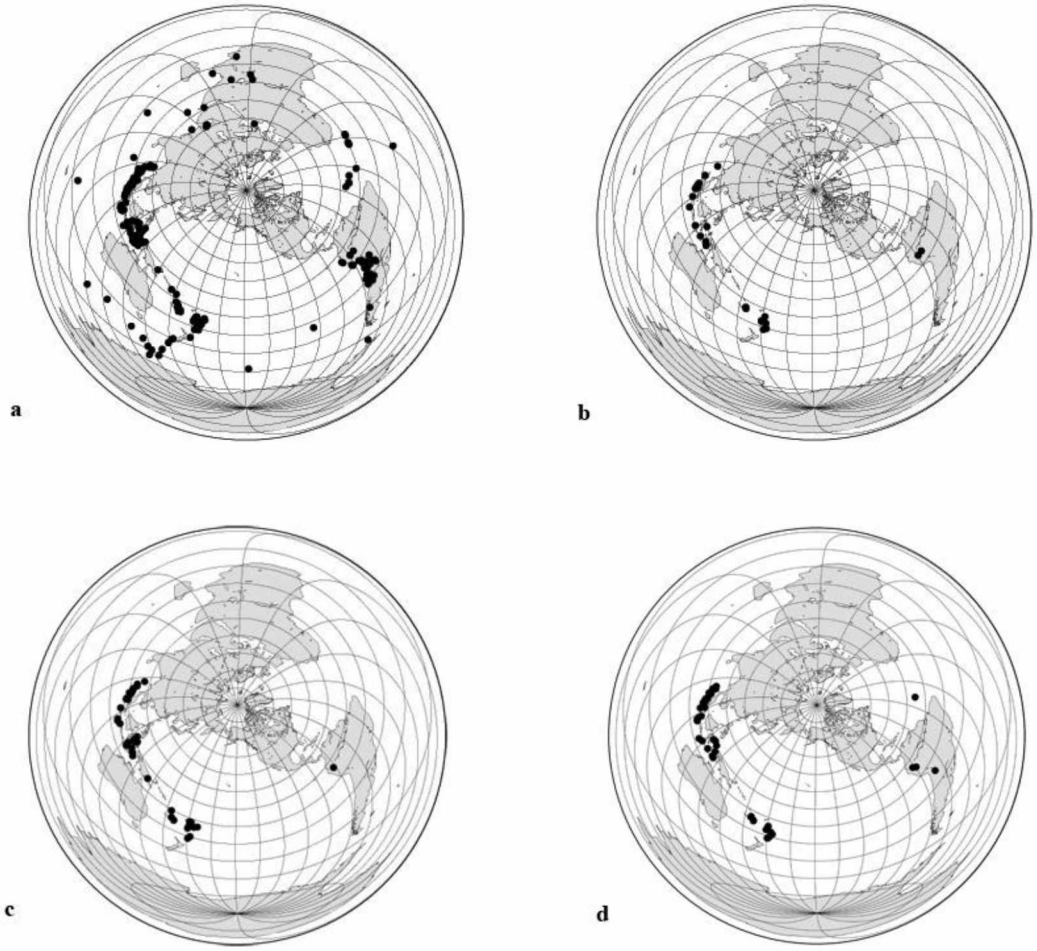

Figure 2.1: Map of events extracted and used
This figure relates the events extracted vs. the events that yielded results. 2.1a shows all events extracted for analysis of the MOOS network and 2.1b shows the events that yielded results. Figure 2.1c shows only the events that yielded results from the ARCTIC network and 2.1d shows only the events that yielded results from the permanent network stations used.

The fast directions (ϕ) and delay times (δt) were found using a grid search. The grid search consisted of rotating the horizontal waveforms through a range of possible fast directions (ϕ) from -90° to 90° and offsetting them by a range of possible delay times (δt) from 0 to 8 seconds. At each point on the grid search a covariance matrix was calculated. The best possible solution minimizes the second and smaller eigenvalue (φ_2) of this matrix. This value, the minimized second eigenvalue φ_{2min} is then used to find the

errors associated with this solution. The results of the grid search are displayed as a normalized second eigenvalue with respect to φ_{2min}. On a contour plot of φ_2/φ_{2min} the 95% confidence region is the 1.11 contour for this data set, with the optimal solution resulting in a value of 1. An example of this analysis can be seen in figures 2.2-2.5.

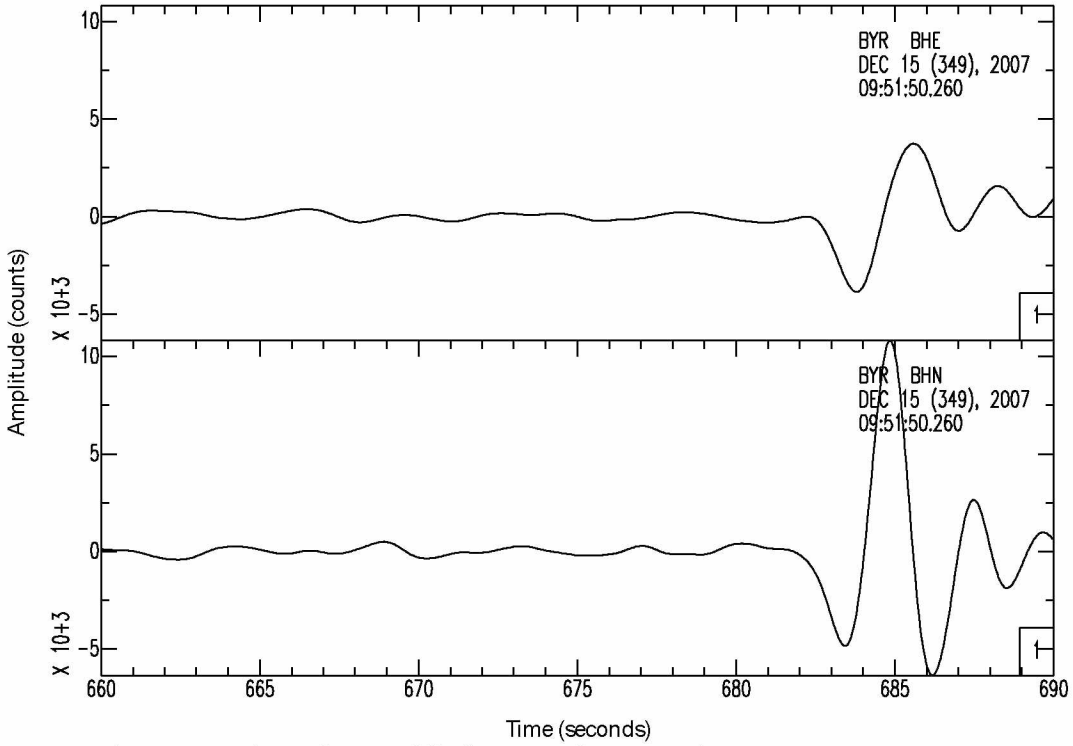

Figure 2.2 Thirty second time window of SKS wave before analysis.
This figure shows the SKS wave isolated in a 30 second time window on the horizontal components. The east-west component is on the top and north-south component is on the bottom. Note that they are plotted on the same scale. This event was recorded on the MOOS station BYR on December 15, 2007.

After calculating the splitting parameters and 95% confidence regions, the wave forms were again visually analyzed to identify null readings. This was done with additional visual inspection of the wave forms. The wave forms are rotated to the solution fast direction and offset by the solution delay time. Null readings are observations where the best possible solution returns no energy on the transverse component, an example of

such an event can be seen in figure 2.6. A Null reading arises when a wave has not split. In an anisotropic medium, this happens when waves arrive along the fast or slow directions. This can be checked by rotating the original waves to their great circle path, null readings will only have energy on the radial component.

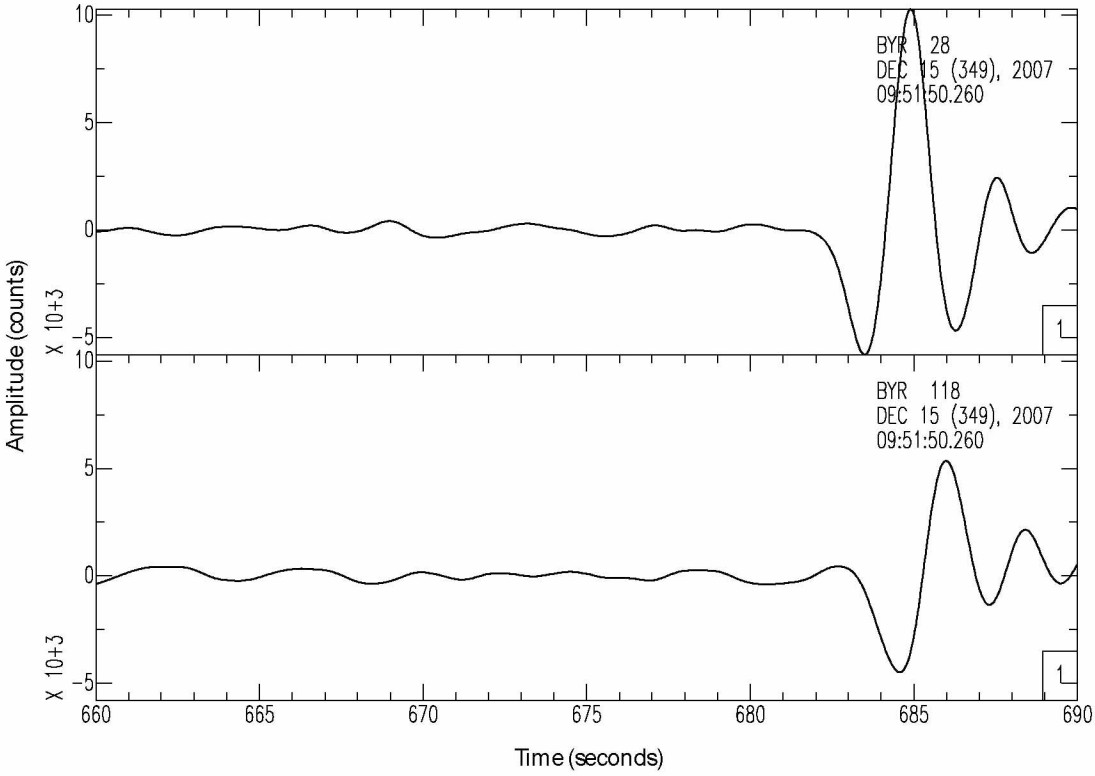

Figure 2.3 SKS wave rotated to fast and slow directions
In this figure the SKS wave from figure 2.2 has been rotated to the calculated fast (top) and slow (bottom) directions. Note the similarity in the wave forms and offset in onset of the SKS wave. Also note that these waveforms are potted on the same scale. This event was recorded on the MOOS station BYR on December 15, 2007.

After determining that the waves from an event are split, the error plot was examined. Events with large errors were thrown out as well as events with non-unique solutions. The error threshold was set to +/- 35 degrees for fast direction and +/- .6 seconds for delay time in the 95% confidence regions after Christensen and Abers (2010).

Any event with 95% confidence regions larger then this bound was thrown out. Non-unique solutions return two or more 95% confidence regions, and an example of this can be seen in figure 2.7. These events were also excluded from the results.

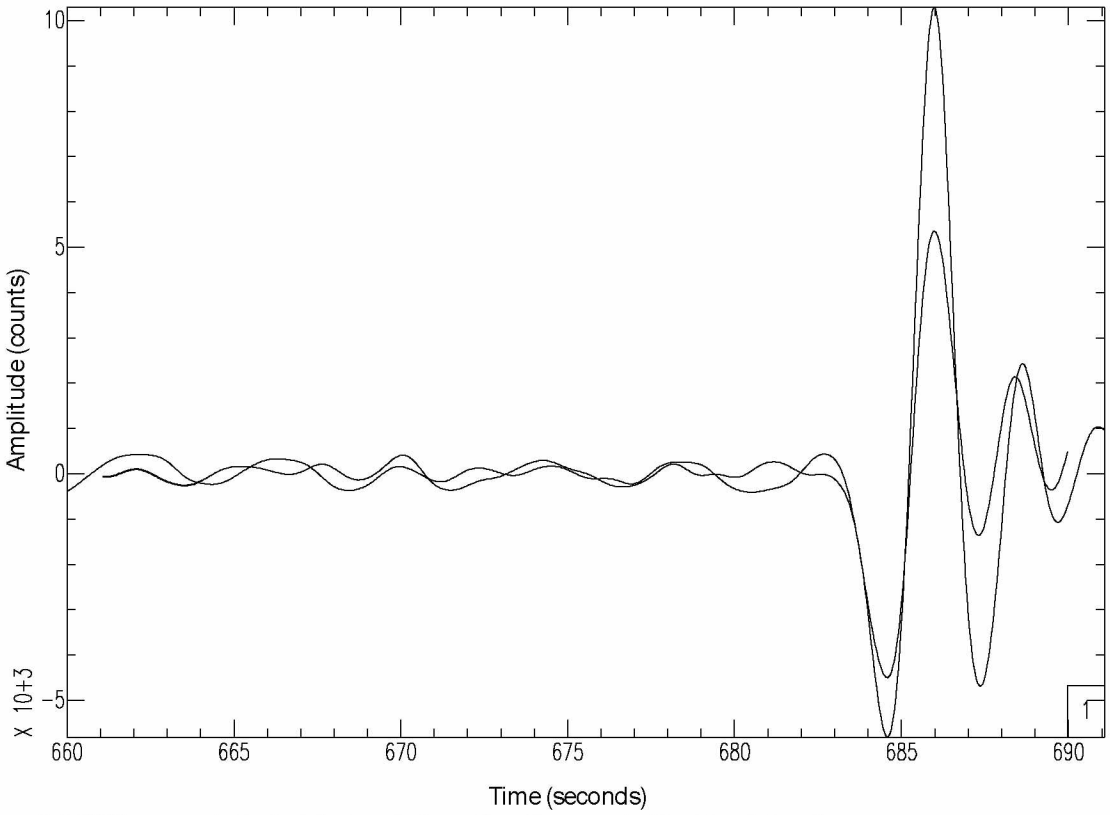

Figure 2.4 SKS wave plotted at fast and slow directions and offset by delay time
This figure shows the SKS wave from figure 2.2 rotated to the fast and slow direction, offset by the delay time and overlaid to show the correlation in the waveform. This event was recorded on the MOOS station BYR on December 15, 2007.

Not all events yielded useable results. Along with null readings, the amplitude of the SKS waves are dependant on the radiation pattern of the event. If the path from source to receiver was along a low energy lobe of the radiation pattern for S waves, then the SKS wave produced from that event was unlikely to have enough amplitude above background to be usable. In addition, waves that came from a back-azimuth aligned with

either the fast direction or slow direction of the anisotropic medium would not be split. All of these properties of an earthquake reduce the number of usable events for the data set. The events used for this study are plotted in figure 2.1 and listed in table 2-1.

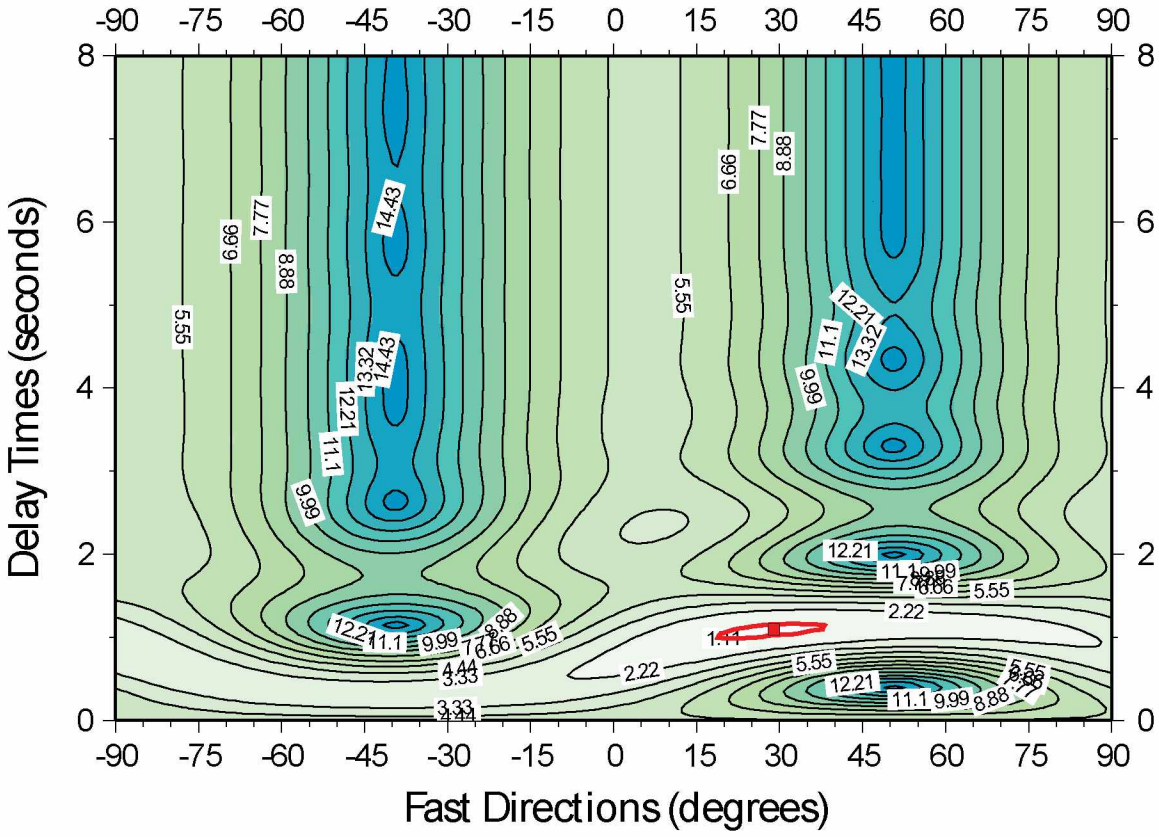

Figure 2.5 Contour plot and 95% confidence region
This figure shows the contour plot associated with the calculation of the fast direction and delay time for the SKS wave in figure 2.2. This event was recorded on the MOOS station BYR on December 15, 2007. The red line indicates the 95% confidence region. Colors range from white within the 95% confidence region to blue for the worst fitting solutions in the grid search.

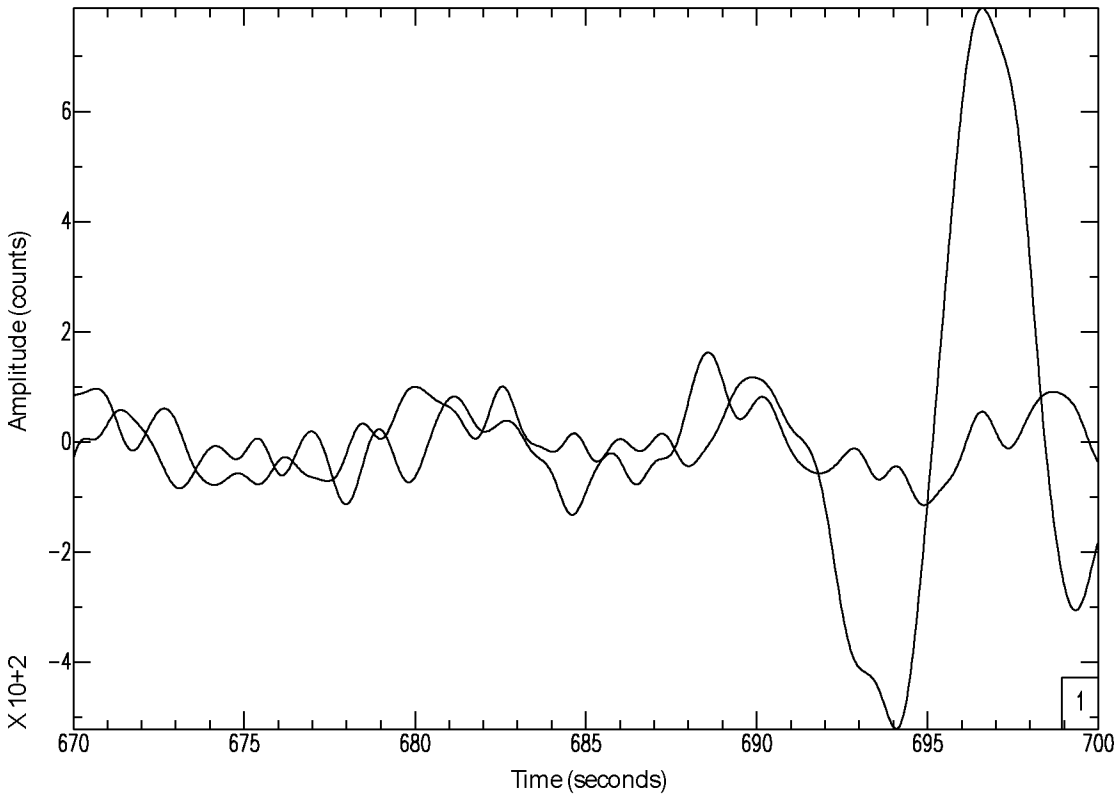

Figure 2.6: Example of a null solution
Null solutions have all the energy on the radial component and no energy on the transverse component. This is an example from the station HEAD from the MOOS network.

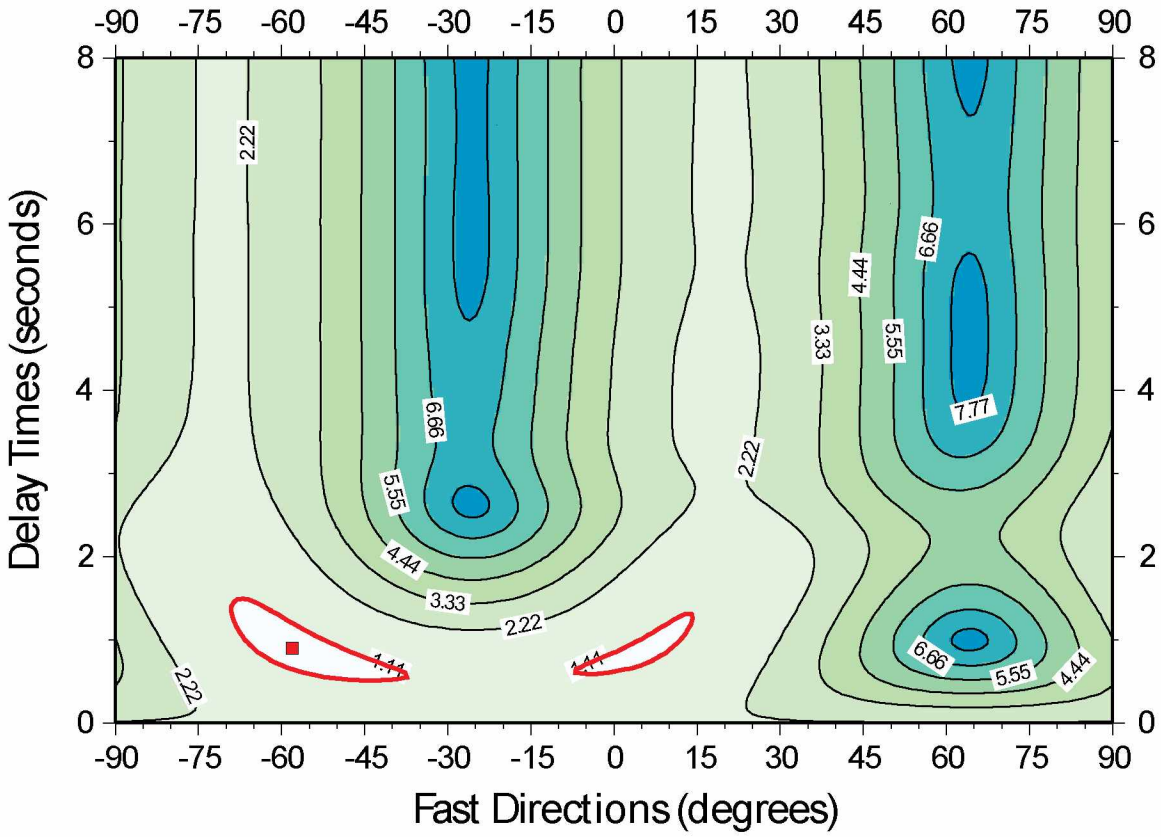

Figure 2.7: Contour plot and 95% confidence region for a non-unique solution
Solutions that return a non-unique solution have more then one 95% confidence region. This event was recoded on the MOOS station DEVL, and is not included in the results for that network. The optimal solution is noted with a red point, and the 95% confidence regions are plotted in red. The color scale grades from white within the 95% confidence region to blue, for the areas of worst fit.

Table 2-1: Table of events used for analysis.
This table shows all events used for the analysis of the data from the BEAAR (Christensen and Abers, 2010), ARCTIC, permanent and MOOS networks.

M/D/Y	Origin Time	Latitude (degrees)	Longitude (degrees)	Depth (km)	Magnitude	Event ID	Network
7/8/1999	04:49.9	-30.25	-178.13	116	5.7	1	BEAAR
7/18/1999	34:03.0	-22.55	179.41	591	6.0	2	BEAAR
7/19/1999	17:03.0	-28.63	-177.61	39	6.5	3	BEAAR
7/28/1999	16:57.0	-28.69	-177.52	33	6.1	4	BEAAR
7/28/1999	08:20.0	-30.29	-178.01	25	6.3	5	BEAAR
8/1/1999	39:04.0	-30.37	-177.83	10	6.5	6	BEAAR
8/12/1999	44:59.0	-1.72	122.46	33	6.2	7	BEAAR
8/14/1999	16:52.0	-5.89	104.71	101	6.4	8	BEAAR
8/25/1999	06:22.0	-19.06	169.61	263	5.7	9	BEAAR
9/15/1999	01:24.0	-20.93	-67.28	218	6.4	10	BEAAR
11/30/1999	01:53.0	-18.90	-69.17	128	6.6	11	BEAAR
11/30/1999	23:34.8	-21.28	169.10	33	5.8	12	BEAAR
12/19/1999	38:32.2	-3.99	131.33	33	5.9	13	BEAAR
12/21/1999	14:57.0	-6.85	105.56	56	6.5	14	BEAAR
3/1/2000	21:01.3	-19.00	-179.36	675	5.8	15	BEAAR
3/3/2000	09:13.0	-7.32	128.49	142	6.4	16	BEAAR
4/11/2000	41:26.1	-27.94	-178.39	201	5.8	17	BEAAR
4/18/2000	28:12.0	-20.66	-176.47	221	6.0	18	BEAAR
4/23/2000	27:23.0	-28.31	-62.99	609	7.0	19	BEAAR
5/4/2000	21:16.0	-1.11	123.57	26	7.6	20	BEAAR
5/14/2000	08:34.0	-4.30	123.16	33	6.3	21	BEAAR
6/4/2000	28:26.0	-4.72	102.09	33	7.9	22	BEAAR
6/6/2000	58:06.0	-5.09	102.70	33	6.2	23	BEAAR
6/7/2000	45:26.0	-4.61	101.91	33	6.7	24	BEAAR
6/14/2000	15:25.0	-25.52	178.05	605	6.4	25	BEAAR
6/16/2000	55:35.0	-33.88	-70.09	120	6.4	26	BEAAR
6/18/2000	44:13.0	-13.80	97.45	10	7.9	27	BEAAR
6/27/2000	37:05.8	-7.10	125.91	496	5.8	28	BEAAR
7/15/2000	13:44.6	-7.03	128.93	217	5.9	29	BEAAR
7/31/2000	01:49.0	-29.28	-176.35	10	6.2	30	BEAAR
8/7/2000	33:55.0	-7.02	123.36	649	6.5	31	BEAAR
8/15/2000	30:08.0	-31.51	179.73	358	6.6	32	BEAAR
8/24/2000	36:45.3	-6.03	102.69	33	5.9	33	BEAAR
8/28/2000	05:47.0	-4.11	127.39	16	6.8	34	BEAAR
9/2/2000	02:19.0	-20.07	-179.14	688	6.0	35	BEAAR
9/3/2000	21:23.7	-20.55	-177.82	363	5.8	36	BEAAR
9/10/2000	06:15.0	-1.11	129.33	33	6.1	37	BEAAR
12/18/2000	19:21.0	-21.18	-179.12	628	6.6	38	BEAAR
2/13/2001	28:30.0	-4.68	102.56	36	7.2	39	BEAAR
2/16/2001	59:09.0	-7.16	117.49	521	6.1	40	BEAAR
3/11/2001	50:40.4	-25.37	-177.97	231	5.8	41	BEAAR
3/14/2001	56:18.0	0.45	121.89	109	6.0	42	BEAAR

Table 2-1 continued…

5/19/2001	36:25.0	-19.90	-177.52	369	6.0	43	BEAAR
5/25/2001	06:10.0	-7.87	110.18	143	6.3	44	BEAAR
5/26/2001	57:26.0	-20.29	-177.84	407	6.4	45	BEAAR
5/28/2001	37:05.0	-6.61	132.35	33	6.1	46	BEAAR
6/3/2001	41:57.0	-29.67	-178.63	178	7.1	47	BEAAR
6/14/2001	27:04.4	-22.05	-179.46	604	5.7	48	BEAAR
6/19/2001	32:24.0	-22.74	-67.88	147	6.1	49	BEAAR
6/26/2001	18:31.0	-17.75	-71.65	24	6.8	50	BEAAR
7/4/2001	06:31.0	-21.73	-176.71	185	6.5	51	BEAAR
7/5/2001	53:48.0	-16.09	-73.99	62	6.6	52	BEAAR
7/7/2001	38:43.0	-17.54	-72.08	33	7.6	53	BEAAR
7/24/2001	00:09.0	-19.45	-69.26	33	6.3	54	BEAAR
8/5/2001	16:16.0	12.22	93.35	96	6.0	55	BEAAR
1/4/2005	9:13:12.25	10.672	92.362	23.2	6	56	ARCTIC
2/19/2005	0:04:43.59	-5.562	122.129	10	6.3	57	ARCTIC
2/26/2005	12:56:52.62	2.908	95.592	36	6	58	ARCTIC
3/2/2005	10:42:12.23	-6.527	129.933	201.7	7	59	ARCTIC
3/29/2005	5:16:29.85	2.648	96.581	30	5.8	60	ARCTIC
3/30/2005	16:19:41.10	2.993	95.414	22	5.9	61	ARCTIC
3/30/2005	17:41:57.16	-22.459	-179.754	588.7	5.8	62	ARCTIC
4/10/2005	10:29:11.28	-1.644	99.607	19	6.4	63	ARCTIC
4/10/2005	17:24:39.40	-1.591	99.717	30	5.9	64	ARCTIC
4/11/2005	6:11:11.82	2.169	96.759	24	5.9	65	ARCTIC
4/11/2005	17:08:53.94	-21.975	170.612	68	6	66	ARCTIC
4/14/2005	11:29:52.55	-1.915	99.951	33.4	5.8	67	ARCTIC
4/16/2005	16:38:03.90	1.812	97.662	31	6	68	ARCTIC
4/28/2005	14:07:33.70	2.132	96.799	22	5.9	69	ARCTIC
5/10/2005	1:09:05.10	-6.226	103.139	17	5.9	70	ARCTIC
5/14/2005	5:05:18.48	0.587	98.459	34	6.4	71	ARCTIC
5/18/2005	11:37:41.74	5.439	93.357	2.5	6	72	ARCTIC
6/8/2005	6:28:10.92	2.17	96.724	23.5	5.8	73	ARCTIC
6/26/2005	8:23:03.87	1.769	125.825	91.6	6	74	ARCTIC
7/5/2005	1:52:02.95	1.819	97.082	21	6.2	75	ARCTIC
9/4/2005	23:58:34.89	3.004	123.073	443.9	5.8	76	ARCTIC
9/26/2005	1:55:37.67	-5.678	-76.398	115	6.7	77	ARCTIC
10/25/2005	19:40:43.04	-7.154	145.976	175.4	5.8	78	ARCTIC
11/19/2005	14:10:13.03	2.164	96.786	21	6	79	ARCTIC
1/2/2006	22:13:40.49	-19.926	-178.178	582.9	6.5	80	ARCTIC
1/15/2006	11:58:29.12	-7.826	122.597	264.8	6	81	ARCTIC
1/27/2006	16:58:53.67	-5.473	128.131	397	7	82	ARCTIC
2/2/2006	12:48:43.44	-17.747	-178.39	597.5	5.9	83	ARCTIC
2/24/2006	14:15:45.21	-17.995	-179.59	622.4	5.9	84	ARCTIC
2/26/2006	3:08:27.81	-23.607	-179.989	535.2	5.9	85	ARCTIC
4/25/2006	18:26:17.15	1.994	96.995	21	5.8	86	ARCTIC
5/3/2006	15:26:40.29	-20.187	-174.123	55	7.2	87	ARCTIC

Table 2-1 continued…

5/13/2006	3:11:42.94	5.512	94.437	45.6	5.9	88	ARCTIC
5/16/2006	10:39:23.34	-31.779	-179.313	151.6	6.8	89	ARCTIC
5/16/2006	15:28:25.92	0.093	97.05	12	6.6	90	ARCTIC
5/19/2006	14:44:24.90	-0.143	124.713	35	6	91	ARCTIC
5/26/2006	22:53:58.92	-7.961	110.446	12.5	6	92	ARCTIC
6/24/2006	21:15:00.92	-0.39	123.195	26	5.8	93	ARCTIC
7/15/2006	7:10:48.18	-4.451	126.165	367.8	5.8	94	ARCTIC
7/17/2006	8:19:28.75	-9.254	107.411	34	6.1	95	ARCTIC
7/17/2006	15:45:59.82	-9.42	108.319	21	5.9	96	ARCTIC
7/18/2006	3:27:50.38	-0.167	124.956	21.7	5.8	97	ARCTIC
7/23/2006	8:22:04.16	-0.336	123.286	28	5.8	98	ARCTIC
8/7/2006	22:18:54.02	-15.777	167.799	140.6	6	99	ARCTIC
8/11/2006	20:54:14.37	2.403	96.348	22	5.8	100	ARCTIC
8/15/2006	23:53:47.24	-21.189	-176.254	158	5.9	101	ARCTIC
1/31/2007	3:15:52.29	-29.776	-178.002	34	6.1	102	ARCTIC
3/6/2007	3:49:38.90	-0.493	100.498	19	5.9	103	ARCTIC
4/4/2007	11:00:27.44	-20.711	168.828	10	5.8	104	ARCTIC
5/5/2003	15:50:08.47	0.215	127.354	123.6	5.9	105	AEIC/AVO
9/5/2003	1:23:01.96	5.316	95.9	124.8	5.7	106	AEIC/AVO
6/30/2004	23:37:25.45	0.797	124.726	90.8	6	107	AEIC/AVO
7/25/2004	14:35:19.06	-2.427	103.981	582.1	6.8	108	AEIC/AVO
3/2/2005	10:42:12.23	-6.527	129.933	201.7	7	109	AEIC/AVO
3/19/2005	17:34:46.18	-21.893	-179.547	598.7	5.9	110	AEIC/AVO
3/30/2005	16:19:41.10	2.993	95.414	22	5.9	111	AEIC/AVO
4/3/2005	3:10:56.47	2.022	97.942	36	6	112	AEIC/AVO
4/10/2005	10:29:11.28	-1.644	99.607	19	6.4	113	AEIC/AVO
4/11/2005	17:08:53.94	-21.975	170.612	68	6	114	AEIC/AVO
4/16/2005	16:38:03.90	1.812	97.662	31	6	115	AEIC/AVO
4/28/2005	14:07:33.70	2.132	96.799	22	5.9	116	AEIC/AVO
5/10/2005	1:09:05.10	-6.226	103.139	17	5.9	117	AEIC/AVO
5/14/2005	5:05:18.48	0.587	98.459	34	6.4	118	AEIC/AVO
5/19/2005	1:54:52.85	1.989	97.041	30	6.2	119	AEIC/AVO
7/5/2005	1:52:02.95	1.819	97.082	21	6.2	120	AEIC/AVO
7/30/2005	15:13:20.12	5.177	94.476	38	5.8	121	AEIC/AVO
9/26/2005	1:55:37.67	-5.678	-76.398	115	6.7	122	AEIC/AVO
5/16/2006	10:39:23.34	-31.779	-179.313	151.6	6.8	123	AEIC/AVO
5/16/2006	15:28:25.92	0.093	97.05	12	6.6	124	AEIC/AVO
6/24/2006	21:15:00.92	-0.39	123.195	26	5.8	125	AEIC/AVO
7/17/2006	8:19:28.75	-9.254	107.411	34	6.1	126	AEIC/AVO
7/17/2006	15:45:59.82	-9.42	108.319	21	5.9	127	AEIC/AVO
7/23/2006	8:22:04.16	-0.336	123.286	28	5.8	128	AEIC/AVO
8/2/2006	14:45:04.63	-11.167	116.85	15	5.9	129	AEIC/AVO
8/11/2006	20:54:14.37	2.403	96.348	22	5.8	130	AEIC/AVO
9/16/2006	9:45:23.91	-3.08	129.441	17	5.9	131	AEIC/AVO
4/4/2007	11:00:27.44	-20.711	168.828	10	5.8	132	AEIC/AVO

Table 2-1 continued…

7/21/2007	15:34:52.60	-22.151	-65.777	289.5	5.8	133	AEIC/AVO
8/8/2007	17:05:04.92	-5.859	107.419	280	6.5	134	AEIC/AVO
9/13/2007	3:35:28.72	-2.13	99.627	22	6.3	135	AEIC/AVO
9/13/2007	16:09:16.39	-3.158	101.533	48.8	6.1	136	AEIC/AVO
9/14/2007	6:01:32.27	-4.075	101.169	23	5.9	137	AEIC/AVO
9/20/2007	8:31:14.49	-1.999	100.141	30	6.3	138	AEIC/AVO
10/5/2007	7:17:52.81	-25.189	179.459	509.4	6	139	AEIC/AVO
10/24/2007	21:02:50.48	-3.896	101.017	20	6.1	140	AEIC/AVO
12/9/2007	7:28:20.82	-25.996	-177.514	152.5	7	141	AEIC/AVO
12/15/2007	9:39:52.89	-6.613	131.094	50.7	6	142	AEIC/AVO
1/4/2008	7:29:18.30	-2.782	101.032	35	5.9	143	AEIC/AVO
2/25/2008	8:36:33.03	-2.486	99.972	25	6.4	144	AEIC/AVO
3/29/2008	17:30:50.15	2.855	95.296	20	5.8	145	AEIC/AVO
4/9/2008	12:46:12.72	-20.071	168.892	33	6.3	146	AEIC/AVO
8/26/2008	21:00:36.61	-7.641	-74.377	154	6	147	AEIC/AVO
9/10/2008	13:08:14.91	8.092	-38.718	10	6.3	148	AEIC/AVO
9/29/2008	15:19:31.59	-29.756	-177.683	36	6.5	149	AEIC/AVO
12/6/2008	10:55:27.09	-7.398	124.738	405.4	6.1	150	AEIC/AVO
12/11/2008	21:40:52.35	0.06	123.427	133.2	6.1	151	AEIC/AVO
1/19/2009	3:35:18.84	-22.596	170.911	12	5.7	152	AEIC/AVO
2/18/2009	21:53:45.16	-27.424	-176.33	25	6.8	153	AEIC/AVO
5/16/2009	0:53:52.74	-31.519	-178.792	54.6	6.1	154	AEIC/AVO
7/13/2009	10:52:20.22	-9.13	119.315	67.2	5.7	155	AEIC/AVO
9/2/2009	7:55:01.05	-7.782	107.297	46	6.8	156	AEIC/AVO
9/30/2009	10:16:09.25	-0.72	99.867	81	7.1	157	AEIC/AVO
10/24/2009	14:40:43.72	-6.133	130.385	130	6.7	158	AEIC/AVO
2/7/2010	22:28:20.60	-23.319	-179.877	544	5.6	159	AEIC/AVO
7/17/2006	15:45:59.82	-9.42	108.319	21	5.9	160	MOOS
8/11/2006	20:54:14.37	2.403	96.348	22	5.8	161	MOOS
12/22/2006	19:50:44.63	10.653	92.361	24	5.7	162	MOOS
7/1/2007	14:34:12.02	-5.929	130.564	134.6	5.8	163	MOOS
7/12/2007	5:23:49.34	-7.933	-74.379	152.1	5.9	164	MOOS
7/17/2007	9:39:27.81	-26.206	-177.744	10	5.7	165	MOOS
7/21/2007	13:27:04.41	-8.133	-71.272	644.9	6.2	166	MOOS
8/17/2007	2:16:30.64	-5.301	129.469	21.9	5.9	167	MOOS
9/12/2007	23:49:03.72	-2.625	100.841	35	6.6	168	MOOS
9/13/2007	16:09:16.39	-3.158	101.533	48.8	6.1	169	MOOS
9/19/2007	7:27:50.70	-2.746	100.892	35	5.7	170	MOOS
9/20/2007	8:31:14.49	-1.999	100.141	30	6.3	171	MOOS
10/2/2007	3:43:40.34	-4.237	101.221	31.7	5.7	172	MOOS
10/5/2007	7:17:52.81	-25.189	179.459	509.4	6	173	MOOS
10/13/2007	17:45:53.18	-21.23	169.195	37	5.8	174	MOOS
10/16/2007	21:05:43.27	-25.775	179.53	509.3	6.2	175	MOOS
11/19/2007	0:52:12.51	-21.185	-178.752	558.3	6.2	176	MOOS
11/25/2007	19:53:07.96	-8.225	118.453	35	6.2	177	MOOS

Table 2-1 continued…

12/15/2007	9:39:52.89	-6.613	131.094	50.7	6	178	MOOS
1/4/2008	7:29:18.30	-2.782	101.032	35	5.9	179	MOOS
2/24/2008	14:46:21.47	-2.405	99.931	22	6	180	MOOS
2/25/2008	8:36:33.03	-2.486	99.972	25	6.4	181	MOOS
2/25/2008	18:06:03.90	-2.332	99.891	25	6	182	MOOS
2/25/2008	21:02:18.42	-2.245	99.808	25	6.2	183	MOOS
4/9/2008	11:23:40.35	-20.185	168.905	35	5.7	184	MOOS
4/11/2008	17:45:05.64	-20.404	168.818	35	5.7	185	MOOS
8/4/2008	20:45:13.97	-5.916	130.195	173.9	6.1	186	MOOS
8/26/2008	3:07:29.50	-6.338	104.469	21.7	5.7	187	MOOS
10/5/2008	9:12:36.07	-30.184	-177.176	10	5.8	188	MOOS
12/6/2008	10:55:27.09	-7.398	124.738	405.4	6.1	189	MOOS
12/11/2008	21:40:52.35	0.06	123.427	133.2	6.1	190	MOOS
12/30/2008	19:49:52.61	-4.297	101.217	20	5.7	191	MOOS
4/15/2009	20:01:34.38	-3.117	100.469	20	6.1	192	MOOS
5/16/2009	0:53:52.74	-31.519	-178.792	54.6	6.1	193	MOOS
8/16/2009	7:38:21.70	-1.479	99.49	20	6.5	194	MOOS
8/16/2009	12:49:00.09	-1.448	99.433	21	6	195	MOOS

3. Results

The results from the MOOS and ARCTIC deployments are discussed below. In addition, individual measurements for each station are plotted in the appendices. The results from the ARCTIC network are presented in Appendix A, the results from the BEAAR network (Christensen and Abers, 2010) are in Appendix B, and the results from the MOOS network are in Appendix C.

3.1 MOOS

Shear wave splitting results from the MOOS network stations are listed in table 3-1 and plotted in figure 3.1. There are 173 individual splitting results. Splitting observations are plotted at the 100km projection of the individual ray paths, so back-azimuth behavior of the measurements can be observed. The 100km depth is chosen simply to separate the observations at each station and does not necessarily represent the anisotropic region. Due to the large number of observations, results are also plotted as back-azimuth averages in figure 3.2, and those results are presented in table 3-2. In addition, fast direction and delay times are plotted against back-azimuth in appendix C. In general, shear wave splitting measurements show fast directions parallel to Pacific plate motion. The northwest to southeast directions are very consistent throughout the network, and delay times range from .2 to 2 seconds. For most stations, fast directions are not dependent on the back-azimuth of the events.

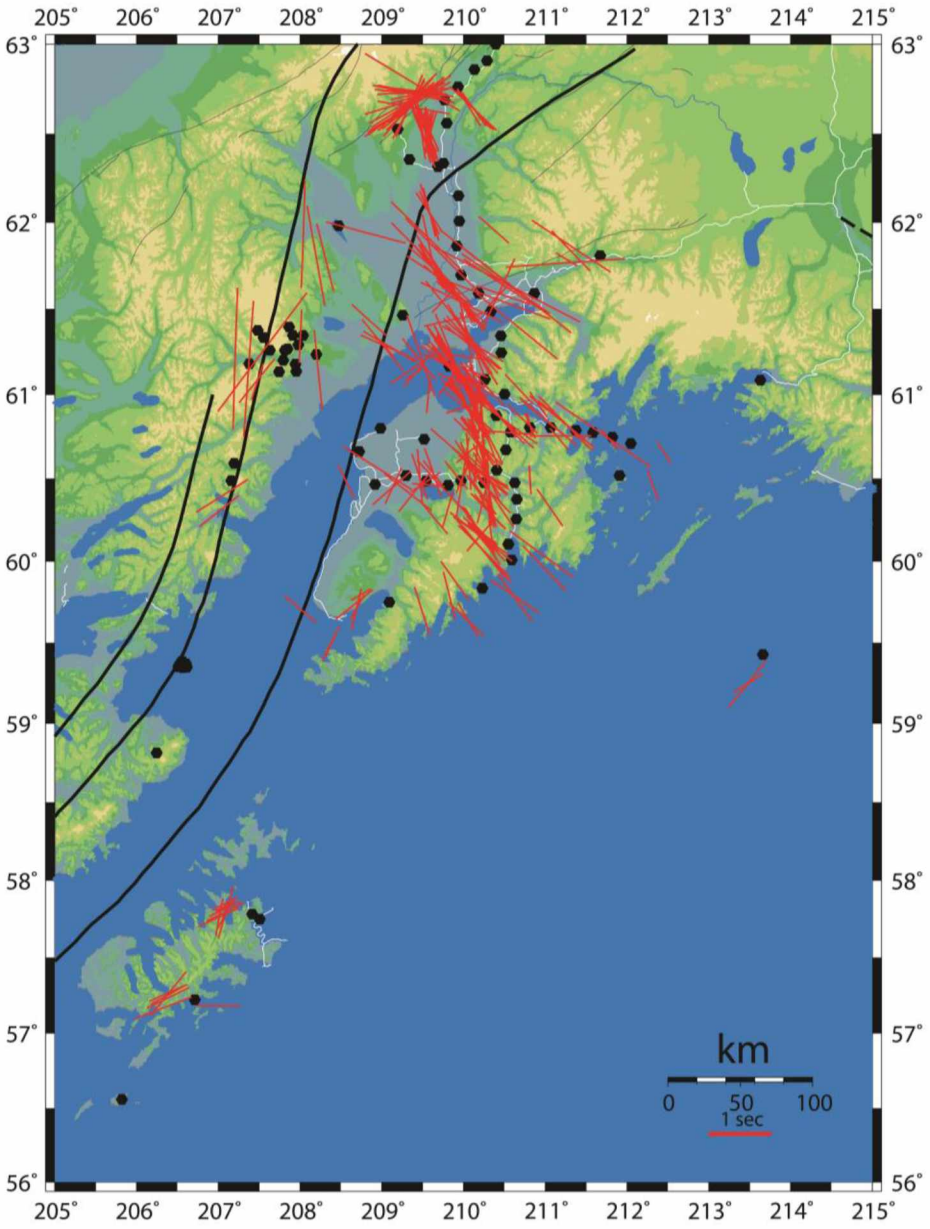

Figure 3.1: Results from the MOOS network.
Results from the MOOS network are plotted along with results from the permanent stations. Results are plotted as a vector oriented in the fast direction with a length proportional to the delay time. Individual results are plotted at the 100km projection of the ray. This is done to separate measurements by back-azimuth so any azimuthal dependence can be seen.

Permanent stations within the MOOS network and surrounding area were also included in the project, adding 107 additional individual measurements to the MOOS dataset (Bellesiles et al., 2009). These stations are permanent stations operated by AEIC (Alaska Earthquake Information Center), as well as stations from the AVO (Alaska Volcano Observatory) volcano monitoring network. These results are also in table 3-1 and plotted in figure 3.1 and for the remainder of the thesis will be discussed as part of the MOOS network.

Apart from the dominant fast direction normal to the trench, there are several stations that have a significantly different fast direction. The first group of stations are northern stations that sample the mantle wedge. The station at Byers Lake (BYR) is included in this group. This station shows two distinct fast directions with a strong dependence on back-azimuth. Rays approaching from the west transverse the mantle wedge, while rays approaching from the south and east transverse only the very thin nose of the mantle wedge. BYR was also a station in the BEAAR network (Christensen and Abers, 2010), and results for both networks are combined for this site. Other stations in this group are SKN, the Mt Spurr stations (SPCG, SPBG, and SPCR), and the Mt Redoubt stations (RDJH and RDWB). All of these stations lie above the mantle wedge and have fast directions that are subparallel to the contours of the subducting slab.

The second group of stations that have fast directions significantly different from the dominant trench-normal fast directions are located on western Kenai Peninsula, Kodiak Island and Middleton Island. The Kodiak Island stations (KDAK and OHAK) have a NE to SW fast direction which is, parallel to the strike of the trench. These

stations are located south of the 50km subducting slab contour in a region of the subduction zone with no mantle wedge. Middleton Island (MID) is located in the Gulf of Alaska, offshore from Price William Sound, significantly closer to the trench. This station also has fast directions that are parallel to the trench. The western Kenai stations (BRLK, CNP and HOM) all have fast directions parallel to the trench as well.

Unfortunately, the MOOS network has a limited back-azimuth coverage (100-300 degrees) with a majority of events coming from the west. This limits analysis of dipping and multiple anisotropic layers. There are two areas of low data return: Cook Inlet and Prince William Sound.

Stations located in the Prince William Sound region (WHIT, PERI, PORT, MAIN, BLAK) display low data return. This could be ocean noise related to the stations being located on small islands and close to the shore. Cook Inlet is a large sedimentary basin northwest of the Kenai Peninsula. The basin is part of a northeast trending collisional forearc and is bounded on the west and north by volcanic and plutonic rocks, on the east and south by the Chugach and Kenai mountains and is part of the accretion prism of the subduction zone (Hartz et al., 2009). The stations COOK, MPEN, NSKI, BING, and SOLD are located within Cook Inlet basin, and there are only 5 individual results for this region (table 3-1). This is possibly due to the effect the basin has on the waves coming into the station and most likely does not reflect a lack of splitting.

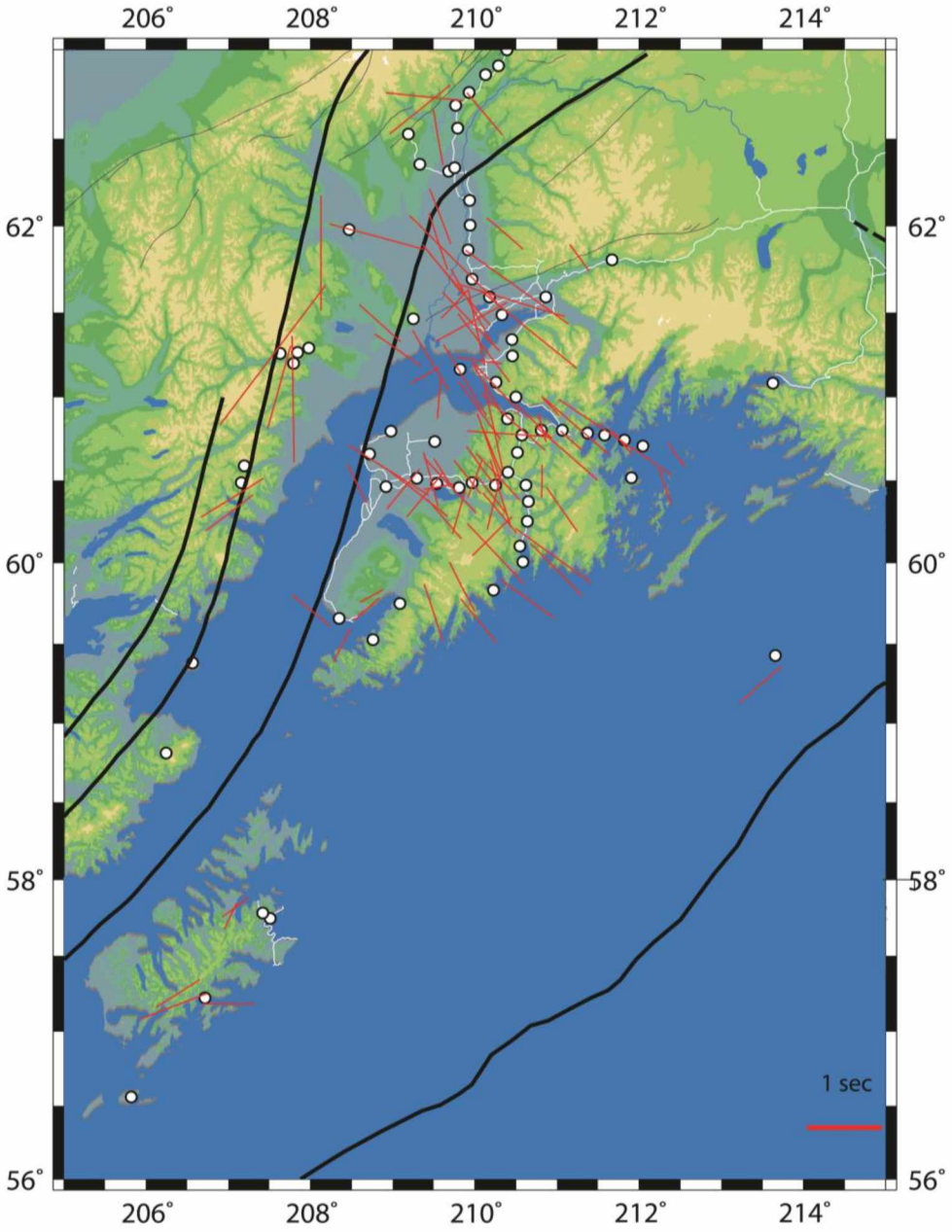

Figure 3.2: Back-azimuth average results from the MOOS network.
Results from the MOOS network and permanent stations, plotted as back-azimuth averages. Results are plotted as a vector oriented in the fast direction with a length proportional to the delay time. Individual results are plotted at the 100km projection of the ray. This is done to separate measurements by back-azimuth so any azimuthal dependence can be seen.

In addition to these two major low data return locations, there were also volcano stations. Volcanoes can be noisy, and while there was limited recovery on Mt Redoubt

and Mt Spurr, the stations on Mt St Augustine yielded no results. Mt St Augustine is also located on an island in the Cook Inlet.

3.2 ARCTIC

Results from the shear wave splitting observations of the ARCTIC network are listed in table 3-1 and plotted in figure 3.3. There are 205 individual measurements. In general, fast directions are consistently NE/SW, rotating to NNE/SSW in the far northern stations. The transition between these can be seen in figure 3.3 at the south end of the Brooks Range. Station CHS, located at Atigun Pass, shows fast directions that deviate from this trend. Over a ten degree back-azimuth range (284 to 294 degrees), there are eight results with a fast direction that is WNW to ESE (around -70). At this time there is not enough information to determine the cause of this anomalous fast direction.

Results from the westward line (RBY, GTM, and NOM) are shown for completeness. The stations RBY and GTM have the same general result as the rest of the N/S line. NOM shows a N/S fast direction, which does not fit the general trend and is probably related to extensional tectonics that are well known in the Seward Peninsula. The delay times range from .5 to 1.5 seconds. Average results for each station can be seen in figure 3.4, and delay time vs. back-azimuth plots and fast direction vs back-azimuth plots can be seen in Appendix A.

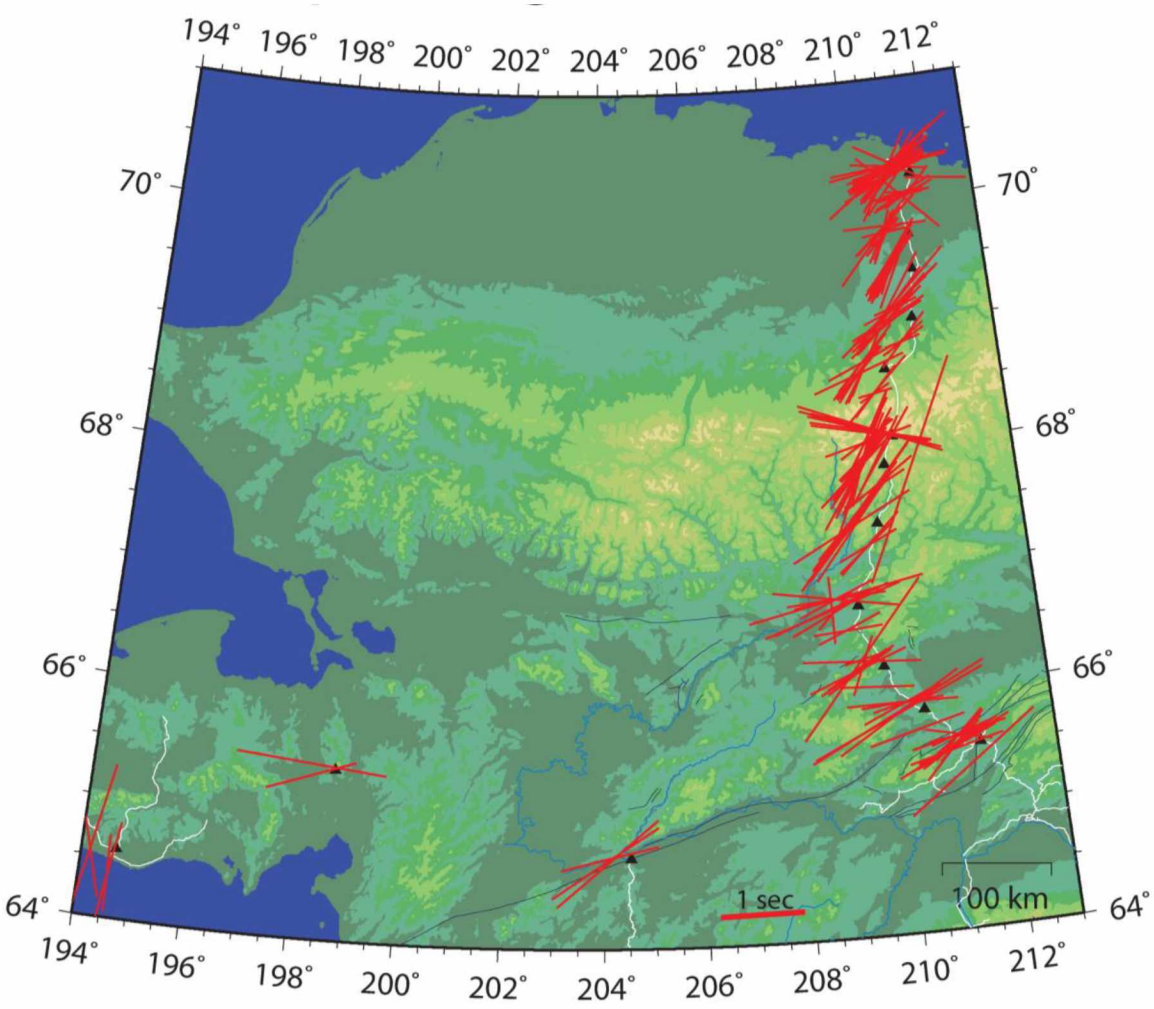

Figure 3.3: Results from the ARCTIC network.
Results from the ARCTIC network. Results are plotted as a vector oriented in the fast direction with a length proportional to the delay time. Individual results are plotted at the 100km projection of the ray. This is done to separate measurements by back-azimuth so any azimuthal dependence can be seen.

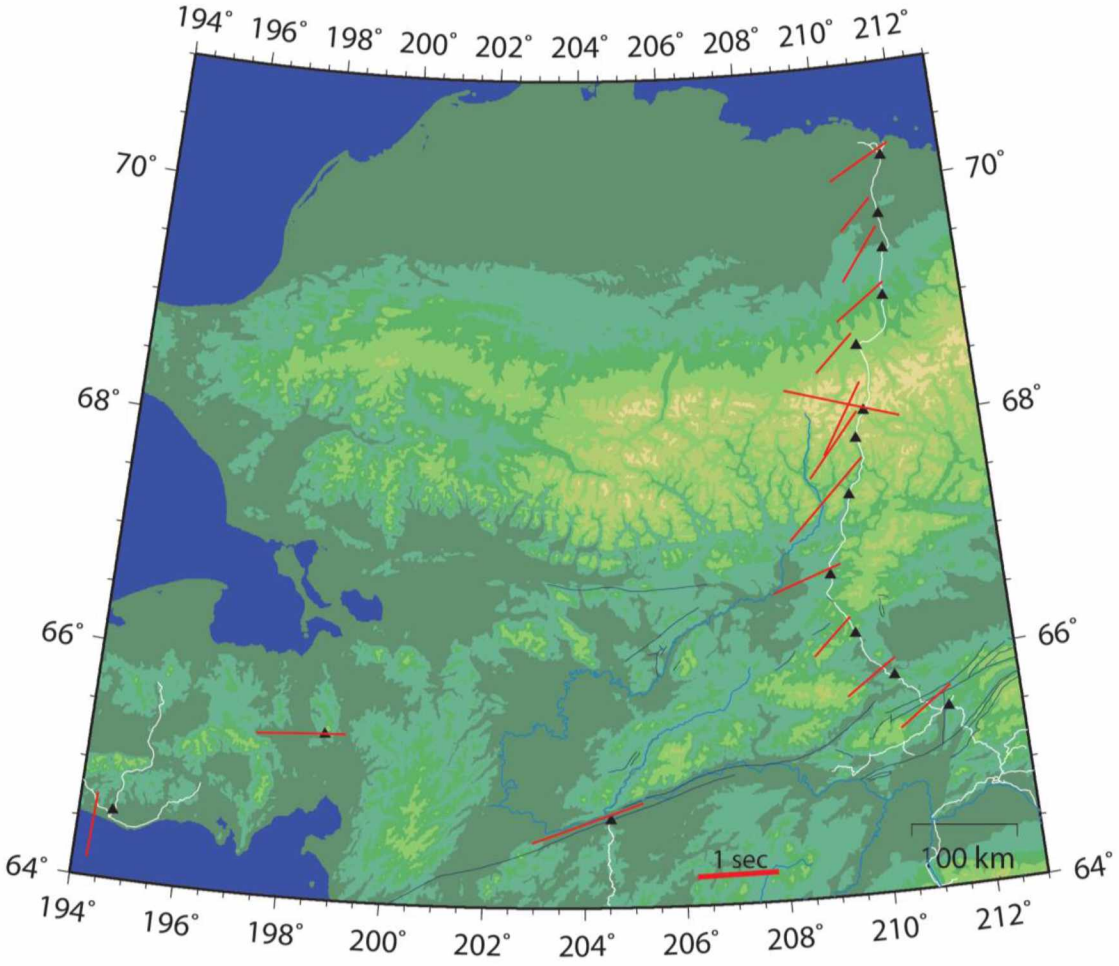

Figure 3.4: Results from the ARCTIC network plotted as back-azimuth averages.
The average splitting measurements for each back-azimuth for each station in the ARCTIC network. Results are plotted as a vector oriented in the fast direction with a length proportional to the delay time. Individual results are plotted at the 100km projection of the ray. This is done to separate measurements by back-azimuth so any azimuthal dependence can be seen.

Table 3-1: Results from all stations.
The ARCTIC results (Litherland et al., 2007 and this thesis), MOOS results (this thesis) and BEAAR results (Christensen and Abers, 2010) are listed. Event numbers are from table 2-1.

Station Name	Back Azimuth (degrees)	Distance (degrees)	Fast Direction (degrees)	Error (degrees)	Delay Time (seconds)	Error (seconds)	Event	Network
BMQ	293	97	46	36/103	0.76	0.29/1.73	73	ARCTIC
BMQ	265	86	49	38/60	1.26	1.08/1.45	74	ARCTIC
BMQ	292	97	40	36/46	1.14	0.79/1.51	75	ARCTIC
BMQ	268	86	46	30/63	0.98	0.74/1.24	76	ARCTIC
BMQ	107	89	25	23/27	2.84	2.32/3.45	77	ARCTIC
BMQ	265	96	33	19/48	1.32	0.98/1.57	81	ARCTIC
BMQ	261	92	19	5/56	0.74	0.39/1.43	82	ARCTIC
BMQ	208	88	63	54/71	0.84	0.72/0.98	84	ARCTIC
BMQ	292	97	41	37/45	1.16	0.91/1.47	86	ARCTIC
BMQ	205	102	56	45/74	1.06	0.74/1.42	89	ARCTIC
BMQ	292	98	40	31/58	0.70	0.35/1.37	90	ARCTIC
BMQ	266	88	34	23/45	1.64	1.3/1.99	91	ARCTIC
BMQ	276	101	24	17/32	1.84	1.31/2.34	92	ARCTIC
BMQ	267	89	40	32/49	1.16	0.96/1.34	93	ARCTIC
BMQ	263	92	33	23/43	1.12	0.94/1.32	94	ARCTIC
BMQ	277	103	27	23/31	1.30	1.02/1.59	95	ARCTIC
BMQ	267	89	44	30/58	0.98	0.76/1.2	97	ARCTIC
BMQ	293	97	50	42/66	0.76	0.48/1.17	99	ARCTIC
CBM	292	97	77	31/98	0.42	0.31/1.2	75	ARCTIC
CBM	268	86	60	42/73	0.86	0.66/1.09	76	ARCTIC
CBM	292	97	40	27/53	2.36	1.78/2.95	79	ARCTIC
CBM	264	96	59	29/77	0.64	0.39/0.96	81	ARCTIC
CBM	205	100	-86	-117/-73	0.88	0.48/1.4	89	ARCTIC
CBM	265	88	69	56/77	1.26	0.81/1.68	91	ARCTIC
CBM	262	91	59	50/68	0.92	0.74/1.13	94	ARCTIC
CBM	277	103	22	14/44	0.74	0.37/1.22	95	ARCTIC
CBM	265	86	60	47/70	1.04	0.81/1.25	96	ARCTIC
CBM	288	98	-86	-104/-74	1.40	0.8/1.99	102	ARCTIC
CHS	259	92	27	10/51	0.82	0.63/1.03	59	ARCTIC
CHS	293	96	-72	-91/-60	1.42	0.66/2.22	60	ARCTIC
CHS	294	96	-67	-70/-66	1.80	1.51/2.01	61	ARCTIC
CHS	289	99	-71	-74/-69	1.54	1.23/1.83	63	ARCTIC
CHS	217	94	35	29/40	1.34	1.01/1.66	67	ARCTIC
CHS	288	99	-76	-86/-68	1.46	0.86/1.87	67	ARCTIC
CHS	292	97	-69	-74/-64	1.44	1.07/1.8	68	ARCTIC
CHS	284	102	-77	-81/-74	1.44	1.08/1.79	70	ARCTIC
CHS	291	98	-70	-75/-66	1.36	0.94/1.76	71	ARCTIC
CHS	266	86	32	14/62	1.12	0.85/1.44	74	ARCTIC
CHS	292	97	-70	-74/-68	1.74	1.36/2.04	75	ARCTIC
CHS	269	86	29	18/44	1.24	0.91/1.56	76	ARCTIC

Table 3-1 continued…

CHS	267	89	58	36/73	0.78	0.63/0.99	93	ARCTIC
CHS	263	92	76	32/89	1.08	0.61/1.47	94	ARCTIC
CHS	221	89	32	24/38	1.08	0.9/1.25	98	ARCTIC
FRB	294	96	49	44/56	0.94	0.7/1.19	73	ARCTIC
FRB	293	97	42	35/49	1.74	1.31/2.21	75	ARCTIC
FRB	294	96	90	53/111	0.98	0.59/1.58	79	ARCTIC
FRB	266	97	30	17/58	0.60	0.4/0.87	81	ARCTIC
FRB	267	89	20	9/42	0.66	0.37/1	91	ARCTIC
FRB	277	101	49	34/75	0.46	0.32/0.67	92	ARCTIC
FRB	268	90	43	27/63	0.58	0.47/0.76	93	ARCTIC
FRB	264	92	24	14/37	0.64	0.51/0.78	94	ARCTIC
FRB	280	103	70	35/91	0.44	0.31/0.76	95	ARCTIC
FRB	279	103	84	62/96	0.58	0.42/0.83	95	ARCTIC
FRB	268	90	30	18/50	0.70	0.41/1.08	97	ARCTIC
FRB	222	91	37	32/40	0.96	0.72/1.17	98	ARCTIC
FRB	294	96	50	43/60	1.00	0.67/1.45	99	ARCTIC
GBN	292	97	86	69/99	1.18	0.87/1.67	73	ARCTIC
GBN	291	97	-80	-87/-75	1.52	1.18/1.87	75	ARCTIC
GBN	268	86	70	60/79	1.48	1.05/1.89	76	ARCTIC
GBN	292	97	79	66/91	2.14	1.59/2.75	79	ARCTIC
GBN	264	96	45	10/68	0.60	0.37/0.9	81	ARCTIC
GBN	260	92	64	47/72	1.14	0.54/1.95	82	ARCTIC
GBN	207	87	86	81/91	0.82	0.74/0.88	84	ARCTIC
GBN	207	93	67	51/83	0.82	0.66/0.96	85	ARCTIC
GBN	291	97	67	58/78	0.96	0.85/1.08	86	ARCTIC
GBN	265	88	72	60/79	1.72	0.94/2.3	91	ARCTIC
GBN	265	86	-1	-16/32	0.80	0.52/1.17	96	ARCTIC
GBN	292	97	81	69/91	1.02	0.85/1.25	99	ARCTIC
GTM	254	91	71	46/97	1.10	0.9/1.3	81	ARCTIC
GTM	281	93	-84	-91/-79	1.80	1.21/2.42	86	ARCTIC
ICT	266	87	47	34/60	1.02	0.83/1.22	74	ARCTIC
ICT	293	97	53	44/72	1.18	0.72/1.76	75	ARCTIC
ICT	269	87	64	39/86	0.92	0.59/1.4	76	ARCTIC
ICT	294	97	52	43/67	1.58	0.92/2.3	79	ARCTIC
ICT	207	91	60	43/102	0.58	0.33/0.89	80	ARCTIC
ICT	266	97	63	42/79	0.92	0.6/1.19	81	ARCTIC
ICT	262	93	58	34/74	1.08	0.73/1.7	82	ARCTIC
ICT	209	90	75	62/89	0.44	0.37/0.51	84	ARCTIC
ICT	208	95	43	31/60	0.82	0.55/1.04	85	ARCTIC
ICT	293	97	52	45/61	1.50	1.11/1.96	86	ARCTIC
ICT	297	94	72	52/122	0.38	0.16/0.69	88	ARCTIC
ICT	206	103	54	42/71	0.56	0.42/0.81	89	ARCTIC
ICT	293	98	68	45/104	0.70	0.45/1.26	90	ARCTIC
ICT	267	89	50	36/64	1.18	0.95/1.44	91	ARCTIC
ICT	268	90	47	31/64	0.92	0.67/1.19	93	ARCTIC

Table 3-1 continued…

ICT	289	98	49	38/64	1.24	0.75/2.08	102	ARCTIC
LMW	295	98	73	51/97	0.70	0.5/1.02	58	ARCTIC
LMW	260	92	77	69/84	1.16	0.95/1.37	59	ARCTIC
LMW	295	98	-76	-108/-61	0.80	0.52/1.36	61	ARCTIC
LMW	289	100	88	48/114	0.50	0.32/1.25	63	ARCTIC
LMW	293	98	55	39/106	0.68	0.34/1.19	68	ARCTIC
LMW	293	98	78	61/94	1.16	0.88/1.43	69	ARCTIC
LMW	293	98	48	39/66	0.80	0.57/1.06	75	ARCTIC
LMW	270	87	63	51/73	1.20	0.98/1.42	76	ARCTIC
LMW	293	98	47	38/65	0.82	0.5/1.21	86	ARCTIC
LMW	206	100	55	51/60	1.92	1.7/2.15	89	ARCTIC
LMW	292	100	83	56/100	0.72	0.52/1.16	90	ARCTIC
LMW	267	89	44	25/62	1.06	0.83/1.28	91	ARCTIC
LMW	268	90	68	39/90	0.98	0.56/1.52	93	ARCTIC
LMW	264	92	66	56/74	1.08	0.89/1.29	94	ARCTIC
LMW	278	104	49	34/70	0.66	0.51/0.87	95	ARCTIC
LMW	267	87	65	56/74	1.50	1.29/1.7	96	ARCTIC
LMW	268	90	59	47/70	0.94	0.75/1.12	97	ARCTIC
LMW	294	98	52	37/86	0.68	0.45/1.15	99	ARCTIC
NOM	278	91	10	1/20	1.92	1.04/2.88	79	ARCTIC
NOM	251	89	-16	-30/8	1.04	0.45/1.36	81	ARCTIC
NOM	193	89	-2	-39/18	0.92	0.56/1.28	85	ARCTIC
NOM	192	97	8	0/13	1.18	0.59/1.76	89	ARCTIC
PRB	301	89	-59	-90/-45	0.88	0.53/1.33	56	ARCTIC
PRB	268	95	55	34/80	0.72	0.53/1.06	57	ARCTIC
PRB	260	93	46	35/56	0.62	0.53/0.73	59	ARCTIC
PRB	294	96	54	46/67	1.86	1.12/2.45	60	ARCTIC
PRB	296	96	53	49/59	1.38	1.13/1.64	61	ARCTIC
PRB	209	95	84	59/109	0.68	0.49/0.92	62	ARCTIC
PRB	290	99	73	65/81	0.92	0.82/1.01	63	ARCTIC
PRB	290	99	70	62/81	0.92	0.82/1.04	64	ARCTIC
PRB	294	96	68	54/86	0.94	0.74/1.24	65	ARCTIC
PRB	218	96	-83	-126/-59	0.30	0.2/0.67	66	ARCTIC
PRB	290	99	77	57/101	0.90	0.69/1.12	67	ARCTIC
PRB	293	96	58	45/77	0.82	0.61/1.11	68	ARCTIC
PRB	294	96	62	51/79	1.02	0.8/1.33	69	ARCTIC
PRB	285	102	77	62/90	1.06	0.92/1.22	70	ARCTIC
PRB	292	97	-81	-112/-62	0.90	0.68/1.37	71	ARCTIC
PRB	298	94	62	51/76	1.14	0.81/1.5	72	ARCTIC
PRB	294	96	62	55/70	1.12	0.97/1.31	73	ARCTIC
PRB	267	87	70	45/85	0.90	0.63/1.22	74	ARCTIC
PRB	294	96	54	48/61	1.14	0.96/1.39	75	ARCTIC
PRB	270	87	30	13/49	1.18	0.82/1.57	76	ARCTIC
PRB	109	89	-82	-125/-70	0.72	0.46/1.22	77	ARCTIC
PRB	245	89	41	11/63	0.84	0.46/1.26	78	ARCTIC

Table 3-1 continued…

PRB	294	96	85	62/107	1.38	1.16/1.64	79	ARCTIC
PRB	208	92	56	40/97	0.48	0.23/0.98	80	ARCTIC
PRB	266	97	50	42/59	0.90	0.82/1	81	ARCTIC
PRB	262	93	67	50/77	1.12	0.78/1.55	82	ARCTIC
PRB	208	90	81	71/91	0.62	0.54/0.68	83	ARCTIC
PRB	209	91	84	73/93	0.52	0.45/0.58	84	ARCTIC
PRB	209	96	78	49/110	0.40	0.24/0.64	85	ARCTIC
PRB	294	96	60	53/71	1.04	0.83/1.27	86	ARCTIC
PRB	204	92	67	53/86	0.78	0.62/1.07	87	ARCTIC
PRB	207	104	82	52/109	0.48	0.33/0.79	89	ARCTIC
PRB	293	98	82	62/98	1.44	1.12/1.86	90	ARCTIC
PRB	267	89	45	16/74	0.78	0.55/1.39	91	ARCTIC
PRB	278	101	38	27/53	1.12	0.78/1.44	92	ARCTIC
PRB	268	90	65	47/80	0.82	0.6/1.07	93	ARCTIC
PRB	264	93	55	47/63	0.82	0.72/0.93	94	ARCTIC
PRB	280	103	55	32/93	0.70	0.47/1.44	95	ARCTIC
PRB	279	103	73	61/83	0.94	0.8/1.15	95	ARCTIC
PRB	206	102	64	46/99	0.74	0.56/1.15	101	ARCTIC
PRB	220	96	-44	-54/-36	1.28	0.75/1.7	103	ARCTIC
RBY	259	94	50	26/73	1.58	0.95/1.88	81	ARCTIC
RBY	262	87	57	49/63	1.52	1.34/1.71	93	ARCTIC
RBY	272	101	77	66/83	1.20	0.87/1.53	95	ARCTIC
SAG	294	96	42	35/61	0.76	0.3/1.3	73	ARCTIC
SAG	266	87	36	19/55	0.76	0.53/0.98	74	ARCTIC
SAG	293	97	38	35/44	0.92	0.59/1.29	75	ARCTIC
SAG	269	87	38	26/53	0.74	0.55/0.97	76	ARCTIC
SAG	244	88	26	-11/54	0.66	0.44/0.89	78	ARCTIC
SAG	266	97	33	19/50	0.64	0.48/0.82	81	ARCTIC
SAG	262	93	24	4/64	0.50	0.29/1.02	82	ARCTIC
SAG	209	90	43	40/47	0.72	0.55/0.84	84	ARCTIC
SAG	294	96	43	37/53	0.88	0.52/1.36	86	ARCTIC
SAG	297	94	39	31/47	1.02	0.86/1.14	88	ARCTIC
SAG	277	101	40	16/76	0.94	0.61/1.4	92	ARCTIC
SAG	268	90	31	19/48	0.72	0.49/1.04	93	ARCTIC
SAG	264	92	32	27/37	0.64	0.57/0.72	94	ARCTIC
SAG	268	90	32	20/45	0.82	0.6/1.06	97	ARCTIC
SAG	222	90	34	32/36	0.98	0.89/1.08	98	ARCTIC
SAG	206	93	47	40/53	1.38	1.05/1.65	100	ARCTIC
TFS	292	97	45	37/59	0.88	0.54/1.31	75	ARCTIC
TFS	269	86	44	26/62	0.80	0.57/1.02	76	ARCTIC
TFS	293	96	67	40/96	0.90	0.46/1.48	79	ARCTIC
TFS	207	91	80	51/117	0.42	0.2/0.7	80	ARCTIC
TFS	265	96	28	-1/52	0.58	0.42/0.85	81	ARCTIC
TFS	208	89	61	54/69	0.42	0.35/0.47	84	ARCTIC
TFS	208	95	43	33/59	0.78	0.46/1.07	85	ARCTIC

Table 3-1 continued…

TFS	293	97	43	36/53	1.12	0.74/1.57	86	ARCTIC
TFS	206	103	46	41/52	1.04	0.78/1.32	89	ARCTIC
TFS	266	89	71	38/83	1.16	0.67/1.76	91	ARCTIC
TFS	267	89	44	24/62	0.82	0.58/1.1	93	ARCTIC
TFS	263	92	32	24/40	0.78	0.69/0.88	94	ARCTIC
TFS	279	103	29	20/47	0.90	0.51/1.38	95	ARCTIC
TFS	278	103	45	33/59	0.68	0.54/0.88	95	ARCTIC
TFS	266	86	39	22/60	0.82	0.61/1.07	96	ARCTIC
TFS	267	89	41	19/62	0.74	0.45/1.03	97	ARCTIC
WSM	292	97	41	36/46	1.76	1.39/2.16	73	ARCTIC
WSM	265	86	42	11/67	1.58	1.07/2.08	74	ARCTIC
WSM	292	97	43	38/50	1.64	1.3/1.95	75	ARCTIC
WSM	268	86	42	25/59	1.42	1.11/1.73	76	ARCTIC
WSM	292	97	41	34/49	2.18	1.71/2.63	79	ARCTIC
WSM	208	88	51	46/58	0.88	0.68/1.07	84	ARCTIC
WSM	207	93	65	51/85	0.78	0.49/1.11	85	ARCTIC
WSM	292	97	45	40/53	1.34	1.03/1.64	86	ARCTIC
WSM	205	101	47	39/63	1.00	0.6/1.46	89	ARCTIC
WSM	291	99	41	35/50	2.14	1.41/2.77	90	ARCTIC
WSM	263	92	39	22/57	1.52	1.24/1.75	94	ARCTIC
WSM	267	89	63	49/74	1.62	1.21/2.11	97	ARCTIC
WSM	293	97	43	38/49	1.62	1.22/2.02	99	ARCTIC
YRT	292	98	87	78/93	0.98	0.73/1.22	75	ARCTIC
YRT	269	86	64	58/71	2.36	2.07/2.62	76	ARCTIC
YRT	292	98	-89	-100/-81	1.32	0.87/1.84	86	ARCTIC
YRT	205	100	76	64/87	1.18	0.96/1.44	89	ARCTIC
YRT	292	99	77	59/89	0.74	0.56/0.97	90	ARCTIC
YRT	266	88	66	59/73	2.26	1.75/2.69	91	ARCTIC
YRT	267	89	59	54/65	1.72	1.44/2.02	97	ARCTIC
YRT	288	99	67	35/87	1.02	0.6/1.45	102	ARCTIC
BERG	263	93	26	18/36	0.7	0.5/0.9	157	AEIC
BRLK	285	100	60	23/86	0.35	0.22/0.67	156	AEIC
BRLK	257	90	14	5/26	0.68	0.47/0.92	157	AEIC
BRLK	105	90	-18	-43/1	0.8	0.57/1.11	146	AEIC
BRLK	261	94	29	6/72	0.45	0.22/0.7	149	AEIC
BRLK	266	88	52	39/65	0.75	0.53/0.99	150	AEIC
CNP	265	98	25	9/44	0.52	0.36/0.7	154	AEIC
CNP	257	90	27	9/58	0.52	0.34/0.8	157	AEIC
FIB	258	91	56	41/71	0.4	0.34/0.47	108	AEIC
FIB	216	89	5	-27/31	0.56	0.3/0.93	113	AEIC
FIB	290	101	-19	-35/-2	1.35	1.06/1.66	123	AEIC
FIB	258	90	39	20/68	0.54	0.36/0.82	157	AEIC
FIB	283	100	-39	-50/-26	0.85	0.69/0.99	107	AEIC
FIB	266	87	56	45/67	0.85	0.68/1.07	106	AEIC

Table 3-1 continued…

HOM	286	100	-50	-64/-33	0.66	0.47/0.87	156	AEIC
KDAK	264	97	24	5/54	0.35	0.2/0.65	154	AEIC
KDAK	274	102	64	53/71	0.65	0.54/0.76	155	AEIC
KDAK	285	100	60	23/86	0.35	0.22/0.67	156	AEIC
KDAK	287	99	64	29/86	0.35	0.2/0.54	117	AEIC
KDAK	265	87	11	-2/33	0.6	0.33/0.99	124	AEIC
KDAK	273	103	16	9/29	0.85	0.47/1.34	126	AEIC
KDAK	280	99	64	45/77	0.55	0.42/0.68	107	AEIC
KDAK	264	85	66	39/76	0.7	0.38/1.05	106	AEIC
KDAK	291	97	62	26/99	0.45	0.32/0.61	105	AEIC
MID	207	93	58	36/91	0.55	0.29/0.9	148	AEIC
MID	208	89	39	31/52	0.95	0.5/1.38	140	AEIC
OHAK	283	101	39	28/54	0.9	0.73/1.06	143	AEIC
OHAK	274	102	64	56/71	0.74	0.64/0.83	155	AEIC
OHAK	284	100	66	48/85	0.66	0.54/0.82	156	AEIC
OHAK	255	88	69	59/75	0.96	0.53/1.31	157	AEIC
OHAK	104	107	90	65/101	0.7	0.32/1.18	132	AEIC
OHAK	281	102	61	43/79	0.65	0.54/0.81	136	AEIC
PMR	208	87	-51	-58/-44	1.65	1.37/1.93	109	AEIC
PMR	267	99	-71	-84/-63	0.9	0.65/1.8	154	AEIC
PMR	288	101	-56	-60/-51	1.7	1.44/1.95	112	AEIC
PMR	264	87	44	22/76	0.4	0.22/0.64	104	AEIC
PMR	291	101	-52	-60/-40	1.85	1.18/2.68	123	AEIC
PMR	268	89	25	17/34	1.25	0.95/1.56	127	AEIC
PMR	292	99	-52	-57/-48	2.65	2.19/3.15	119	AEIC
PMR	284	100	-57	-62/-53	1.55	1.33/1.72	107	AEIC
PMR	288	102	-63	-72/-55	2.65	2.06/3.29	134	AEIC
PMR	258	91	-70	-81/-60	1.7	1.48/1.91	141	AEIC
RC01	286	102	-61	-76/-44	1.05	0.9/1.26	142	AEIC
RC01	293	99	-36	-43/-28	1.6	1.37/1.8	144	AEIC
RC01	218	88	71	54/103	0.55	0.29/0.97	131	AEIC
RC01	293	99	-22	-36/-7	1.8	1.49/2.14	110	AEIC
RC01	291	99	-27	-38/-17	1.15	0.99/1.29	111	AEIC
RC01	287	101	-49	-56/-40	1.3	1.13/1.46	112	AEIC
RC01	264	86	39	28/52	0.5	0.4/0.61	104	AEIC
RC01	291	99	-36	-46/-25	1.4	1.19/1.6	114	AEIC
RC01	291	101	-29	-40/-19	1.25	1.03/1.42	123	AEIC
RC01	292	99	-28	-39/-17	1.5	1.25/1.73	115	AEIC
RC01	290	100	-37	-46/-29	1.15	1.01/1.34	117	AEIC
RC01	292	99	-30	-37/-22	1.2	1.04/1.34	118	AEIC
RC01	277	104	-41	-55/-28	1.05	0.78/1.27	125	AEIC
RC01	276	104	-40	-54/-27	0.95	0.73/1.19	126	AEIC
RC01	268	101	-70	-92/-43	0.6	0.4/0.8	128	AEIC
RC01	278	101	-42	-54/-30	0.75	0.57/0.98	133	AEIC
RC01	292	99	-36	-45/-27	1.55	1.34/1.79	129	AEIC

Table 3-1 continued…

RC01	283	100	-42	-48/-36	1.1	1.01/1.15	107	AEIC
RC01	295	98	-29	-45/-17	1.45	1.26/1.62	120	AEIC
RC01	266	87	34	20/48	0.45	0.37/0.62	106	AEIC
RC01	294	97	-71	-86/-9	1.1	0.98/1.44	105	AEIC
RC01	287	102	-31	-43/-19	1.25	1.05/1.5	134	AEIC
RC01	285	102	-54	-64/-42	0.95	0.89/1.01	135	AEIC
RC01	285	103	-42	-54/-29	1.3	1.08/1.51	136	AEIC
RC01	287	101	-55	-70/-39	1.4	1.19/1.62	137	AEIC
RC01	106	90	-43	-57/-18	0.65	0.44/1	146	AEIC
RC01	208	90	-34	-45/-24	1.1	0.93/1.32	138	AEIC
RC01	285	103	-31	-44/-17	0.95	0.78/1.17	139	AEIC
RDJH	201	90	58	38/73	0.98	0.71/1.34	152	AVO
RDWB	202	94	52	43/66	0.8	0.46/1.16	153	AVO
SAW	288	102	-57	-61/-50	1.5	0.95/1.96	143	AEIC
SAW	279	104	-44	-57/-27	0.88	0.67/1.1	155	AEIC
SAW	259	91	86	77/97	1.9	1.73/2.07	141	AEIC
SAW	264	95	-59	-81/-26	0.4	0.23/0.72	149	AEIC
SKN	217	88	-10	-20/2	1.6	1.25/1.97	145	AEIC
SKN	104	108	-75	-79/-71	1.3	0.83/1.71	132	AEIC
SKN	203	94	-14	-35/11	1.1	0.82/1.47	148	AEIC
SKN	256	90	2	-7/10	1.7	1.46/1.96	141	AEIC
SPBG	256	90	2	-4/8	2.25	2.1/2.36	108	AVO
SPBG	203	96	39	26/53	0.9	0.67/1.12	122	AVO
SPBG	65	94	3	-22/30	0.85	0.53/1.21	147	AVO
SPBG	202	93	18	4/56	0.6	0.22/1.2	148	AVO
SPCG	258	87	37	28/46	2.35	2.02/2.68	130	AVO
SPCR	256	90	4	-4/12	2.15	2.02/2.31	108	AVO
SPCR	105	88	-6	-16/0	1.25	0.78/1.86	121	AVO
SSN	207	88	-39	-54/13	0.36	0.13/0.77	158	AEIC
SSN	214	90	-39	-58/12	1.04	0.6/1.62	151	AEIC
SSN	203	91	-66	-73/-53	1	0.56/1.48	152	AEIC
SSN	203	94	-60	-65/-52	0.95	0.7/1.17	148	AEIC
SSN	262	94	-48	-61/-34	0.75	0.45/0.97	149	AEIC
SWD	287	102	-33	-51/-23	0.8	0.6/1.06	143	AEIC
SWD	294	100	-39	-50/-28	1.2	1.02/1.38	144	AEIC
SWD	291	101	-59	-88/-9	0.55	0.22/2.29	123	AEIC
SWD	292	100	-37	-55/-17	0.7	0.59/0.9	115	AEIC
SWD	288	101	41	28/54	0.66	0.58/0.75	156	AEIC
SWD	282	104	-42	-60/-28	0.65	0.54/0.96	116	AEIC
SWD	290	100	-45	-57/-32	0.6	0.49/0.7	117	AEIC
SWD	291	100	-32	-48/-19	0.95	0.83/1.14	119	AEIC
SWD	283	100	-41	-67/-25	0.55	0.4/0.74	107	AEIC
SWD	295	98	-44	-63/-22	0.65	0.49/0.8	120	AEIC
SWD	294	97	-51	-65/-40	0.7	0.53/0.81	105	AEIC
SWD	287	102	-33	-44/-25	1.1	0.88/1.3	134	AEIC

Table 3-1 continued…

SWD	285	103	-52	-66/-37	1.25	1.07/1.48	136	AEIC
SWD	287	102	-56	-68/-44	1.05	0.93/1.22	137	AEIC
SWD	107	89	-54	-63/-45	1.25	1.04/1.43	146	AEIC
ALPI	286	102	-34	-55/-13	1.12	0.87/1.34	178	MOOS
ALPI	287	102	-49	-59/-36	1.22	1.02/1.43	180	MOOS
ALPI	287	102	-60	-70/-47	1.12	0.79/1.4	181	MOOS
ALPI	286	102	-32	-42/-22	1.50	1.3/1.71	191	MOOS
ALPI	286	102	-33	-39/-26	1.14	1.02/1.25	167	MOOS
ALPI	285	102	-42	-51/-33	1.22	1.12/1.33	168	MOOS
ALPI	287	101	-21	-30/-11	1.06	0.94/1.17	170	MOOS
ALPI	281	103	-51	-64/-38	1.12	0.95/1.28	186	MOOS
ALPI	285	103	-30	-44/-15	1.06	0.85/1.27	171	MOOS
ALPI	208	90	-43	-56/4	0.92	0.34/1.25	172	MOOS
ALPI	263	94	-82	83/-63	0.62	0.44/0.77	188	MOOS
AVAL	288	102	-43	-51/-33	1.00	0.85/1.2	193	MOOS
AVAL	287	102	-34	-43/-23	1.40	1.04/1.79	180	MOOS
AVAL	287	102	-7	-22/9	1.18	0.96/1.39	181	MOOS
AVAL	286	103	-3	-22/11	1.10	0.76/1.47	191	MOOS
AVAL	104	91	-35	-45/-25	0.72	0.63/0.81	165	MOOS
AVAL	286	102	-11	-21/-2	1.16	0.96/1.35	167	MOOS
AVAL	284	102	-2	-25/31	1.02	0.76/1.28	170	MOOS
BIGB	287	102	-40	-46/-34	1.26	1.15/1.36	180	MOOS
BIGB	287	102	-34	-49/-19	1.46	1.16/1.72	182	MOOS
BIGB	258	90	43	23/75	0.54	0.27/0.84	185	MOOS
BIGB	281	103	-49	-68/-29	1.06	0.81/1.33	186	MOOS
BIGB	203	94	-12	-29/8	1.04	0.78/1.31	187	MOOS
BING	103	92	-43	-52/-34	1.02	0.86/1.17	165	MOOS
BING	285	101	-58	-65/-50	1.28	0.83/1.68	167	MOOS
BLAK	288	103	-44	-58/-13	1.00	0.7/1.33	180	MOOS
BLAK	288	102	-45	-55/-33	1.20	0.88/1.55	182	MOOS
BLAK	260	91	-41	-58/-23	0.44	0.34/0.52	185	MOOS
BLAK	287	102	-51	-57/-45	1.18	0.99/1.37	167	MOOS
BLAK	288	102	-50	-63/-20	1.10	0.66/1.49	170	MOOS
BLAK	264	95	-90	75/-76	0.98	0.67/1.23	188	MOOS
BYR	257	101	-80	-87/-73	1.16	0.96/1.35	180	MOOS
BYR	218	89	-8	-16/0	0.92	0.78/1.07	183	MOOS
BYR	218	89	-20	-30/-10	1.26	1.02/1.5	184	MOOS
BYR	259	90	40	29/51	1.22	1.02/1.43	166	MOOS
BYR	286	101	85	70/-84	1.16	0.83/1.5	167	MOOS
BYR	287	101	-83	81/-71	1.02	0.75/1.29	170	MOOS
BYR	207	91	-17	-26/-8	0.82	0.76/0.89	172	MOOS
BYR	217	90	-15	-29/1	1.08	0.82/1.32	173	MOOS
BYR	207	92	-5	-17/8	0.82	0.69/0.96	174	MOOS
BYR	267	98	50	26/71	0.96	0.7/1.24	176	MOOS

Table 3-1 continued…

BYR	257	91	28	19/38	1.08	0.98/1.16	177	MOOS
CASW	287	101	-18	-44/8	0.94	0.7/1.17	179	MOOS
CASW	287	101	-16	-35/-2	0.78	0.63/0.96	180	MOOS
CASW	287	101	-14	-37/6	0.80	0.62/1	182	MOOS
CASW	104	92	-49	-57/-37	0.64	0.44/0.79	165	MOOS
CASW	286	101	-24	-36/-14	0.76	0.64/0.89	167	MOOS
CASW	287	101	-34	-59/-12	0.74	0.51/0.96	170	MOOS
CASW	207	86	-45	-70/-22	1.66	1.5/1.89	175	MOOS
DEVL	288	101	-50	-67/-10	0.78	0.45/1.18	194	MOOS
DEVL	286	102	-47	-66/-23	0.52	0.32/0.72	178	MOOS
DEVL	287	102	-5	-20/3	0.90	0.61/1.26	180	MOOS
DEVL	286	102	-49	-64/-34	1.60	1.13/1.99	191	MOOS
DEVL	205	95	14	-33/24	0.78	0.29/1.39	192	MOOS
DEVL	258	90	9	0/19	1.26	0.85/1.56	162	MOOS
DEVL	107	90	-3	-21/11	0.46	0.35/0.6	163	MOOS
DEVL	104	91	-3	-18/6	0.38	0.28/0.49	165	MOOS
DEVL	259	90	22	5/41	0.54	0.4/0.66	185	MOOS
DEVL	286	102	-22	-42/-5	0.68	0.52/0.87	167	MOOS
DEVL	285	102	-48	-65/-28	0.64	0.5/0.78	168	MOOS
DEVL	287	102	-33	-47/-17	0.78	0.62/0.97	170	MOOS
DEVL	281	103	-47	-62/-24	0.42	0.24/0.62	186	MOOS
DEVL	263	94	24	12/43	0.50	0.27/0.71	188	MOOS
DEVL	285	103	-23	-46/6	0.60	0.37/0.9	190	MOOS
DIVI	287	102	-41	-53/2	0.68	0.46/0.97	180	MOOS
DIVI	286	102	-28	-52/-2	0.56	0.39/0.84	167	MOOS
DIVI	285	102	-45	-64/-27	0.80	0.67/0.94	168	MOOS
DIVI	287	102	-7	-28/7	1.12	0.69/1.62	170	MOOS
HEAD	288	102	-44	-53/-33	1.08	0.92/1.27	193	MOOS
HEAD	287	102	-45	-59/-25	1.16	0.9/1.46	180	MOOS
HEAD	104	91	-44	-50/-37	0.98	0.9/1.06	165	MOOS
HEAD	286	102	-40	-51/-27	1.04	0.77/1.31	167	MOOS
HEAD	287	102	-41	-53/-28	1.32	1.03/1.6	170	MOOS
HOLG	107	90	-36	-57/-15	0.92	0.68/1.15	163	MOOS
HOLG	205	89	-31	-47/3	0.64	0.38/1.01	164	MOOS
HOLG	104	91	-56	-61/-50	0.92	0.83/0.99	165	MOOS
HOLG	258	90	-14	-30/1	0.76	0.49/0.98	185	MOOS
HOLG	286	102	-36	-46/-25	0.76	0.64/0.88	167	MOOS
HOLG	208	89	-47	-68/-24	0.76	0.53/1.01	172	MOOS
HOPE	288	101	-36	-45/-26	0.92	0.84/1.03	193	MOOS
HOPE	288	101	-44	-62/-23	1.22	0.93/1.57	194	MOOS
HOPE	286	102	-32	-45/-19	1.06	0.85/1.25	178	MOOS
HOPE	287	102	-31	-53/-10	0.64	0.49/0.85	180	MOOS
HOPE	287	102	-40	-56/-21	0.90	0.62/1.9	181	MOOS
HOPE	286	102	-30	-55/-2	1.08	0.75/1.4	191	MOOS
HOPE	107	90	-22	-54/2	0.42	0.33/0.55	163	MOOS

Table 3-1 continued…

HOPE	104	92	-15	-34/-3	0.38	0.3/0.46	165	MOOS
HOPE	286	102	-21	-32/-11	1.04	0.81/1.29	167	MOOS
HOPE	285	102	-38	-49/-26	0.98	0.86/1.09	168	MOOS
HOPE	286	102	-41	-56/-26	1.02	0.81/1.23	169	MOOS
HOPE	281	103	-50	-65/-35	0.98	0.67/1.27	186	MOOS
HOPE	285	103	-41	-55/-27	1.08	0.81/1.34	171	MOOS
HOPJ	287	102	-20	-28/-11	1.48	1.32/1.66	180	MOOS
HOPJ	287	102	-27	-39/-13	1.42	0.95/1.8	181	MOOS
HOPJ	293	99	-4	-15/5	1.44	1.18/1.71	160	MOOS
HOPJ	286	102	-21	-34/-11	0.84	0.66/1.06	167	MOOS
HOPJ	287	102	-4	-34/16	0.90	0.57/1.51	170	MOOS
INDI	287	102	-13	-37/5	0.90	0.56/1.27	179	MOOS
INDI	287	102	-35	-48/-16	0.92	0.78/1.1	180	MOOS
INDI	107	90	-35	-56/-1	0.48	0.28/0.7	163	MOOS
INDI	104	91	-52	-66/-14	0.36	0.19/0.58	165	MOOS
INDI	286	102	-31	-44/-18	0.72	0.58/0.86	167	MOOS
INDI	285	102	-35	-48/-22	0.76	0.64/0.88	168	MOOS
INDI	287	101	-15	-38/6	0.72	0.57/0.97	170	MOOS
KASH	287	101	-12	-30/1	0.74	0.5/1.05	180	MOOS
KASH	287	101	-46	-62/-32	1.60	1.22/2.03	182	MOOS
KNIK	286	102	-30	-47/-9	0.70	0.49/0.94	178	MOOS
KNIK	287	102	-50	-66/-32	1.04	0.87/1.21	179	MOOS
KNIK	287	102	-43	-50/-35	1.16	1/1.33	180	MOOS
KNIK	287	102	-64	-81/-46	1.44	1.05/1.77	181	MOOS
KNIK	259	91	-39	-54/-24	1.52	1.41/1.65	185	MOOS
KNIK	285	102	-44	-61/-29	1.14	0.96/1.31	168	MOOS
KNIK	287	101	-38	-52/-25	1.12	0.94/1.3	170	MOOS
KNIK	257	91	78	53/-80	1.04	0.79/1.22	177	MOOS
LSKI	259	90	49	30/69	0.80	0.59/1.02	166	MOOS
LSKI	262	94	25	4/46	0.62	0.48/0.76	188	MOOS
LSUM	288	101	5	-3/10	1.40	1.07/1.67	193	MOOS
LSUM	288	101	-37	-55/-17	0.90	0.65/1.16	194	MOOS
LSUM	287	102	-15	-36/-3	0.94	0.75/1.19	180	MOOS
LSUM	287	102	-32	-51/-11	0.86	0.69/1.08	182	MOOS
LSUM	286	102	-46	-71/-14	1.06	0.79/1.33	191	MOOS
LSUM	286	102	-19	-32/-7	0.76	0.63/0.91	167	MOOS
LSUM	285	102	-24	-40/-6	0.82	0.63/1	168	MOOS
LSUM	287	101	-33	-42/-22	0.94	0.82/1.06	170	MOOS
LSUM	281	103	-38	-55/-21	0.60	0.42/0.78	186	MOOS
LSUM	267	89	50	32/70	0.58	0.4/0.76	189	MOOS
MAIN	105	91	-20	-40/-1	0.52	0.37/0.68	165	MOOS
MOOP	286	102	-57	-68/-47	0.86	0.74/1.01	178	MOOS
MOOP	287	102	-7	-33/8	1.28	0.72/1.87	179	MOOS
MOOP	287	102	-46	-58/-26	0.94	0.69/1.24	180	MOOS
MOOP	287	102	-8	-26/9	0.92	0.71/1.13	181	MOOS

Table 3-1 continued…

MOOP	287	102	-25	-36/-14	1.04	0.89/1.2	182	MOOS
MOOP	286	102	-32	-46/-17	0.82	0.63/1.02	167	MOOS
MOOP	285	102	-62	-76/-47	0.78	0.64/0.93	168	MOOS
NANC	287	102	-27	-35/-18	0.80	0.7/0.88	180	MOOS
NANC	276	104	-57	-66/-45	0.94	0.73/1.15	159	MOOS
NANC	292	99	-45	-57/-32	1.80	1.5/2.11	160	MOOS
NANC	286	101	-49	-57/-40	0.98	0.83/1.12	167	MOOS
NANC	286	101	-39	-63/-17	0.90	0.64/1.08	169	MOOS
NANC	287	101	-31	-46/-17	0.82	0.69/0.95	170	MOOS
NANC	285	103	-38	-55/-21	0.90	0.71/1.07	171	MOOS
NANC	299	93	-32	-49/-13	0.86	0.62/1.09	161	MOOS
NANC	299	93	-32	-49/-13	0.86	0.62/1.09	161	MOOS
NSKI	203	95	-26	-41/-6	0.58	0.38/0.97	192	MOOS
PERI	106	91	-34	-50/19	0.40	0.32/0.49	165	MOOS
PERI	287	103	-56	-62/-51	1.82	1.52/2.12	167	MOOS
PORT	287	102	-46	-66/-13	0.66	0.34/1.03	167	MOOS
RUSS	286	102	-19	-34/-9	0.80	0.65/0.98	179	MOOS
RUSS	286	102	-18	-49/0	0.44	0.33/0.72	180	MOOS
RUSS	204	95	16	-19/28	0.62	0.27/1.19	192	MOOS
RUSS	286	102	-38	-60/-10	0.48	0.33/0.71	167	MOOS
RUSS	262	94	-85	64/90	0.52	0.28/0.75	188	MOOS
RUSS	262	94	-85	-90/-72	0.52	0.28/0.75	188	MOOS
RUSS	267	88	57	39/89	0.56	0.29/0.82	189	MOOS
SNUG	286	102	-39	-57/-15	0.58	0.41/0.83	167	MOOS
SOLD	103	92	-52	-64/-40	0.96	0.74/1.17	165	MOOS
TUPA	287	102	-55	-61/-49	1.38	1.06/1.77	180	MOOS
TUPA	287	102	-47	-55/-38	1.38	1.05/1.7	182	MOOS
TUPA	285	102	-43	-50/-37	1.06	0.9/1.24	167	MOOS
TUPA	287	102	-38	-55/1	0.76	0.44/1.24	170	MOOS
TUPA	263	95	-86	81/-74	1.12	0.85/1.33	188	MOOS
USKI	286	102	-5	-22/6	0.88	0.6/1.18	179	MOOS
USKI	258	90	39	27/59	0.78	0.54/0.98	162	MOOS
USKI	106	90	-37	-51/-24	0.78	0.64/0.9	163	MOOS
USKI	205	90	-40	-58/-2	0.70	0.4/1.15	164	MOOS
USKI	104	92	-35	-45/-26	0.60	0.53/0.68	165	MOOS
USKI	286	101	-19	-29/-10	0.76	0.66/0.86	170	MOOS
WHIT	288	102	-50	-55/-44	1.20	0.98/1.44	180	MOOS
WHIT	105	91	-40	-53/-23	0.42	0.33/0.53	165	MOOS
WHIT	287	102	-51	-61/-38	1.04	0.81/1.28	167	MOOS
AND	207	99	85	73/97	1.40	1.24/1.56	32	BEAAR
AND	115	116	83	60/102	0.80	0.57/1.09	26	BEAAR
AND	209	93	-86	-103/ -73	1.14	0.92/1.35	25	BEAAR
AND	285	102	42	32/54	1.08	0.69/1.52	22	BEAAR

Table 3-1 continued…

ANT	262	87	42	29/55	1.76	1.41/2.12	37	BEAAR
ANT	208	86	-25	-37/-10	0.66	0.50/0.84	35	BEAAR
ANT	262	91	59	43/77	1.96	1.52/2.50	34	BEAAR
ANT	206	97	-4	-33/21	0.44	0.31/0.60	32	BEAAR
ANT	264	95	60	47/74	0.72	0.53/0.92	31	BEAAR
ANT	285	113	72	70/75	1.38	1.04/1.66	27	BEAAR
ANT	209	92	-3	-12/6	0.50	0.38/0.61	25	BEAAR
ANT	285	102	73	47/95	0.64	0.48/0.90	24	BEAAR
ANT	283	103	68	46/88	0.66	0.45/0.92	33	BEAAR
ANT	206	86	-23	-35/-7	0.64	0.42/0.87	36	BEAAR
BYR	106	114	-32	-44/-20	0.70	0.60/0.80	19	BEAAR
BYR	107	103	-40	-50/-28	0.72	0.51/0.92	11	BEAAR
BYR	107	103	-36	-50/-12	0.66	0.39/1.00	54	BEAAR
BYR	108	100	-43	-52/-32	0.86	0.62/1.12	50	BEAAR
BYR	109	98	-41	-51/-24	0.74	0.43/1.10	52	BEAAR
BYR	204	95	-24	-32/-14	0.62	0.50/0.74	6	BEAAR
BYR	204	95	0	-12/11	0.62	0.51/0.73	5	BEAAR
BYR	204	94	-25	-35/-11	0.66	0.47/0.87	3	BEAAR
BYR	204	95	17	-5/35	0.64	0.49/0.77	1	BEAAR
BYR	205	87	-22	-30/-14	0.88	0.76/1.00	51	BEAAR
BYR	205	95	-7	-12/-1	0.70	0.63/0.76	47	BEAAR
BYR	205	93	11	-20/40	0.68	0.49/0.85	17	BEAAR
BYR	206	97	9	-14/28	0.58	0.45/0.69	32	BEAAR
BYR	206	86	-17	-29/-3	0.84	0.66/1.02	45	BEAAR
BYR	207	87	-5	-16/8	0.76	0.62/0.88	38	BEAAR
BYR	207	86	-15	-26/-2	0.88	0.73/1.01	35	BEAAR
BYR	208	85	-9	-32/24	0.70	0.39/1.06	15	BEAAR
BYR	208	88	-19	-30/-7	0.84	0.67/0.99	2	BEAAR
BYR	208	91	-4	-13/6	0.82	0.70/0.94	25	BEAAR
BYR	217	90	-14	-23/-4	1.06	0.89/1.23	12	BEAAR
BYR	256	90	47	37/57	0.96	0.85/1.06	46	BEAAR
BYR	259	92	59	51/66	1.54	1.38/1.70	29	BEAAR
BYR	264	95	49	37/61	0.92	0.81/1.02	31	BEAAR
BYR	265	92	57	49/66	1.42	1.22/1.62	21	BEAAR
BYR	266	89	62	47/76	1.36	1.09/1.64	20	BEAAR
BYR	267	90	46	32/61	1.30	1.10/1.51	7	BEAAR
BYR	269	97	35	24/46	0.76	0.69/0.85	40	BEAAR
BYR	275	101	75	65/83	0.82	0.66/0.96	44	BEAAR
BYR	280	103	78	64/91	0.76	0.59/0.94	14	BEAAR
BYR	281	102	-78	-85/-71	1.34	1.06/1.61	8	BEAAR
BYR	283	102	-85	-96/-75	1.26	1.00/1.52	23	BEAAR
BYR	283	102	89	83/94	0.90	0.76/1.07	39	BEAAR
BYR	284	102	-87	-98/-78	1.04	0.76/1.33	22	BEAAR
BYR	106	105	-47	-57/-37	1.02	0.75/1.28	10	BEAAR
BYR	205	86	-29	-47/20	0.58	0.19/1.10	18	BEAAR

Table 3-1 continued…

BYR	205	91	-13	-30/21	0.68	0.25/1.10	41	BEAAR
BYR	206	86	-18	-26/-9	0.82	0.71/0.94	36	BEAAR
BYR	207	88	-21	-31/-12	0.82	0.73/0.92	48	BEAAR
BYR	218	87	-22	-35/-8	1.12	1.01/1.22	9	BEAAR
BYR	259	92	51	27/83	1.10	0.85/1.31	16	BEAAR
BYR	261	87	53	42/64	1.52	1.21/1.84	37	BEAAR
BYR	261	93	23	6/49	1.06	0.86/1.27	28	BEAAR
BYR	284	102	-79	-89/-71	1.18	0.78/1.55	24	BEAAR
BYR	299	91	-59	-70/-48	1.76	1.39/2.08	55	BEAAR
BYR	206	85	-14	-29/10	0.78	0.33/1.08	43	BEAAR
BYR	268	89	73	59/85	1.40	1.25/1.58	42	BEAAR
BYR	261	90	55	46/64	1.68	1.48/1.88	34	BEAAR
BYR	204	95	-7	-31/19	0.56	0.38/0.76	5	BEAAR
CAR	262	87	38	29/48	2.26	2.00/2.50	37	BEAAR
CAR	263	91	50	39/61	1.94	1.61/2.28	34	BEAAR
CAR	285	103	76	59/96	1.22	0.92/1.58	24	BEAAR
CAR	284	103	45	31/59	0.90	0.70/1.11	23	BEAAR
CAR	285	103	61	51/70	1.11	0.89/1.40	22	BEAAR
CAR	263	94	61	12/79	1.58	1.39/1.71	28	BEAAR
CZN	264	88	83	76/88	2.18	1.59/2.61	37	BEAAR
CZN	206	95	65	46/90	2.40	1.93/2.86	30	BEAAR
CZN	262	94	80	75/85	3.18	2.84/3.52	29	BEAAR
DH1	301	91	39	32/44	0.88	0.79/0.97	55	BEAAR
DH1	111	97	-49	-61/-11	0.62	0.32/1.14	52	BEAAR
DH1	110	100	-60	-65/-48	0.98	0.48/1.38	50	BEAAR
DH1	206	96	24	18/30	1.08	0.77/1.41	47	BEAAR
DH1	257	91	32	28/35	1.20	1.15/1.26	46	BEAAR
DH1	277	102	26	21/31	0.82	0.72/0.92	44	BEAAR
DH1	270	89	30	14/44	1.40	1.29/1.53	42	BEAAR
DH1	270	98	21	14/27	1.00	0.92/1.08	40	BEAAR
DH1	209	88	26	3/38	0.82	0.46/1.16	38	BEAAR
DH1	263	88	34	26/42	1.56	1.39/1,72	37	BEAAR
DH1	263	91	49	31/67	1.22	0.98/1.47	34	BEAAR
DH1	265	95	23	13/34	0.98	0.89/1.08	31	BEAAR
DH1	210	92	19	12/24	0.66	0.50/0.82	25	BEAAR
DH1	285	103	27	16/37	1.94	1.58/2.38	23	BEAAR
DH1	263	94	19	4/32	1.10	0.99/1.20	28	BEAAR
DH1	260	93	29	25/34	1.04	0.97/1.11	29	BEAAR
DH2	264	88	17	5/41	0.96	0.66/1.42	37	BEAAR
DH2	264	95	-1	-15/15	0.74	0.27/1.11	28	BEAAR
DH2	261	93	9	-5/56	0.62	0.24/1.28	29	BEAAR
DH3	110	102	-73	-102/-66	0.78	0.22/1.39	54	BEAAR
DH3	111	99	-73	-76/-70	1.20	0.98/1.45	50	BEAAR
DH3	110	105	88	64/108	1.36	0.80/1.82	49	BEAAR
DH3	207	96	42	37/48	1.12	0.83/1.42	47	BEAAR

Table 3-1 continued…

DH3	264	95	-44	-58/-31	0.58	0.39/0.74	28	BEAAR
DH3	272	99	-23	-35/-15	0.82	0.51/1.10	40	BEAAR
EFS	107	103	-81	-85/-77	2.12	1.68/2.50	54	BEAAR
EFS	205	88	38	28/51	0.98	0.57/1.28	51	BEAAR
EFS	205	96	60	54/66	0.82	0.70/0.92	47	BEAAR
EFS	256	91	47	29/67	2.12	1.72/2.57	46	BEAAR
EFS	275	101	54	44/63	1.86	1.70/2.02	44	BEAAR
EFS	284	102	46	38/54	1.60	1.19/2.02	39	BEAAR
EFS	261	87	41	30/53	2.22	1.81/2.58	37	BEAAR
EFS	209	92	64	55/74	0.52	0.43/0.60	25	BEAAR
EFS	206	87	60	48/72	0.56	0.41/0.72	36	BEAAR
FID	284	102	-84	-91/-78	1.44	1.10/1.79	24	BEAAR
FID	283	102	-72	-82/-63	1.10	0.89/1.31	23	BEAAR
FID	284	102	-83	-87/-79	1.56	1.32/1.84	22	BEAAR
FID	206	86	-38	-45/-31	1.12	1.01/1.24	36	BEAAR
GNR	206	96	-89	-94/-84	0.70	0.59/0.81	47	BEAAR
GNR	276	102	71	61/81	1.68	1.51/1.87	44	BEAAR
GNR	270	98	87	77/96	1.62	1.27/1.95	40	BEAAR
GNR	285	102	53	43/64	1.28	0.98/1.60	39	BEAAR
GNR	210	93	-87	-110/-69	0.60	0.34/0.87	25	BEAAR
GNR	285	102	83	73/93	1.44	1.19/1.70	24	BEAAR
GNR	263	94	80	66/93	1.70	1.57/1.84	28	BEAAR
GNR	206	92	-88	-111/-75	0.74	0.40/1.11	41	BEAAR
GNR	208	89	-77	-94/-67	0.64	0.32/0.90	48	BEAAR
GOO	110	98	-41	-58/-15	1.04	0.67/1.59	52	BEAAR
GOO	205	87	-20	-29/-11	0.66	0.63/0.71	51	BEAAR
GOO	257	91	52	42/62	1.36	1.16/1.57	46	BEAAR
GOO	276	102	48	42/54	1.06	0.98/1.16	44	BEAAR
GOO	270	98	45	30/62	0.94	0.78/1.10	40	BEAAR
GOO	284	102	52	44/62	0.98	0.79/1.17	39	BEAAR
GOO	208	87	-16	-32/3	0.54	0.38/0.71	38	BEAAR
GOO	208	86	-5	-18/7	0.70	0.63/0.79	35	BEAAR
GOO	262	91	45	35/55	1.86	1.59/2.14	34	BEAAR
GOO	206	98	18	-31/37	0.26	0.13/0.46	32	BEAAR
GOO	209	92	12	-6/28	0.52	0.33/0.70	25	BEAAR
GOO	285	103	59	43/76	0.86	0.63/1.13	24	BEAAR
GOO	285	103	53	43/64	1.04	0.85/1.22	22	BEAAR
GOO	260	93	53	40/66	1.60	1.33/1.89	29	BEAAR
GOO	207	86	-25	-37/-13	0.66	0.59/0.74	36	BEAAR
GOO	208	88	-14	-32/6	0.74	0.55/0.90	48	BEAAR
HURN	107	103	-54	-66/-30	1.10	0.53/1.90	54	BEAAR
HURN	110	98	-49	-57/-35	1.52	0.93/2.03	52	BEAAR
HURN	205	87	-36	-40/-30	0.68	0.55/0.80	51	BEAAR
HURN	109	100	-45	-52/-35	1.54	1.23/1.82	50	BEAAR
HURN	205	95	-38	-54/-3	0.38	0.16/0.67	47	BEAAR

Table 3-1 continued…

HURN	256	90	50	31/64	0.84	0.60/1.09	46	BEAAR
HURN	206	86	-43	-50/-31	1.04	0.63/1.44	45	BEAAR
HURN	276	102	36	31/41	0.84	0.74/0.93	44	BEAAR
HURN	269	98	18	6/31	0.70	0.57/0.83	40	BEAAR
HURN	284	102	78	62/90	0.78	0.61/1.05	39	BEAAR
HURN	207	87	-33	-49/7	0.68	0.24/1.28	38	BEAAR
HURN	262	87	41	22/61	1.58	1.09/2.18	37	BEAAR
HURN	208	86	-34	-41/-26	0.78	0.59/0.98	35	BEAAR
HURN	262	90	59	45/73	1.38	1.04/1.72	34	BEAAR
HURN	207	97	-23	-39/1	0.36	0.28/0.47	32	BEAAR
HURN	209	92	-9	-20/3	0.46	0.38/0.56	25	BEAAR
HURN	285	102	64	39/109	0.62	0.46/1.49	24	BEAAR
HURN	284	102	87	66/99	0.80	0.55/1.26	22	BEAAR
HURN	266	93	58	45/69	1.34	1.03/1.69	21	BEAAR
HURN	266	90	55	41/67	1.22	1.05/1.40	20	BEAAR
HURN	107	113	-70	-80/-61	1.92	1.72/2.10	19	BEAAR
HURN	205	86	-35	-46/-24	1.82	1.43/2.10	18	BEAAR
HURN	281	103	62	43/82	0.70	0.53/0.86	14	BEAAR
HURN	106	105	-34	-53/-10	0.76	0.42/1.17	10	BEAAR
HURN	281	102	49	34/65	0.66	0.51/0.83	8	BEAAR
HURN	267	91	39	24/53	1.32	1.14/1.50	7	BEAAR
HURN	204	96	-36	-57/15	0.36	0.14/0.85	6	BEAAR
HURN	204	96	-21	-48/12	0.36	0.18/0.62	5	BEAAR
HURN	204	96	-32	-50/24	0.38	0.12/0.85	5	BEAAR
HURN	258	89	58	24/88	0.98	0.63/1.51	13	BEAAR
HURN	262	94	-1	-10/9	0.80	0.67/0.91	28	BEAAR
HURN	259	92	72	61/91	1.36	1.07/1.62	29	BEAAR
HURN	283	103	84	37/102	0.72	0.41/1.50	33	BEAAR
HURN	206	86	-32	-38/-25	0.72	0.55/0.89	36	BEAAR
HURN	205	91	-47	-68/-13	0.92	0.38/1.51	41	BEAAR
HURN	208	88	-16	-31/0	0.82	0.57/1.06	48	BEAAR
MCK	300	91	80	71/88	1.52	1.32/1.71	55	BEAAR
MCK	110	98	-18	-64/8	0.34	0.18/0.93	52	BEAAR
MCK	109	100	-7	-63/6	0.40	0.14/0.86	50	BEAAR
MCK	206	96	-81	-88/-74	0.82	0.61/1.04	47	BEAAR
MCK	257	91	45	34/58	2.44	2.23/2.66	46	BEAAR
MCK	276	102	61	55/68	1.70	1.59/1.81	44	BEAAR
MCK	270	98	76	62/87	1.90	1.73/2.08	40	BEAAR
MCK	285	102	58	51/66	1.66	1.44/1.86	39	BEAAR
MCK	262	87	53	44/62	2.36	1.98/2.74	37	BEAAR
MCK	208	87	86	79/94	0.82	0.68/0.95	32	BEAAR
MCK	210	93	-81	-87/-76	0.76	0.58/0.94	25	BEAAR
MCK	285	103	52	38/68	1.44	1.00/1.98	22	BEAAR
MCK	260	93	54	43/66	2.58	2.38/2.79	29	BEAAR
MCK	284	103	75	59/92	1.04	0.83/1.26	33	BEAAR

Table 3-1 continued…

MHR	110	98	-49	-56/-39	1.20	0.84/1.59	52	BEAAR
MHR	205	87	-44	-50/-37	0.96	0.81/1.12	51	BEAAR
MHR	108	100	-51	-56/-45	1.50	1.11/1.85	50	BEAAR
MHR	205	95	-47	-55/-35	0.64	0.37/0.92	47	BEAAR
MHR	269	98	-11	-25/2	1.10	0.82/1.32	40	BEAAR
MHR	284	102	-83	-91/-79	1.38	0.87/1.79	39	BEAAR
MHR	207	87	-44	-54/-32	1.00	0.61/1.32	38	BEAAR
MHR	206	97	-33	-46/-7	0.54	0.23.0.80	32	BEAAR
MHR	115	115	-44	-57/-30	1.32	1.14/1.40	26	BEAAR
MHR	115	115	-42	-60/0	0.74	0.26/1.29	26	BEAAR
MHR	209	92	-26	-37/-15	0.72	0.54/0.91	25	BEAAR
MHR	284	102	-79	-87/-72	1.82	1.31/2.25	24	BEAAR
MHR	283	102	89	80/97	1.88	1.63/2.12	23	BEAAR
MHR	262	94	4	-10/21	0.52	0.38/0.68	28	BEAAR
MHR	207	88	-34	-44/-24	1.06	0.78/1.32	48	BEAAR
NNA	108	103	72	64/80	2.00	1.79/2.19	54	BEAAR
NNA	270	98	45	29/62	1.76	1.49/2.04	40	BEAAR
NNA	285	102	63	47/79	0.96	0.74/1.18	39	BEAAR
NNA	208	89	89	75/104	1.56	1.06/1.94	38	BEAAR
NNA	208	88	89	74/103	1.28	1.00/1.55	35	BEAAR
NNA	209	93	90	80/100	1.54	1.29/1.77	25	BEAAR
NNA	266	93	33	23/44	1.78	1.51/2.07	21	BEAAR
NNA	267	90	43	32/54	2.00	1.69/2.30	20	BEAAR
NNA	106	114	75	63/88	1.70	1.19/2.16	19	BEAAR
NNA	281	103	67	55/79	1.32	1.03/1.62	14	BEAAR
NNA	107	103	77	61/92	1.40	1.08/1.72	11	BEAAR
NNA	106	105	85	69/100	1.46	1.06/1.85	10	BEAAR
NNA	282	102	59	45/74	1.40	1.09/1.76	8	BEAAR
NNA	268	91	58	43/73	1.76	1.43/2.10	7	BEAAR
NNA	205	97	-89	-104/-77	1.28	0.96/1.65	6	BEAAR
NNA	205	97	-88	-102/-73	1.58	1.23/1.96	5	BEAAR
NNA	205	96	89	68/110	1.64	1.14/2.15	4	BEAAR
NNA	205	96	84	70/96	1.34	0.93/1.78	3	BEAAR
NNA	262	94	50	34/68	0.82	0.67/0.96	28	BEAAR
NNA	206	92	54	38/70	1.72	1.26/2.13	41	BEAAR
PVE	208	91	-36	-49/-19	1.40	1.10/1.60	25	BEAAR
PVE	261	93	77	33/103	0.90	0.66/1.13	28	BEAAR
PVW	204	86	8	-17/22	0.94	0.59/1.23	51	BEAAR
PVW	268	97	47	36/58	1.44	1.32/1.58	40	BEAAR
PVW	283	102	33	27/45	1.08	0.63/1.56	39	BEAAR
PVW	206	86	6	-16/21	1.02	0.55/1.48	38	BEAAR
PVW	260	86	47	37/58	1.84	1.59/2.11	37	BEAAR
PVW	207	85	7	-10/20	1.46	0.90/1.83	35	BEAAR
PVW	261	90	48	41/56	2.12	1.79/2.44	34	BEAAR
PVW	205	87	13	-1/21	0.54	0.24/0.78	32	BEAAR

Table 3-1 continued…

PVW	263	94	31	18/44	1.44	1.33/1.56	31	BEAAR
PVW	202	94	19	-23/41	1.38	0.60/1.93	30	BEAAR
PVW	261	93	43	31/54	1.66	1.52/1.79	28	BEAAR
PVW	258	92	35	29/41	2.02	1.89/21.5	29	BEAAR
PVW	282	103	72	43/98	0.86	0.68/1.40	33	BEAAR
PVW	205	86	26	14/37	1.32	1.03/1.58	36	BEAAR
PYY	115	115	-35	-51/-21	1.28	0.98/1.64	26	BEAAR
PYY	209	92	-22	-36/1	0.62	0.39/0.97	25	BEAAR
PYY	283	102	88	70/104	1.48	1.04/1.86	23	BEAAR
PYY	259	92	64	56/71	1.32	1.12/1.52	29	BEAAR
RCK	206	96	86	79/92	1.02	0.91/1.12	47	BEAAR
RCK	257	91	44	23/64	2.00	1.75/2.27	46	BEAAR
RCK	207	87	76	65/86	0.74	0.61/0.87	45	BEAAR
RCK	276	102	55	44/67	1.80	1.66/1.98	44	BEAAR
RCK	270	98	82	68/94	2.06	1.86/2.27	40	BEAAR
RCK	208	88	78	65/91	0.74	0.62/0.87	38	BEAAR
RCK	209	93	79	68/90	1.08	0.86/1.29	25	BEAAR
RCK	107	103	49	34/71	0.36	0.28/0.49	11	BEAAR
RCK	208	86	60	43/73	2.04	1.84/2.26	15	BEAAR
RCK	262	94	75	57/92	2.12	1.87/2.37	28	BEAAR
RCK	260	93	38	26/50	2.20	2.00/2.41	29	BEAAR
RND	300	91	78	69/89	0.80	0.49/1.08	55	BEAAR
RND	108	103	-60	-72/-2	0.68	0.19/1.53	54	BEAAR
RND	111	98	-65	-71/-54	1.34	0.75/1.91	52	BEAAR
RND	206	88	38	30/48	0.42	0.25/0.59	51	BEAAR
RND	109	100	-72	-77/-66	1.52	1.08/1.89	50	BEAAR
RND	257	91	38	32/44	1.90	1.79/2.00	46	BEAAR
RND	276	102	46	41/51	1.12	1.03/1.22	44	BEAAR
RND	270	98	59	47/70	1.30	1.14/1.48	40	BEAAR
RND	285	102	53	48/57	1.18	1.07/1.32	39	BEAAR
RND	262	87	49	37/60	1.76	1.54/1.99	37	BEAAR
RND	263	91	41	29/53	1.96	1.49/2.45	34	BEAAR
RND	265	95	64	54/74	1.64	1.52/1.77	31	BEAAR
RND	285	113	67	43/91	1.58	1.13/2.32	27	BEAAR
RND	210	92	31	26/36	1.98	1.71/2.23	25	BEAAR
RND	285	103	50	44/56	0.96	0.82/1.10	24	BEAAR
RND	284	103	47	24/70	0.92	0.66/1.20	23	BEAAR
RND	285	103	47	41/54	1.00	0.80/1.19	22	BEAAR
RND	282	103	47	41/53	1.04	0.92/1.16	8	BEAAR
RND	268	91	29	14/43	1.94	1.75/2.13	7	BEAAR
RND	219	88	18	0/34	0.90	0.67/1.12	9	BEAAR
RND	263	94	47	38/56	1.68	1.56/1.81	28	BEAAR
RND	260	93	41	36/47	1.76	1.65/1.89	29	BEAAR
RND	284	104	67	53/81	1.08	0.90/1.28	33	BEAAR
SAN	205	88	42	32/52	1.06	0.89/1.19	51	BEAAR

Table 3-1 continued…

SAN	205	96	54	49/60	1.16	1.07/1.24	47	BEAAR
SAN	257	91	44	33/55	2.54	2.42/2.66	46	BEAAR
SAN	207	87	53	46/61	0.74	0.62/0.86	45	BEAAR
SAN	276	102	55	47/62	2.42	2.31/2.53	44	BEAAR
SAN	206	86	36	17/55	0.84	0.56/1.09	43	BEAAR
SAN	270	98	55	42/67	2.36	2.18/2.52	40	BEAAR
SAN	284	102	50	43/58	1.82	1.59/2.06	39	BEAAR
SAN	262	87	38	19/55	1.46	1.06/1.83	37	BEAAR
SAN	206	98	45	26/63	1.14	1.05/1.21	32	BEAAR
SAN	264	95	58	43/73	2.26	2.08/2.45	31	BEAAR
SAN	262	94	46	33/59	2.38	2.22/2.52	28	BEAAR
SAN	259	93	60	49/72	2.54	2.34/2.74	29	BEAAR
SAN	206	92	48	35/63	2.32	2.13/2.53	41	BEAAR
SBL	108	100	-76	-81/-72	1.98	1.37/2.69	53	BEAAR
SBL	109	98	-78	-86/-73	1.56	0.95/2.14	52	BEAAR
SBL	205	87	22	15/29	1.48	1.38/1.58	51	BEAAR
SBL	108	101	-81	-85/-78	1.56	1.20/1.89	50	BEAAR
SBL	261	90	53	39/68	1.98	1.52/2.39	34	BEAAR
SBL	259	92	43	19/78	2.18	1.59/2.63	29	BEAAR
SBL	283	103	73	59/89	1.06	0.74/1.52	33	BEAAR
SLM	263	91	51	43/59	2.06	1.80/2.31	34	BEAAR
SLM	265	95	43	23/66	1.36	1.07/1.61	31	BEAAR
SLM	285	103	68	60/78	1.40	1.17/1.63	24	BEAAR
SLM	284	103	49	28/73	0.66	0.42/0.89	23	BEAAR
SLM	285	103	55	42/74	1.52	0.97/2.34	22	BEAAR
SLM	263	94	68	44/85	1.76	1.59/1.95	28	BEAAR
SLM	260	93	35	23/46	1.90	1.61/2.17	29	BEAAR
SLM	284	104	71	58/85	1.40	1.12/1.70	33	BEAAR
SLT	285	102	24	13/38	1.98	1.63/2.33	24	BEAAR
SLT	262	94	43	25/61	1.76	1.59/1.92	28	BEAAR
SOB	262	87	63	41/88	1.78	1.21/2.57	37	BEAAR
SOB	206	98	77	66/88	0.86	0.77/0.94	32	BEAAR
SOB	115	115	-88	-104/-67	1.48	1.30/1.70	26	BEAAR
SOB	115	115	-85	-95/-77	1.26	1.04/1.46	26	BEAAR
SOB	209	93	76	47/116	0.46	0.31/0.71	25	BEAAR
SOB	262	94	83	72/93	1.88	1.63/2.10	28	BEAAR
SOB	260	93	58	42/73	2.20	2.03/2.37	29	BEAAR
SOB	207	87	-70	-84/-61	0.74	0.41/1.05	36	BEAAR
TCE	205	97	-21	-34/-7	0.96	0.63/1.24	32	BEAAR
TCE	208	91	-35	-48/-24	1.80	1.58/1.97	25	BEAAR
TCE	284	102	-58	-68/-25	0.66	0.19/1.30	22	BEAAR
TCE	259	92	37	23/53	0.84	0.70/0.99	29	BEAAR
TCE	282	103	-69	-80/-48	1.06	0.45/1.60	33	BEAAR
TCE	206	86	-51	-62/-41	1.80	1.63/1.95	36	BEAAR
TLKY	299	91	-9	-22/4	0.74	0.56/0.90	55	BEAAR

Table 3-1 continued…

TLKY	109	100	-60	-64/-53	1.22	0.66/1.91	53	BEAAR
TLKY	205	86	-31	-42/-21	1.36	1.19/1.52	51	BEAAR
TLKY	108	100	-58	-63/-53	1.06	0.76/1.41	50	BEAAR
TLKY	205	94	-19	-28/-10	1.12	0.88/1.35	47	BEAAR
TLKY	206	85	-15	-22/-6	1.54	1.14/1.91	45	BEAAR
TLKY	275	101	-19	-24/-14	0.88	0.76/0.99	44	BEAAR
TLKY	283	102	-17	-22/-11	0.82	0.70/0.94	39	BEAAR
TLKY	207	86	-18	-30/-8	1.48	1.20/1.75	38	BEAAR
TLKY	207	85	-25	-35/-15	1.38	1.12/1.65	35	BEAAR
TLKY	203	93	-35	-49/-19	1.34	0.82/1.94	30	BEAAR
TLKY	209	91	-9	-17/-2	1.10	0.93/1.26	25	BEAAR
TLKY	283	102	-17	-25/-9	0.74	0.60/0.88	23	BEAAR
TLKY	284	102	-17	-27/-8	0.70	0.53/0.88	22	BEAAR
TLKY	107	113	-45	-51/-39	0.84	0.70/0.97	19	BEAAR
TLKY	280	103	-20	-29/-13	0.82	0.70/0.92	14	BEAAR
TLKY	107	102	-55	-62/-47	0.94	0.56/1.34	11	BEAAR
TLKY	106	105	-58	-71/-45	0.90	0.68/1.09	10	BEAAR
TLKY	281	102	-20	-25/-15	0.86	0.79/0.93	8	BEAAR
TLKY	204	95	-22	-29/-15	1.20	0.99/1.40	6	BEAAR
TLKY	204	93	-23	-34/-11	1.36	1.03/1.68	4	BEAAR
TLKY	204	93	-30	-38/-21	1.48	1.16/1.78	3	BEAAR
TLKY	205	93	-30	-45/-15	1.60	1.42/1.76	17	BEAAR
TLKY	283	103	-26	-53/-10	0.56	0.37/0.89	33	BEAAR
TLKY	207	87	-24	-39/-11	1.26	1.03/1.46	48	BEAAR
WOLF	264	95	38	17/59	0.64	0.51/0.75	31	BEAAR
WOLF	208	91	-11	-25/4	0.72	0.59/0.85	25	BEAAR
WOLF	261	93	34	21/46	0.76	0.66/0.86	28	BEAAR
WOLF	259	92	49	33/64	1.12	0.90/1.34	29	BEAAR
WOLF	206	86	-12	-28/5	0.74	0.63/0.85	36	BEAAR
WON	106	104	55	41/72	0.86	0.67/1.10	54	BEAAR
WON	108	101	-85	-106/-74	0.98	0.65/1.55	53	BEAAR
WON	109	99	47	34/85	0.88	0.52/1.41	52	BEAAR
WON	204	87	26	17/35	1.76	1.44/1.96	51	BEAAR
WON	108	101	50	42/60	0.98	0.78/1.16	50	BEAAR
WON	204	95	39	33/49	0.96	0.62/1.29	47	BEAAR
WON	255	90	50	32/65	2.56	2.33/2.78	46	BEAAR
WON	205	86	35	30/40	1.38	1.08/1.69	45	BEAAR
WON	274	101	41	36/46	1.94	1.81/2.07	44	BEAAR
WON	268	97	30	21/39	2.20	2.02/2.40	40	BEAAR
WON	283	102	35	30/41	1.72	1.36/2.05	39	BEAAR
WON	260	86	47	22/68	2.46	1.95/2.89	37	BEAAR
WON	205	97	45	36/54	1.06	0.89/1.22	32	BEAAR
WON	114	116	43	32/55	0.88	0.65/1.07	26	BEAAR
WON	261	93	40	26/54	2.36	2.11/2.61	28	BEAAR
WON	258	92	36	25/46	2.42	2.21/2.65	29	BEAAR

Table 3-1 continued…

YAN	111	98	-46	-62/-15	0.56	0.33/0.98	52	BEAAR
YAN	109	100	-44	-58/-8	0.36	0.22/0.63	50	BEAAR
YAN	257	91	46	35/57	2.00	1.86/2.14	46	BEAAR
YAN	276	102	57	49/65	1.46	1.33/1.59	44	BEAAR
YAN	270	98	-86	-96/-77	1.98	1.78/2.19	40	BEAAR
YAN	285	102	61	51/72	1.22	0.95/1.49	39	BEAAR
YAN	262	87	44	37/51	2.08	1.88/2.28	37	BEAAR
YAN	265	95	89	79/99	1.84	1.68/2.00	31	BEAAR
YAN	285	113	62	36/94	0.88	0.48/1.71	27	BEAAR
YAN	285	103	38	27/49	1.38	1.06/1.75	24	BEAAR
YAN	285	103	61	50/72	1.32	1.03/1.65	22	BEAAR
YAN	266	93	55	38/72	2.02	1.65/2.40	21	BEAAR
YAN	267	90	58	51/65	2.24	2.07/2.41	20	BEAAR
YAN	282	103	62	42/95	1.36	1.03/2.01	8	BEAAR
YAN	268	91	10	-3/24	1.58	1.23/1.90	7	BEAAR
YAN	263	94	80	70/90	1.86	1.70/2.03	28	BEAAR
YAN	260	93	65	53/76	2.16	1.96/2.35	29	BEAAR
YAN	284	104	54	39/70	1.86	1.61/2.11	33	BEAAR

Table 3-2: Station averages by back-azumith group for all networks.
This table includes the results for each station by back-azimuth average for all stations and all networks.

Station Name	Back-azimuth group	Average Distance (degrees)	Average Fast Direction (degrees)	Fast Direction Error (degrees)	Average Delay Time (seconds)	Delay Time Error (seconds)
BERG	263	93	26	18.4/35.6	0.7	0.5/0.9
BRLK	105	90	-18	-43.07/1.14	0.8	0.57/1.11
BRLK	285	100	60	23.25/86.11	0.35	0.22/0.67
BRLK	260	90	48	17.36/73.53	0.45	0.24/0.75
CNP	260	94	27	9.89/48.97	0.5	0.35/0.73
FIB	216	89	5	-26.59/31.31	0.56	0.3/0.93
FIB	260	89	60	41.5/77.86	0.45	0.35/0.56
FIB	286	100	-31	-45.13/-14.63	0.95	0.72/1.14
HOM	286	100	-50	-63.98/-32.8	0.66	0.47/0.87
KDAK	264	90	25	4.99/61.29	0.4	0.25/0.68
KDAK	282	100	53	27.83/76.13	0.45	0.34/0.63
MID	207	91	48.5	33.54/71.91	0.75	0.4/1.14
OHAK	104	107	90	64.64/100.85	0.7	0.32/1.18
OHAK	255	88	69	59.06/74.5	0.96	0.53/1.31
OHAK	280	101	58	46.74/40.43	0.7	0.61/0.83
PMR	208	87	-51	-58/-44	1.65	1.37/1.93
PMR	288	101	-54	-59.47/-47.64	1.7	1.35/2.1
PMR	264	91	-73	-82.72/-63	1.5	1.12/1.86
RC01	274	98	-31.14	-43.26/-16.05	1.11	0.92/1.32

Table 3-2 continued…

RDJH	201	90	58	38.15/72.69	0.98	0.71/1.34
RDWB	202	94	52	42.8/65.9	0.8	0.46/1.16
SAW	272	98	-36	-54.8/-11.5	0.45	0.23/0.64
SKN	230	89	0	-13.6/11.9	1.55	1.2/1.9
SKN	104	108	-75	-79.08/-70.66	1.3	0.83/1.71
SPBG	182	93	15.5	1.11/36.8	1.15	0.88/1.47
SPCG	258	87	37	28.32/45.99	2.35	2.02/2.68
SPCR	181	89	-1	-9.7/6.23	1.7	1.4/2.085
SSN	207	91	-55	-65.2/-33.37	0.75	0.43/1.18
SSN	262	94	-48	-60.9/-33.85	0.75	0.45/0.97
SWD	289	101	45	26.8/60.3	0.75	0.6/0.9
SWD	107	89	-54	-63/-45	1.25	1.04/1.43
ALPI	262	94	-82	83.22/-62.53	0.62	0.44/0.77
ALPI	208	90	-43	-55.82/4.01	0.92	0.34/1.25
ALPI	286	102	-37	-49.2/-25	1.15	0.99/1.3
AVAL	104	91	-35	-45.2/-24.55	0.72	0.63/0.81
AVAL	286	102	-17	-34.2/-0.77	0.95	0.78/1.17
BIGB	283	102	-40	-50.36/-29.1	1.25	1.08/1.41
BIGB	203	94	-12	-29/8.3	1.04	0.78/1.31
BIGB	258	91	43	22.8/75.4	0.54	0.27/0.84
BING	103	92	-43	-52.36/-34.08	1.02	0.86/1.17
BING	285	101	-58	-65.41/-49.51	1.28	0.83/1.68
BLAK	287	102	-49	-72.5/-15.44	1.15	0.86/1.41
BLAK	260	93	-48	-72.54/-15.4	0.4	0.28/0.57
BYR	107	104	-40	-48.51/-29.2	0.75	0.58/0.9
BYR	208	90	-10	-22.47/5.4	0.75	0.58/0.9
BYR	263	93	51	32.18/71.93	1.05	0.89/1.24
BYR	285	101	-84	-75.63/83.98	1.05	0.73/1.3
CASW	104	92	-49	-57.42/-36.97	0.64	0.44/0.79
CASW	207	86	-45	-70.25/-21.5	1.66	1.5/1.89
CASW	286	101	-21	-39.23/-5.77	0.8	0.62/0.96
DEVL	105	90	1	-14.43/8.94	0.45	0.32/0.55
DEVL	205	95	14	-32.55/24.35	0.78	0.29/1.39
DEVL	260	93	21	9.72/36.8	0.55	0.35/0.74
DEVL	285	101	-36	-55.74/-11.34	0.6	0.4/0.84
DIVI	286	102	-40	-55.6/-7.5	0.7	0.5/0.9
HEAD	104	91	-44	-50.4/-37.4	0.98	0.9/1.06
HEAD	286	102	-43	-54.57/-28.76	1.1	0.89/1.36
HOLG	275	95	-27	-39.77/-14.76	0.75	0.57/0.9
HOLG	206	89	-39	-51.96/-12	0.75	0.44/1.04
HOLG	105	90	-54	-60.99/-46.42	0.9	0.77/1
HOPE	105	90	-16	-41.16/-1.04	0.4	0.31/0.5
HOPE	286	102	-36	-51.6/-18.8	0.95	0.74/1.1
HOPJ	287	101	-12	-26.85/-0.35	1.2	0.9/1.5
INDI	105	90	-43	-65.38/4.44	0.35	0.19/0.63

Table 3-2 continued…

INDI	286	102	-30	-44.61/-12.89	0.8	0.64/0.93
KASH	286	101	-18	-44.01/-0.2	0.8	0.49/1.13
KNIK	286	99	-28.75	-55.13/-29.06	1.14	0.86/1.29
KNIK	257	99	-44	35.22/-61.5	1.1	0.66/1.26
LSKI	260	92	39	18.55/61.13	0.7	0.54/0.85
LSUM	284	101	-18.9	-35.37/-2.2	0.89	0.68/1.09
LSUM	286	102	-22	-42.2/-5.9	0.85	0.65/1.05
MAIN	105	91	-20	-40.17/-1.46	0.52	0.37/0.68
MOOP	286	102	-43	-56.7/-27.1	0.85	0.65/1.04
NANC	288	100	-39	-53.7/-23.6	0.85	0.68/1.05
NSKI	203	95	-26	-40.72/-5.84	0.58	0.38/0.97
PERI	106	91	-34	-50.01/18.54	0.4	0.32/0.49
PERI	287	103	-56	-61.69/-50.55	1.82	1.52/2.12
PORT	287	102	-46	-66.04/-12.64	0.66	0.34/1.03
RUSS	204	95	16	-19/28	0.62	0.27/1.19
RUSS	263	93	80	-77.85/47.5	0.4	0.23/0.55
RUSS	286	102	-32	-58/-2.4	0.5	0.4/0.8
SNUG	286	102	-39	-57.32/-15.3	0.58	0.41/0.83
SOLD	103	92	-52	-64.47/-40.28	0.96	0.74/1.17
TUPA	263	95	-86	80.59/-73.74	1.12	0.85/1.33
TUPA	286	102	-48	-55.7/-38.25	1.15	0.87/1.46
USKI	105	91	-38	-49.12/-26.64	0.65	0.55/0.75
USKI	205	89	-40	-57.63/-2.48	0.7	0.4/1.15
USKI	258	90	39	26.5/59.4	0.78	0.54/0.98
USKI	286	102	-15	-27.83/-3.8	0.75	0.63/0.91
WHIT	227	102	-49	-55.55/-41.18	1.1	0.885/1.35
WHIT	105	91	-40	-53/-23	0.42	0.33/0.53
BMQ	259	94	40	34/49	1	0.7/1.33
CBM	268	94	47	31/66	0.65	0.45/0.85
CHS	255	94	31	22/41	1	0.76/1.2
CHS	295	94	-72	-76/-68	1.45	1.08/1.88
FRB	274	95	46	35/60	0.55	0.38/0.75
GBN	266	93	71	59/81	0.9	0.7/1.06
GTM	268	92	87	75/96	1.1	0.84/1.41
ICT	262	94	55	43/73	0.75	0.5/1.06
LMW	277	95	55	43/71	0.8	0.59/1.07
NOM	228	92	2	-10/10	0.8	0.45/1.21
PRB	260	95	62	52/76	0.85	0.64/1
RBY	264	94	71	47/80	1.45	1.02/1.75
SAG	262	93	37	32/43	0.8	0.61/0.98
TFS	258	94	47	37/58	0.65	0.48/0.87
WSM	264	94	46	39/55	1.35	0.97/1.77
YRT	271	95	56	40/72	0.75	0.49/1.03
AND	115	116	83	60/102	0.8	0.57/1.09
AND	208	96	-87	-101/-73	1.25	1.07/1.46

Table 3-2 continued…

AND	285	102	42	32/54	1.1	0.69/1.52
ANT	207	90	-9	-23/6	0.5	0.36/0.64
ANT	263	91	53	36/70	1.95	1.47/2.53
ANT	284	106	72	67/78	0.7	0.49/0.94
CAR	263	91	46	31/60	1.65	1.45/1.89
CAR	285	103	60	47/75	1.05	0.78/1.37
CZN	263	91	84	78/89	2.75	2.2/3.21
CZN	206	95	65	46/90	2.4	1.93/2.86
DH1	110	98	-57	-64/-36	0.85	0.37/1.32
DH1	208	92	21	12/29	0.75	0.49/0.99
DH1	265	93	27	20/35	1.1	0.99/1.23
DH1	293	97	38	29/46	0.9	0.73/1.04
DH2	263	92	10	-3/32	0.85	0.44/1.57
DH3	110	102	-72	-79/-68	1.2	0.74/1.52
DH3	207	96	42	37/48	1.15	0.83/1.42
DH3	268	97	-33	-49/-21	0.6	0.37/0.84
EFS	107	103	-81	-85/-77	2.12	1.68/2.5
EFS	206	91	60	49/73	0.6	0.45/0.75
EFS	269	95	46	35/58	1.85	1.6/2.15
FID	284	102	-69	-88/-77	1.3	1.09/1.72
GNR	207	92	-87	-99/-77	0.65	0.45/0.88
GNR	276	100	78	66/90	1.6	1.39/1.84
GOO	110	98	-41	-58/-15	1.05	0.67/1.59
GOO	207	89	-21	-47/13	0.7	0.32/0.85
GOO	272	98	48	37/59	1.15	0.93/1.35
HURN	108	104	-54	-63/-41	1.7	1.08/2.12
HURN	206	91	-27	-40/3	0.5	0.28/0.74
HURN	263	91	38	16/69	0.85	0.64/1.27
HURN	282	100	45	34/61	0.75	0.54/0.95
MCK	109	99	-8	-58/7	0.4	0.16/0.88
MCK	208	92	-83	-90/-76	0.85	0.68/1.01
MCK	272	97	52	37/67	1.95	1.66/2.21
MCK	300	91	80	71/88	1.52	1.32/1.71
MHR	112	107	-50	-56/-41	1.3	0.95/1.61
MHR	206	91	-40	-50/-27	0.85	0.52/1.12
MHR	265	96	7	-9/26	0.55	0.35/0.87
MHR	284	102	-83	-90/-76	1.75	1.34/2.14
NNA	107	106	76	62/90	1.7	1.35/2.09
NNA	206	94	87	69/104	1.45	1.13/1.9
NNA	273	97	48	32/67	1.7	1.27/2.11
PVE	208	91	-36	-49/-19	1.4	1.1/1.6
PVE	261	93	77	33/103	0.9	0.66/1.13
PVW	205	86	17	2/28	1.25	0.72/1.57
PVW	267	95	38	27/49	1.6	1.39/1.87
PYY	115	115	-35	-51/-21	1.28	0.98/1.64

Table 3-2 continued…

PYY	209	92	-22	-36/1	0.62	0.39/0.97
PYY	284	102	88	70/104	1.45	1.04/1.86
PYY	259	92	64	56/71	1.32	1.12/1.52
RCK	107	103	50	34/71	0.35	0.28/0.49
RCK	208	90	77	64/89	0.85	0.65/1.02
RCK	265	96	57	36/76	1.95	1.73/2.17
RND	109	100	-68	-74/-56	1.35	0.65/1.92
RND	212	89	25	19/36	1.05	0.4/1.71
RND	263	92	46	35/56	1.7	1.55/1.89
RND	283	104	49	42/57	1.05	0.91/1.24
RND	300	91	78	69/89	0.8	0.49/1.08
SAN	206	91	44	35/56	1.05	0.89/1.17
SAN	267	95	51	39/64	2.4	2.21/2.58
SBL	108	100	-79	-85/-75	1.6	1.06/2.02
SBL	205	87	22	15/29	1.5	1.38/1.58
SBL	260	91	50	32/70	2.15	1.7/2.54
SBL	283	103	73	59/89	1.05	0.74/1.52
SLM	264	93	48	35/62	1.8	1.51/2.12
SLM	285	103	74	59/92	1.2	0.88/1.54
SLT	262	94	43	25/61	1.75	1.59/1.92
SLT	285	102	24	13/38	2	1.63/2.33
SOB	115	115	-84	-95/-73	1.4	1.18/1.56
SOB	207	95	-75	-89/-66	0.8	0.63/0.95
SOB	262	91	71	55/86	2.15	1.81/2.59
TCE	206	91	-34	-49/-20	1.7	1.03/2
TCE	283	102	-62	-72/-36	0.85	0.27/1.39
TCE	259	92	37	23/53	0.85	0.7/0.99
TLKY	107	104	-54	-61/-46	0.9	0.66/1.09
TLKY	205	90	-21	-34/-8	1.3	0.96/1.67
TLKY	281	102	-18	-25/-12	0.85	0.72/0.93
TLKY	299	91	-8	-22/4	0.75	0.57/0.9
WOLF	207	88	-12	-26/4	0.75	0.61/0.85
WOLF	261	93	38	22/54	0.75	0.62/0.9
WON	109	104	49	38/67	0.9	0.63/1.18
WON	205	91	39	32/47	1.1	0.81/1.39
WON	266	94	39	30/49	2.2	1.94/2.45
YAN	110	99	-48	-61/-14	0.45	0.24/0.77
YAN	273	98	57	37/78	1.8	1.55/2.09

4. Discussion

Results from the MOOS and ARCTIC experiments represent two distinctly different and separate shear wave splitting provinces. Recently published results from the BEAAR (Broadband Experiment Across the Alaska Range) experiment serve to fill in the gap between MOOS and ARCTIC and allow us to extend the observations across Alaska in a north/south line. These combined results not only allow us to interpret the flow regime across the statewide transect, but also allow us to test hypotheses suggested by the BEAAR results. The combined results are shown in figure 4.1. It is clear from this figure that there are two dominant and perpendicular splitting directions across Alaska. These two regimes are separated by the subducting Pacific plate which forms the boundary between the two regimes. Fast directions north of the slab are parallel to the strike of the slab in the NE to SW direction, while fast directions south of the slab are in the direction of plate motion in the NW to SE direction. These two regimes will be discussed separately in the following sections.

4.1 North of the Subducted Pacific Plate

North of the subducting Pacific plate, fast directions are consistently NE/SW, parallel to the strike of the subducting plate (and trench). This direction is observed not only at stations above the mantle wedge, but north across Alaska to the Beaufort Sea. Christensen and Abers (2010) proposed that the results from the BEAAR experiment indicate along-strike flow in the mantle wedge. This conclusion was reached in part from the observation that splitting times increased with path length through the mantle wedge.

Path average delay times were plotted against ray path lengths in the wedge as measured from the top of the slab to the Moho; this assumes negligible mantle lithosphere in the overriding plate. A good correlation ($R^2 = 0.75$) was seen between the two parameters (figure 4.2). From this figure you can see that delay times have a clear linear relationship with the path length in the mantle wedge. Using this information Christensen and Abers (2010) calculate an apparent mantle wedge anisotropy of 7.9 ± 0.9% for a V_s= 4.4 km/s. The y intercept is small, 0.27 ± 0.15 s, indicating that the splitting in the wedge dominates the splitting measurements. The large splitting times seen above the mantle wedge decrease sharply for stations north of the mantle wedge, indicating a decrease in anisotropy and possibly flow (figure 4.3). The end of the mantle wedge was defined by Christensen and Abers (2010) as the farthest north extent of the slab as defined by the seismicity. In figure 4.3 the station AND represents the farthest north extent of the mantle wedge. The anisotropy value of 7.9 ± 0.9% is comparable to the value for the Ryukyu arc, which was calculated by Long and van der Hilst (2005) to be 10% in the wedge.

Splitting measurements above the mantle wedge at station SKN, as well as the Mt Spurr and Mt Redoubt stations, indicate that the fast directions remain parallel to the strike of the subducted slab along the contours of the subducted slab to the southwest. Along-strike flow in the mantle wedge may be generated by gradual flattening of the slab or perhaps due to edge effects from its proximity to the end of the Pacific plate.

While the fast directions are fairly consistent across all of northern Alaska, from the mantle wedge near the Alaska Range to the Arctic Ocean, the anisotropy may be explained by different processes. Continental lithosphere is generally too heterogeneous

to produce a coherent fast direction over large areas, and thus is not considered as a possible source of the observed anisotropy. This leaves two possible sources for the anisotropy seen in northern Alaska: either fossil lithosphere anisotropy or anisotropy from current asthenospheric flow. Fossil lithospheric anisotropy reflects frozen-in "fossil" strain in the sub-continental lithosphere due to vertically coherent deformation during the last major episode of tectonic activity (Silver 1996). Silver and Chan (1988, 1991) invoked fossil anisotropy to explain the fast direction observed at station COL in Fairbanks, Alaska. This conclusion was reached in part due to the similarity of the measured fast direction to the EW strike of the Denali fault and Alaska Range to the south, and the Tintina-Kaltag fault to the north. They further argued that the EW fast direction at COL is not in the direction of calculated APM (absolute plate motion). While fossil anisotropy is possible, Alaska was formed by a variety of tectonic processes including north-south collision in Arctic Alaska and accretion of many terranes from the south, which makes it unlikely that any fabric would be constant throughout the state, and thus, it is an unlikely explanation for the entire data set.

The second possible source for anisotropy in the stations north of the mantle wedge is asthenospheric flow in the direction of plate motion. In figure 4.4 absolute plate motion directions are plotted along with fast directions from the ARCTIC and northern BEAAR stations. Absolute plate motion of the North American plate in this region has an azimuth of 206 degrees (southwest), which was calculated from the NUVEL-1a plate motion model with no net rotation (DeMets et al., 1990). There is little to no relative movement between northern Alaska and stable North America (Freymueller et al., 2008).

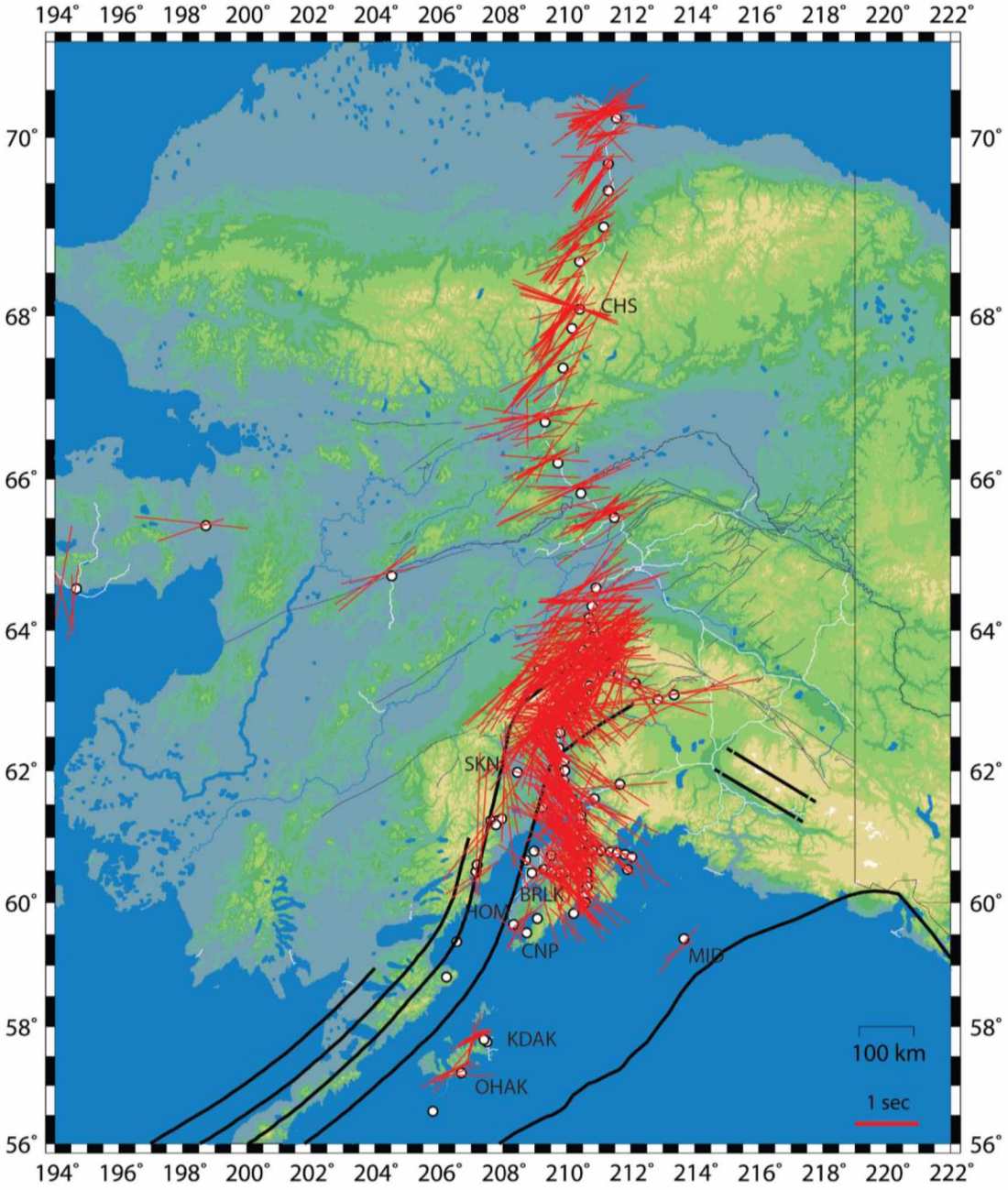

Figure 4.1: Map of all results from all networks.
This map shows the shear wave splitting results from all the networks, including the results from Christensen and Abers (2010). Wadati-Benioff zone contours are plotted at 0, 50, 100, and 150 km. Station names are stations mentioned in the text.

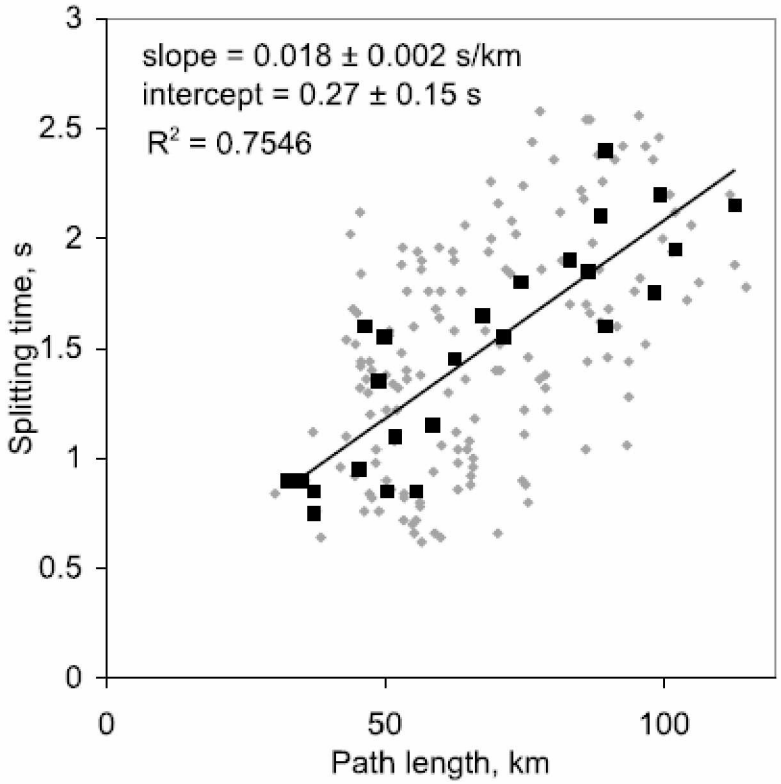

Figure 4.2: Splitting time vs. path length in the wedge.
This figure is from Christensen and Abers (2010). Splitting delay time versus path length within mantle wedge for paths that show slab-parallel fast directions. Path lengths calculated between slab surface and Moho. Black squares show delay times for path averages, and small gray diamonds show individual measurements. Line shows linear regression on path-averaged delay times.

This direction is approximately consistent with the fast directions observed in the Brooks Range and North Slope. The stations on the North Slope and Brooks Range have a more NNE to SSW fast direction. While the vectors do not exactly match, errors in the splitting directions and variability in the absolute plate motion vector from reference frame arguments (e.g. DeMets et al., 1990 and Gripp and Gordon, 2002) suggest a possible correlation.

The splitting observations can be interpreted to reflect regional flow in the approximately direction of North American plate motion for most of northern Alaska. As

seen in the ARCTIC results in figure 4.4, fast directions in the south of the network and the fast directions in the northern part of the BEAAR network (Christensen and Abers 2010) show fast directions along the strike of the subducting slab. The observation that fast directions seen in the mantle wedge persist north to the Brooks Range was unexpected. Computer modeling of the effect of the flat slab subduction and the edge of the slab on the mantle flow field, published by Jadamec and Billen (2010) includes some E-W flow as far north as Fairbanks and offers a possible explanation for this observation.

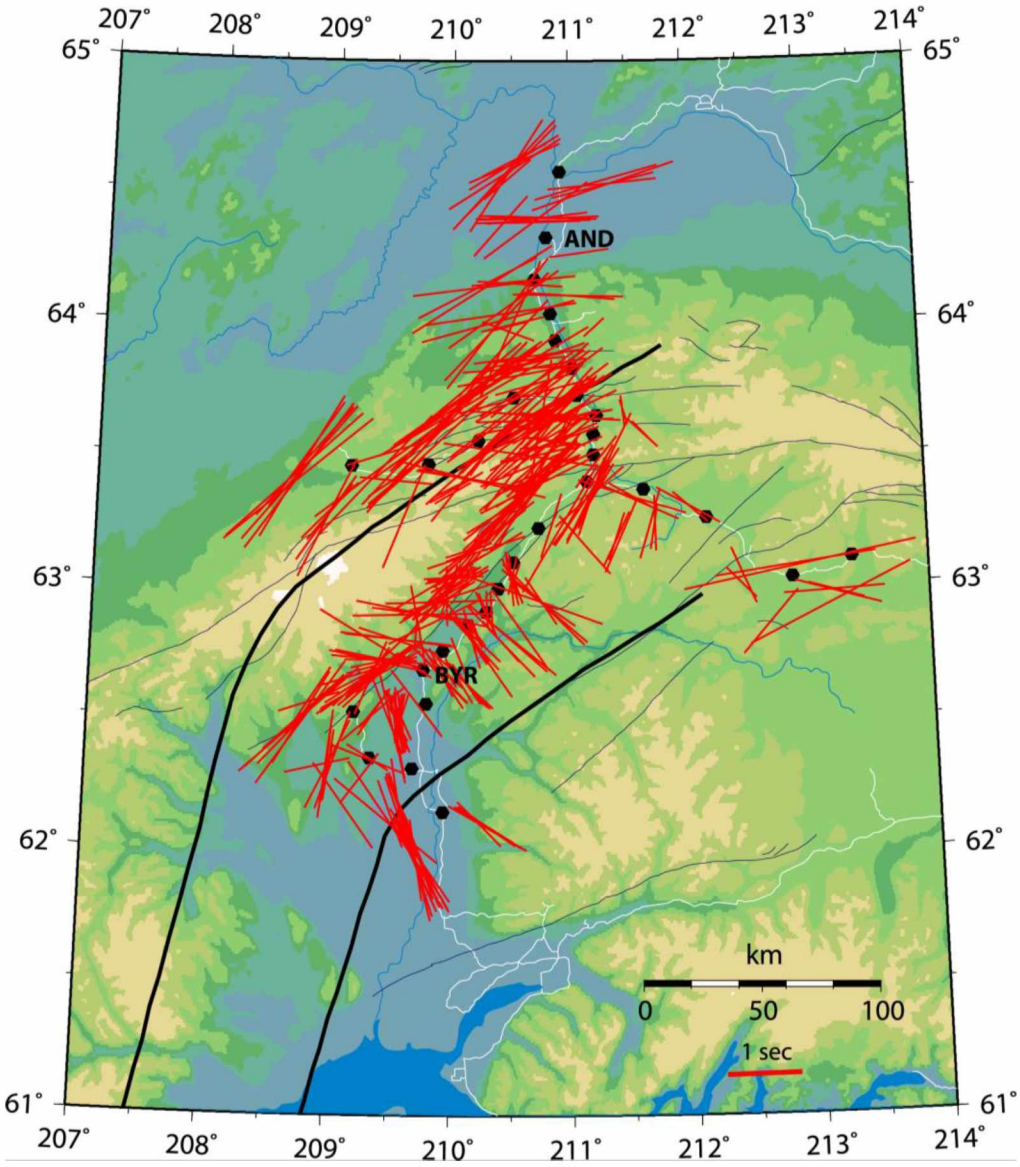

Figure 4.3: Results from the BEAAR network.
Results from the BEAAR network (Christensen and Abers, 2010). Results are plotted as a vector oriented in the fast direction with a length proportional to the delay time. Individual results are plotted at the 100 km projection of the ray. This is done to separate measurements by back-azimuth so any azimuthal dependence can be seen.

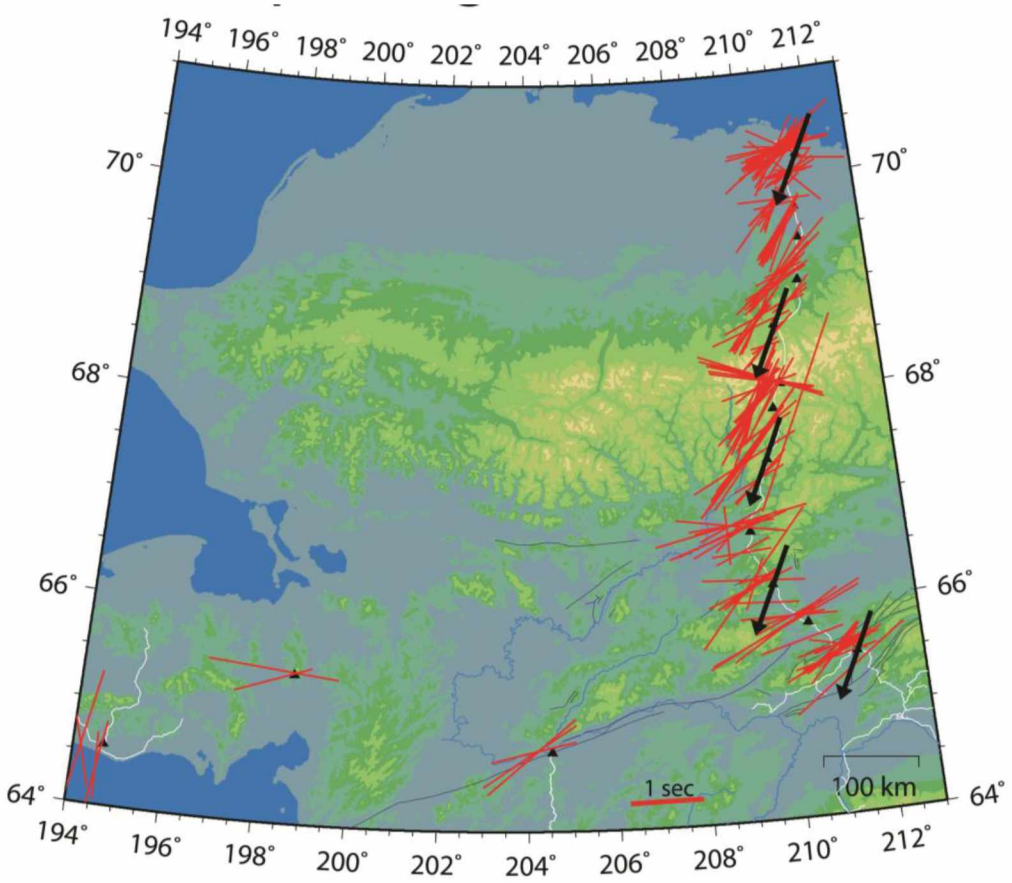

Figure 4.4: Map of ARCTIC results plotted with absolute plate motion vectors.
This map shows absolute plate motion vectors for North America plotted along with the ARCTIC results for several stations. Each vector was individually calculated for the station location where it is plotted, and has an arbitrary length.

4.2 South of the Subducted Pacific Plate

South of the 70 km contour of the subducting Pacific plate, fast directions are generally trench perpendicular, in the direction of Pacific plate motion. Christensen and Abers (2010) noted the occurrence of trench perpendicular fast directions in the BEAAR data for stations directly above the thin cold nose of the mantle wedge. This region of the mantle wedge may have the proper conditions for b-type lattice preferred orientation (LPO), with fast splitting directions perpendicular to the flow direction (Jung and Karato, 2001; Mizukami et al., 2004; Katayama and Karato, 2006; Karato et al., 2008; Kneller et al., 2005, 2008). While this argument can be used to explain the 90 degree change in fast direction, Christensen and Abers (2010) argued against this explanation due to the fact that it was unlikely that the thin mantle wedge could produce the delay times observed. The region of the mantle wedge below the southern BEAAR stations is only 10-30 km thick, and even with the unreasonably high 10% anisotropy, this thickness could only produce 0.2-0.7 sec of splitting, less than the 1-1.7 sec seen in this region. The MOOS results confirm that these fast directions continue south, outside of the region where the mantle wedge exists, and thus substantiates the conclusion that these fast directions are not due to b-type fabric in the mantle wedge.

Anisotropy south of the subducting Pacific plate must then be related to either fossil anisotropy within the subducting plate (including the subducted Yakutat terrane) or from asthenospheric flow beneath the plate. The oceanic plate is not usually cited as a location of significant splitting. Normal oceanic crust has 2-3% anisotropy (Shearer and

Orcutt, 1986) and would not be considered thick enough to produce 1 sec of delay times. However, in Alaska the slab is thicker and is not just oceanic crust.

As stated previously, in this region the Yakutat block is being partially accreted and subducted. The subducted Yakutat block crust is 20-30 km thick near the trench (Christeson et al., 2010) and is subducted to 130km with a thickness of 11-22 km (Ferris et al., 2003; Rossi et al., 2006; Rondenay et al., 2008). There is some controversy as to the exact structure of the Yakutat block. There are two cross sections published, one with the Yakutat block sitting on top of a Pacific plate basement (Fuis et al., 2008), and the second with the Yakutat block as a thick oceanic plateau without Pacific plate basement (Christeson et al., 2010).

The Yakutat block basement was formed at ~50 Ma (Christeson et al., 2010) and, assuming that the Yakutat block has no Pacific plate basement (Christeson et al., 2010), the block would have a 50 km mantle lithosphere under the 11-22 km of crust, based on the cooling relationship between thickness of oceanic lithosphere and time. Assuming vertically coherent anisotropy, the effective anisotropic thickness is ~60-70 km. Using the equation from Wolfe and Solomon (1998) $\delta t = L\frac{\delta\beta}{\beta_0}$, where δt is the delay time, β_0 is the isotropic averaged shear wave velocity, $\delta\beta$ is a dimensionless anisotropy value, and 100* $\delta\beta$ is the percent anisotropy, the percent anisotropy required for 1 sec of splitting in this layer can be calculated. Using the P-wave velocities from Christeson et al. (2010), and the relationship of $V_s = \frac{1}{\sqrt{3}}V_p$ between P wave velocity and S wave velocity, ~6% anisotropy would be able to produce the delay times of around 1 sec that

are seen in the data. This model, in which splitting is due to anisotropy in the Yakutat block, has several inherent assumptions which may or may not be true. The first assumption is that the Pacific plate basement does not underlie the Yakutat block, which is not clear based on the two seismic profiles recently published (Christeson et al., 2010 and Fuis et al., 2008). The second is that there is vertically coherent anisotropy in one direction throughout the entire 70 km lithosphere of the block. If either of these assumptions is false, then this model cannot be used to explain the data. For example, a 20 km thick anisotropic layer requires 20% anisotropy to produce the 1 second splitting seen, which is greater than the single-crystal anisotropy of olivine at 18%, and unreasonable.

Unlike the stations on the central and eastern Kenai Peninsula, which show fast directions that are trench normal, data from the outlying areas not underlain by the Yakutat block show fast directions parallel to the strike of the subducting slab. The data from these other stations can be used to test if the anisotropy is within the Yakutat block. If the subducted Yakutat block is the source of the observed anisotropy, stations located outside the Yakutat block might show substantially different fast directions. In fact, most of the stations located off of the subducted Yakutat block have fast directions, parallel to the trench. These include stations on Kodiak Island, western Kenai Peninsula, and Middleton Island. Middleton Island (MID) is not above the Yakutat block (Fuis et al., 2008) and while data return at this station was low, it shows a trench-parallel fast direction from two observations. The Kodiak Island stations also show trench-parallel fast directions and have slightly lower delay times (around 0.7 sec). Stations located in

western Kenai Peninsula show a change in character from the other Kenai Peninsula stations. The stations HOM, CNP and BRLK, located in southwestern Kenai Peninsula, have trench-parallel fast directions. The stations in northwestern Kenai Peninsula have a low data recovery. These results are more varied in direction than the rest of the Kenai Peninsula data set, but do show trench-parallel fast directions as well. In a model that includes anisotropy in the Yakutat block, the observed fast directions require two sources of anisotropy: trench-normal fossil anisotropy within the subducted Yakutat block with a fast direction that just happens to be in the direction of convergence, underlain by trench-parallel flow in the sub-slab mantle.

If the trench-normal anisotropy is not related to the subduction of the Yakutat block, then it must originate from mantle flow beneath the Pacific plate. Christensen and Abers (2010) preferred this model as an explanation for their trench-normal fast directions. The fact that the fast directions are in the general direction of plate motion tends to support this hypothesis. In addition, the flattening of the slab in this region may help to entrain flow in the direction of slab flattening. Trench-parallel fast directions located away from the region of flat slab subduction would indicate a complex mantle flow field that changes direction over short distances. Trench-parallel fast directions in the Kodiak Islands region would indicate along-trench flow. The transition into flow in the direction of plate motion in the flat slab portion of the subduction zone system, would occur in the relatively small area of Cook Inlet and western Kenai Peninsula. The trench-parallel fast direction of Middleton Island would seem to indicate that the plate-motion fast directions are confined to the region of flab slab subduction of the Yakutat block. At

this time, the data are insufficient to determine if the anisotropy is due to a complex flow field due to the flattening of the subduction zone or to two layers of anisotropy: fossil anisotropy in the subducted Yakutat block and trench-parallel sub-slab mantle flow.

4.3 Global model and comparisons to other subduction zones

The global model, developed by Long and Silver (2008), provides a base model to which we can compare our results. Long and Silver (2008) took a global data set of subduction zone splitting measurements and looked for correlation with various subduction zone parameters. They separated their data set into observations of splitting in the mantle wedge and sub-slab mantle.

For the mantle wedge, a simple 2D corner flow model would produce flow in the direction of subduction, driven by entrained flow. This model would imply an increase in anisotropy, and thus delay times, with increased convergence velocity and slab dip. However, Long and Silver (2008) did not see a correlation between these parameters and the delay time. Also, fast directions observed in the mantle wedge data set were both trench-normal and trench-parallel. Several other parameters were compared to the splitting parameters, and the only correlation seen was between delay time and trench migration rate, normalized by convergence rate (V_{norm}). This was defined as the absolute value of the trench migration rate relative to the mantle, over the convergence rate of the subduction zone. This value measures the importance of the migration of the trench (or slab) relative to the convergence of the two plates. When trench migration dominates, splitting is due to flow parallel to the trench, producing trench-parallel fast directions, and when convergence dominates, splitting is due to corner flow and fast directions are

normal to the trench. If V_{norm} is less than ~0.2, then the system is dominated by convergence and the flow is due to corner flow producing trench-normal fast direction and increased delay times. If V_{norm} is greater than 0.6, then the system is dominated by trench migration, the delay times are increased, and the fast direction is trench-parallel. Between these two populations, delay times are very low, and splitting is thought to be minimal or not present due to a lack of a coherent flow field.

Rondenay et al. (2010) calculated V_{norm} for Alaska as a range from 0.3 to 0.65. This was based on the range of dates proposed for the initiation of subduction of the Yakutat block, which was considered to be between 12 Ma and 5.6 Ma. Based on these results, central Alaska is dominated by trench migration, and the expected flow direction is trench-parallel. This is the flow direction seen in the BEAAR network in the mantle wedge (Christensen and Abers, 2010). Along-strike flow in the mantle wedge has also been seen in the Aleutian subduction zone by Yang et al. (1995), who studied local splitting in the Shumagin Islands segment of the Aleutian-Alaska subduction zone. In this section of the subduction zone, the plate convergence is almost perfectly normal to the trench and it has a rate of 62 mm/yr. This section is also the transition from ocean-continent subduction to ocean-ocean subduction. The majority of the fast directions are trench-parallel and the splitting in the Shumagin Islands was interpreted as anisotropy in the mantle wedge. These results are consistent with the model of trench-parallel fast directions in the mantle wedge, and these results were included in Long and Silver (2008).

Long and Silver (2008) also examined the sub-slab splitting dataset. First they tested the idea that the splitting near the trench was due to anisotropy within the slab. Delay times would then be expected to increase with increasing age, and therefore thickness of the oceanic plate, and fast directions would be parallel to transform faults in the plate. This trend was not seen by Long and Silver (2008), eliminating the slab from consideration.

In the sub-slab mantle the classic model for flow from plate tectonics implies entrained flow below the slab, which would produce trench-normal fast directions. However, in the global database the sub-slab measurements were dominantly trench-parallel (Long and Silver, 2008), with the major exception being Cascadia. Long and Silver (2008) observed that there was a strong correlation between trench migration rates and delay times for the sub-slab mantle. They concluded that flow in the sub-slab mantle is due to flow parallel to the slab that is induced by trench migration. Subduction systems with high trench migration rates showed larger delay time (Tonga and Calabria), and systems with little to no migration had low delay time (Aleutians and Ryukyu). Long and Silver (2008) concluded that this result implies that there is a barrier to entrained flow at the top or base of the mantle transition zone, and the migration of the trench relative to the mantle forces material around the slab edge and along the arc.

The empirical relationship between the absolute value of trench migration is linear and yielded an equation to predict delay times based on absolute trench migration relative to the mantle, where $\partial t = 0.026(|V_T|) + 0.17$. This equation can be used to predict the expected delay times for south central Alaska. Using the results from

Rondenay et al. (2010), with a trench migration rate of 17mm/yr or 36 mm/yr, the predicted flow field would be trench-parallel fast directions for the majority of the stations and a delay time range of 0.612 seconds to 1.106 seconds. This is in good agreement with the delay times measured in the network. However, the fast directions for the majority of the stations are not trench parallel, but trench perpendicular. Thus, this model does not hold for the bulk of stations located in the region that sample the sub-slab mantle. The magnitude of delay times calculated also agrees with the stations on Kodiak Island, which do have trench-parallel fast directions, but this calculation does not apply to this subset of data. The calculations used for southern Alaska are based on the trench migration due to the subduction of the Yakutat block, which has little to no effect on the Kodiak section of the subduction zone.

5. Conclusion: Final model for Splitting Observations in Alaska

The Alaska dataset covers three distinct regions that I interpret to be dominated by different processes. The models and interpretations offered by Long and Silver (2008) and Christensen and Abers (2010) serve as a starting point in the development of a model to explain the Alaska SKS wave splitting data set. Christensen and Abers (2010) observed fast directions that are parallel to the strike of the slab above the mantle wedge, and interpreted these to reflect trench-parallel flow in the mantle wedge. Their results are in agreement with the Long and Silver (2008) global model for anisotropy in subduction zones. This segment of the Aleutian-Alaska subduction zone is dominated by trench (or slab) migration due to the subduction of the Yakutat block, and according to the model

this should produce trench-parallel fast directions in the mantle wedge, which are indeed present in the data set.

North of the mantle wedge, delay times drop slightly and fast directions remain in the same orientation until the line crosses into the Brooks Range where the fast directions are a more NNE/SSW direction. This is consistent with the direction of absolute plate motion in northern Alaska. Splitting observations in northern Alaska are therefore interpreted as flow in the mantle, transitioning from flow along strike with the subducting plate in the mantle wedge, to flow in the direction of absolute plate motion, with a region between the mantle wedge and the Brooks Range where orientation of the fast directions remains the same as in the wedge, but delay times decrease in magnitude.

South of the mantle wedge, the dominant fast direction is in the direction of plate motion (trench-normal), however, there is a secondary trench-parallel fast direction seen in the western Kenai Peninsula, Kodiak Island and Middleton Island. Any interpretation would have to be able to explain both of these observations. The simple relationship between trench migration rate and delay time proposed by Long and Silver (2008) predicts trench-parallel flow in south-central Alaska with delay times around 1 second. While the magnitude of splitting is in agreement, the direction (at least for the dominant fast direction) is not. For these results, two interpretations will be considered. One is a two-source model in which the trench-normal fast directions are due to anisotropy in the Yakutat block, and the second source is the predicted trench-parallel flow in the sub-slab mantle (figure 5.1). The second interpretation is that all splitting is due to sub-slab mantle

flow, complicated by the processes of shallowing of the subduction zone and the proximity of the slab edge to the east (figure 5.2).

The interpretation of the Yakutat block as the source of anisotropy has several implications for the pattern of shear wave splitting observations expected. In this interpretation, fast directions measured over the Yakutat block are a result of anisotropy within the block, and fast directions measured off of the block are due to mantle flow below the slab. Normally, the slab is oceanic crust and is not thick enough to be a significant contributor to splitting observations. However, in this case, the slab is the Yakutat block, and with its greater thickness it must be considered as a possible source. In this model, sub-slab mantle flow would be considered to be trench-parallel throughout the region.

This interpretation explains the two fast directions observed in different places. The stations on western Kenai Peninsula show trench-parallel fast directions along with Kodiak Island and Middleton Island. Another strong piece of evidence for this interpretation is the station on Middleton Island (MID). This island is thought to be on Pacific plate oceanic crust and not to be underlain by the Yakutat block. There was low data recovery from this station, possibly due to ocean noise, and there are only 2 results. However, this station shows a trench-parallel fast direction, which in this interpretation would be due to trench-parallel flow in the sub-slab mantle.

The major problem with this interpretation is low data recovery in key locations. The station HOLG was thought to be on the edge of the Yakutat block, if not off of the block. This station had a consistent trench-normal fast direction. Stations that are known

to be off of the Yakutat block (HOM, CNP, BRLK) had low data recovery, as well as the stations in the Cook Inlet and Middleton Island. In order to determine if this interpretation is optimal for the region, greater data coverage is needed in this key area, where subduction changes from Yakutat block subduction to normal slab subduction. The fundamental problem with this interpretation is that it assumes that the Yakutat block is homogenous enough, and anisotropic enough, to produce 1 second splitting times. Assuming the entire 70 km lithosphere is anisotropic in the same direction, the Yakutat block would have to be 6% anisotropic to produce a 1 second delay time. Direct measurements of anisotropy within the slab would be needed to confirm if this was a realistic value.

Sub-slab flow in the asthenosphere is the second interpretation. In this interpretation, flow beneath the subducting Pacific plate and Yakutat block is responsible for all of the splitting seen. The different fast directions represent changes in flow below the plate. The sub-slab flow changes from trench-parallel near Kodiak Island to entrained flow below the slab in the direction of plate motion in the eastern Kenai Peninsula and Prince William Sound region. This flow could be due to the gradual shallowing of the subducting slab with time as the Yakutat block is subducted.

The major problem with this interpretation is the sharp transition from trench-parallel to trench-normal in the Cook Inlet – Kenai Peninsula region. Regional flow in the sub-slab could then be considered to be trench-parallel for the entire subduction system, except in the regions of flat slab subduction and the edge of the plate, where flow is being entrained.

At this time, it is not possible to distinguish between these two models. It is possible that the true source of anisotropy is a combination of these two models. Despite this drawback, a model of flow for a transect across the state of Alaska has emerged from this study. North of the mantle wedge, flow is in the direction of absolute plate motion, which rotates into trench-parallel flow in the mantle wedge, caused by trench migration relative to the mantle, and south of the wedge, fast directions are either due to flow below the slab or anisotropy within the slab itself.

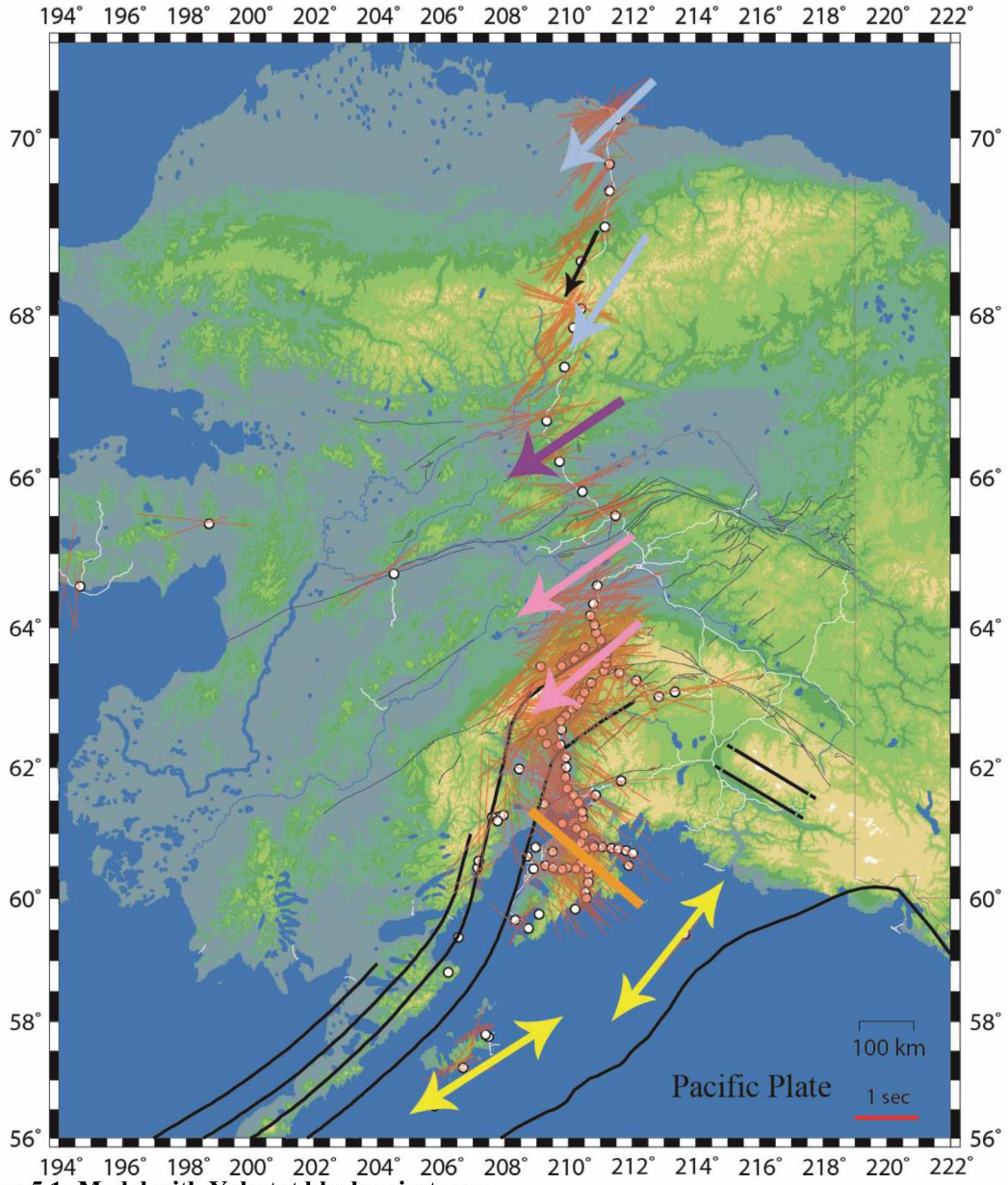

Figure 5.1: Model with Yakutat block anisotropy.
In this figure, the model of flow in Alaska includes trench-parallel flow as well as fossil anisotropy in the Yakutat block. Large arrows represent constrained flow directions (based on fast direction measurements). Solid lines represent fossil anisotropy (based on fast direction measurements). The yellow arrows represent sub-slab flow below the Yakutat block and Pacific plate. This model includes two anisotropic sources in south central Alaska: sub-slab flow is trench parallel (yellow), and the Yakuat block has a fossil anisotropy (orange). To the north, in the mantle wedge, flow is along strike with the slab (pink). Farther north, regional flow is in the direction of absolute plate motion (blue). The black arrow represents the absolute plate motion direction for North America calculated at that point. The purple arrow represents the area of transition between the two flow fields, with the same fast direction as the mantle wedge, but smaller delay times. Flow direction in the far north is inferred from the plate motion direction. This inference is also used in the mantle wedge, assuming a gradient from the plate motion direction to that of along strike.

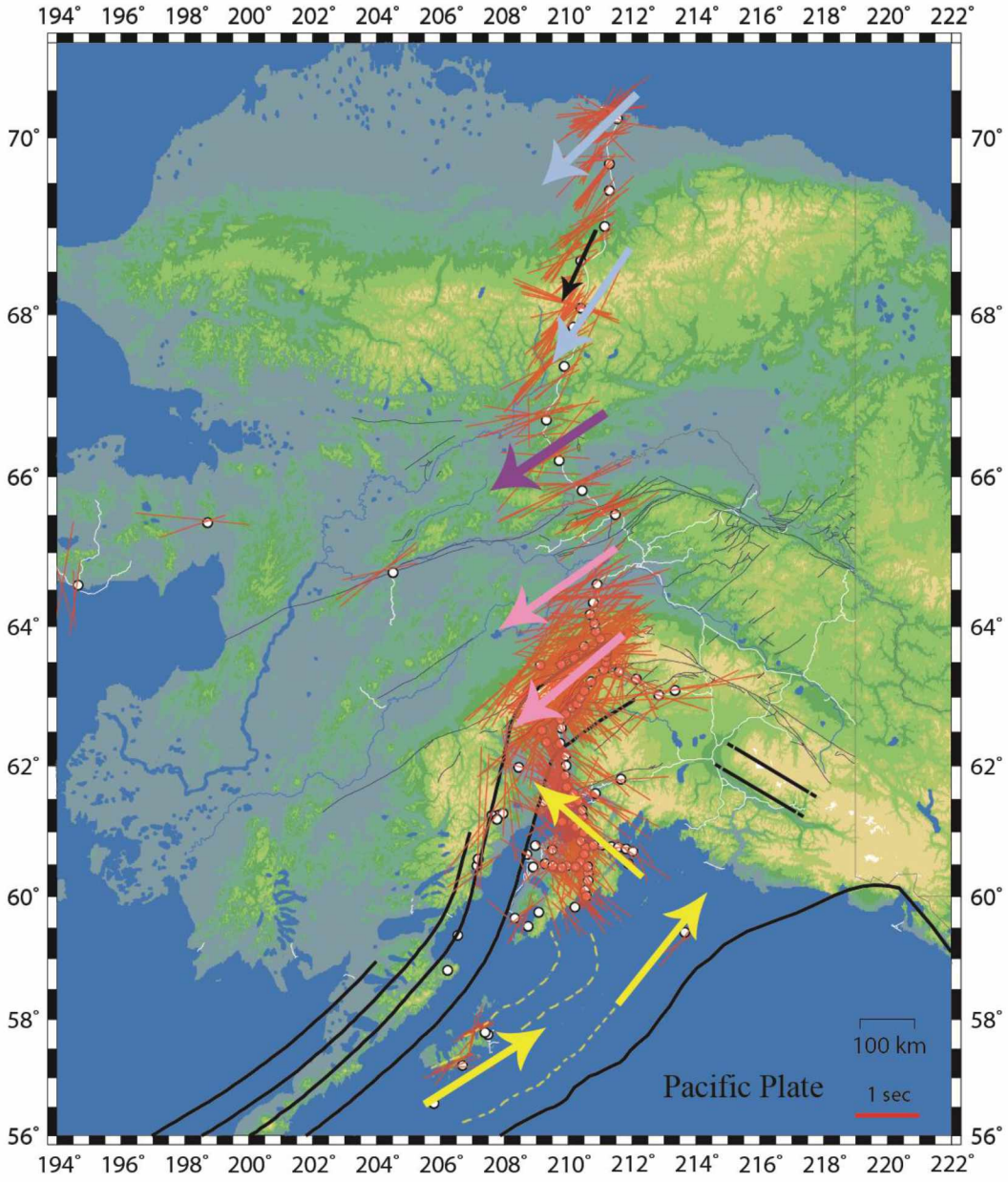

Figure 5.2: Model with entrained flow under the slab
In this figure, the model of flow in Alaska includes an entrained flow field in south central Alaska. Large arrows are constrained flow directions (based on fast direction measurements) and dashed lines are inferred flow lines. In this model, the sub-slab flow is entrained and changes from trench parallel to trench normal in the region of flat slab subduction (yellow). The direction of the sub-slab flow is inferred from entrainment. North, in the mantle wedge, flow is along strike with the slab (pink). North of this regional flow is in the direction of absolute plate motion (blue). The black arrow represents the absolute plate motion direction for North America calculated at that point. The purple arrow represents the area of transition between the two flow fields, with the same fast direction as the mantle wedge, but smaller delay times. Flow direction for the far north is inferred from the plate motion direction. This inference is also used in the mantle wedge, assuming a gradient from the plate motion direction to that of along strike.

References:

Bellesiles, A. K., Christensen, D. H., Entwistle, E., Litherland, M., Abers, G. A., and Song, X., 2009, Shear-wave splitting observations of mantle anisotropy beneath Alaska: AGU Fall Meeting Abstracts, p. B1812+.

Bird, K. J., and Molenaar, C. M., 1992, The North Slope foreland basin, Alaska, in Macqueen, R. W., and Leckie, D. A., eds., Foreland basins and fold belts: Tulsa, OK, United States (USA), American Association of Petroleum Geologists, p. 363-393.

Bruns, T. R., 1983, Model for the origin of the Yakutat block, an accreting terrane in the northern Gulf of Alaska: Geology, v. 11, no. 12, p. 718-721.

Christensen, D. H., and Abers, G. A., 2010, Seismic anisotropy under central Alaska from SKS splitting observations: Journal of Geophysical Research, v. 115, no. B04315, p. 12.

Christeson, G. L., Gulick, S. P. S., Avendonk, H. J. A. v., Worthington, L. L., Reece, R. S., and Pavlis, T. L., 2010, The Yakutat terrane: Dramatic change in crustal thickness across the Transition fault, Alaska: Geology, v. 38, no. 10, p. 895-898.

DeMets, C., Gordon, R. G., Argus, D. F., and Stein, S., 1990, Current plate motions: Geophysical Journal International, v. 101, no. 2, p. 425-478.

Doser, D. I., and Veilleux, A. M., 2009, A Comprehensive Study of the Seismicity of the Kenai Peninsula-Cook Inlet Region, South-Central Alaska: Bulletin of the Seismological Society of America, v. 99, no. 4, p. 2208-2222.

Eberhart-Phillips, D., Christensen, D.H., Brocher, T.M., Hansen, R., Ruppert, N.A., Haeussler, P.J. and Abers, G.A., 2006. Imaging the transition from Aleutian subduction to Yakutat collision in central Alaska, with local earthquakes and active source data, Journal of Geophysical Research, 111, B11303.

Ferris, A., Abers, G. A., Christensen, D. H., and Veenstra, E., 2003, High resolution image of the subducted Pacific (?) plate beneath central Alaska, 50-150 km depth: Earth and Planetary Science Letters, v. 214, no. 3-4, p. 575-588.

Fischer, K. M., Fouch, M. J., Weins, D. A., and Boettcher, M. S., 1998, Anisotropy and flow in Pacific subduction zone back-arcs: Pure and Applied Geophysics, v. 151, p. 463-475.

Fischer, K. M., Parmentier, E. M., Stine, A. R., and Wolf, E. R., 2000, Modeling anisotropy and plate-driven flow in the Tonga subduction zone back arc: Journal of Geophysical Research, v. 105, no. B7, p. 16181-16191.

Fletcher, H. J., and Freymueller, J. T., 1999, New GPS constraints on the motion of the Yakutat block: Geophysical Research Letters, v. 26, no. 19, p. 3029-3032.

Fouch, M. J., and Rondenay, S., 2006, Seismic anisotropy beneath stable continental interiors: Physics of the Earth and Planetary Interiors, v. 158, no. 2-4, p. 292-320.

Freymueller, J.T., Cohen, S.C., Cross, R., Elliott, J., Fletcher, H.J., Larsen, C., Hreinsd´ottir, S. and Zweck, C., 2008. Active deformation processes in alaska, based on 15 years of gps measurements. in Active Tectonics and Seismic Potential of Alaska ed. Jeffrey T. Freymueller, P. J. H., Robert L. Wesson, Göran Ekström. American Geophysical Union.

Fuis, G. S., Moore, T. E., Plafker, G., Brocher, T. M., Fisher, M. A., Mooney, W. D., Nokleberg, W. J., Page, R. A., Beaudoin, B. C., Christensen, N. I., Levander, A. R., Lutter, W. J., Saltus, R. W., and Ruppert, N. A., 2008, Trans-Alaska Crustal Transect and continental evolution involving subduction underplating and synchronous foreland thrusting: Geology, v. 36, no. 3, p. 267-270.

Gripp, A.E. and Gordon, R.G., 2002. Young tracks of hotspots and current plate velocities, Geophysical Journal International, 150, 321-361.

Gutscher, M.-A., and Peacock, S. M., 2003, Thermal models of flat subduction and the rupture zone of great subduction earthquakes: Journal of Geophysical Research, v. 108, no. B1, p. 2009.

Hall, C. E., Fischer, K. M., Parmentier, E. M., and Blackman, D. K., 2000, The influence of plate motions on three-dimensional back arc mantle flow and shear wave splitting: Journal of Geophysical Research, v. 105, no. B12, p. 28009-28033.

Hartz, J. D., Kremer, M. C., Krouskop, D. L., Silliphant, L. J., Houle, J. A., Anderson P.C., and LePain, D. L., 2009, Preliminary engineering and geological evaluation of remaining Cook Inlet gas reserves: Alaska Division of Oil and Gas report, in Decker, P. L., ed., available online at: http://www.dog.dnr.state.ak.us/oil/, p. 37.

Ismail, W. B., and Mainprice, D., 1998, An olivine fabric database: an overview of upper mantle fabrics and seismic anisotropy: Tectonophysics, v. 296, p. 145-157.

Jadamec, M.A., and Billen, M.I., 2010, Reconciling surface plate motions with rapid three-dimensional mantle flow around a slab edge: Nature, v. 465, p. 338-341.

Johnson, J. M., Satake, K., Holdahl, S. R., and Sauber, J., 1996, The 1964 Prince William Sound earthquake: Joint inversion of tsunami and geodetic data: Journal of Geophysical Research, v. 101, no. B1, p. 523-532.

Jung, H., and Karato, S., 2001, Water-induced fabric transitions in olivine Science, v. 293, p. 1460-1463.

Karato, S., Jung, H., Katayama, I., and Skemer, P., 2008, Geodynamic significance of seismic anisotropy of the upper mantle: New insights from laboratory studies: Annual Review of Earth and Planetary Sciences, v. 36, p. 59-95.

Katayama, I., and Karato, S., 2006, Effect of temperature on the B- to C-type olivine fabric transition and implication for flow pattern in subduction zones: Physics of the Earth and Planetary Interiors, v. 157, no. 1-2, p. 33-45.

Kneller, E. A., Long, M. D., and van Keken, P. E., 2008, Olivine fabric transitions and shear wave anisotropy in the Ryukyu subduction system: Earth and Planetary Science Letters, v. 268, no. 3-4, p. 268-282.

Kneller, E. A., and van Keken, P. E., 2007, Trench-parallel flow and seismic anisotropy in the Mariana and Andrea subduction systems: Nature, v. 450, p. 1222-1226.

Kneller, E. A., van Keken, P. E., Karato, S., and Park, J., 2005, B-type olivine fabric in the mantle wedge: Insights from high-resolution non-Newtonian subduction zone models: Earth and Planetary Science Letters, v. 237, no. 3-4, p. 781-797.

Lahr, J. C., and Plafker, G., 1980, Holocene Pacific-North American plate interaction in southern Alaska: Implications for the Yakataga seismic gap: Geology, v. 8, no. 10, p. 483-486.

Litherland, M., Christensen, D., and Song, X., 2007, Mantle Anisotropy in Northern Alaska: Analysis of ARCTIC Seismic Data Using Shear Wave Splitting: AGU Fall Meeting Abstracts.

Long, M. D., Gao, H., Klaus, A., Wagner, L. S., Fouch, M. J., James, D. E., and Humphreys, E., 2009, Shear wave splitting and the pattern of mantle flow beneath eastern Oregon: Earth and Planetary Science Letters, v. 288, no. 3-4, p. 359-369.

Long, M. D., Hager, B. H., De Hoop, M. V., and Van Der Hilst, R. D., 2007, Two-dimensional modeling of subduction zone anisotropy with application to southwestern Japan: Geophysical Journal International, v. 170, no. 2, p. 839-856.

Long, M. D., and Silver, P., 2008, The Subduction Zone Flow Field from Seismic Anisotropy: A Global View: Science, v. 319, no. 18 January 2008, p. 315-318.

Long, M. D., and Silver, P. G., 2009, Shear Wave Splitting and Mantle Anisotropy: Measurements, Interpretations, and New Directions: Surveys in Geophysics, v. 30, no. 4-5, p. 407-461.

Long, M. D., and Van der Hilst, R. D., 2005, Estimating Shear-Wave Splitting Parameters from Broadband Recordings in Japan: A Comparison of Three Methods: Bulletin of the Seismological Society of America, v. 95, no. 4, p. 1346-1358.

Mainprice, D., 2007, Seismic anisotropy of the deep Earth from a mineral and rock physics perspective, in Schubert, G., ed., Treatise on Geophysics: Oxford, Elsevier, p. 437-492.

Meade, C., Silver, P. G., and Kaneshima, S., 1995, Laboratory and seismological observations of lower mantle isotropy: Geophysical Research Letters, v. 22, no. 10, p. 1293-1296.

Mizukami, T., Wallis, S. R., and Yamamoto, J., 2004, Natural examples of olivine lattice preferred orientation patterns with a flow normal a-axis maximum: Nature, v. 427, no. 6973, p. 432-436.

Moore, T. E., Wallace, W. K., Bird, K. J., Karl, S. M., Mull, C. G., and Dillon, J. T., 1994, Chapter 3: Geology of northern Alaska, in Plafker, G., and Berg, H. C., eds., The geology of Alaska: The Geology of North America: Boulder, Colorado, Geological Society of America, p. 49-140.

Naugler, F. P., and Wageman, J. M., 1973, Gulf of Alaska: Magnetic Anomalies, Fracture Zones, and Plate Interaction: Geological Society of America Bulletin, v. 84, no. 5, p. 1575-1584.

Nicholas, A., and Christensen, N. I., 1987, Formation of anisotropy in upper mantle peridotites - A review, in Fuchse, K., and Froidevaux, C., eds., Compositions, structure and dynamics of the lithosphere - asthenosphere system, Geodynamics series, Volume 16: Washington, D.C., American Geophysical Union.

Niu, F., and Perez, A. M., 2004, Seismic anisotropy in the lower mantle: A comparison of waveform splitting of SKS and SKKS: Geophysical Research Letters, v. 31, no. 24, p. L24612.

Oleskevich, D. A., Hyndman, R. D., and Wang, K., 1999, The updip and downdip limits to great subduction earthquakes: Thermal and structural models of Cascadia, south Alaska, SW Japan, and Chile: Journal of Geophysical Research, v. 104, no. B7, p. 14965-14991.

Page, R. A., Stephens, C. D., and Lahr, J. C., 1989, Seismicity of the Wrangell and Aleutian Wadati-Benioff Zones and the North American Plate Along the Trans-Alaska Crustal Transect, Chugach Mountains and Copper River Basin, Southern Alaska: Journal of Geophysical Research, v. 94, no. B11, p. 16059-16082.

Plafker, G. and Berg, H.C., 1994. Overview of the geology and tectonic evolution of Alaska, edn, Vol., pp. Pages, Geological Society of America, Boulder, CO.

Ratchkovski, N. A., and Hansen, R. A., 2002, New Evidence for Segmentation of the Alaska Subduction Zone: Bulletin of the Seismological Society of America, v. 92, no. 5, p. 1754-1765.

Restivo, A., and Helffrich, G., 2006, Core–mantle boundary structure investigated using SKS and SKKS polarization anomalies: Geophysical Journal International, v. 165, no. 1, p. 288-302.

Rondenay, S., Abers, G. A., and van Keken, P. E., 2008, Seismic imaging of subduction zone metamorphism: Geology, v. 36, no. 4, p. 275-278.

Rondenay, S., Montési, L.G.J., and Abers, G.A., 2010, New geophysical insight into the origin of the Denali volcanic gap: Geophysical Journal International, v. 182, p. 613-630.

Rossi, G., Abers, G. A., Rondenay, S., and Christensen, D. H., 2006, Unusual mantle Poisson's ratio, subduction, and crustal structure in central Alaska: Journal Geophysical Research, v. 111, no. B9, p. B09311.

Savage, M. K., 1999, Seismic anisotropy and mantle deformation: What have we learned from shear wave splitting?: Reviews of Geophysics, v. 37, no. 1, p. 65-106.

Shearer, P. M., and Orcutt, J. A., 1986, Compressional and shear wave anisotropy in the oceanic lithosphere - the Ngendei seismic refraction experiment: Geophysical Journal of the Royal Astronomical Society, v. 87, no. 3, p. 967-1003.

Silver, P. G., 1996, Seismic anisotropy beneath the continents: Probing the depths of geology: Annual Review of Earth and Planetary Sciences, v. 24, p. 385-432.

Silver, P. G., and Chan, W. W., 1988, Implications for continental structure and evolution from seismic anisotropy: Nature, v. 335, p. 34-39.

Silver, P. G., and Chan, W. W., 1991, Shear Wave Splitting and Subcontinental Mantle Deformation: Journal of Geophysical Research, v. 96, no. B10, p. 16429-16454.

Stein, S., and Wysession, M., 2003, An Introduction to Seismology, Earthquakes, and Earth Structure Geological Magazine, Oxford: Blackwell Science, xi + 498 p.

Stone, D. B., and Wallace, W. K., 1987, A Geological Framework of Alaska: Episodes, v. 10, no. 4, p. 283-289.

Taber, J. J., Billington, S., and Engdahl, E. R., 1991, Seismicity of the Aleutian Arc, in D.B. Slemmons et al., ed., Neotectonics of North America: Boulder, Colo., Geologic Society of America, p. 29-46.

Walker, K. T., Bokelmann, G. H. R., and Klemperer, S. L., 2001, Shear wave splitting to test mantle deformation models around Hawaii: Geophysical Research Letters, v. 28, no. 22, p. 4319-4322.

Wolfe, C. J., and Solomon, S. C., 1998, Shear-Wave Splitting and Implications for Mantle Flow Beneath the MELT Region of the East Pacific Rise: Science, v. 280, no. 5367, p. 1230-1232.

Yang, X., Fischer, K. M., and Abers, G. A., 1995, Seismic anisotropy beneath the Shumagin Islands segment of the Aleutian-Alaska Subduction zone: Journal of Geophysical Research, v. 100, no. B9, p. 165-177.

Zhang, S., Karato, S., Gerald, J. F., Faul, U. H., and Zhou, Y., 2000, Simple shear deformation of olivine aggregates: Tectonophysics, v. 316, p. 133-152.

Zweck, C., Freymueller, J. T., and Cohen, S. C., 2002, The 1964 great Alaska earthquake: present day and cumulative postseismic deformation in the western Kenai Peninsula: Physics of the Earth and Planetary Interiors, v. 132, no. 1-3, p. 5-20.

Appendix A

Splitting results from the ARCTIC network. Error bars represent 95% confidence region.

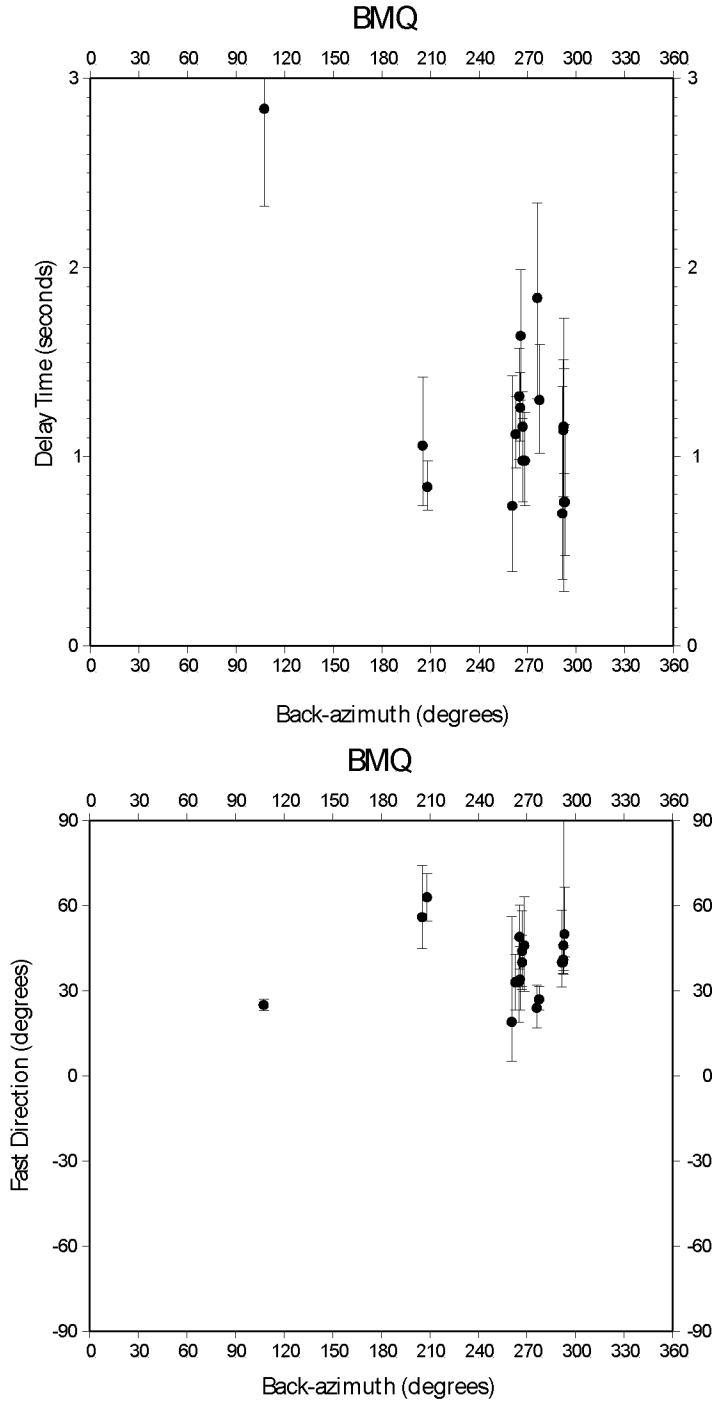

Figure A.1: Station BMQ from the ARCTIC network.
Delay times vs. back-azimuth (top) and fast direction vs. back-azimuth (bottom).

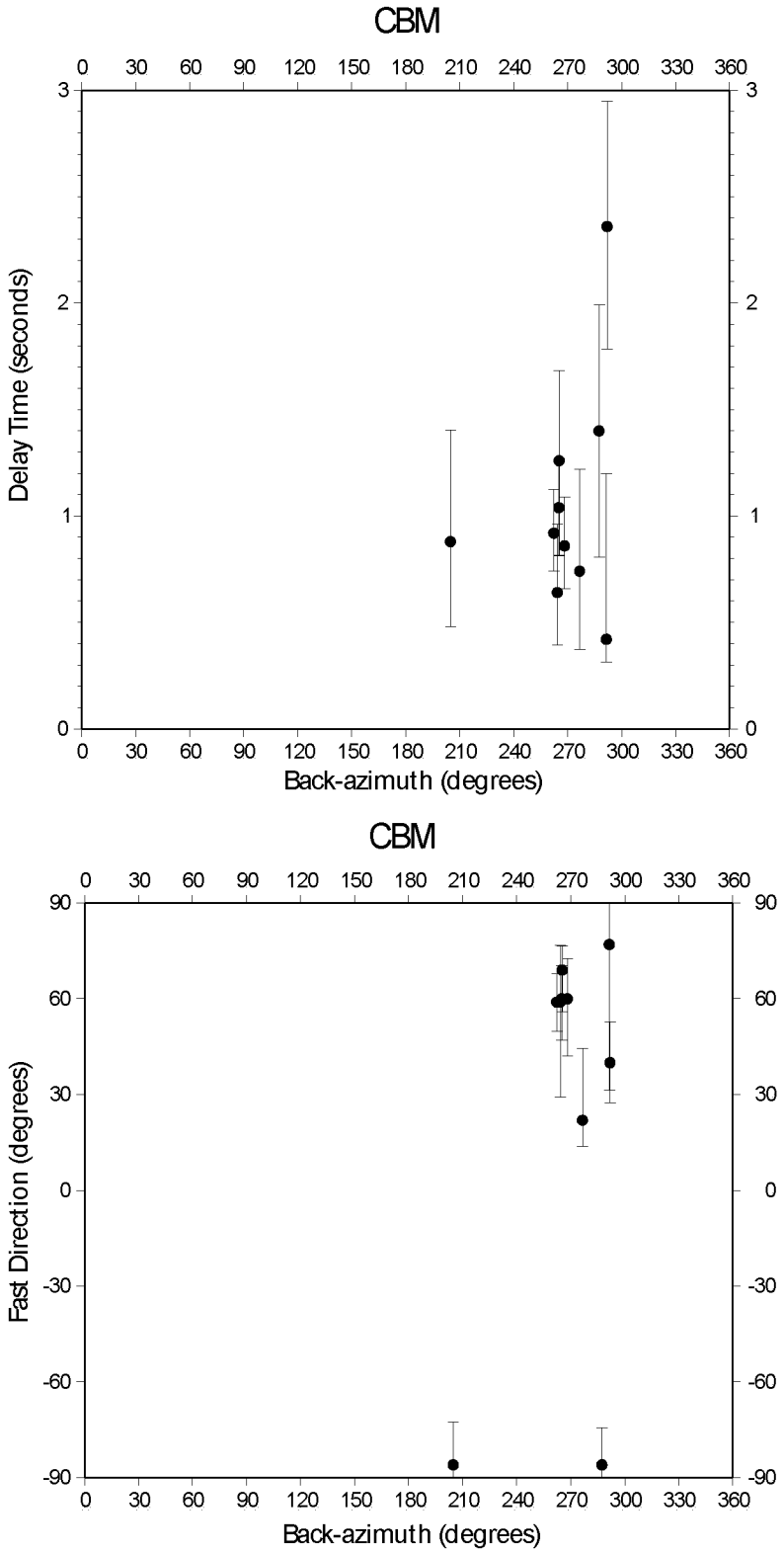

Figure A.2: Station CBM from the ARCTIC network.
Delay times vs. back-azimuth (top) and fast direction vs. back-azimuth (bottom).

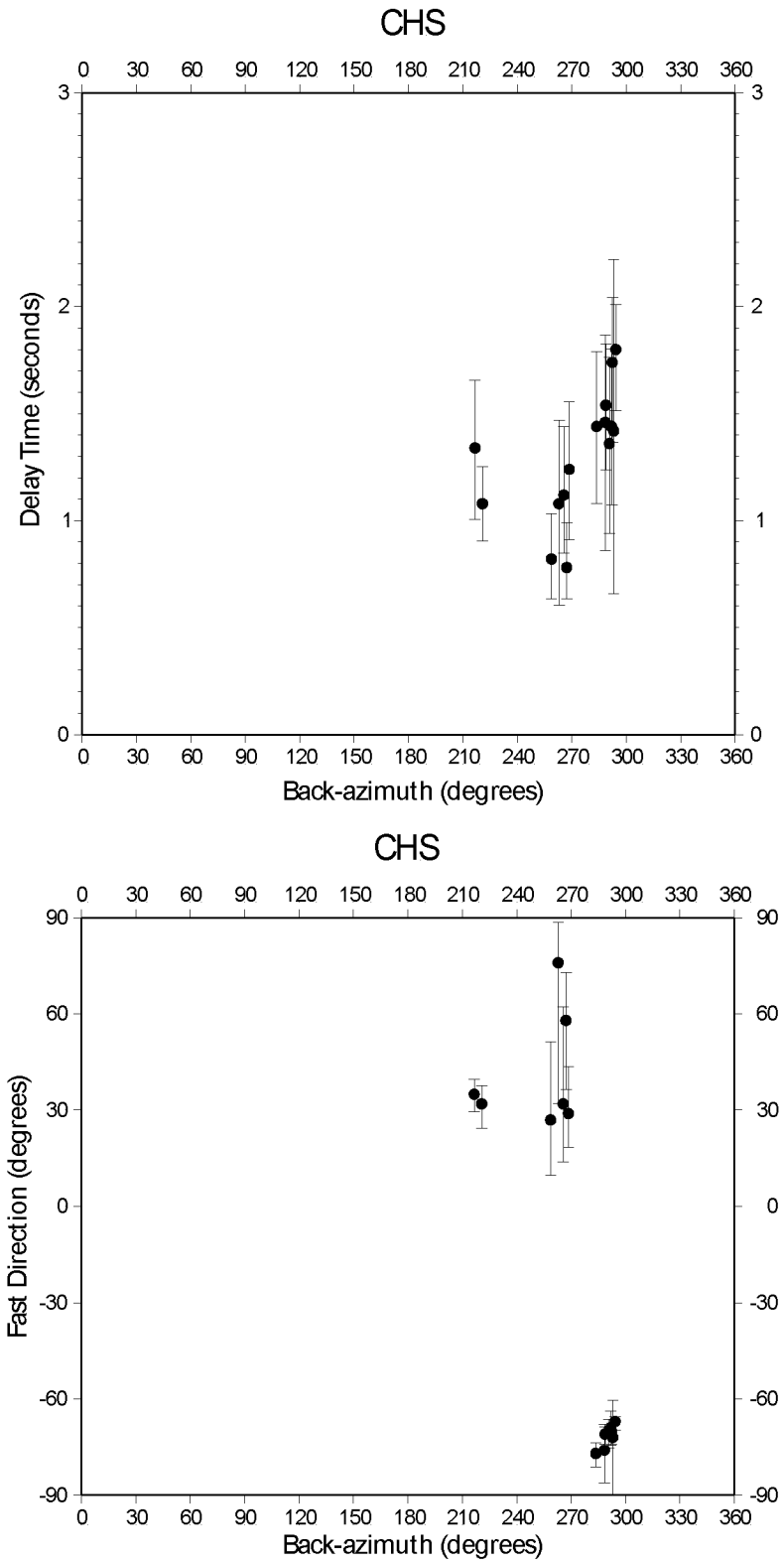

Figure A.3: **Station CHS from the ARCTIC network.**
Delay times vs. back-azimuth (top) and fast direction vs. back-azimuth (bottom).

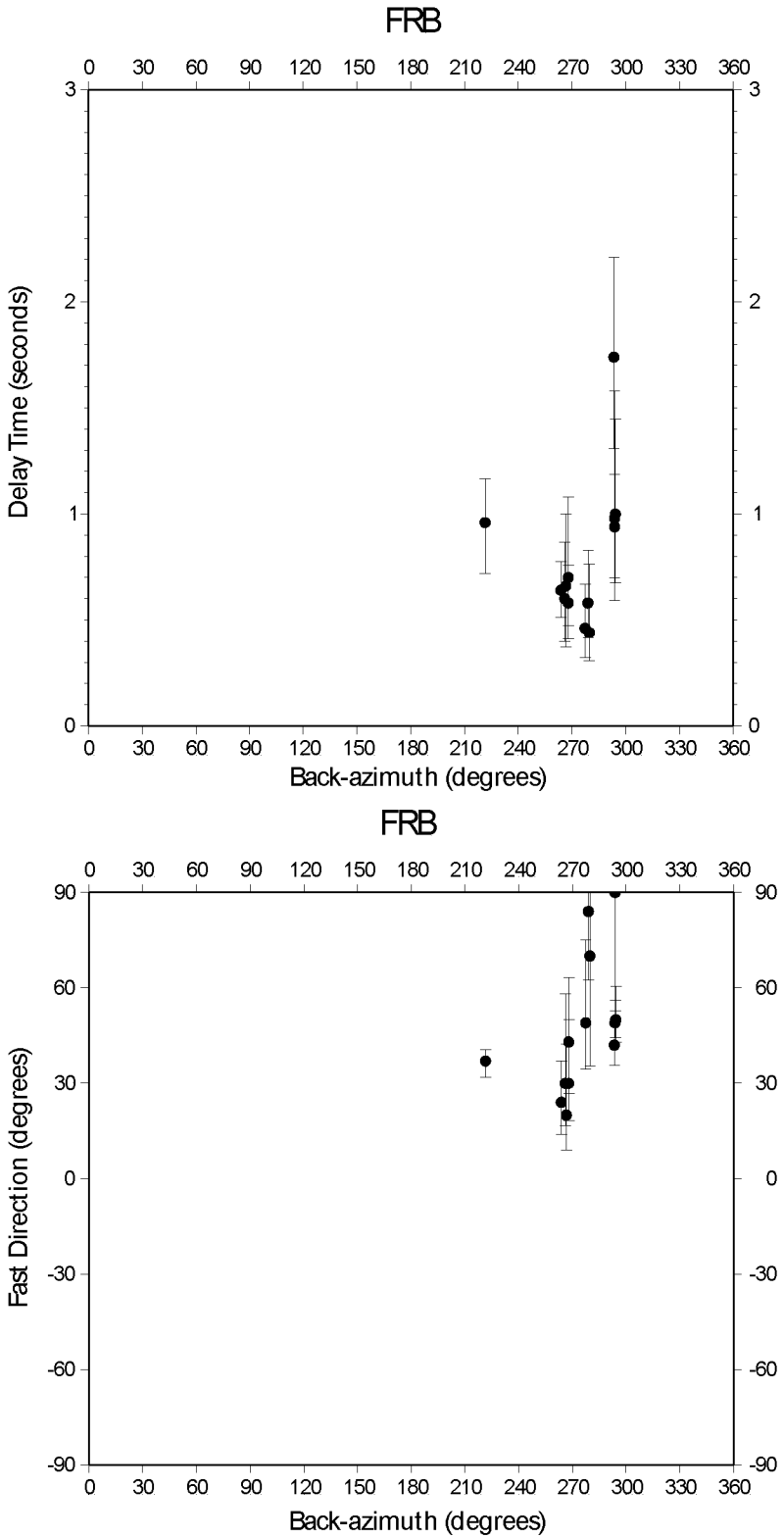

Figure A.4: Station FRB from the ARCTIC network.
Delay times vs. back-azimuth (top) and fast direction vs. back-azimuth (bottom).

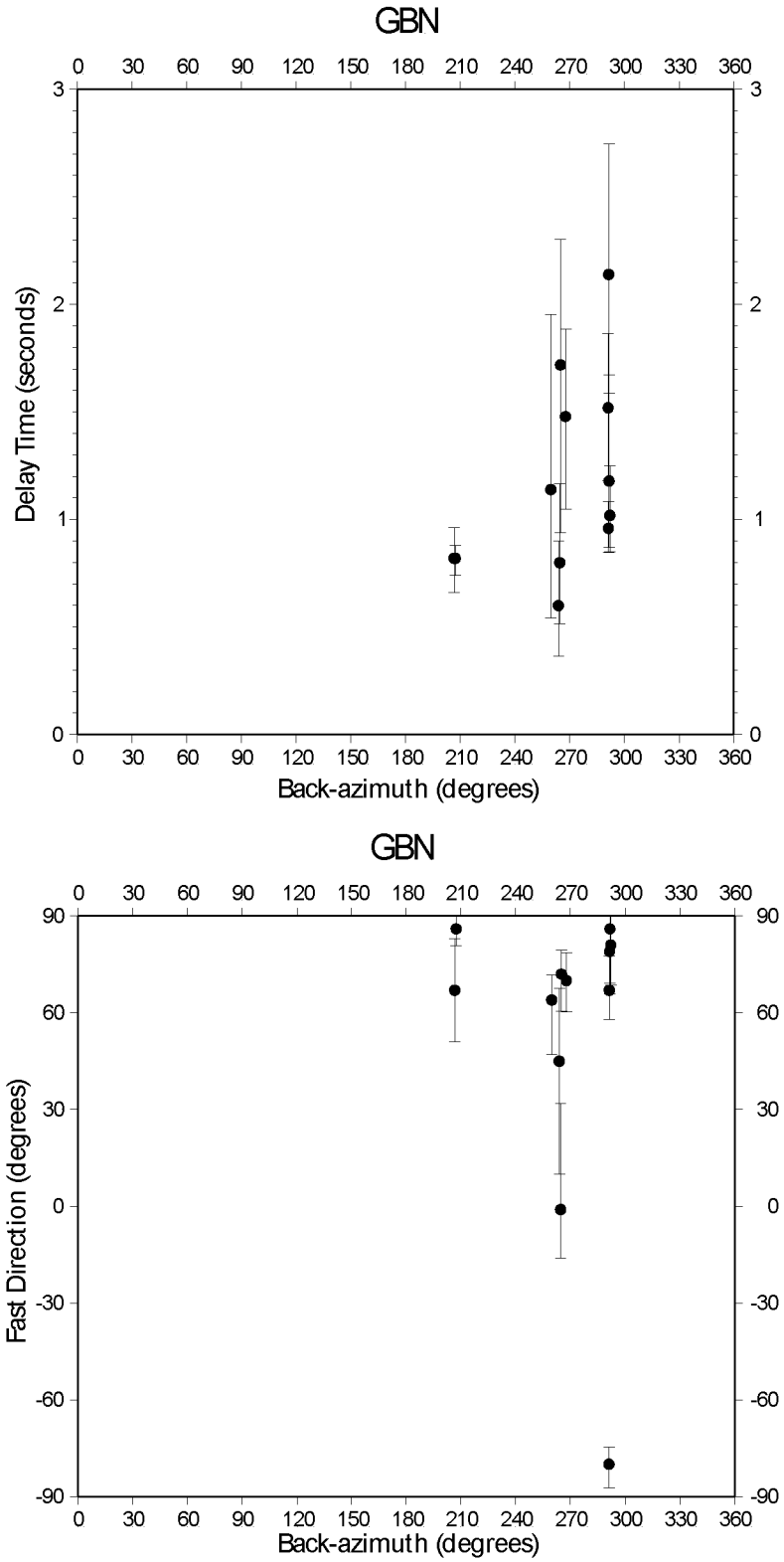

Figure A.5: Station GBN from the ARCTIC network.
Delay times vs. back-azimuth (top) and fast direction vs. back-azimuth (bottom).

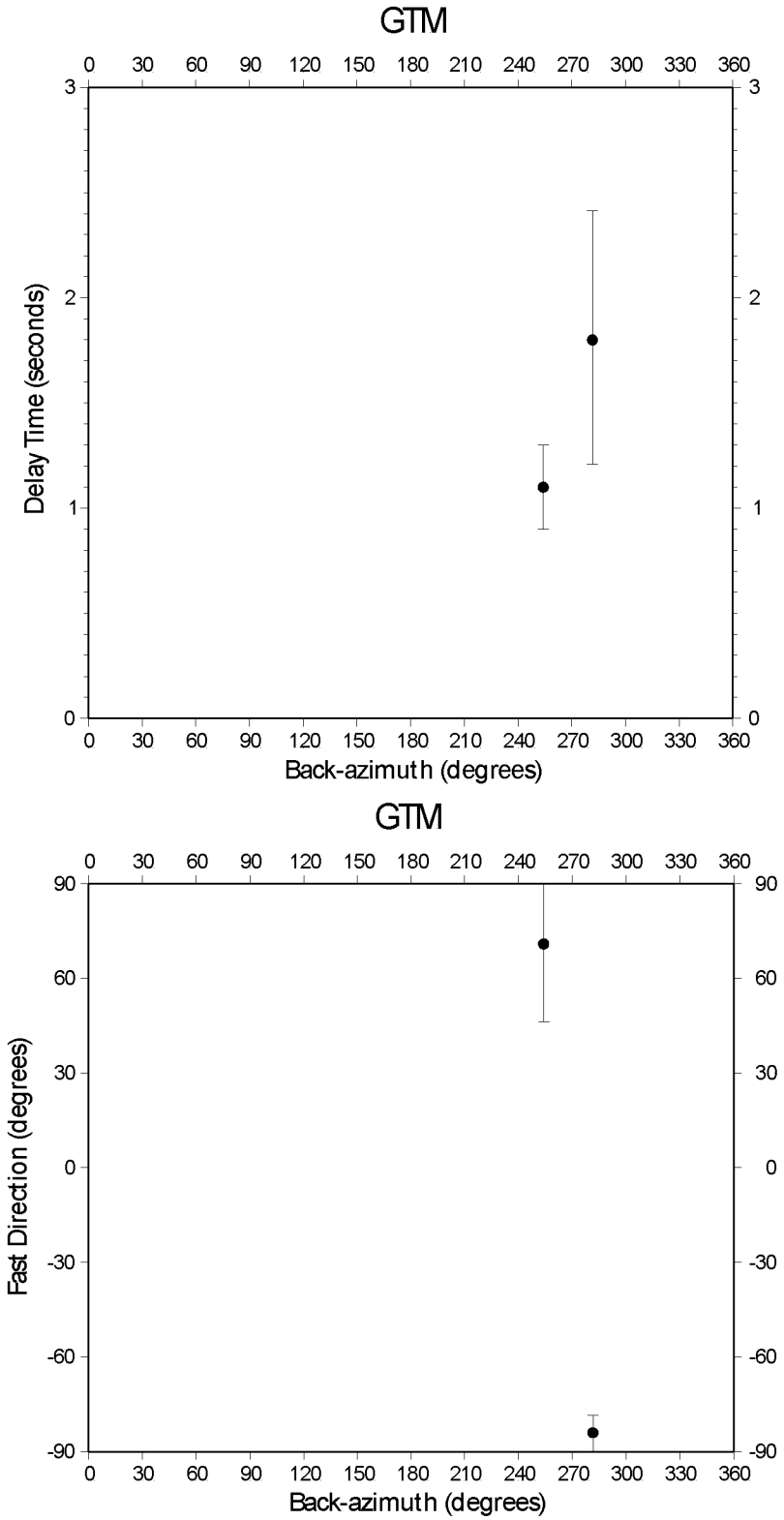

Figure A.6: Station GTM from the ARCTIC network.
Delay times vs. back-azimuth (top) and fast direction vs. back-azimuth (bottom).

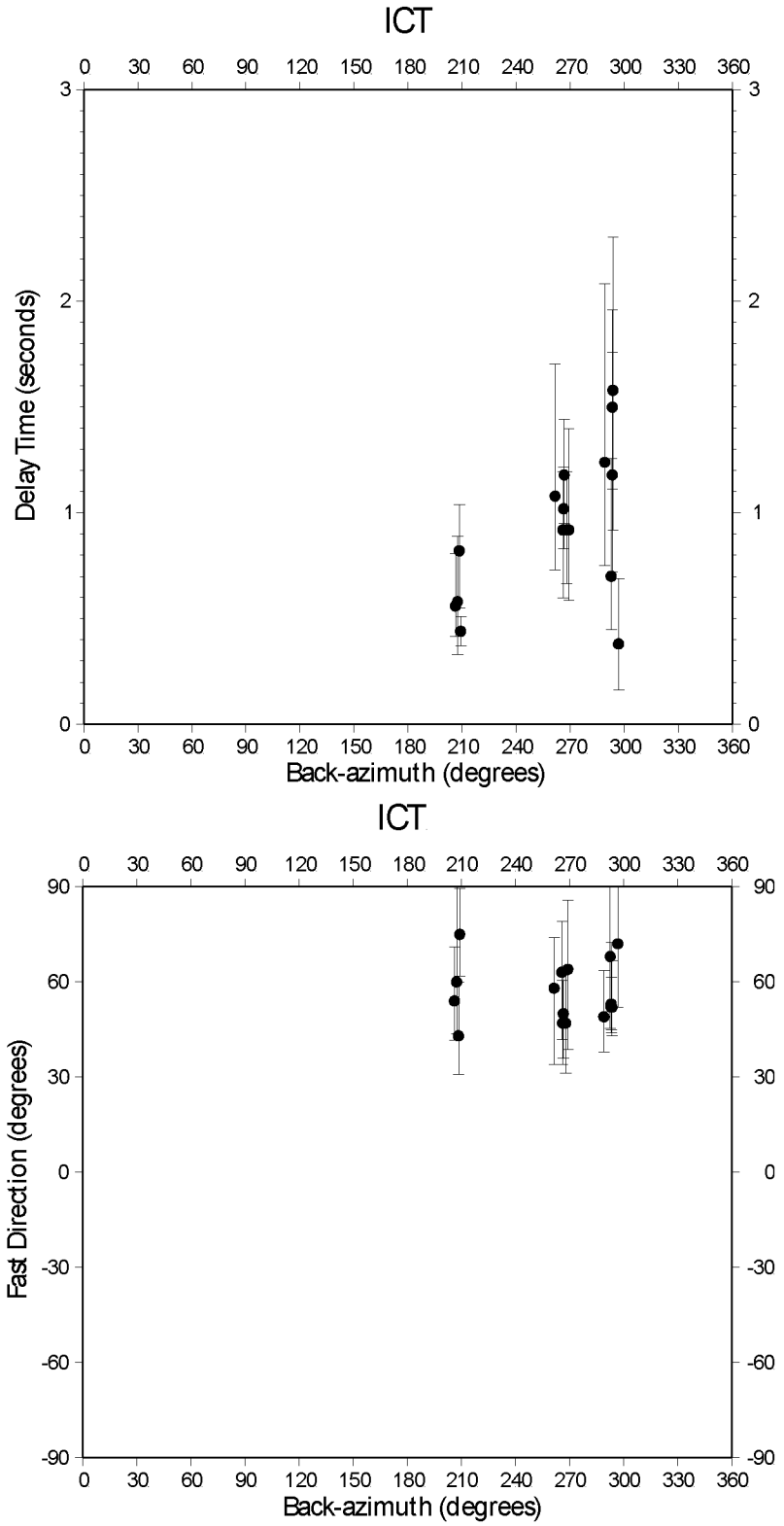

Figure A.7: Station ICT from the ARCTIC network.
Delay times vs. back-azimuth (top) and fast direction vs. back-azimuth (bottom).

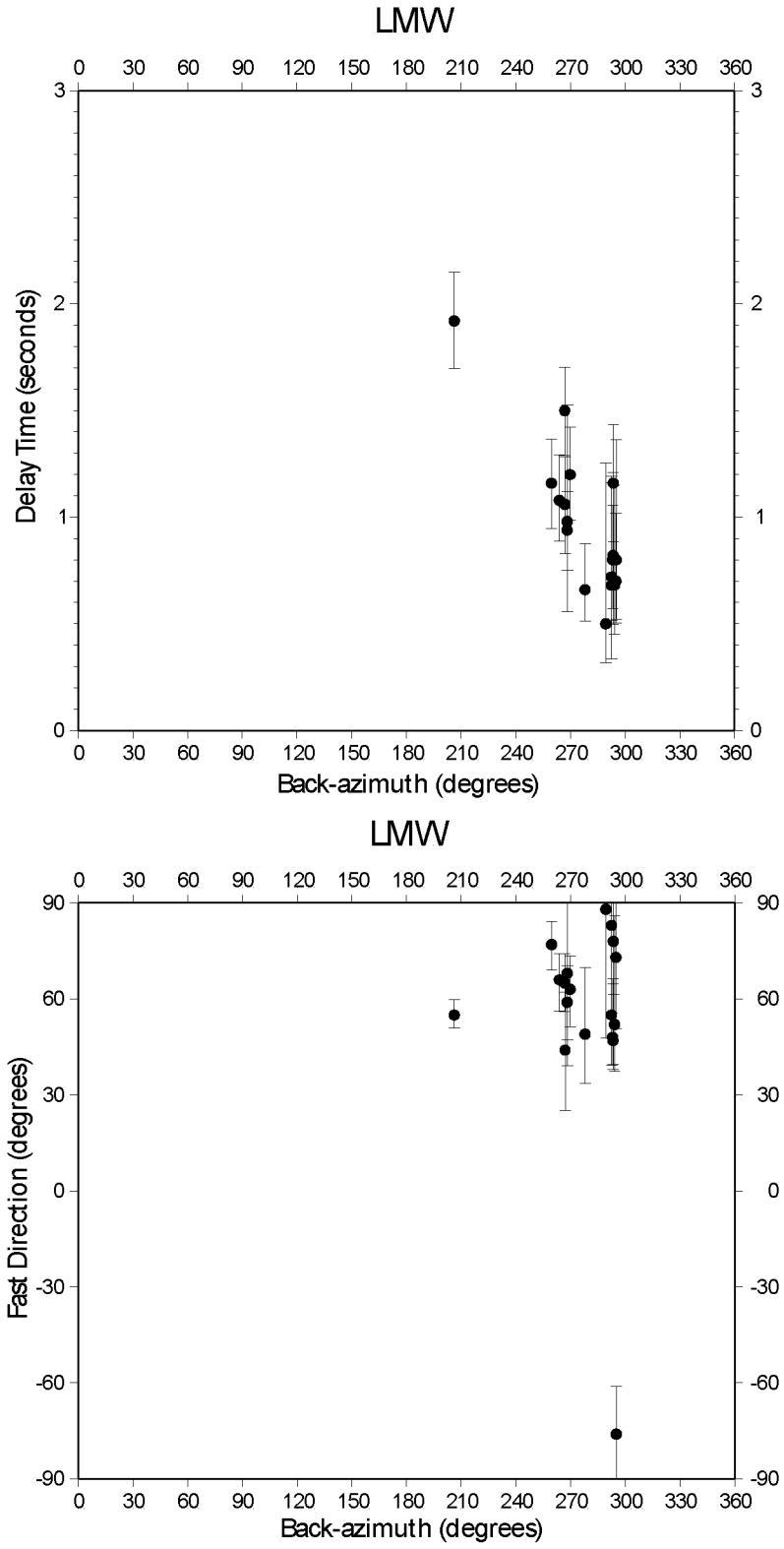

Figure A.8: Station LMW from the ARCTIC network.
Delay times vs. back-azimuth (top) and fast direction vs. back-azimuth (bottom).

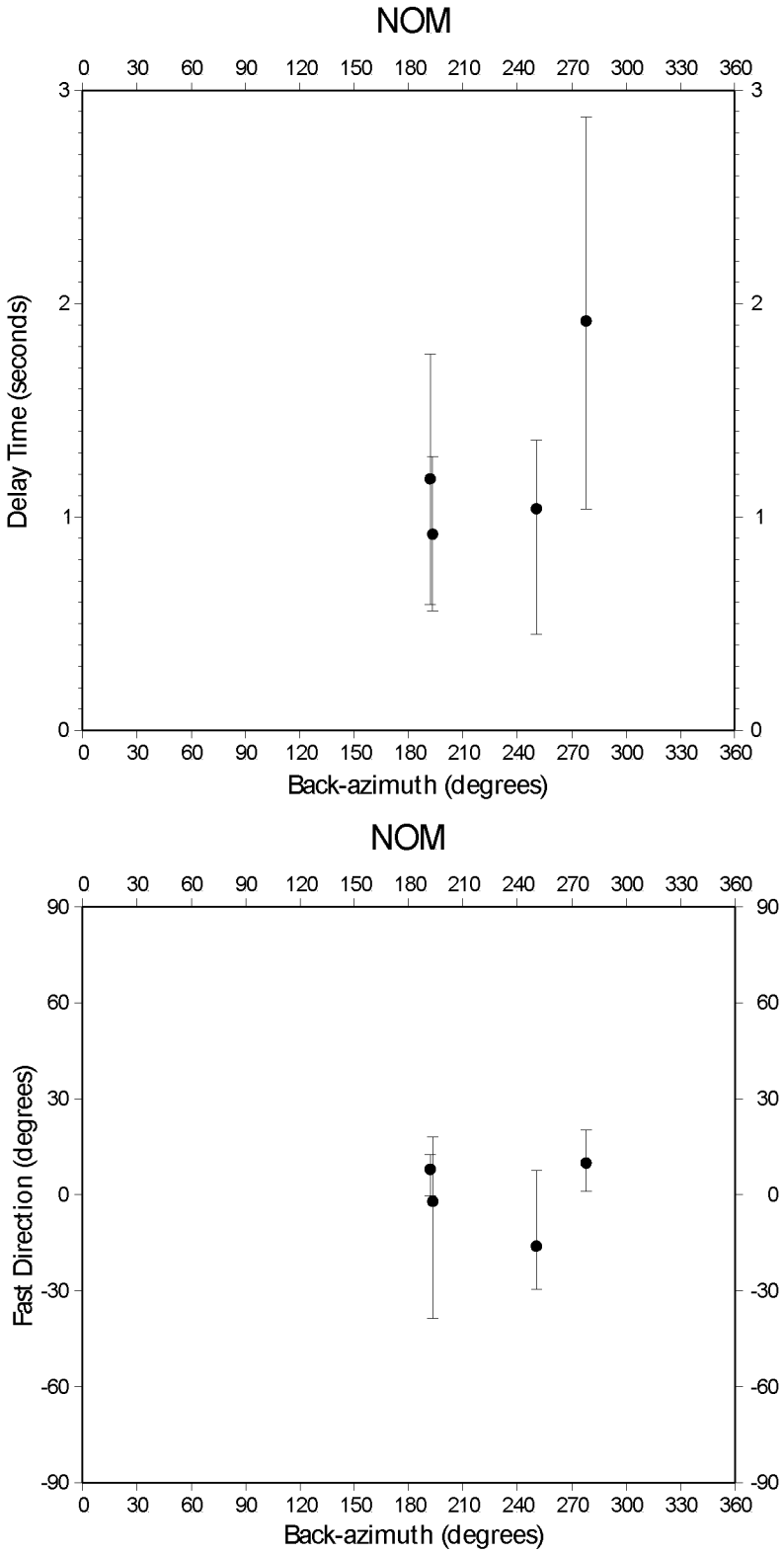

Figure A.9: Station NOM from the ARCTIC network.
Delay times vs. back-azimuth (top) and fast direction vs. back-azimuth (bottom).

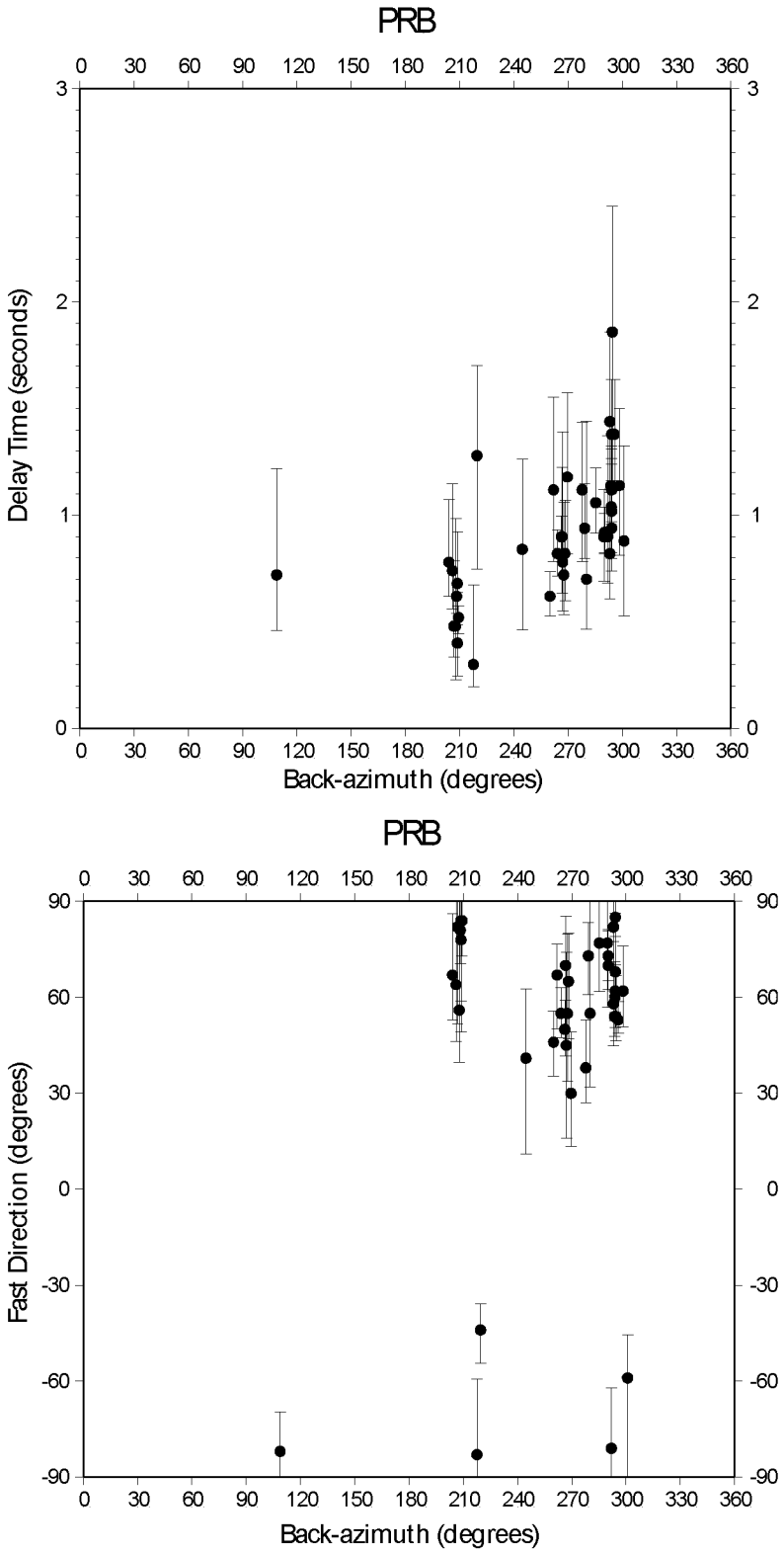

Figure A.10: Station PRB from the ARCTIC network.
Delay times vs. back-azimuth (top) and fast direction vs. back-azimuth (bottom).

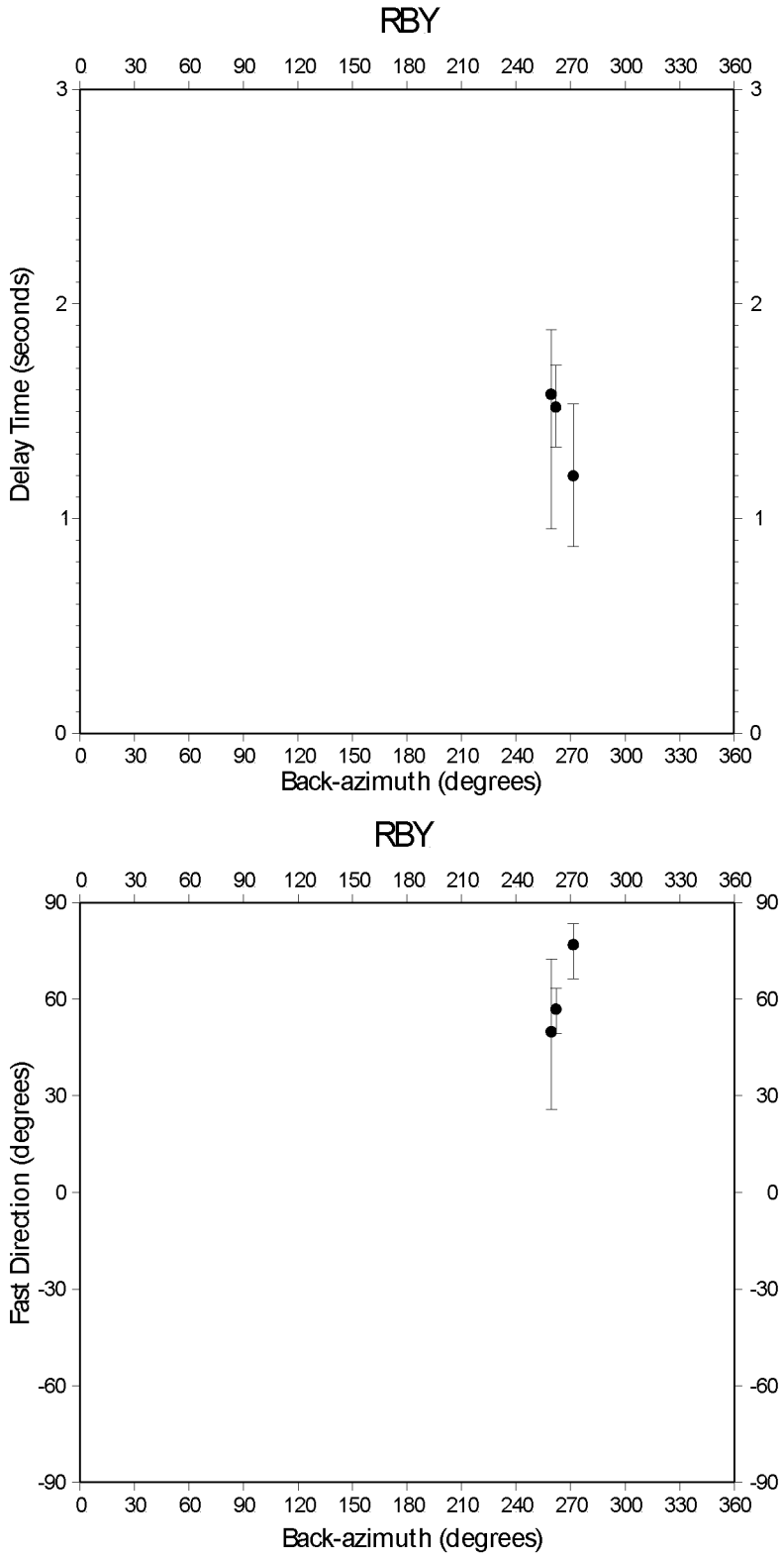

Figure A.11: Station RBY from the ARCTIC network.
Delay times vs. back-azimuth (top) and fast direction vs. back-azimuth (bottom).

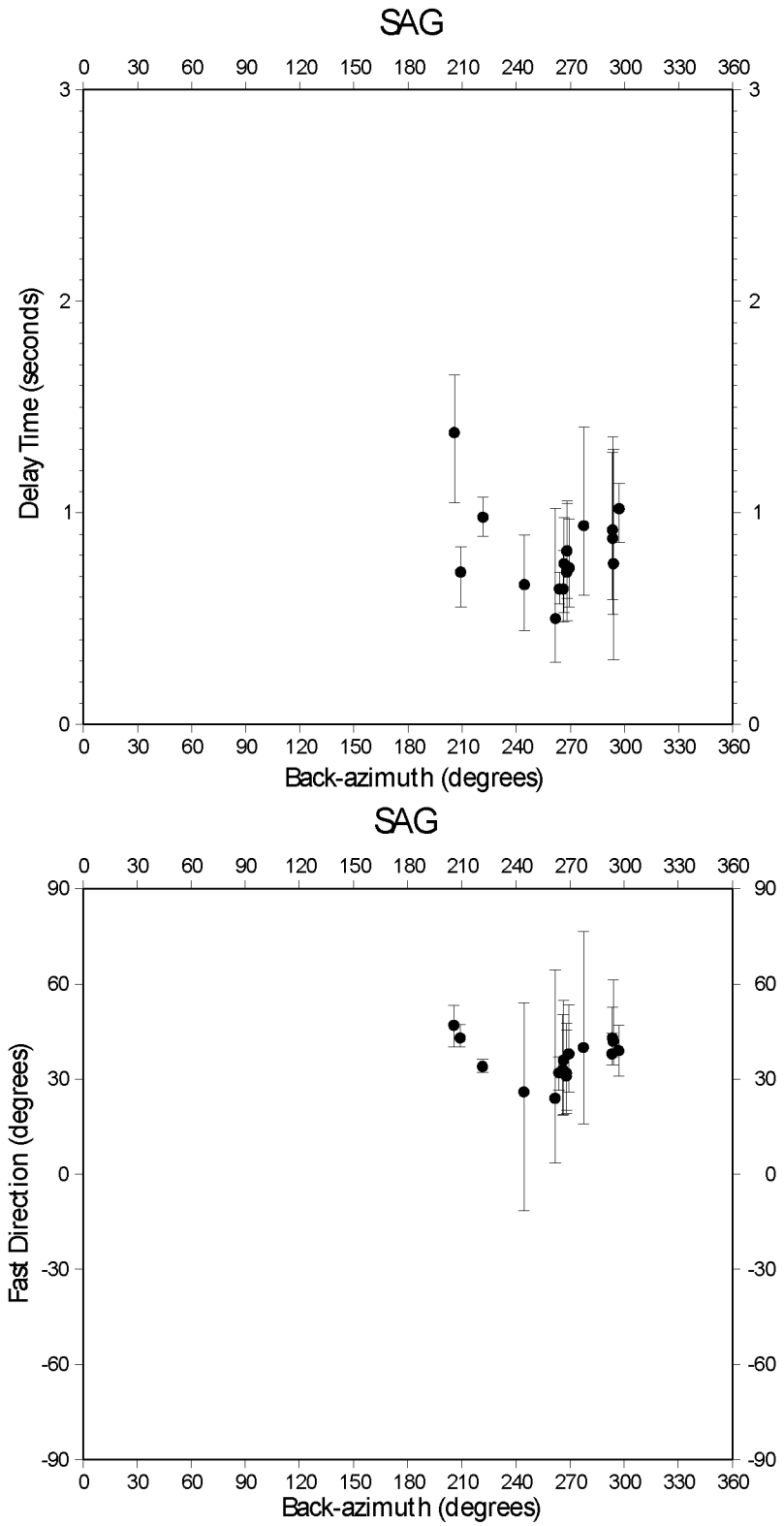

Figure A.12: Station SAG from the ARCTIC network.
Delay times vs. back-azimuth (top) and fast direction vs. back-azimuth (bottom).

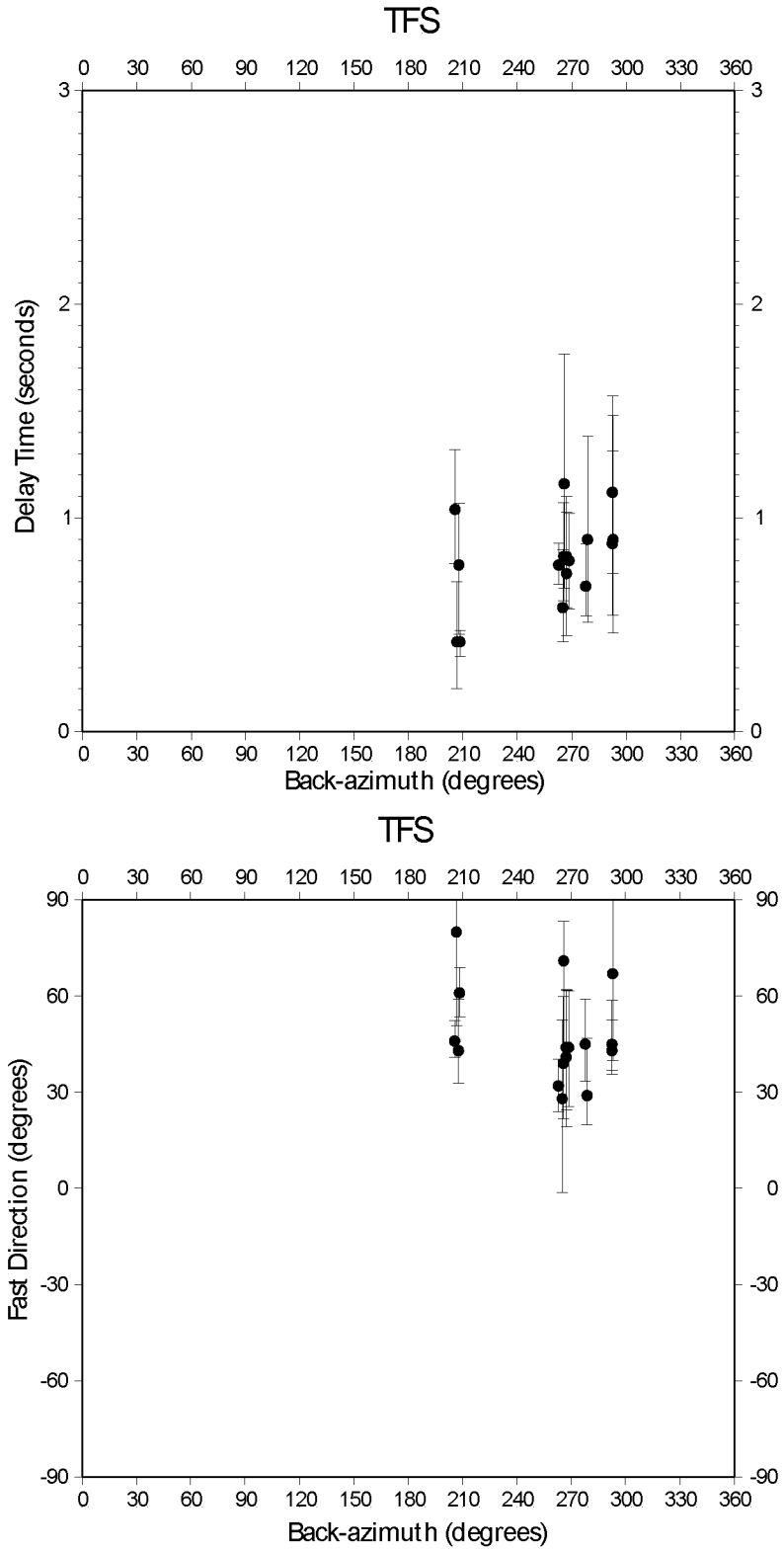

Figure A.13: Station TFS from the ARCTIC network.
Delay times vs. back-azimuth (top) and fast direction vs. back-azimuth (bottom).

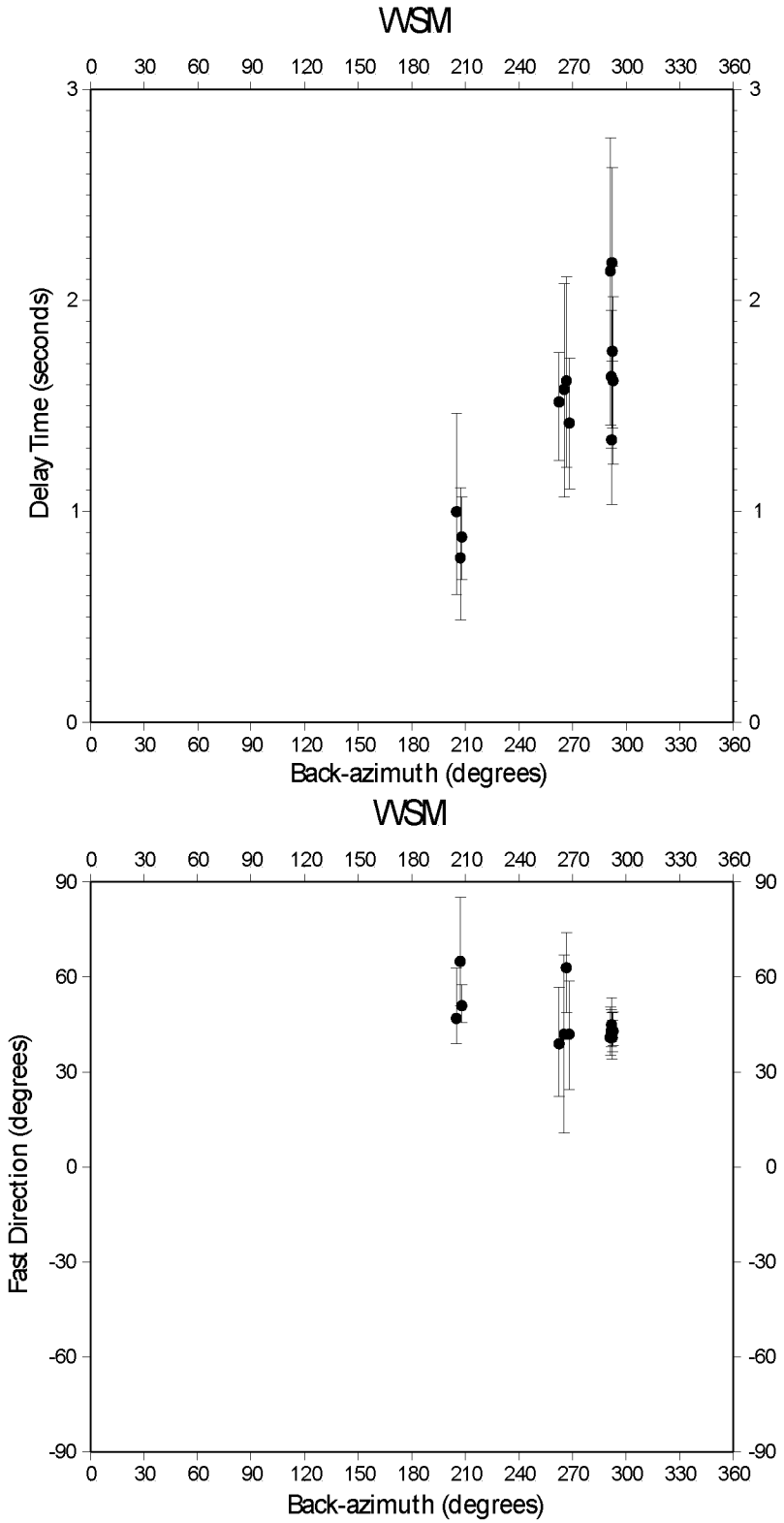

Figure A.14: Station WSM from the ARCTIC network.
Delay times vs. back-azimuth (top) and fast direction vs. back-azimuth (bottom).

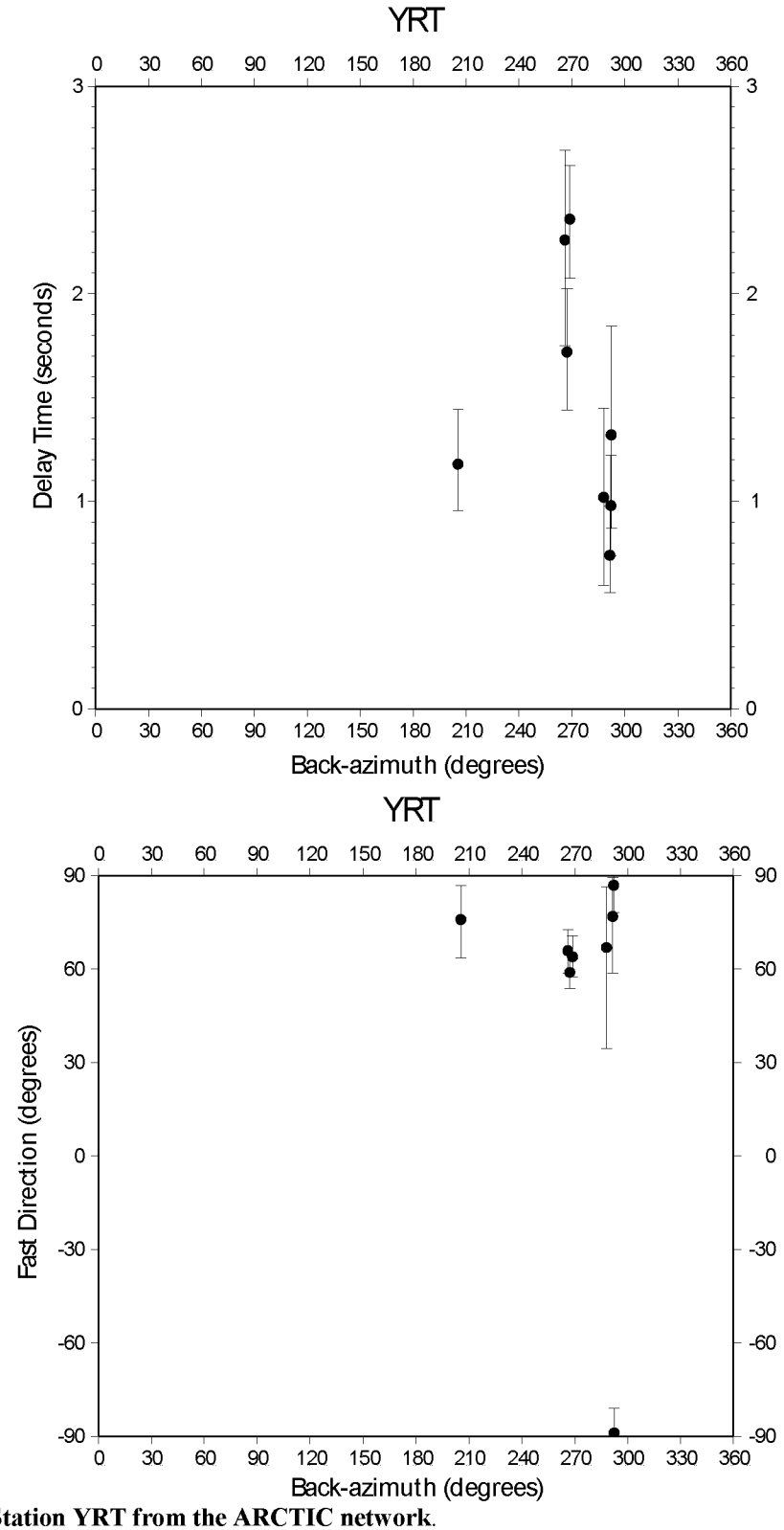

Figure A.15: Station YRT from the ARCTIC network.
Delay times vs. back-azimuth (top) and fast direction vs. back-azimuth (bottom).

Appendix B

Splitting results from the BEAAR network. Error bars represent 95% confidence region.

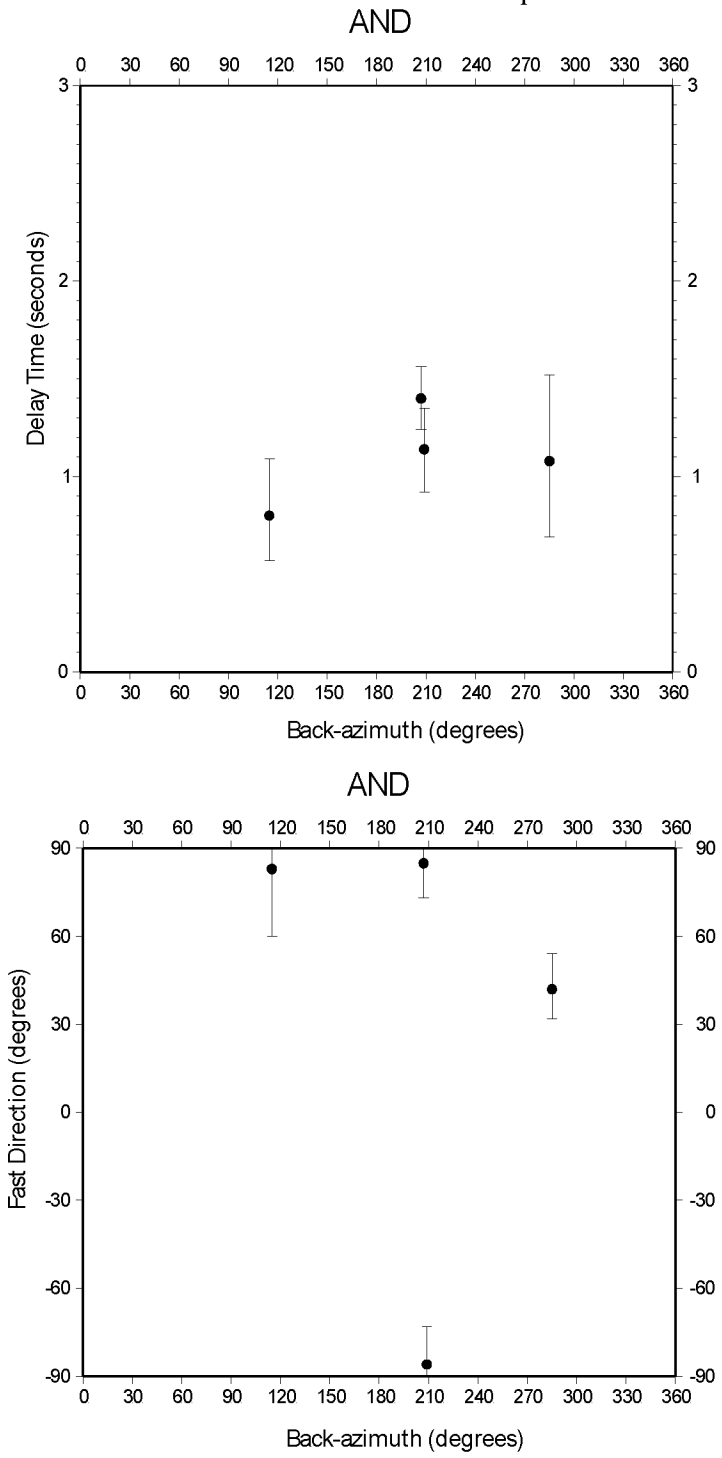

Figure B.1: Station AND from the BEAAR network.
Delay times vs. back-azimuth (top) and fast direction vs. back-azimuth (bottom).

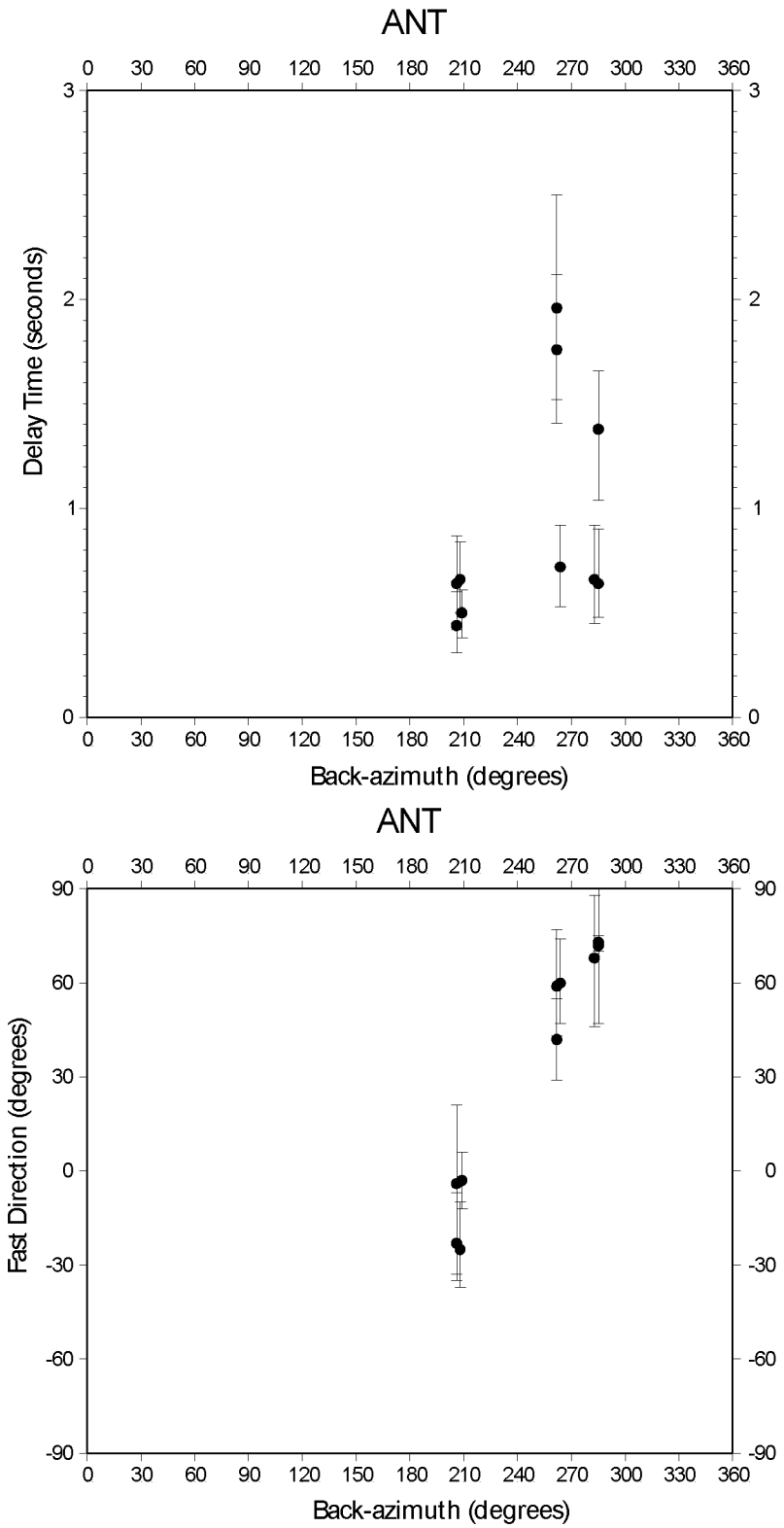

Figure B.2: Station ANT from the BEAAR network.
Delay times vs. back-azimuth (top) and fast direction vs. back-azimuth (bottom).

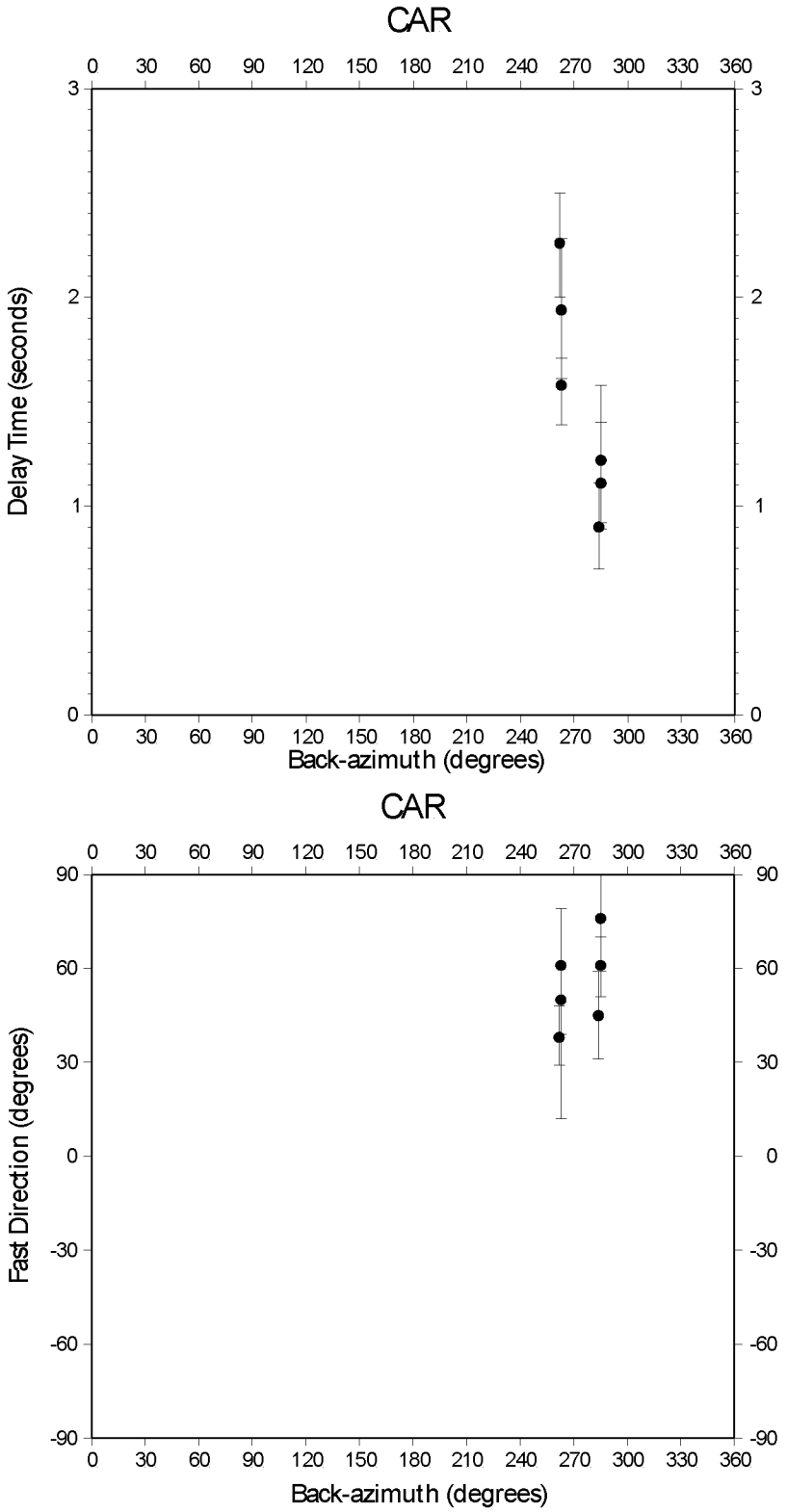

Figure B.3: Station CAR from the BEAAR network.
Delay times vs. back-azimuth (top) and fast direction vs. back-azimuth (bottom).

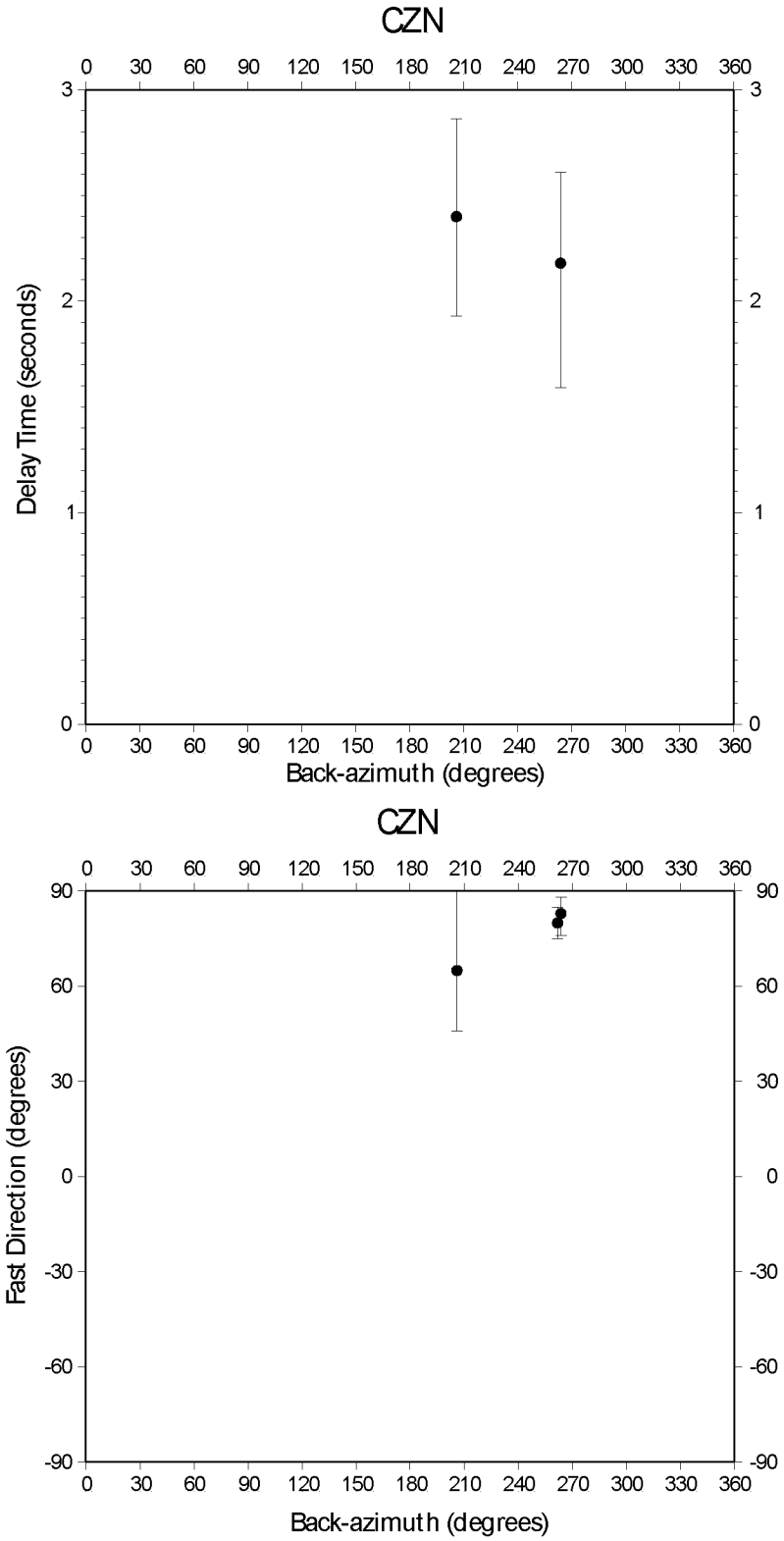

Figure B.4: Station CZN from the BEAAR network.
Delay times vs. back-azimuth (top) and fast direction vs. back-azimuth (bottom).

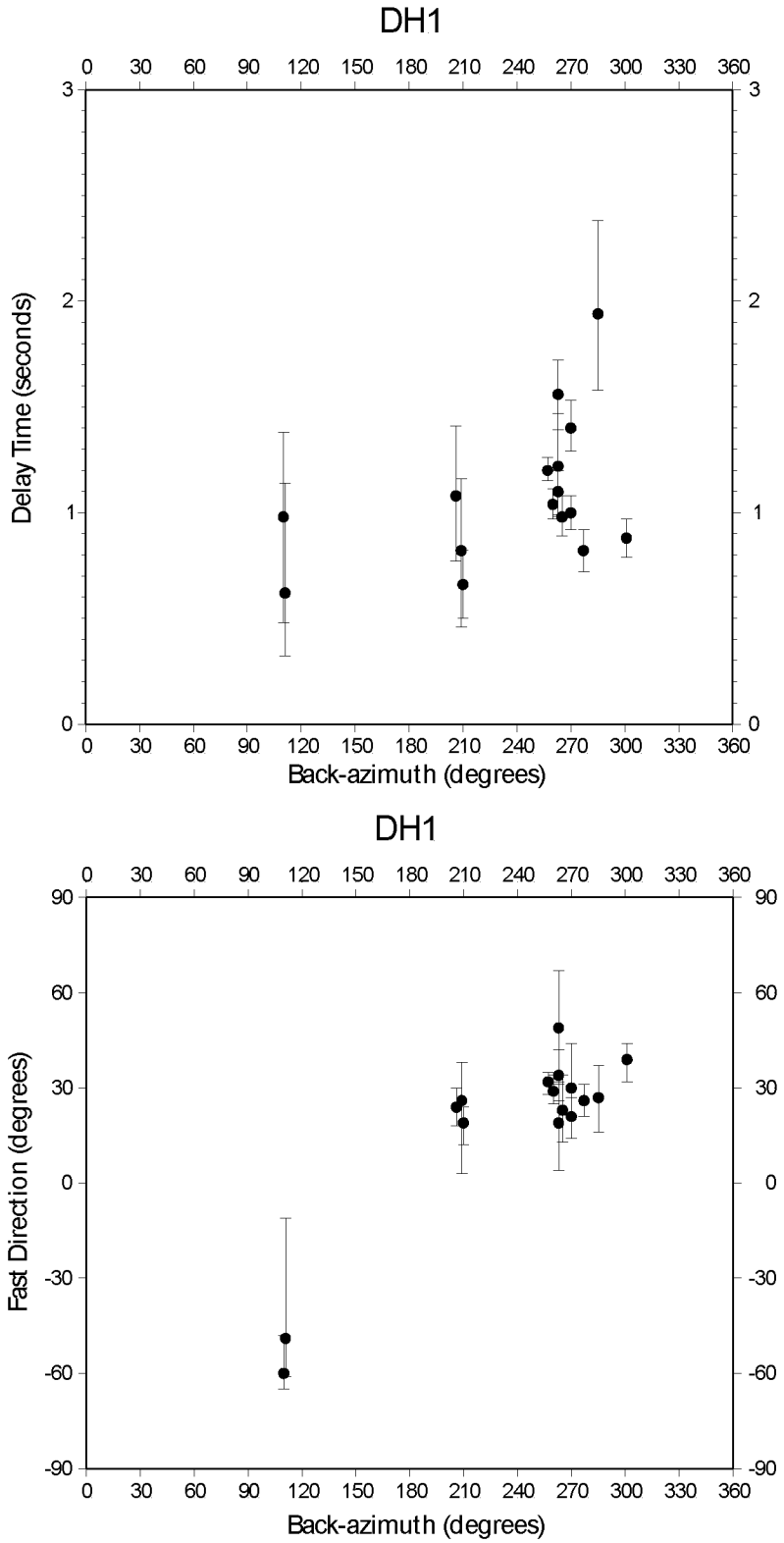

Figure B.5: Station DH1 from the BEAAR network.
Delay times vs. back-azimuth (top) and fast direction vs. back-azimuth (bottom).

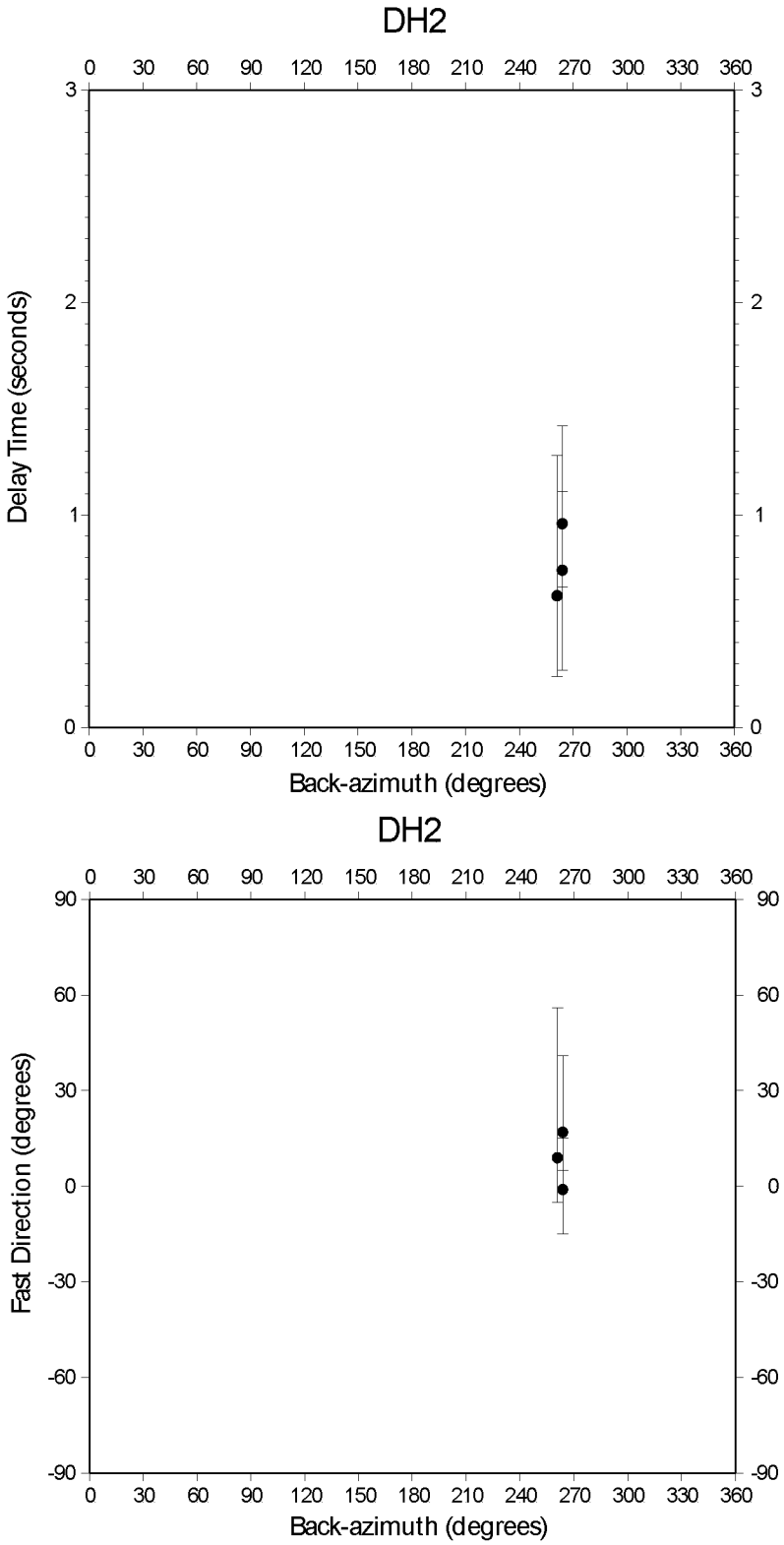

Figure B.6: Station DH2 from the BEAAR network.
Delay times vs. back-azimuth (top) and fast direction vs. back-azimuth (bottom).

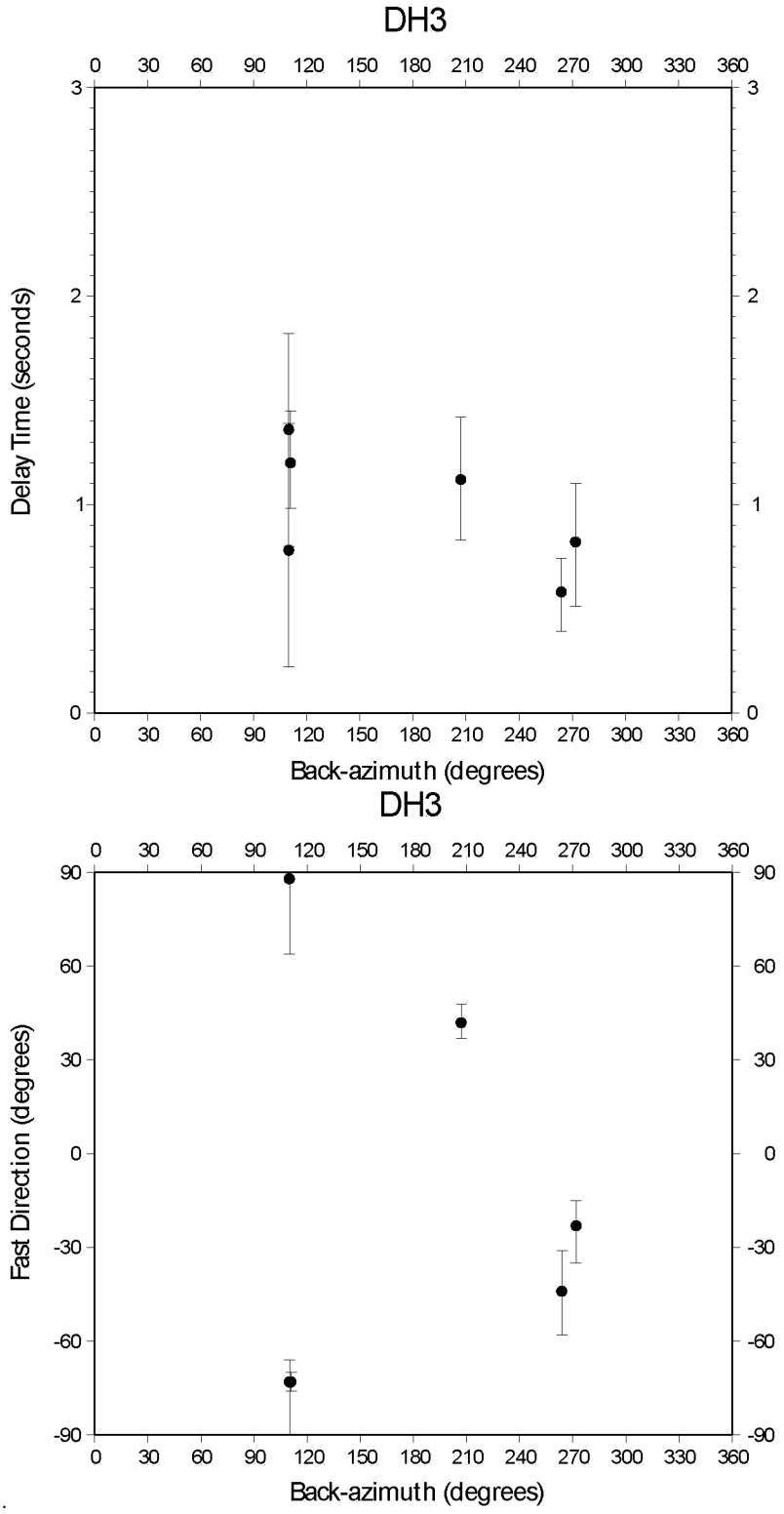

Figure B.7: Station DH3 from the BEAAR network.
Delay times vs. back-azimuth (top) and fast direction vs. back-azimuth (bottom).

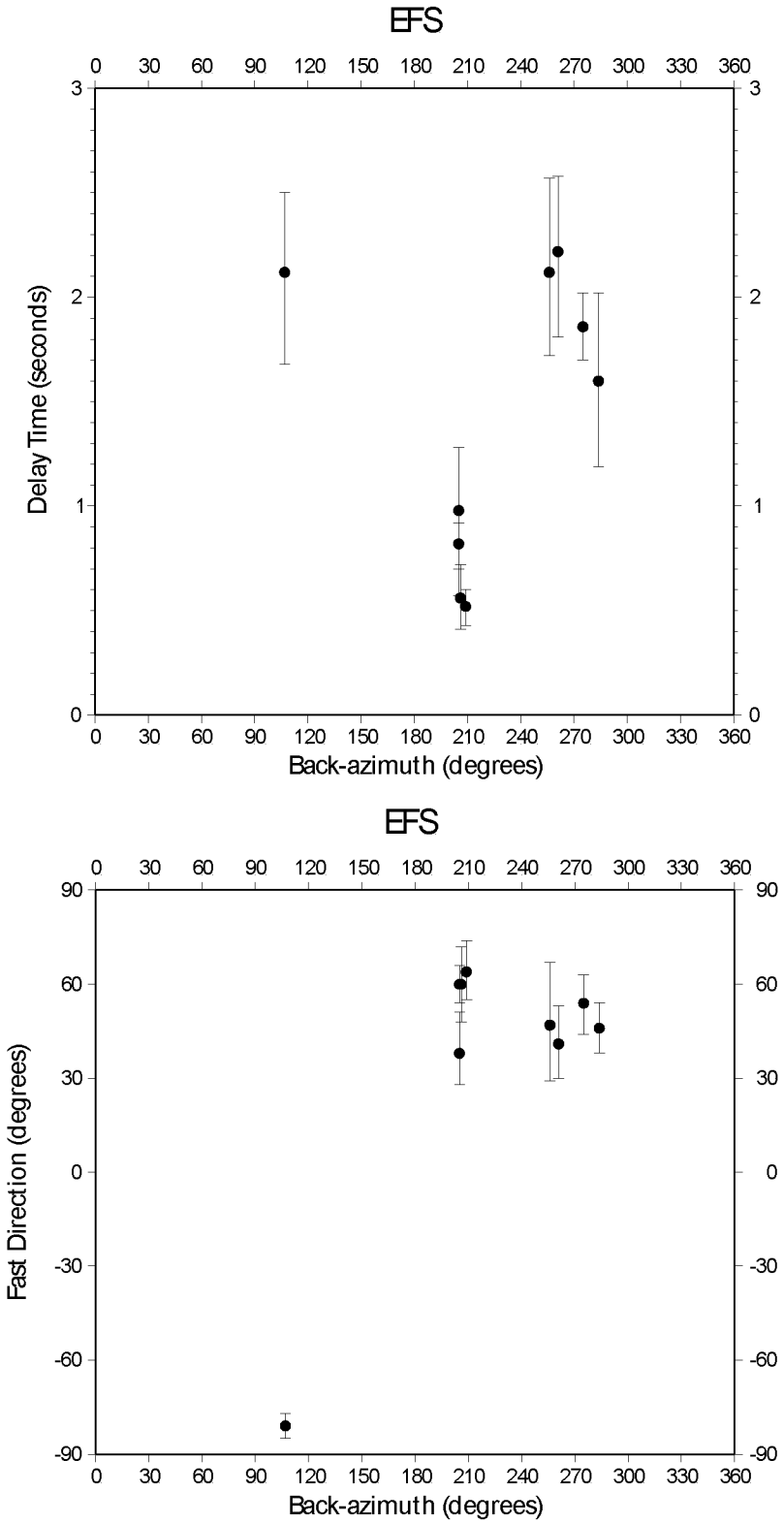

Figure B.8: Station EFS from the BEAAR network.
Delay times vs. back-azimuth (top) and fast direction vs. back-azimuth (bottom).

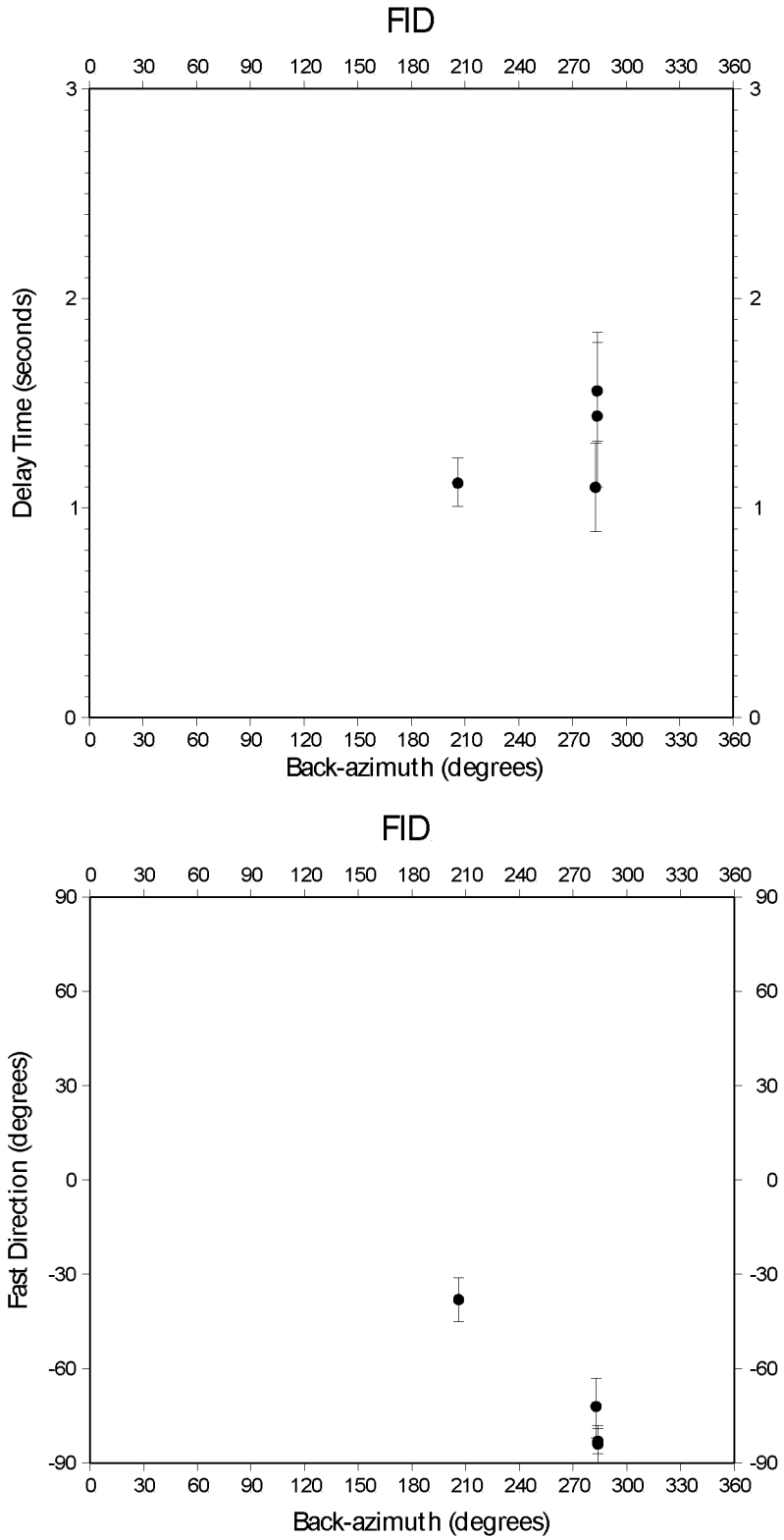

Figure B.9: Station FID from the BEAAR network.
Delay times vs. back-azimuth (top) and fast direction vs. back-azimuth (bottom).

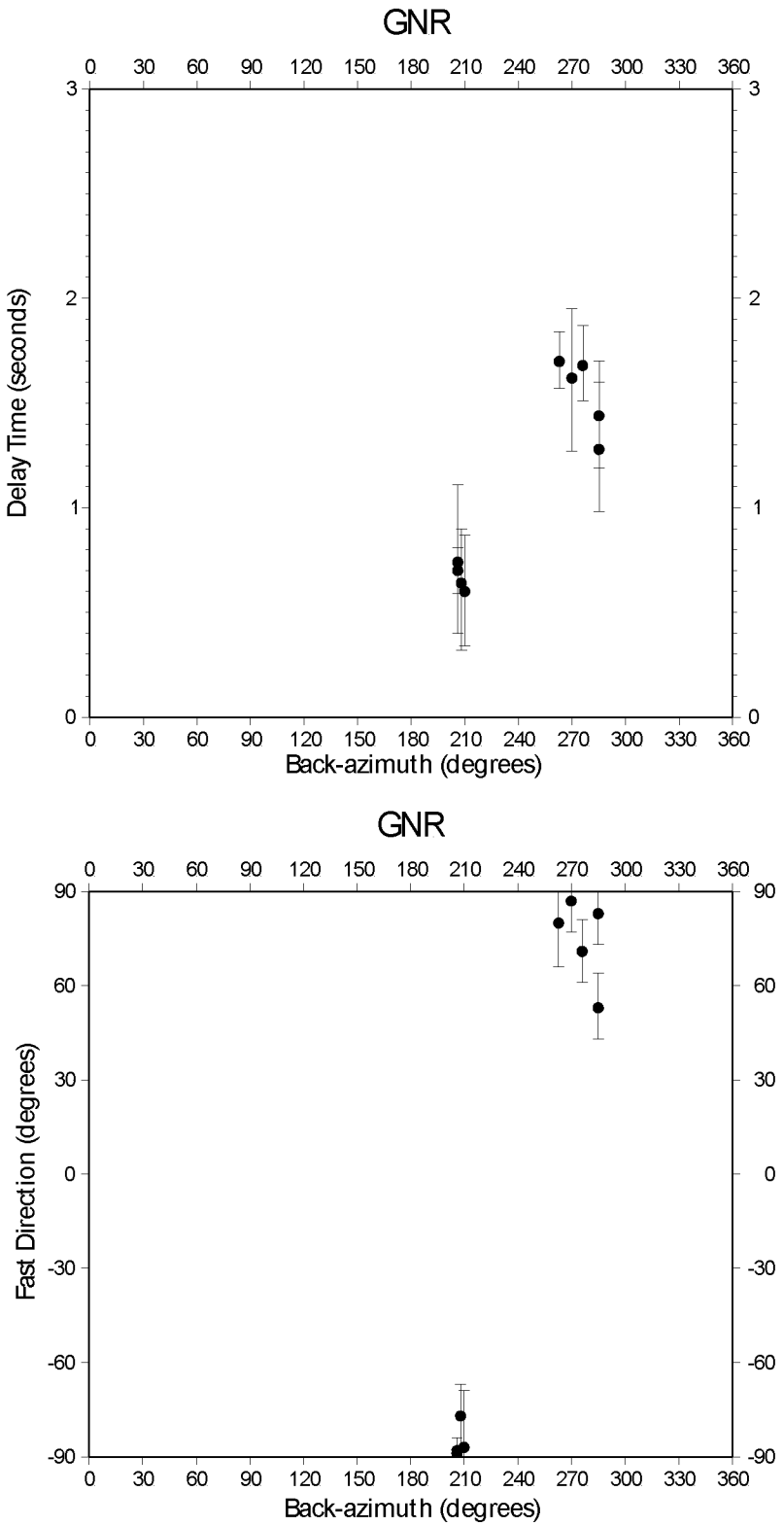

Figure B.10: Station GNR from the BEAAR network.
Delay times vs. back-azimuth (top) and fast direction vs. back-azimuth (bottom).

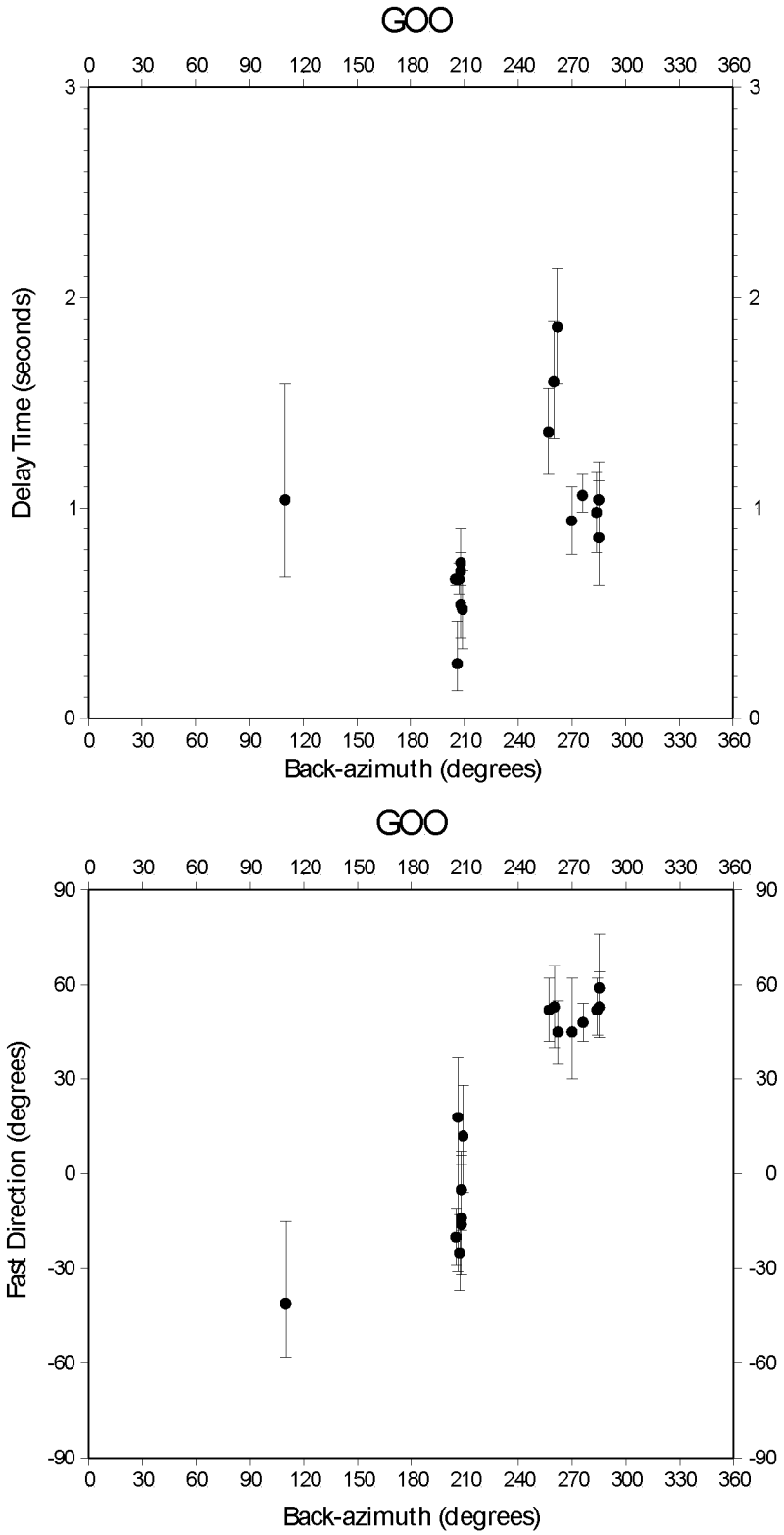

Figure B.11: Station GOO from the BEAAR network.
Delay times vs. back-azimuth (top) and fast direction vs. back-azimuth (bottom).

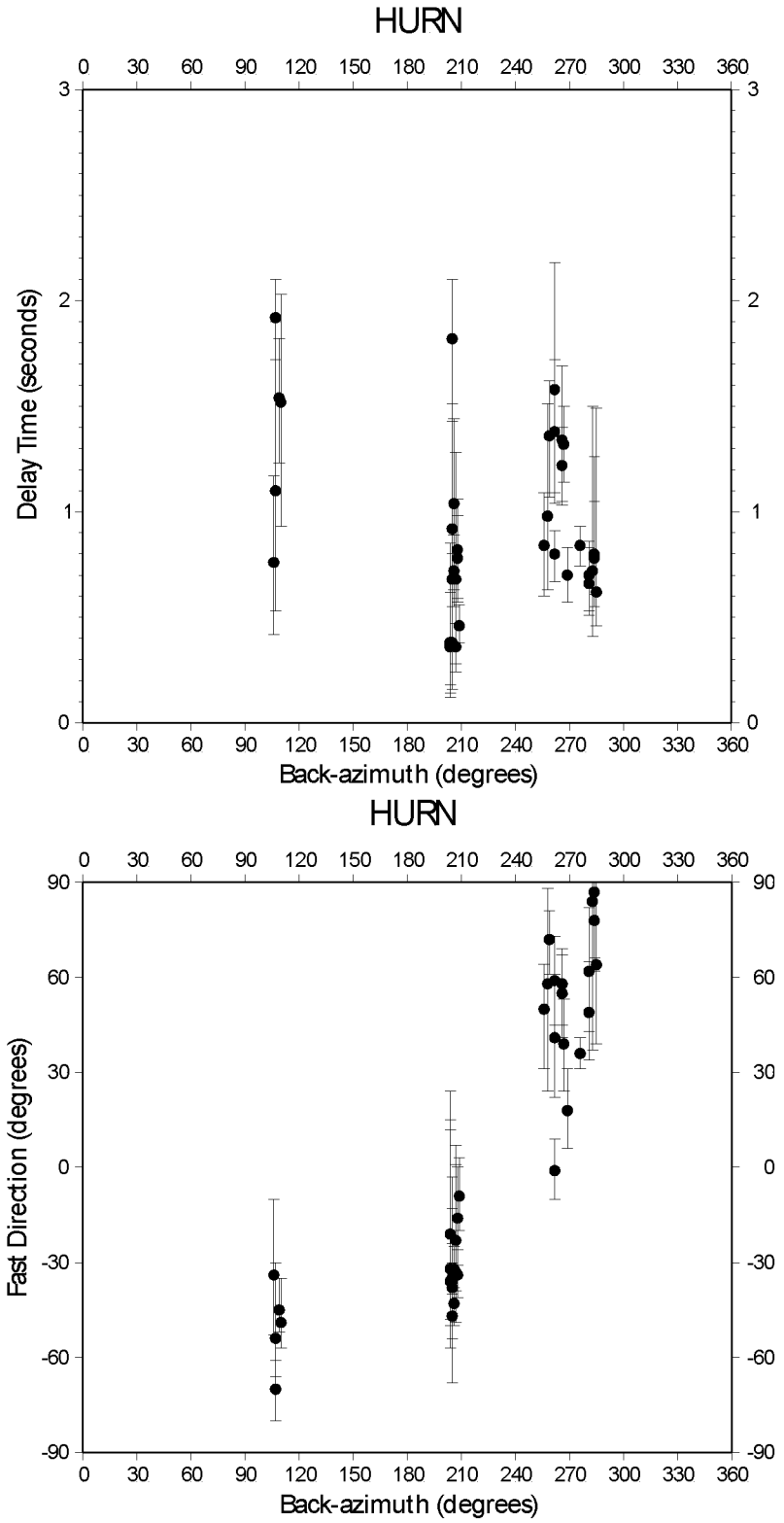

Figure B.12: Station HURN from the BEAAR network.
Delay times vs. back-azimuth (top) and fast direction vs. back-azimuth (bottom).

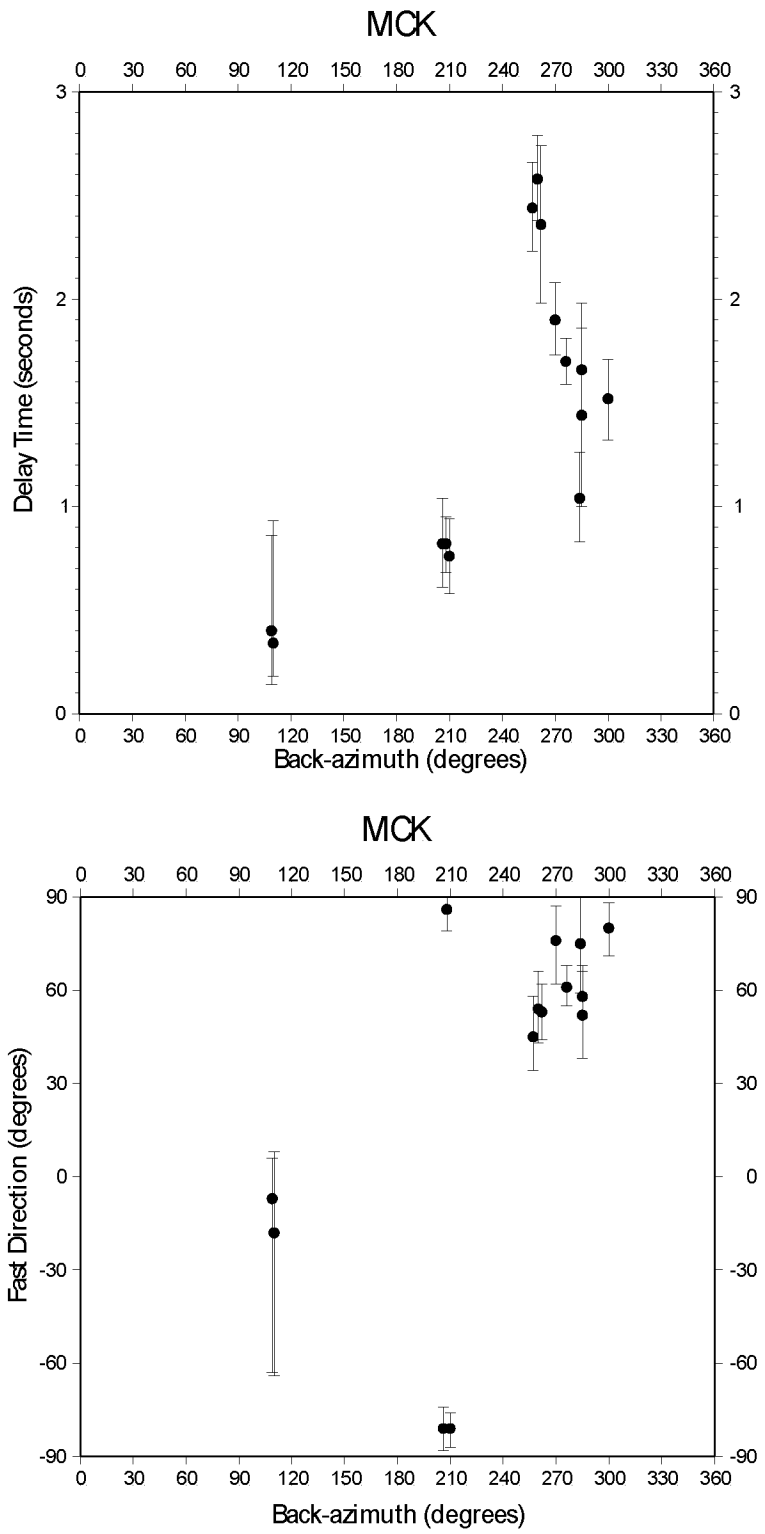

Figure B.13: Station MCK from the BEAAR network.
Delay times vs. back-azimuth (top) and fast direction vs. back-azimuth (bottom).

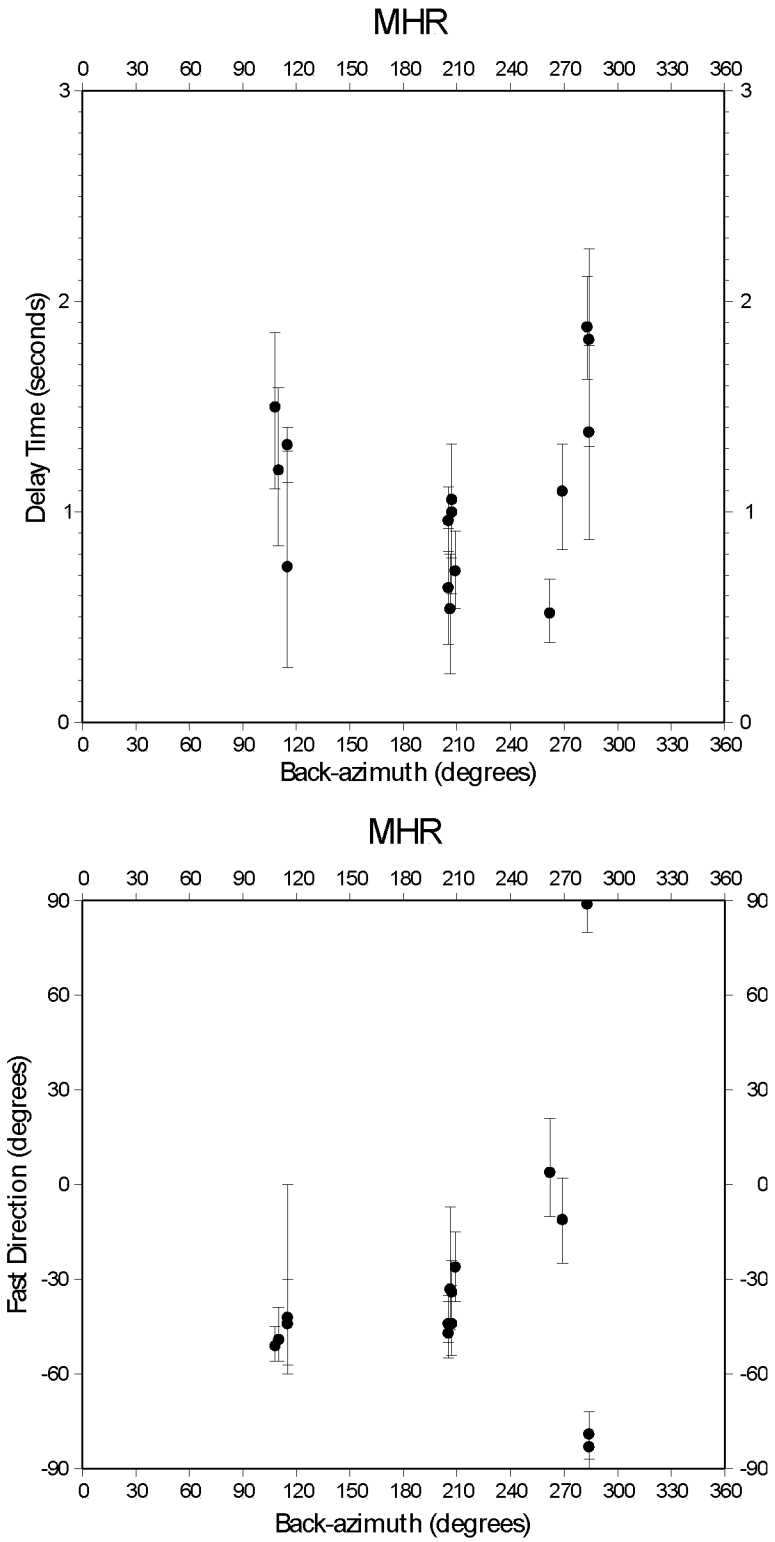

Figure B.14: Station MHR from the BEAAR network.
Delay times vs. back-azimuth (top) and fast direction vs. back-azimuth (bottom).

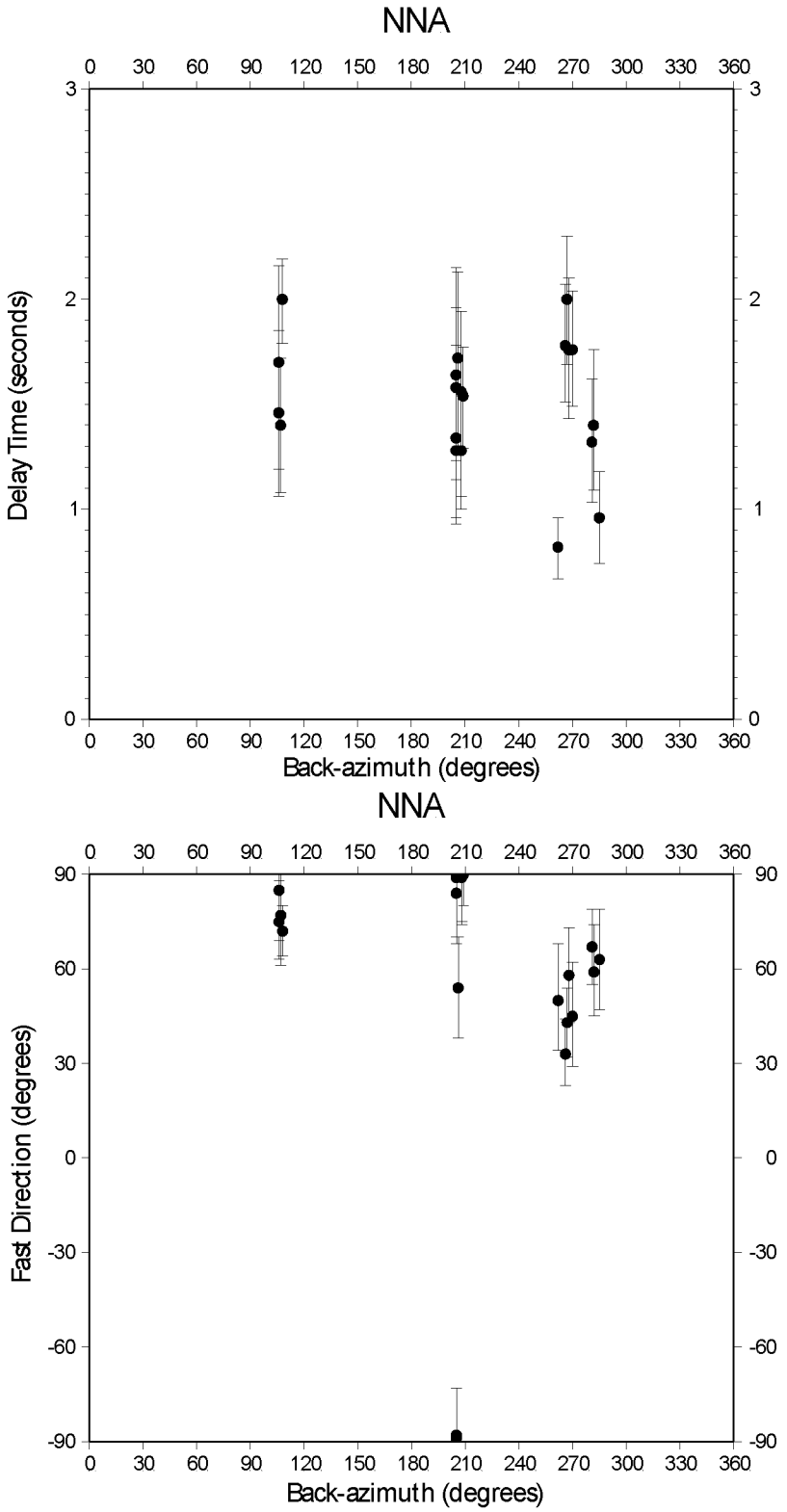

Figure B.15: Station NNA from the BEAAR network.
Delay times vs. back-azimuth (top) and fast direction vs. back-azimuth (bottom).

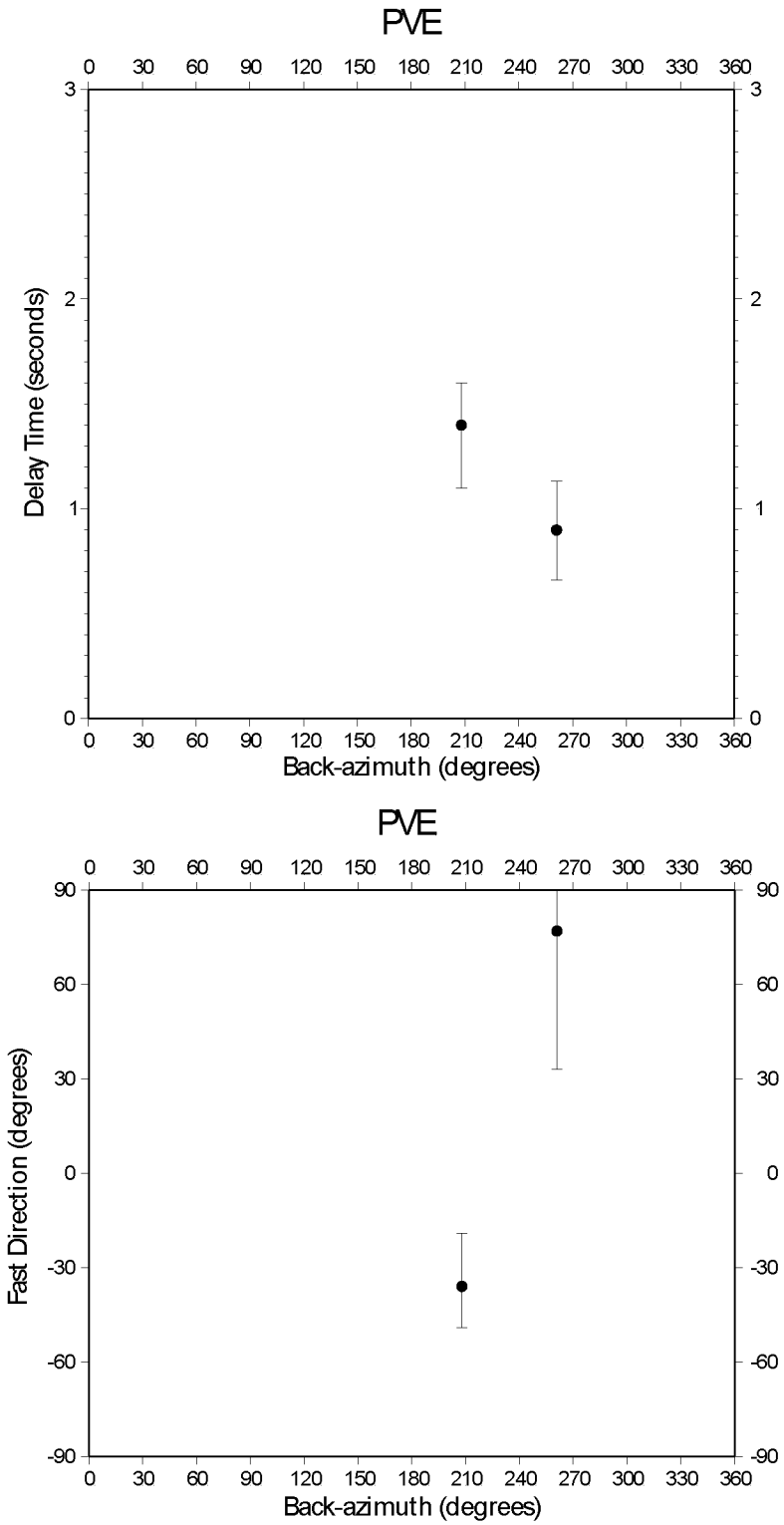

Figure B.16: Station PVE from the BEAAR network.
Delay times vs. back-azimuth (top) and fast direction vs. back-azimuth (bottom).

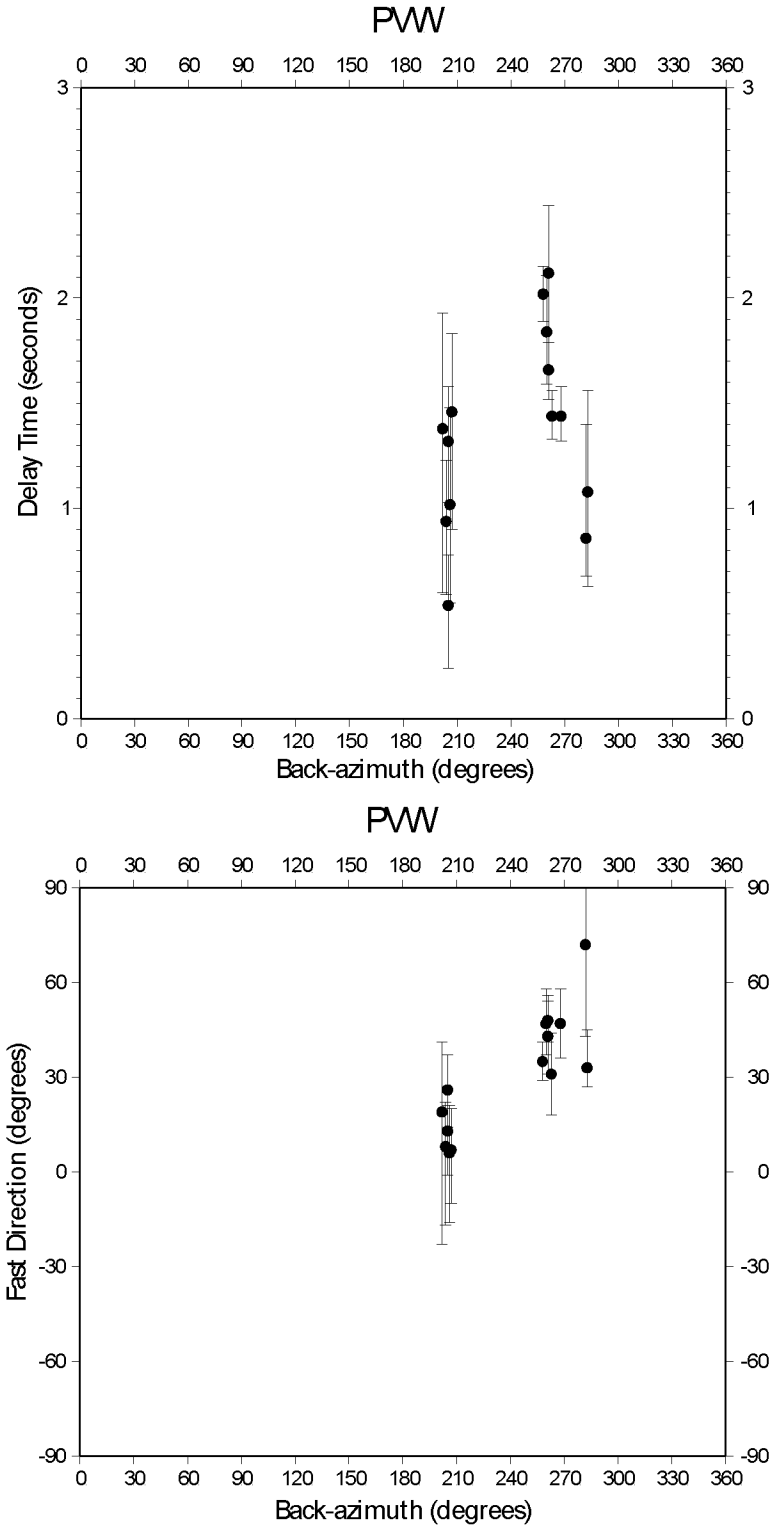

Figure B.17: Station PVW from the BEAAR network.
Delay times vs. back-azimuth (top) and fast direction vs. back-azimuth (bottom).

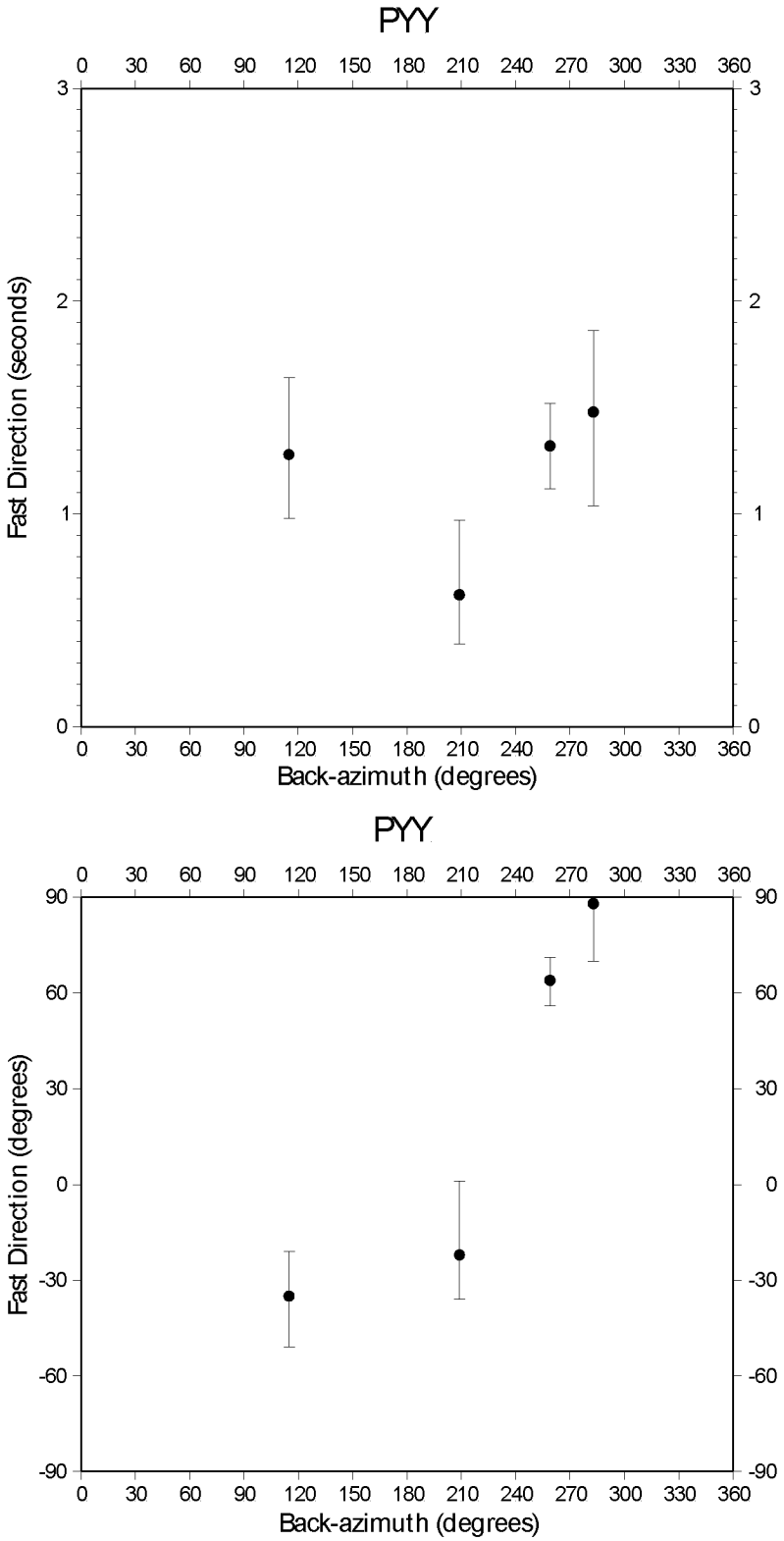

Figure B.18: Station PYY from the BEAAR network.
Delay times vs. back-azimuth (top) and fast direction vs. back-azimuth (bottom).

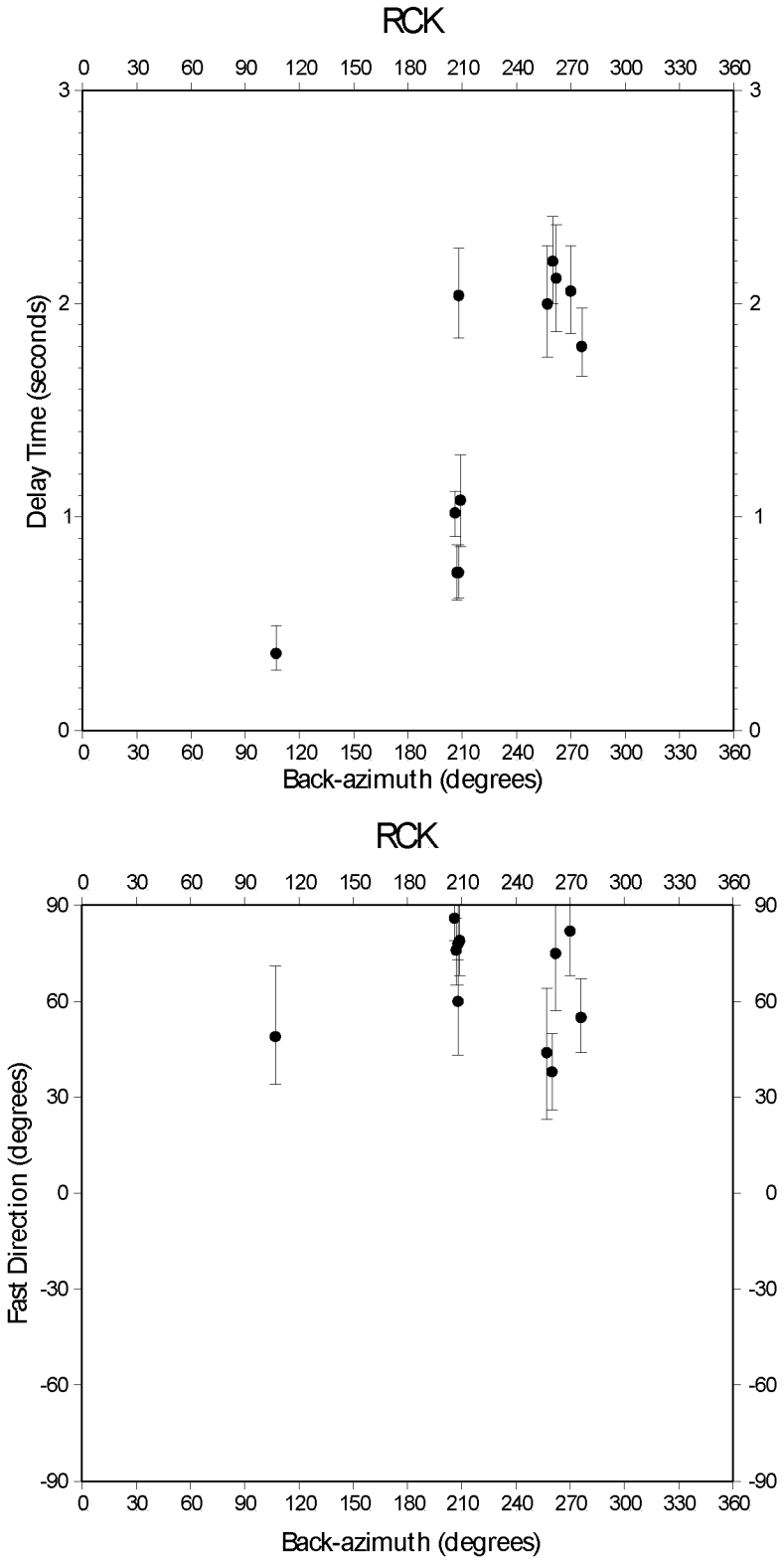

Figure B.19: Station RCK from the BEAAR network.
Delay times vs. back-azimuth (top) and fast direction vs. back-azimuth (bottom).

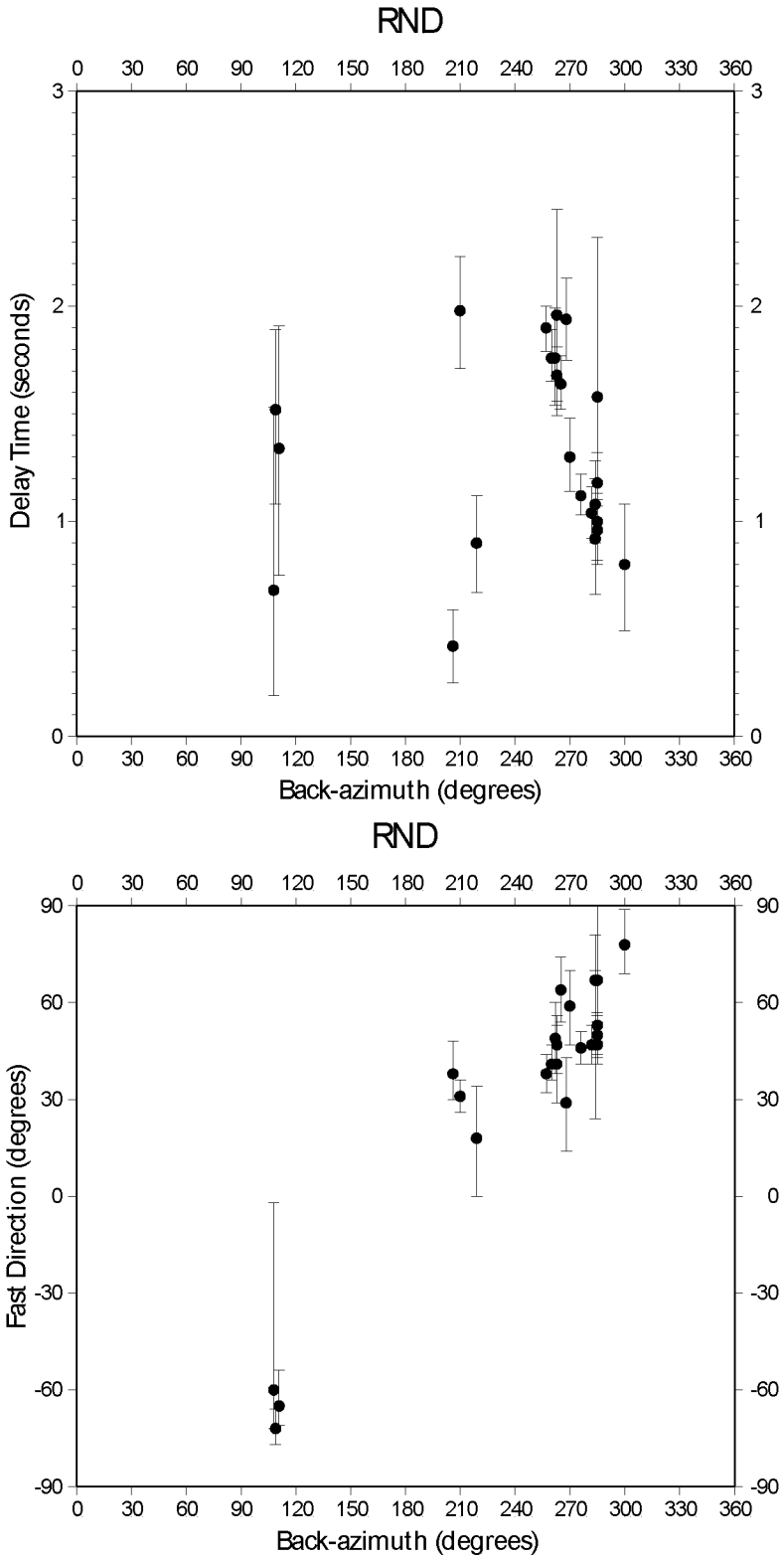

Figure B.20: Station RND from the BEAAR network.
Delay times vs. back-azimuth (top) and fast direction vs. back-azimuth (bottom).

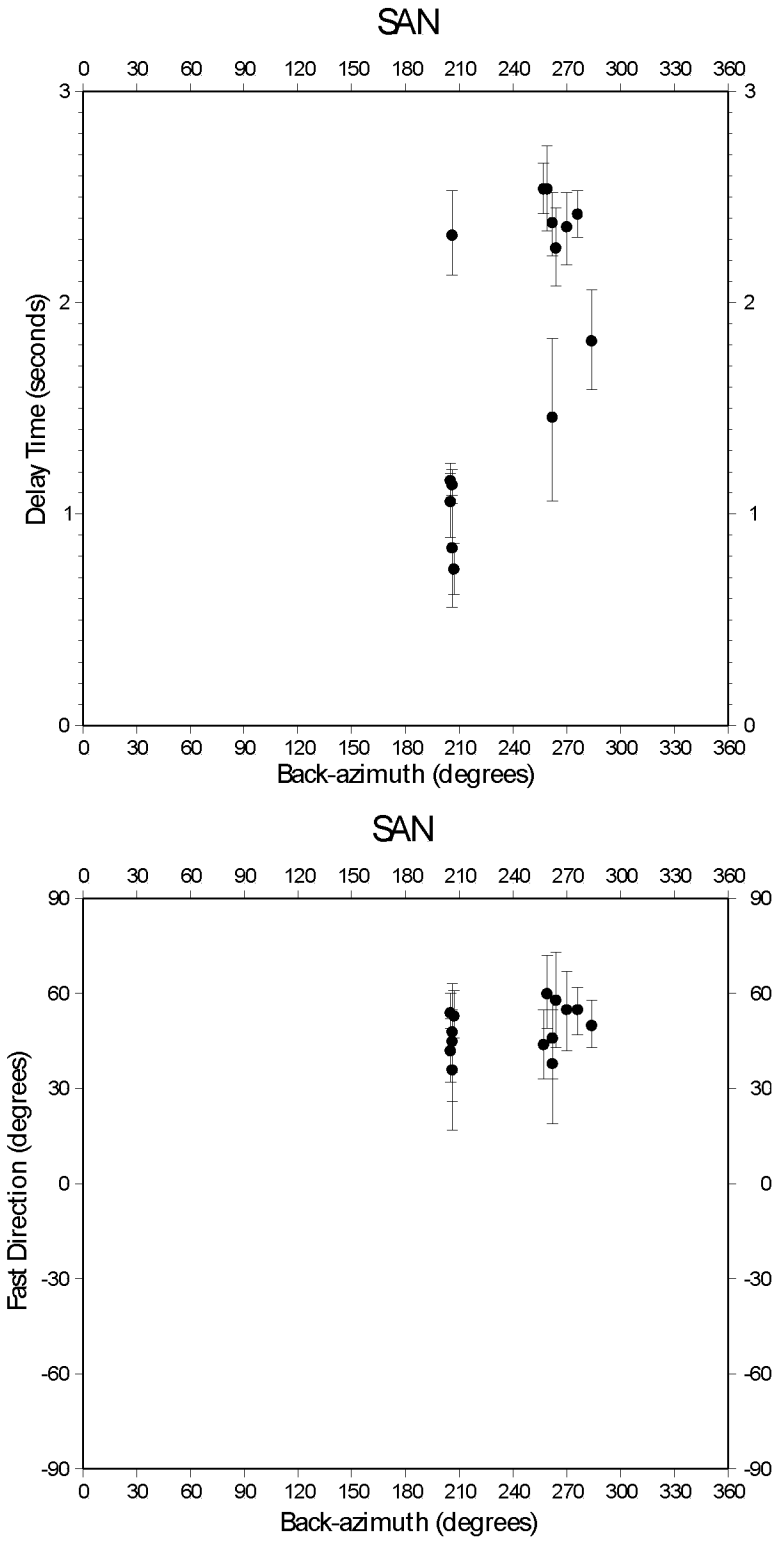

Figure B.21: Station SAN from the BEAAR network.
Delay times vs. back-azimuth (top) and fast direction vs. back-azimuth (bottom).

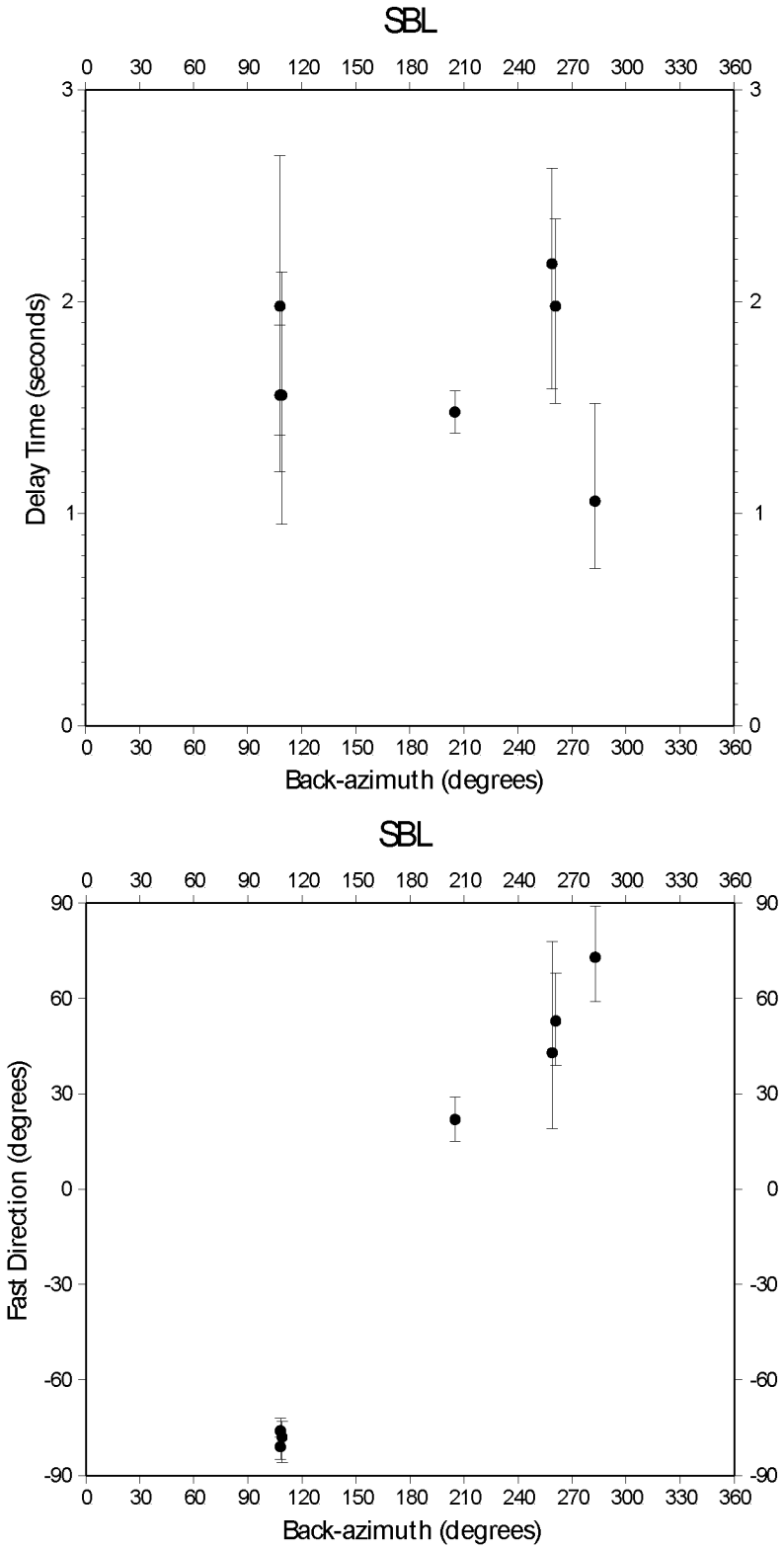

Figure B.22: Station SBL from the BEAAR network.
Delay times vs. back-azimuth (top) and fast direction vs. back-azimuth (bottom).

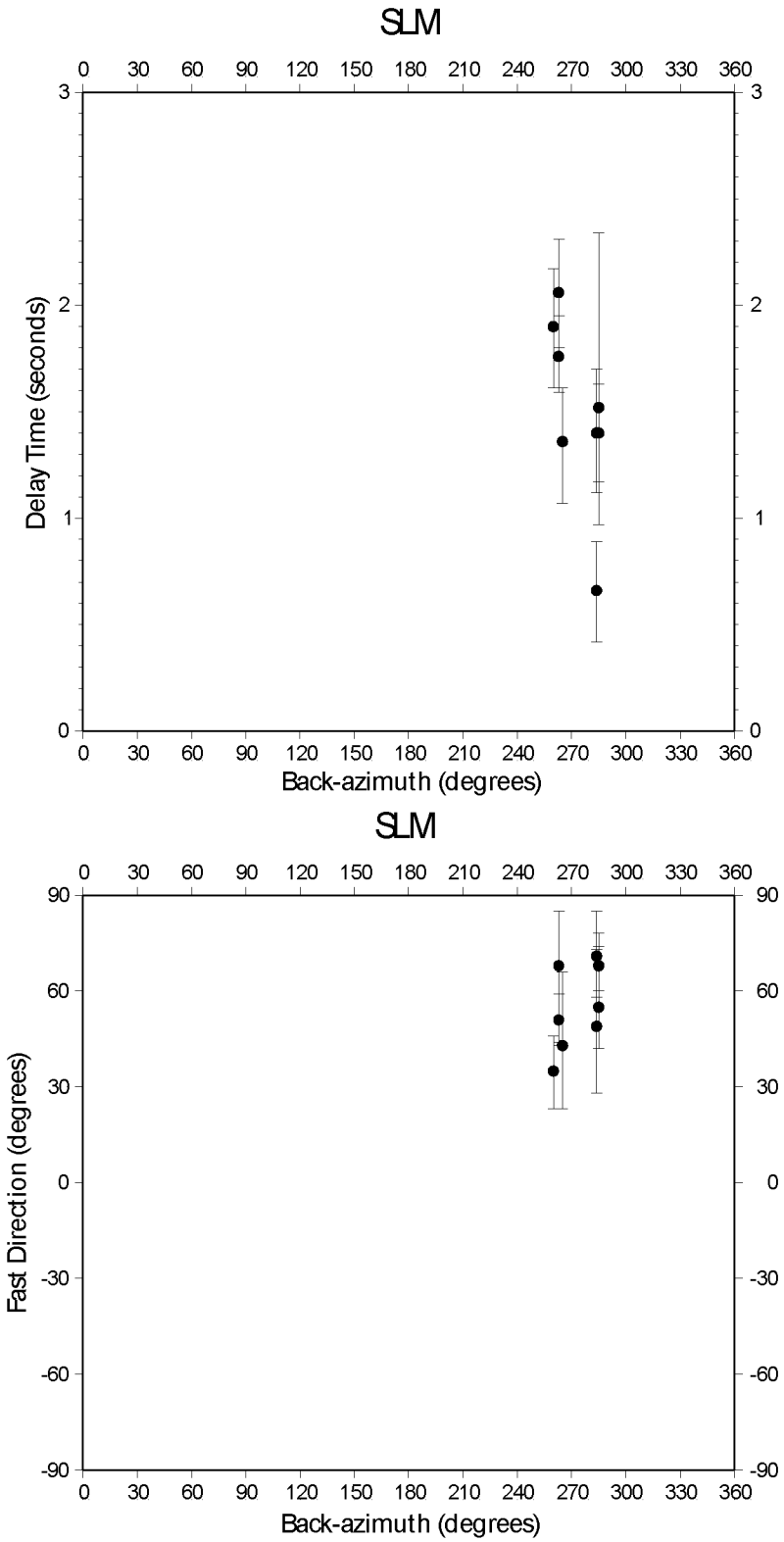

Figure B.23: Station SLM from the BEAAR network.
Delay times vs. back-azimuth (top) and fast direction vs. back-azimuth (bottom).

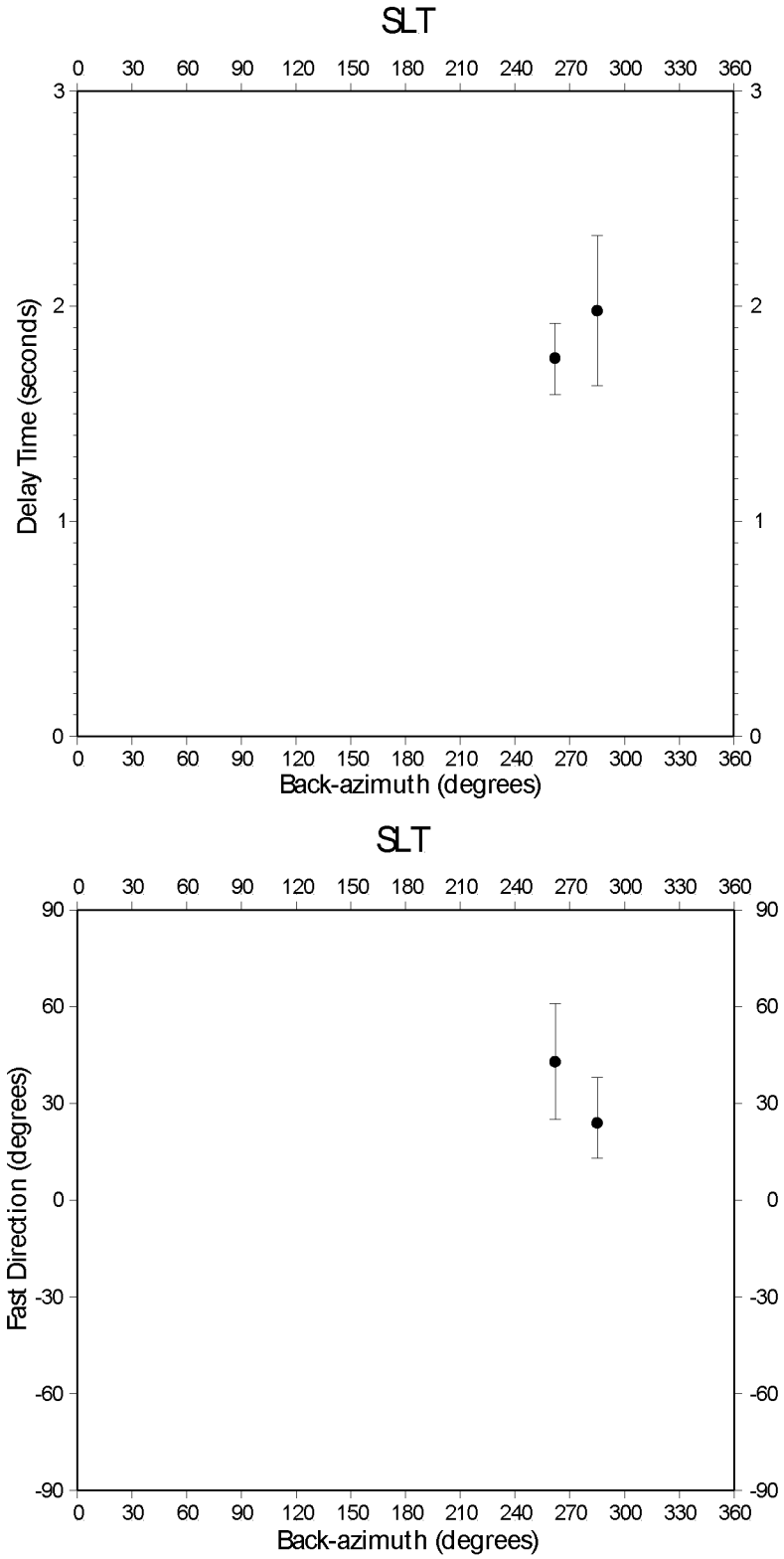

Figure B.24: Station SLT from the BEAAR network.
Delay times vs. back-azimuth (top) and fast direction vs. back-azimuth (bottom).

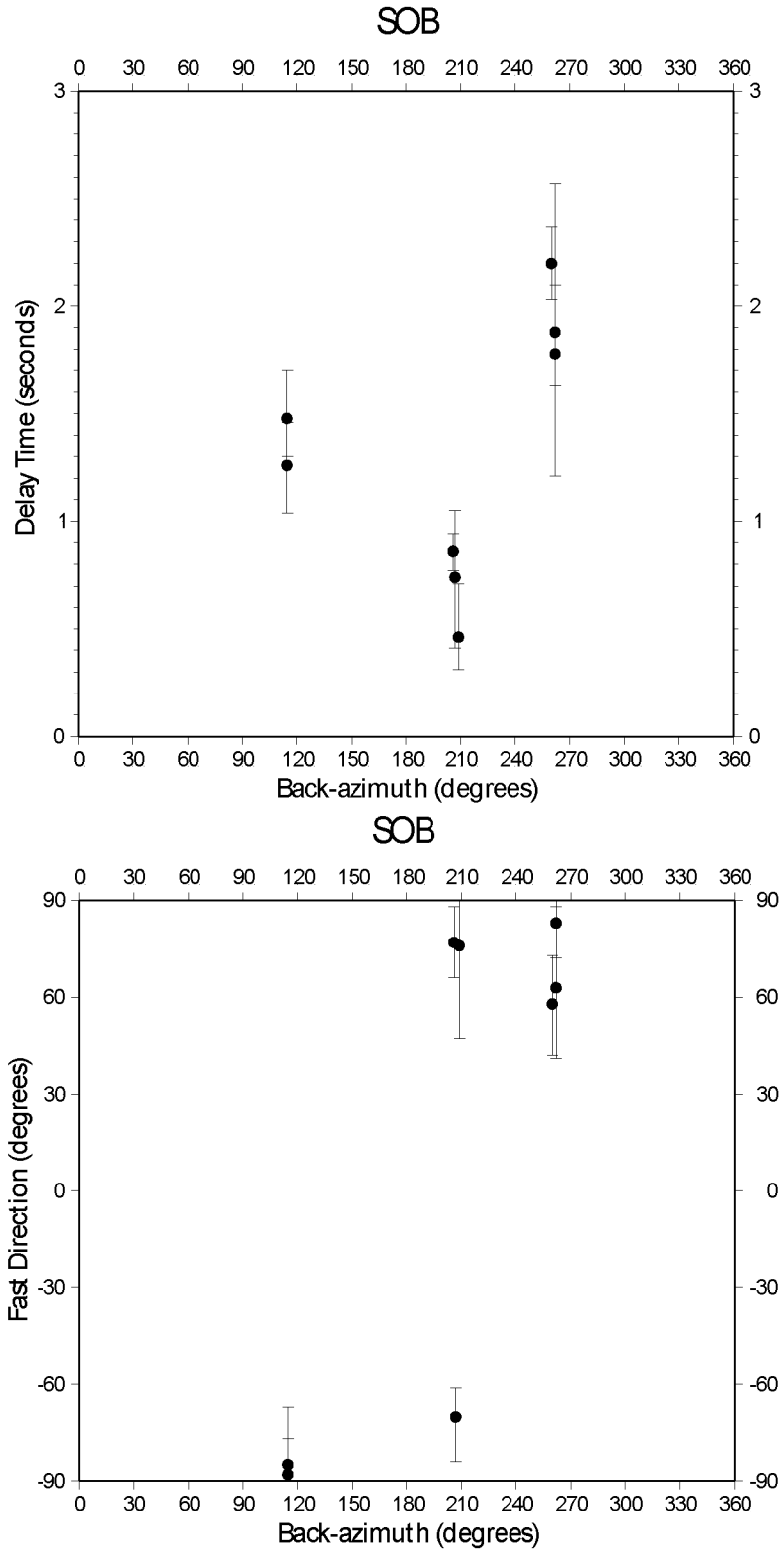

Figure B.25: Station SOB from the BEAAR network.
Delay times vs. back-azimuth (top) and fast direction vs. back-azimuth (bottom).

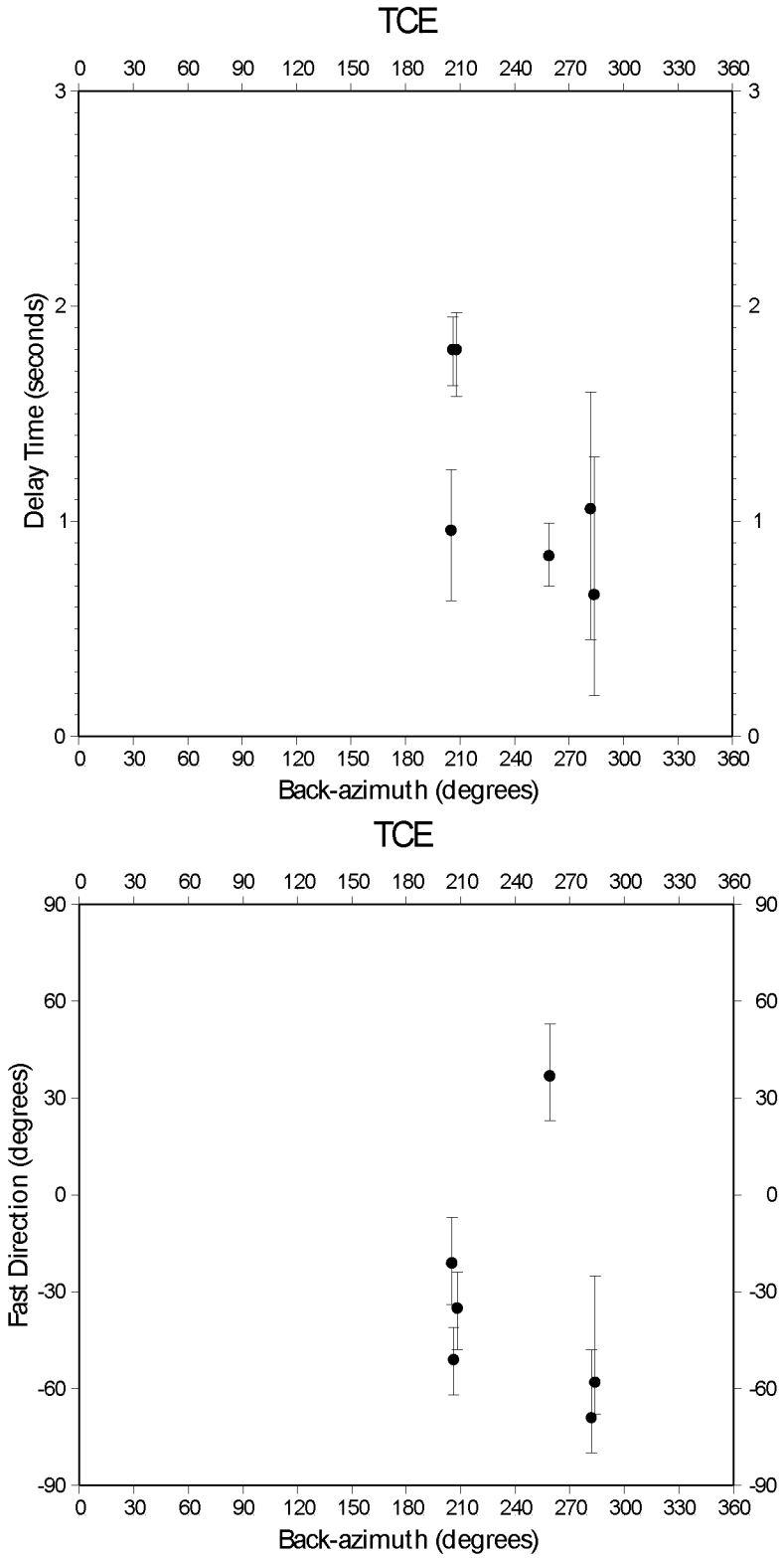

Figure B.26: Station TCE from the BEAAR network.
Delay times vs. back-azimuth (top) and fast direction vs. back-azimuth (bottom).

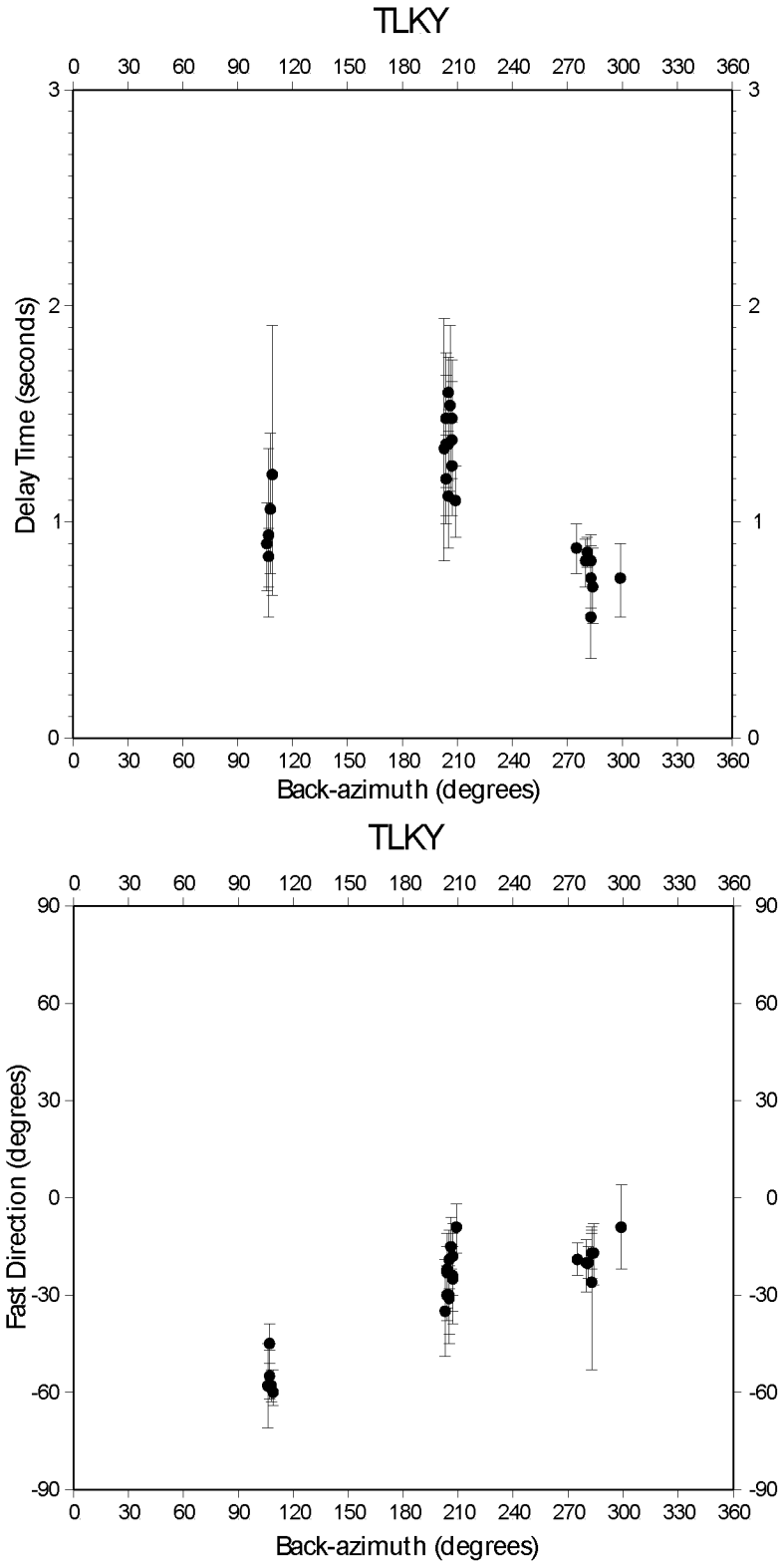

Figure B.27: Station TLKY from the BEAAR network.
Delay times vs. back-azimuth (top) and fast direction vs. back-azimuth (bottom).

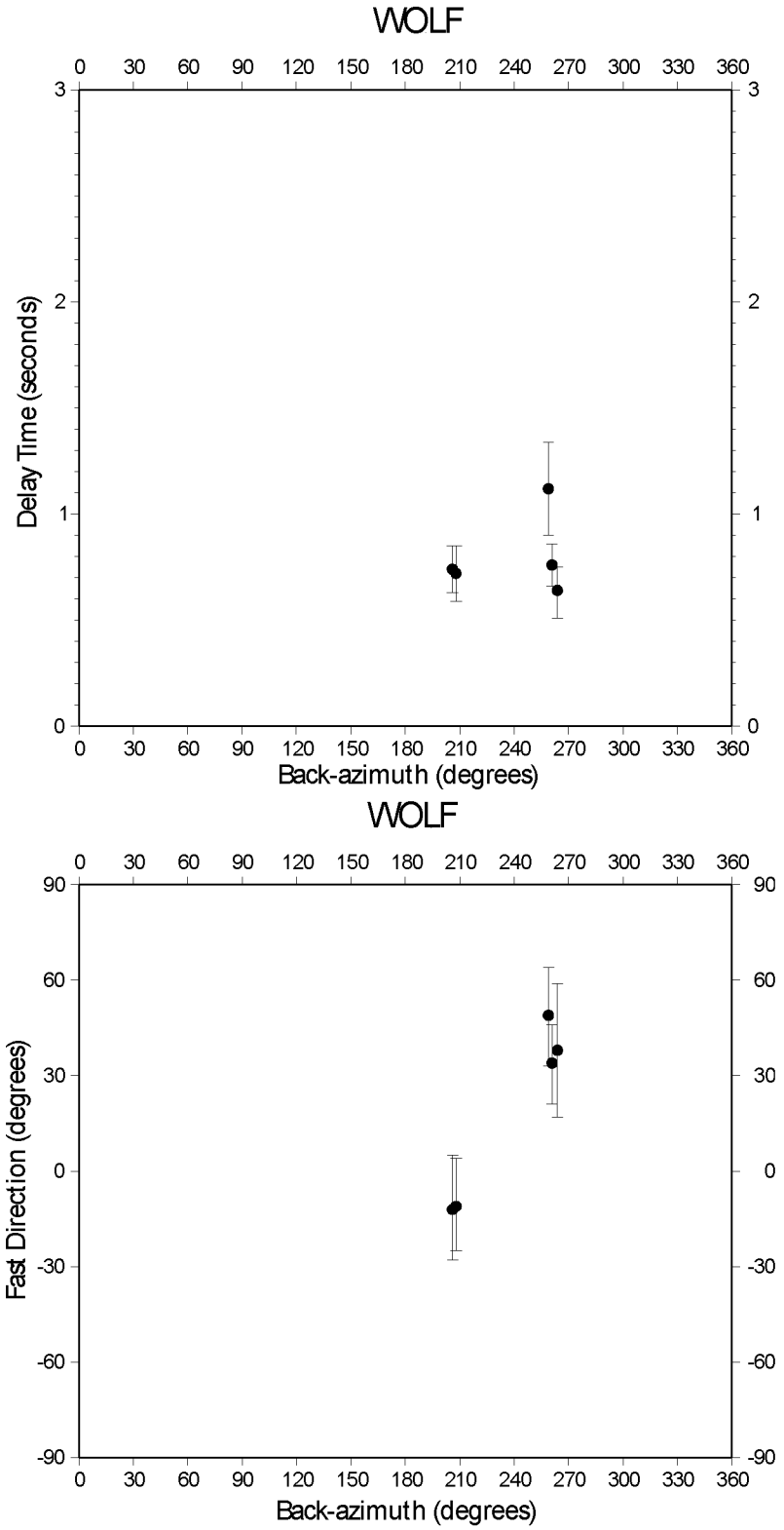

Figure B.28: Station WOLF from the BEAAR network.
Delay times vs. back-azimuth (top) and fast direction vs. back-azimuth (bottom).

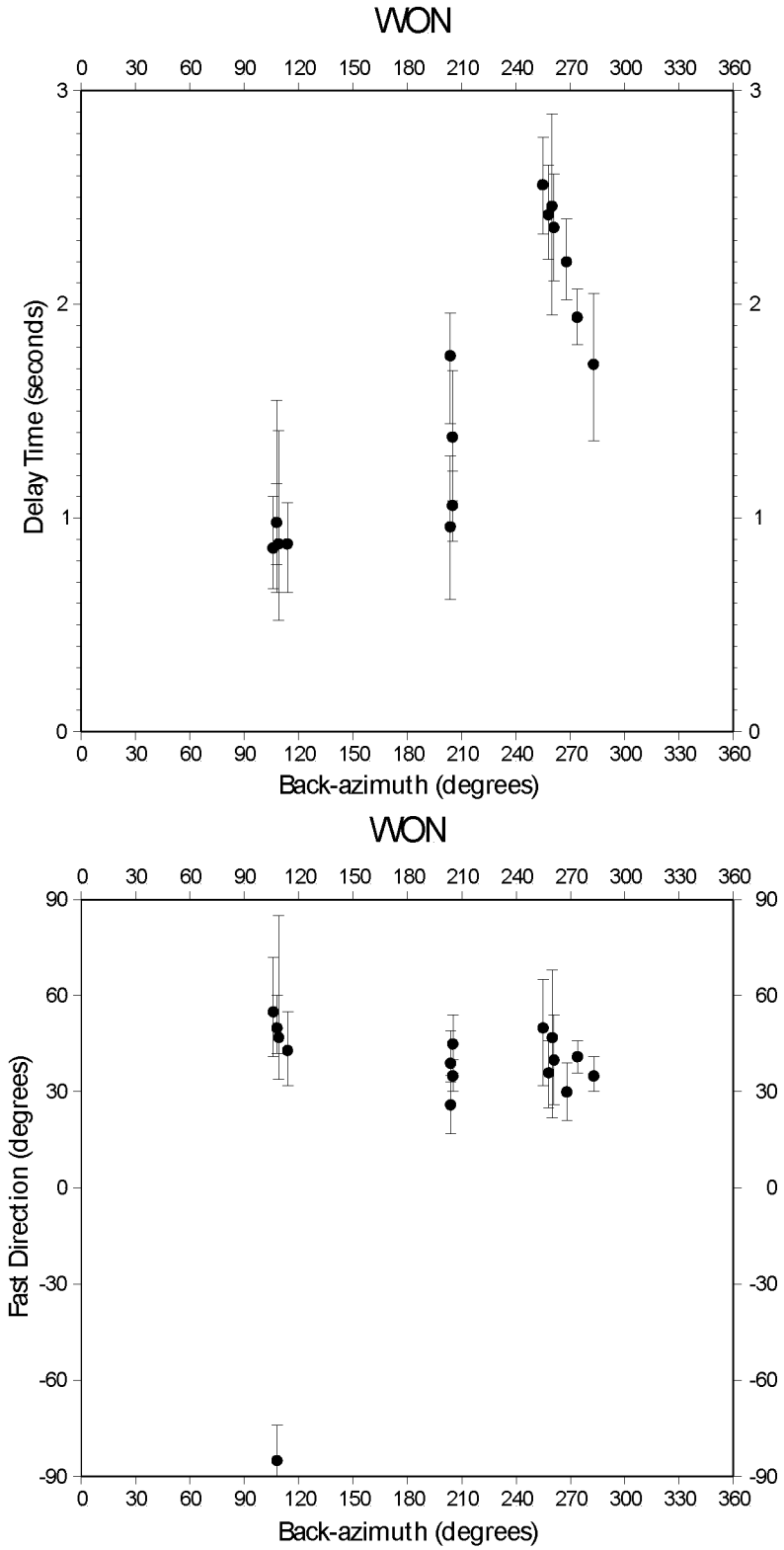

Figure B.29: Station WON from the BEAAR network.
Delay times vs. back-azimuth (top) and fast direction vs. back-azimuth (bottom).

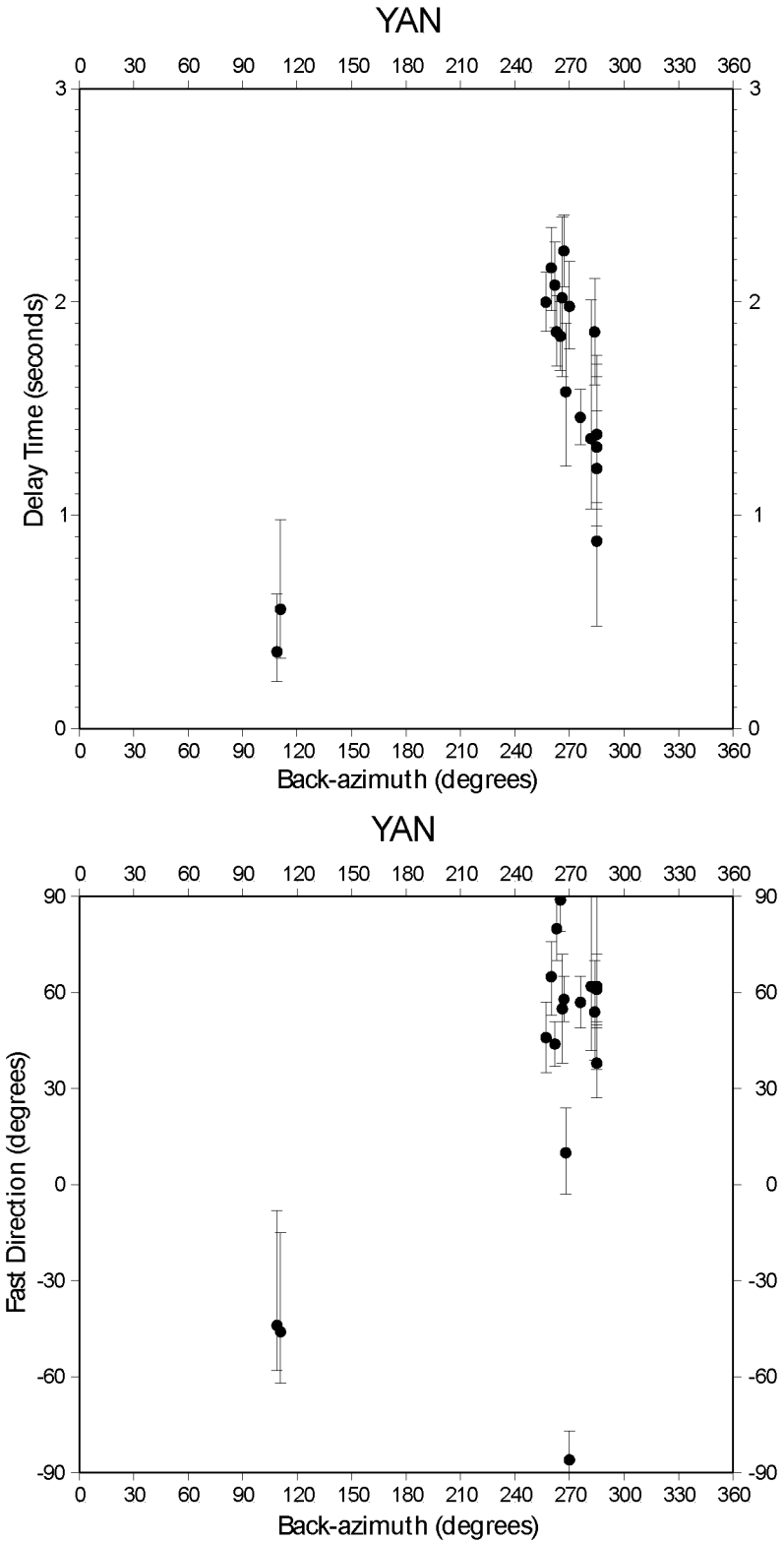

Figure B.30: Station YAN from the BEAAR network.
Delay times vs. back-azimuth (top) and fast direction vs. back-azimuth (bottom).

Appendix C

Splitting results from the MOOS network. Error bars represent 95% confidence region.

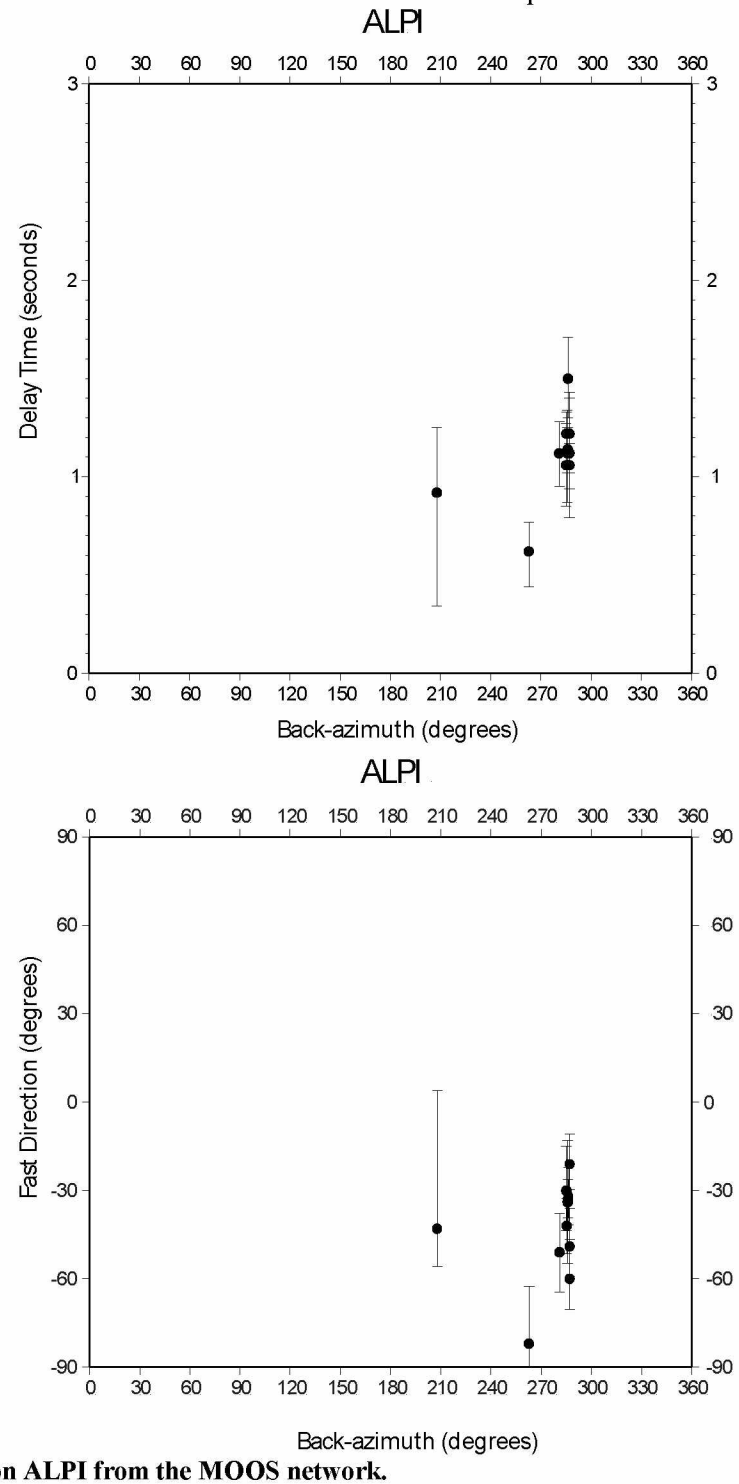

Figure C.1: Station ALPI from the MOOS network.
Delay times vs. back-azimuth (top) and fast direction vs. back-azimuth (bottom).

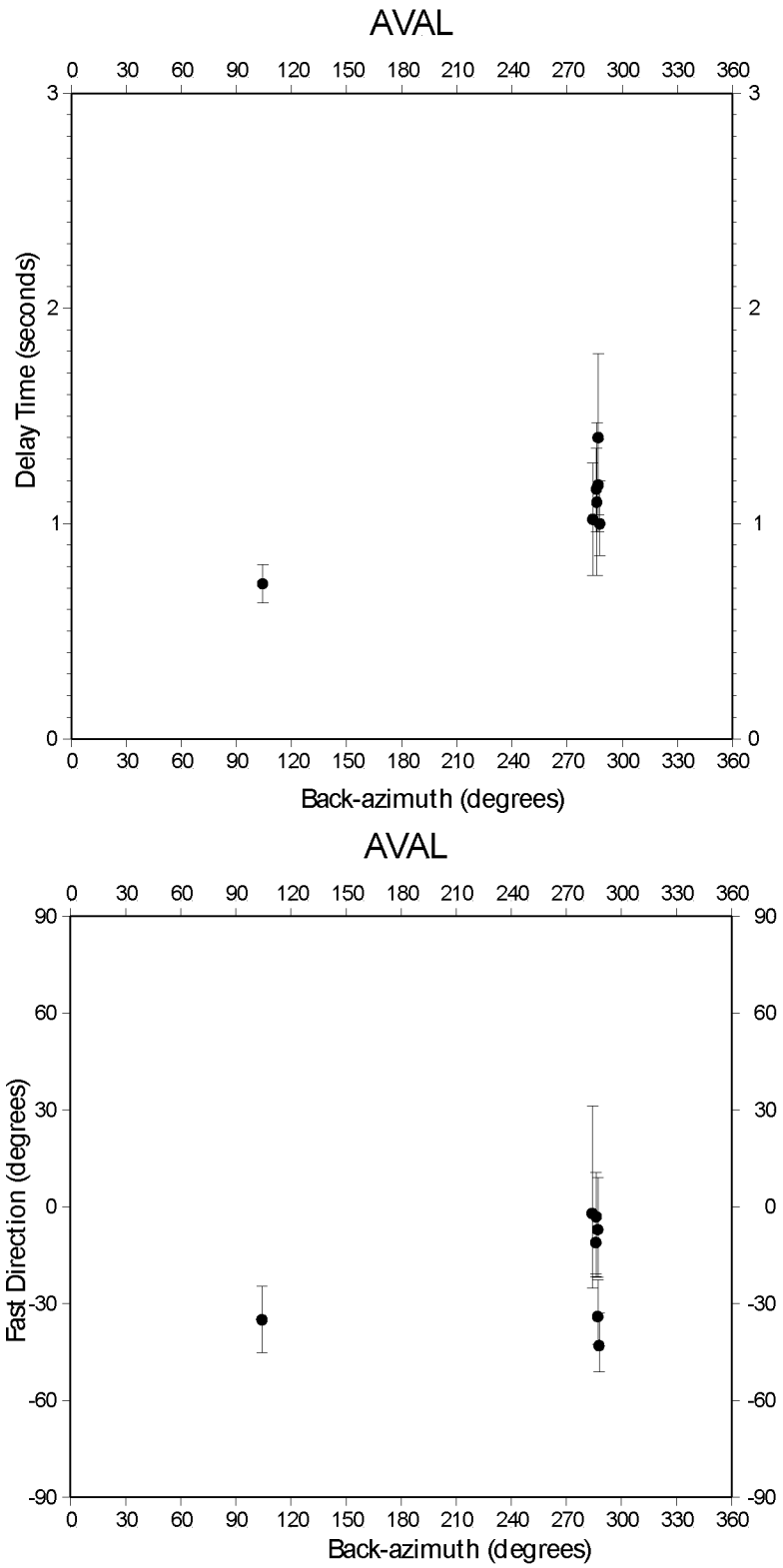

Figure C.2: Station AVAL from the MOOS network.
Delay times vs. back-azimuth (top) and fast direction vs. back-azimuth (bottom).

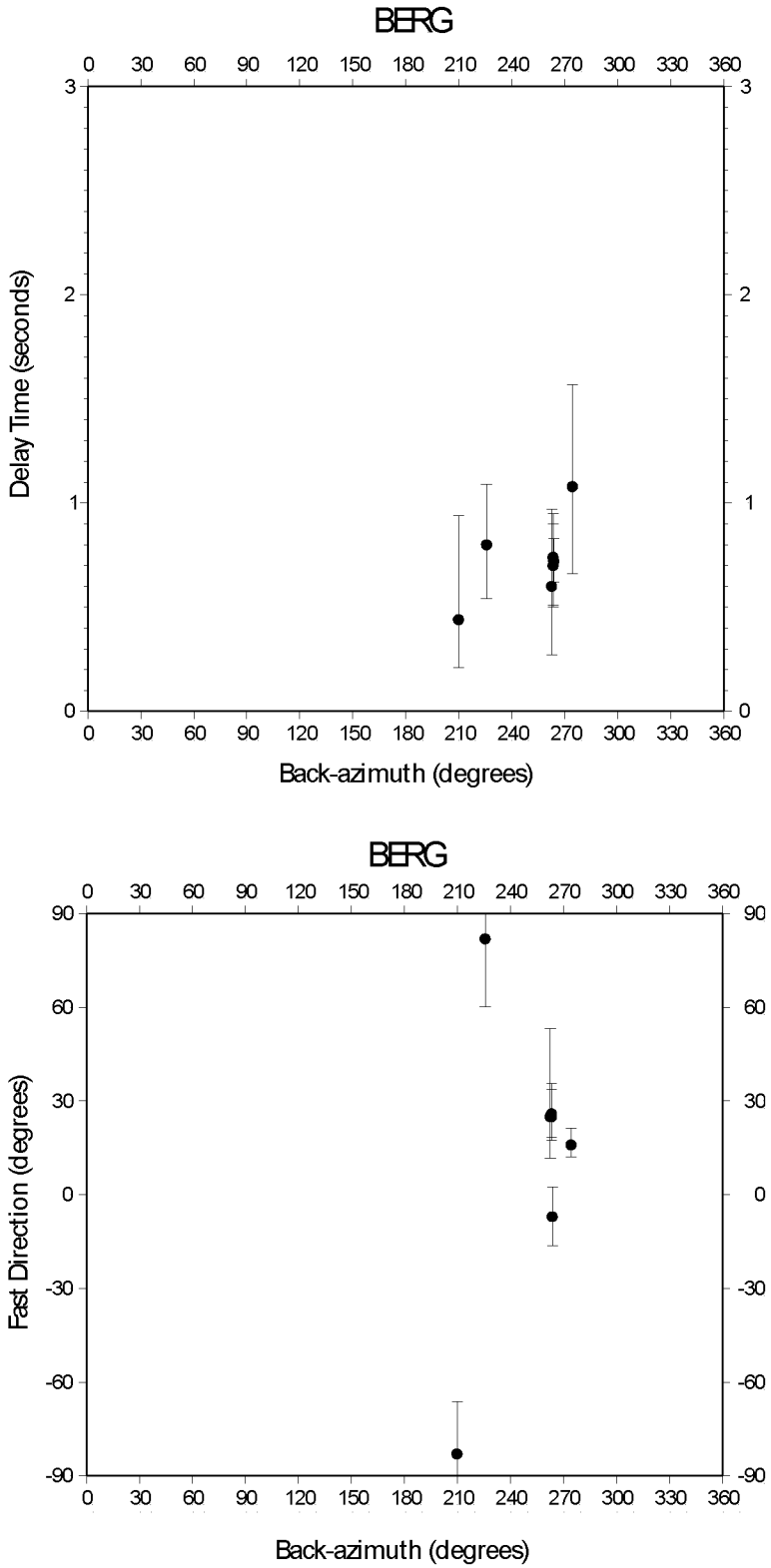

Figure C.3: Station BERG from the AEIC network.
Delay times vs. back-azimuth (top) and fast direction vs. back-azimuth (bottom).

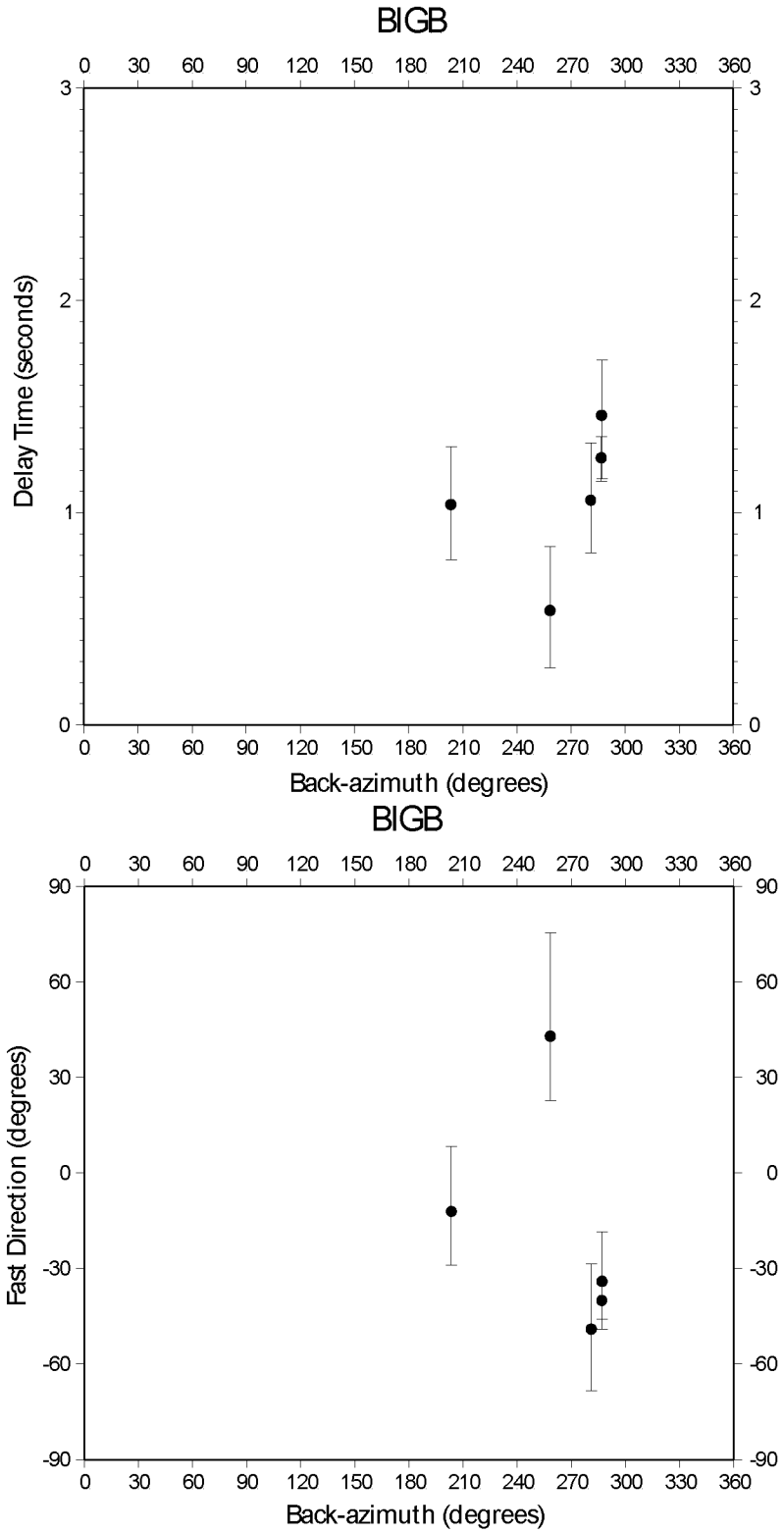

Figure C.4: Station BIGB from the MOOS network.
Delay times vs. back-azimuth (top) and fast direction vs. back-azimuth (bottom).

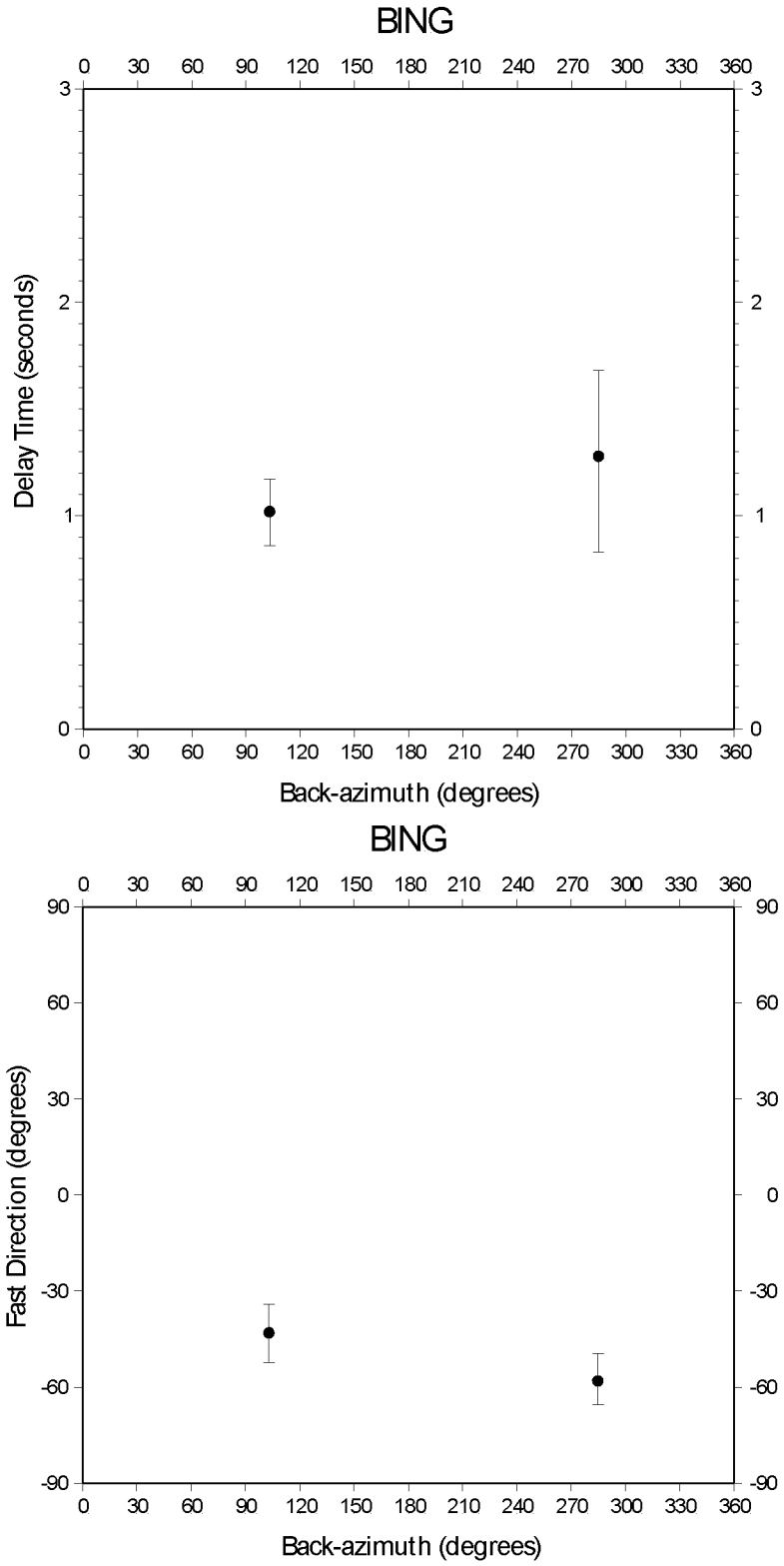

Figure C.5: Station BING from the MOOS network.
Delay times vs. back-azimuth (top) and fast direction vs. back-azimuth (bottom).

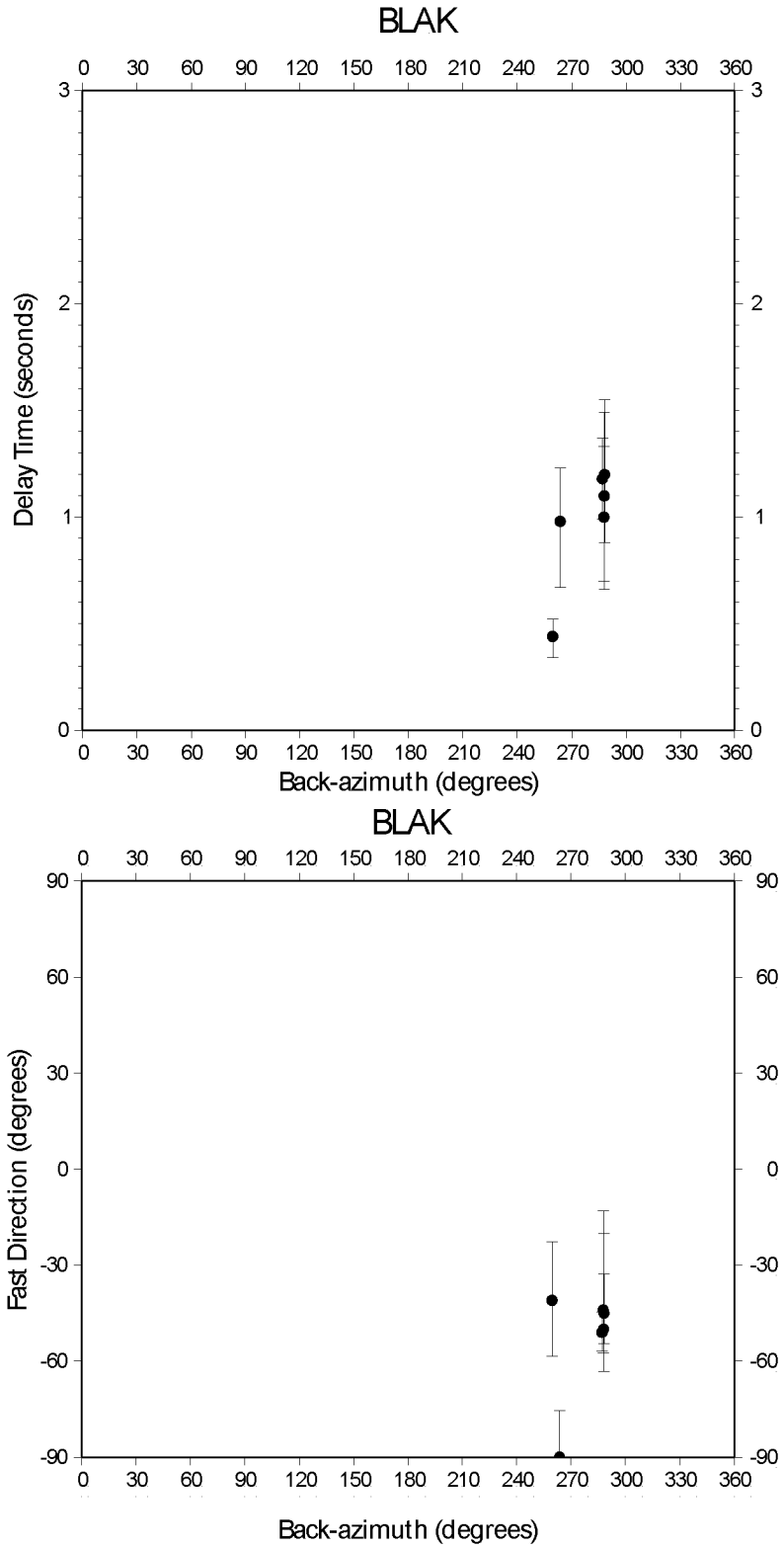

Figure C.6: Station BLAK from the MOOS network.
Delay times vs. back-azimuth (top) and fast direction vs. back-azimuth (bottom).

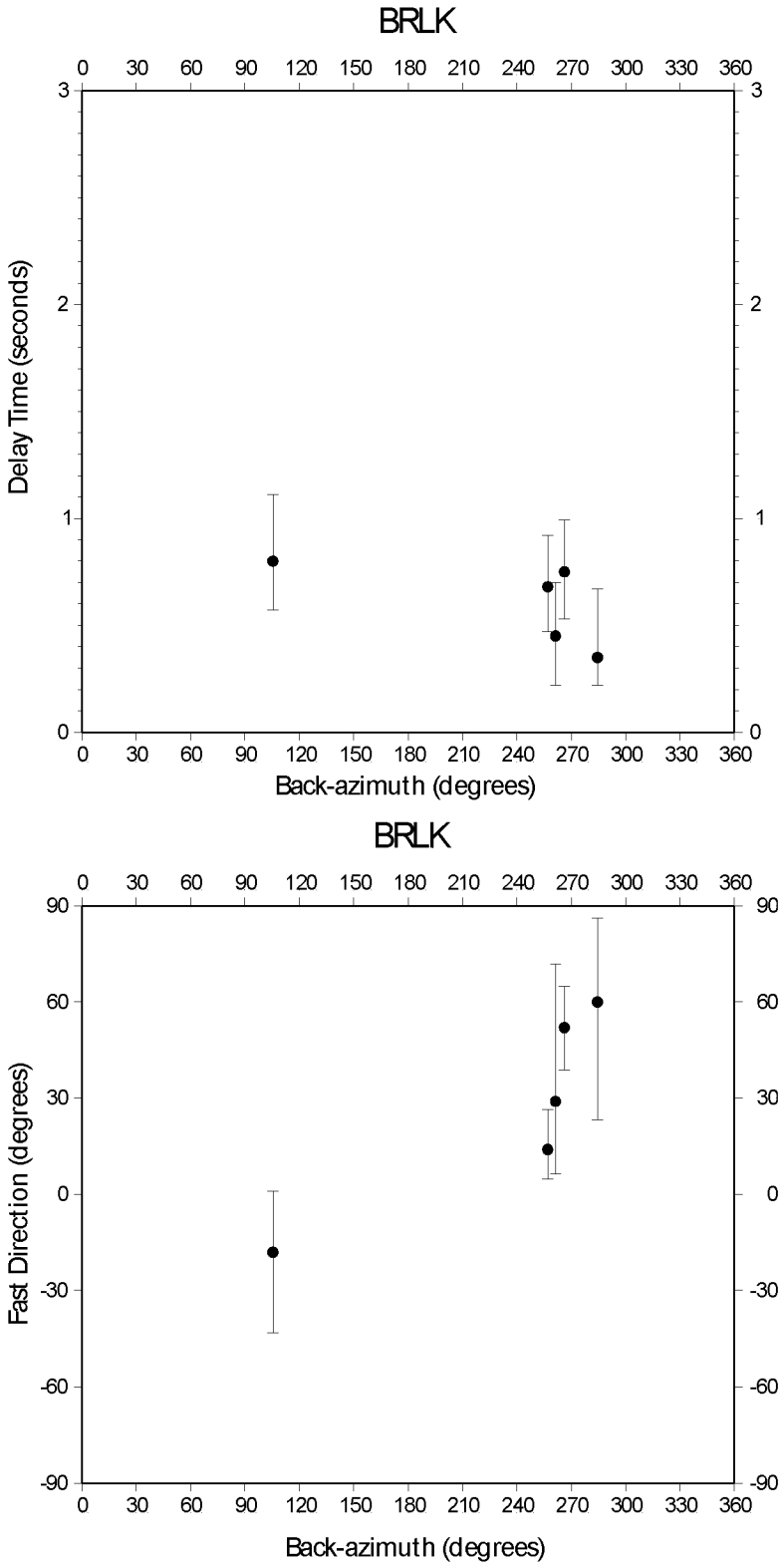

Figure C.7: Station BRLK from the AEIC network.
Delay times vs. back-azimuth (top) and fast direction vs. back-azimuth (bottom).

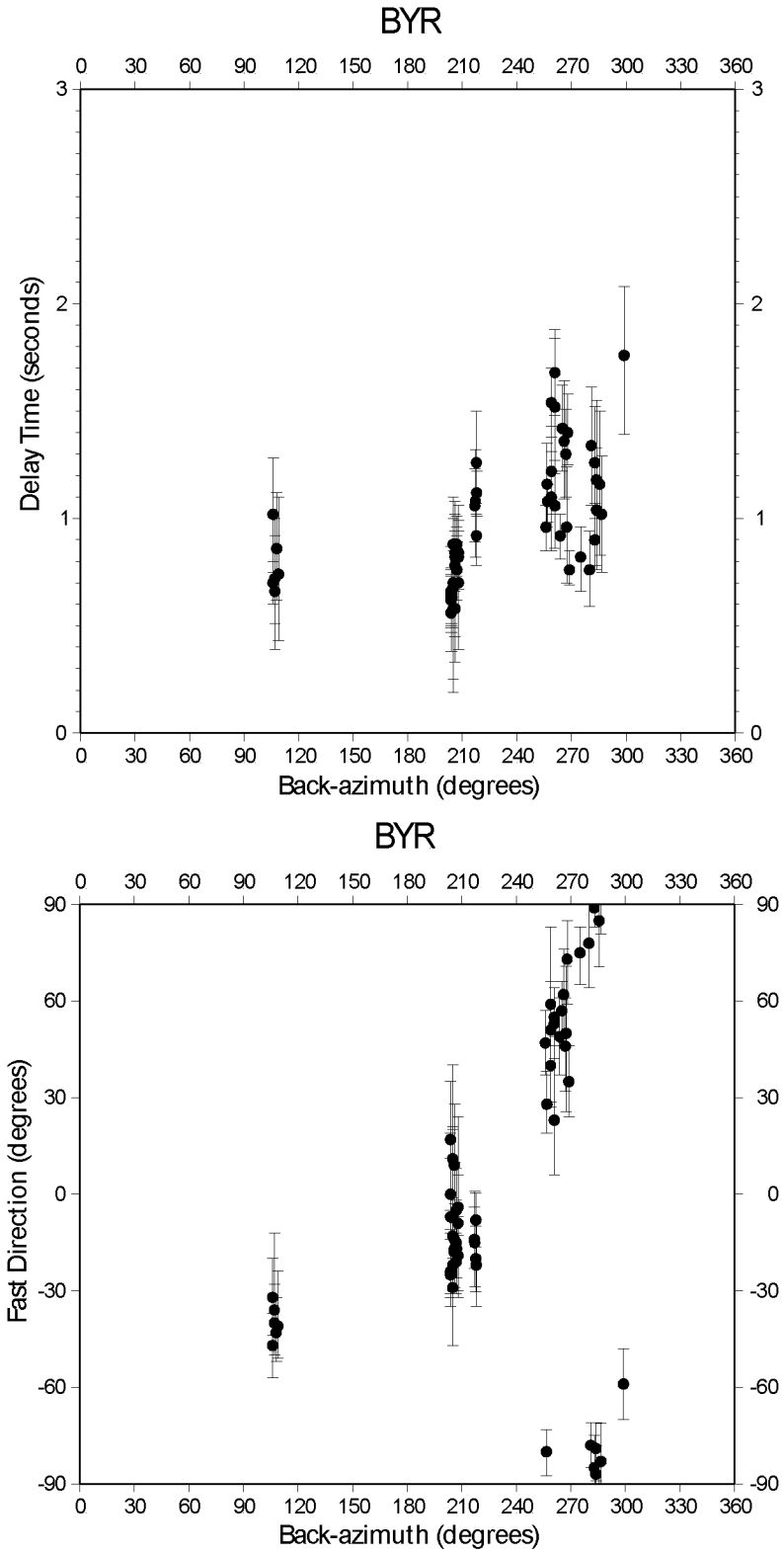

Figure C.8: Station BYR from the MOOS and BEAAR networks.
Delay times vs. back-azimuth (top) and fast direction vs. back-azimuth (bottom).

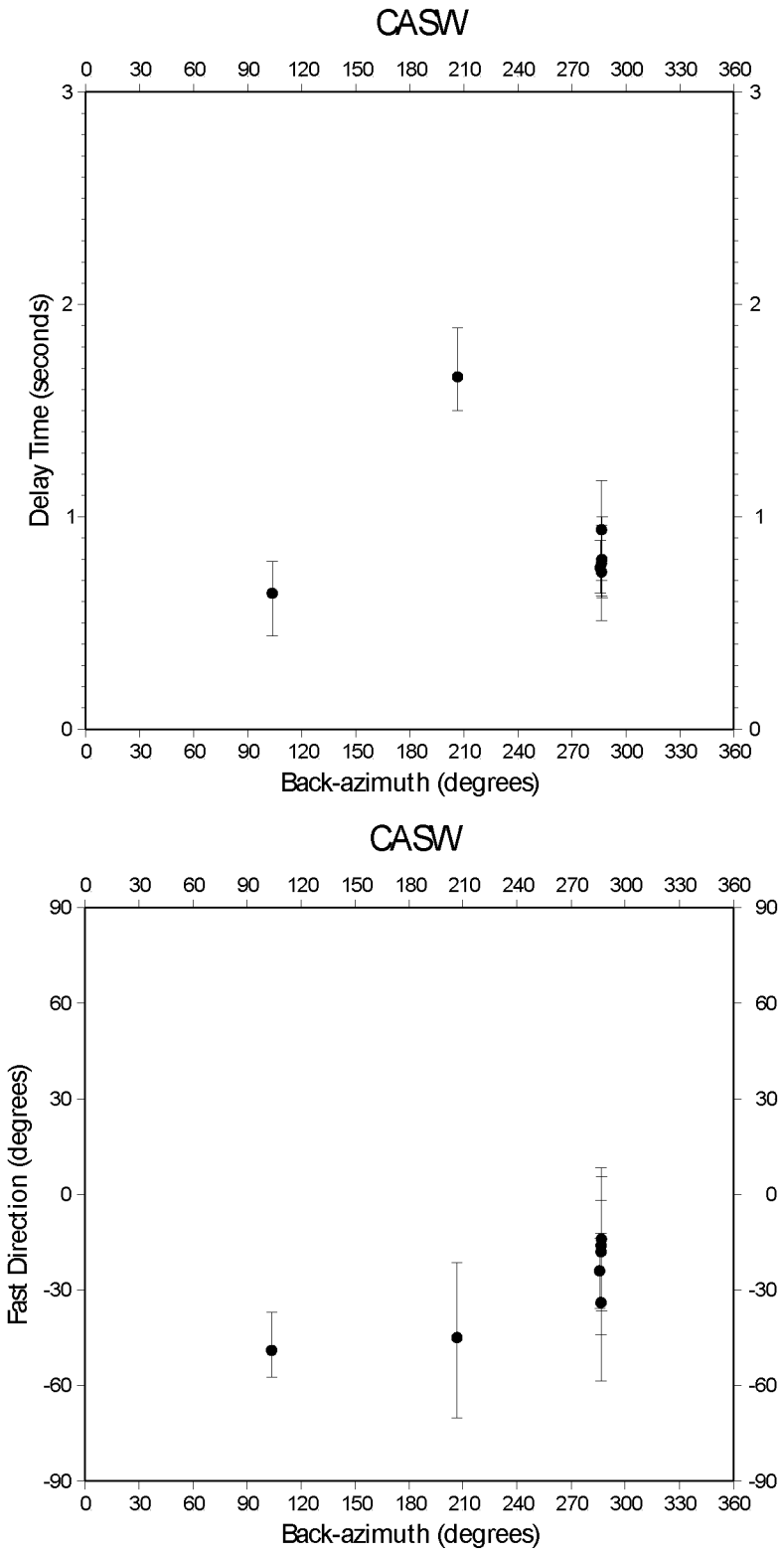

Figure C.9: Station CASW from the MOOS network.
Delay times vs. back-azimuth (top) and fast direction vs. back-azimuth (bottom).

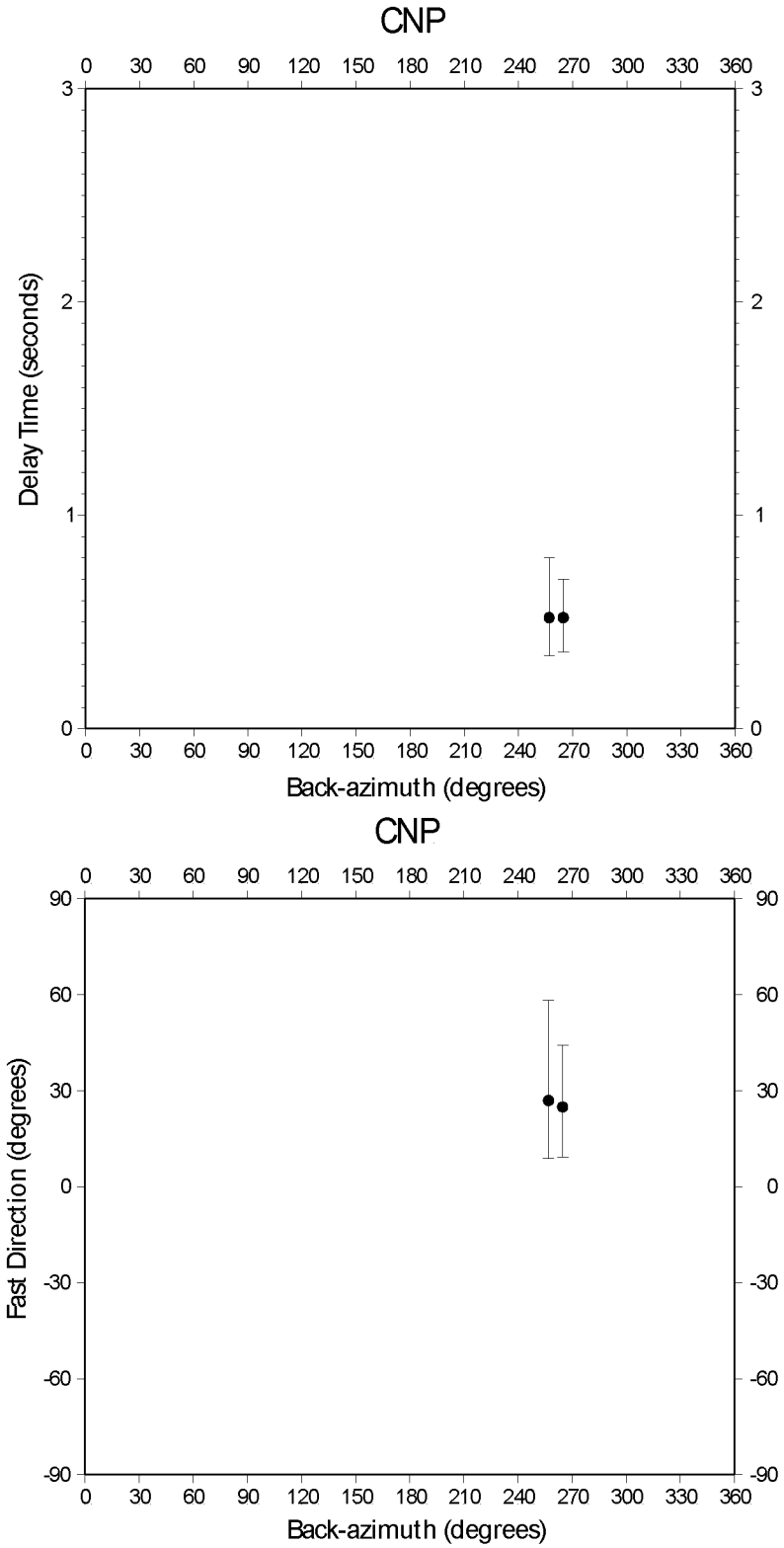

Figure C.10: Station CNP from the AEIC network.
Delay times vs. back-azimuth (top) and fast direction vs. back-azimuth (bottom).

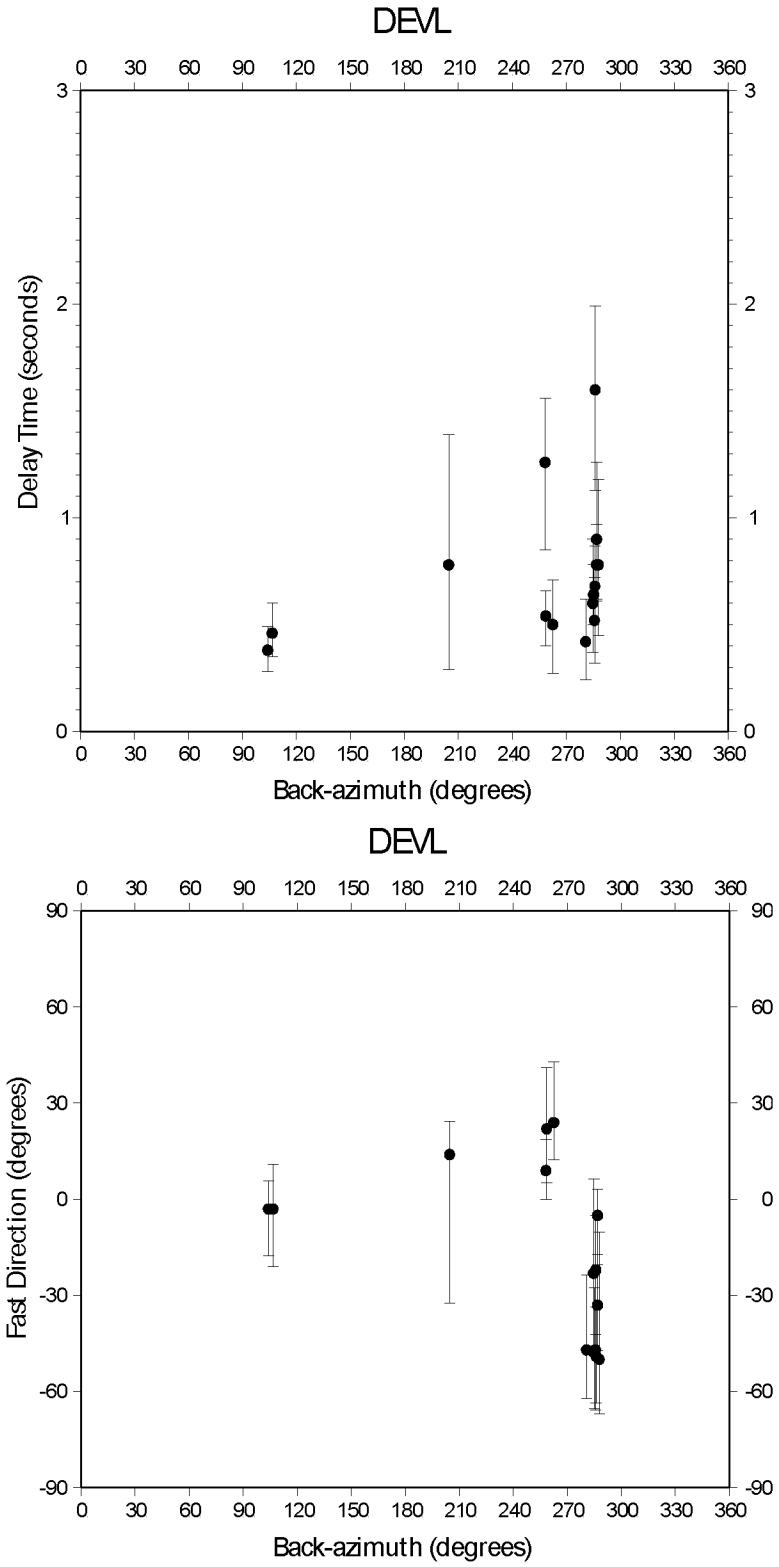

Figure C.11: Station DEVL from the MOOS network.
Delay times vs. back-azimuth (top) and fast direction vs. back-azimuth (bottom).

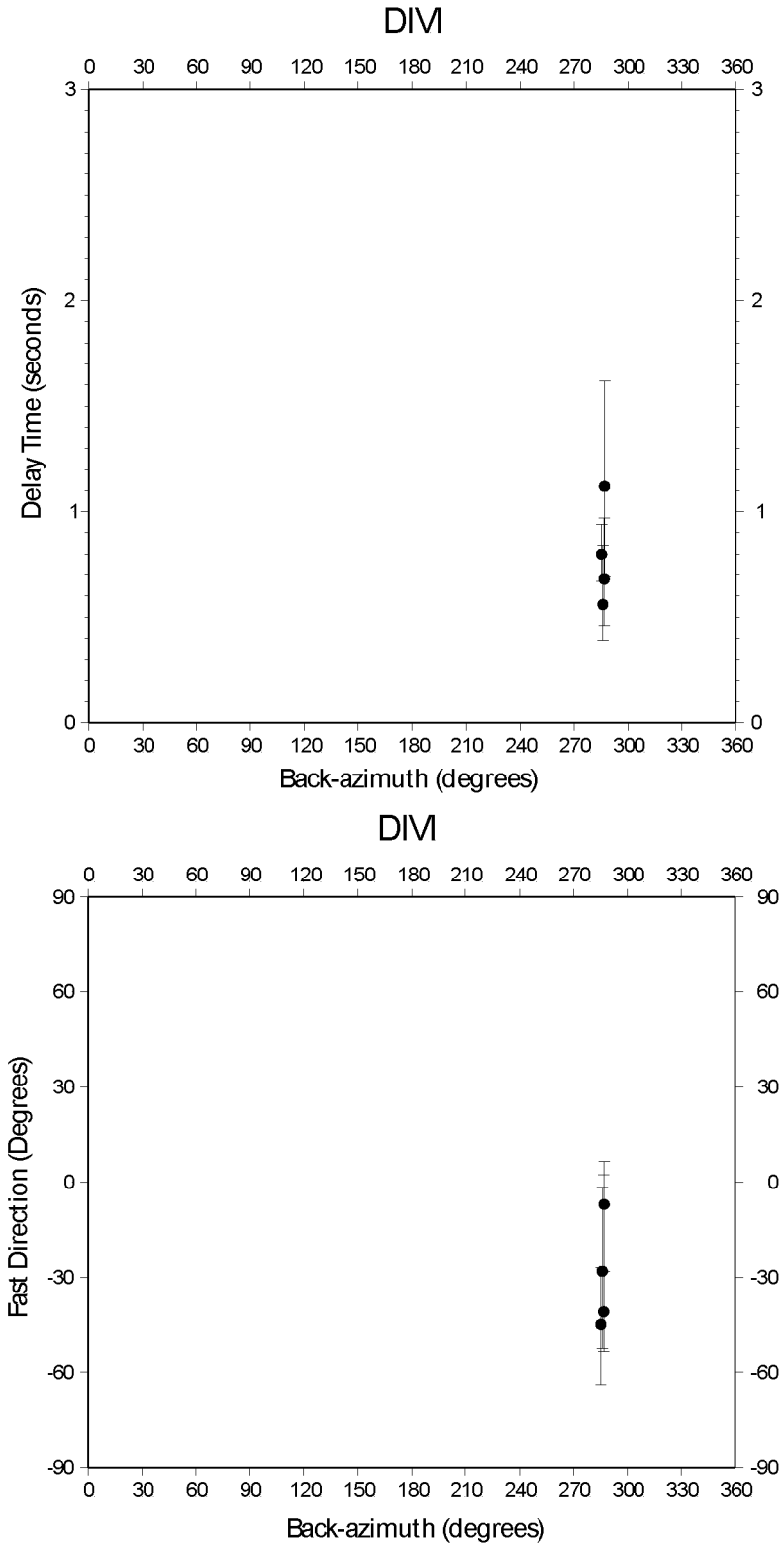

Figure C.12: Station DIVI from the MOOS network.
Delay times vs. back-azimuth (top) and fast direction vs. back-azimuth (bottom).

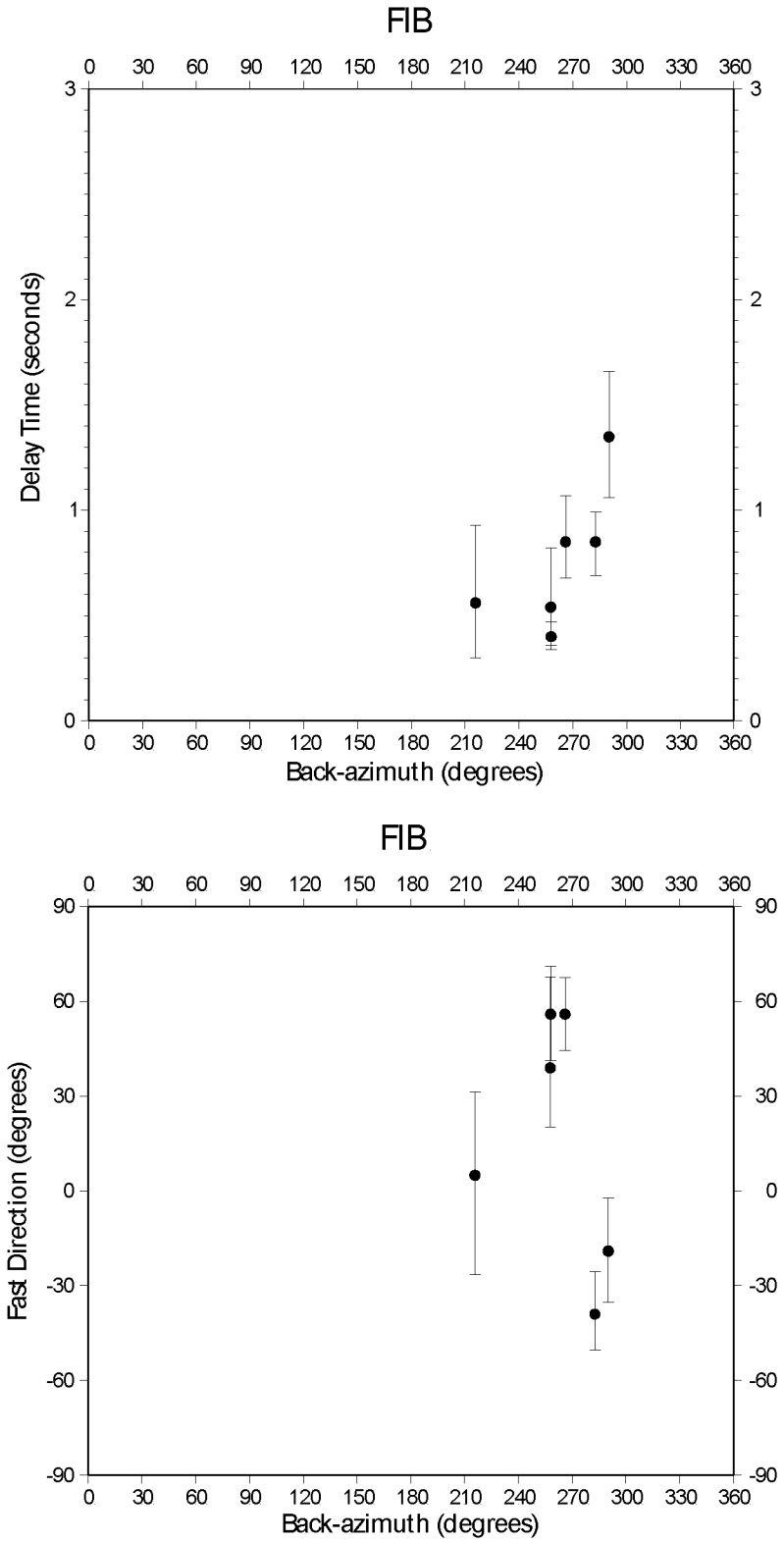

Figure C.13: Station FIB from the AEIC network.
Delay times vs. back-azimuth (top) and fast direction vs. back-azimuth (bottom).

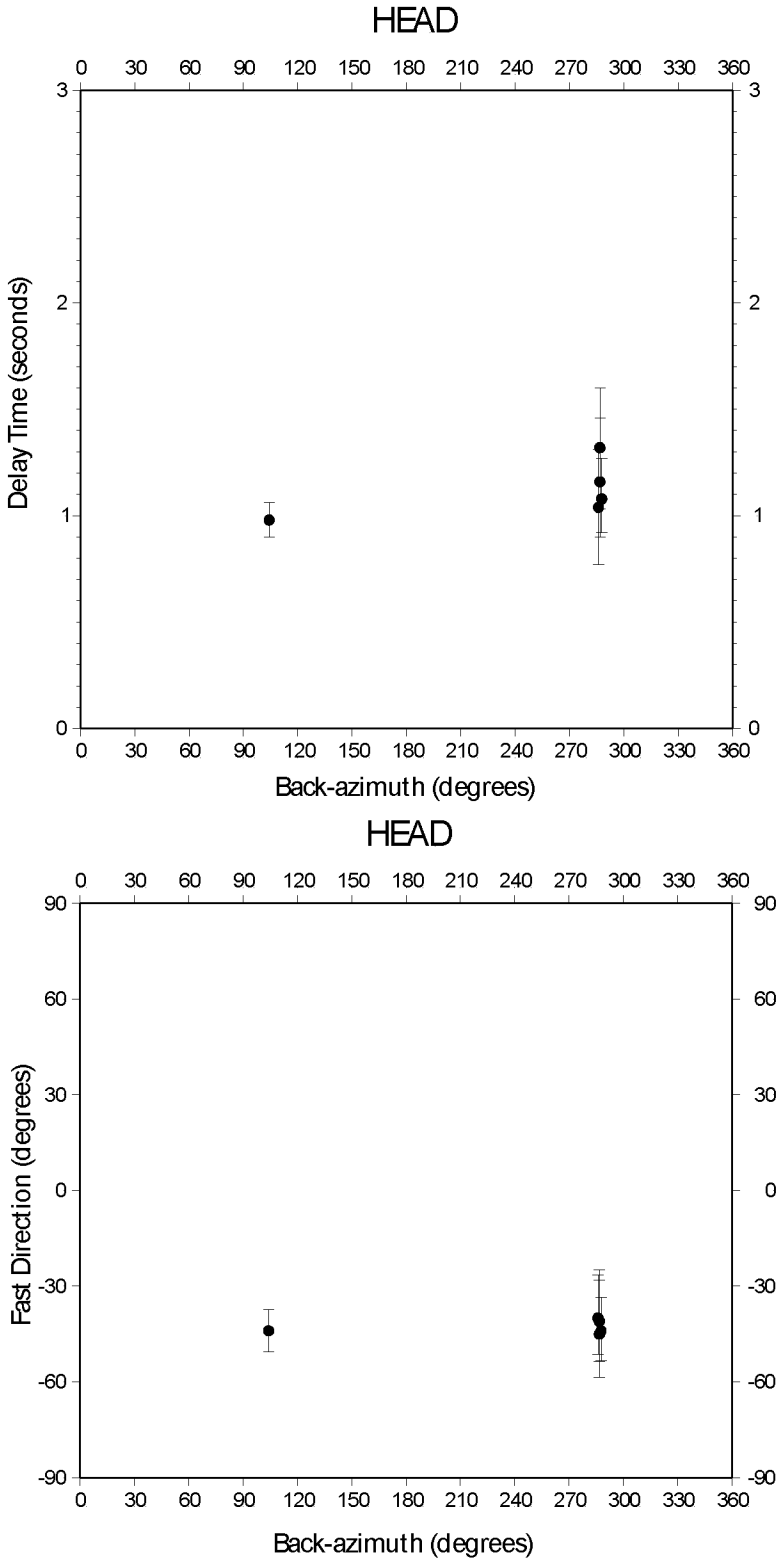

Figure C.14: Station HEAD from the MOOS network.
Delay times vs. back-azimuth (top) and fast direction vs. back-azimuth (bottom).

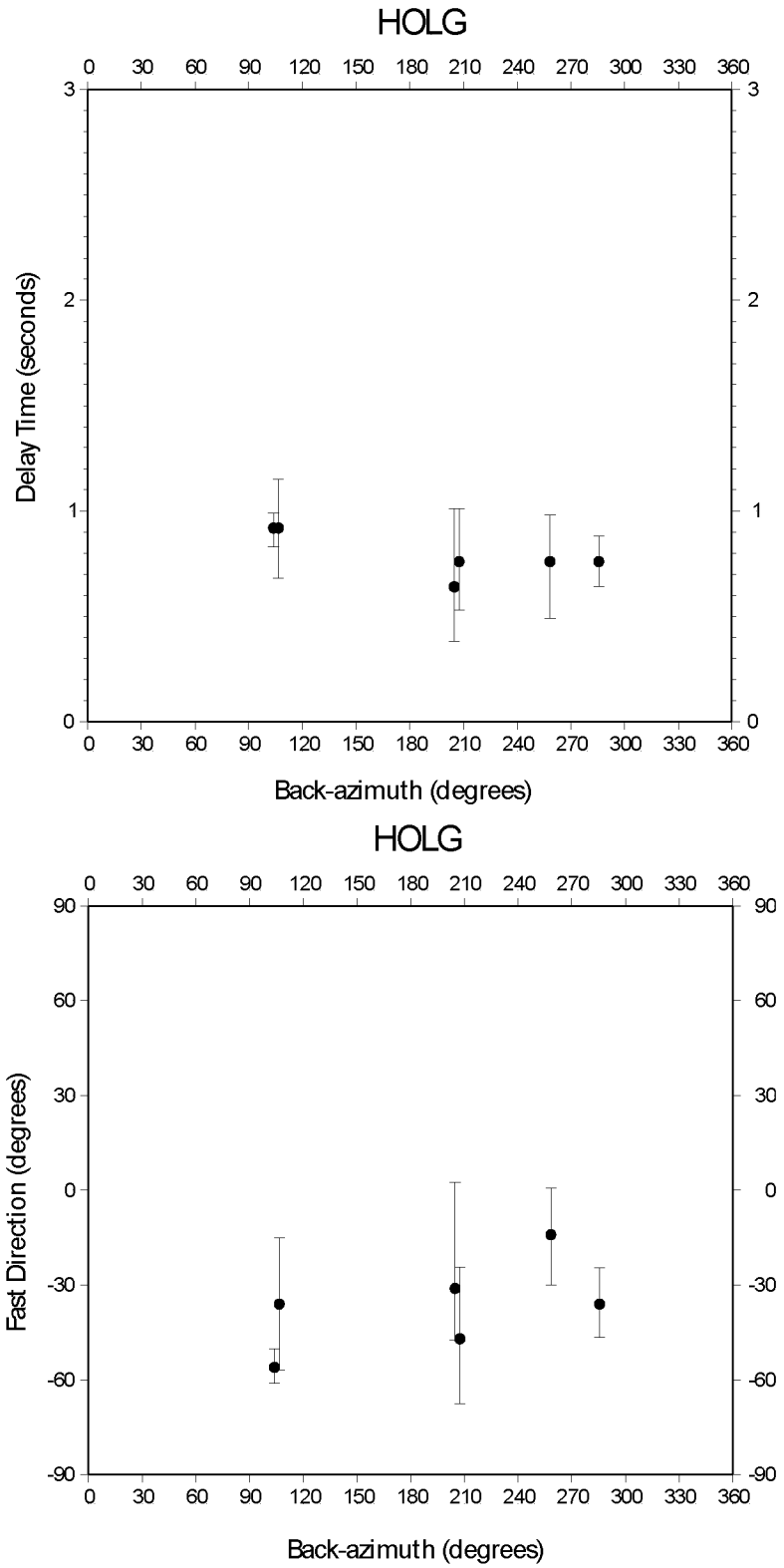

Figure C.15: Station HOLG from the MOOS network.
Delay times vs. back-azimuth (top) and fast direction vs. back-azimuth (bottom).

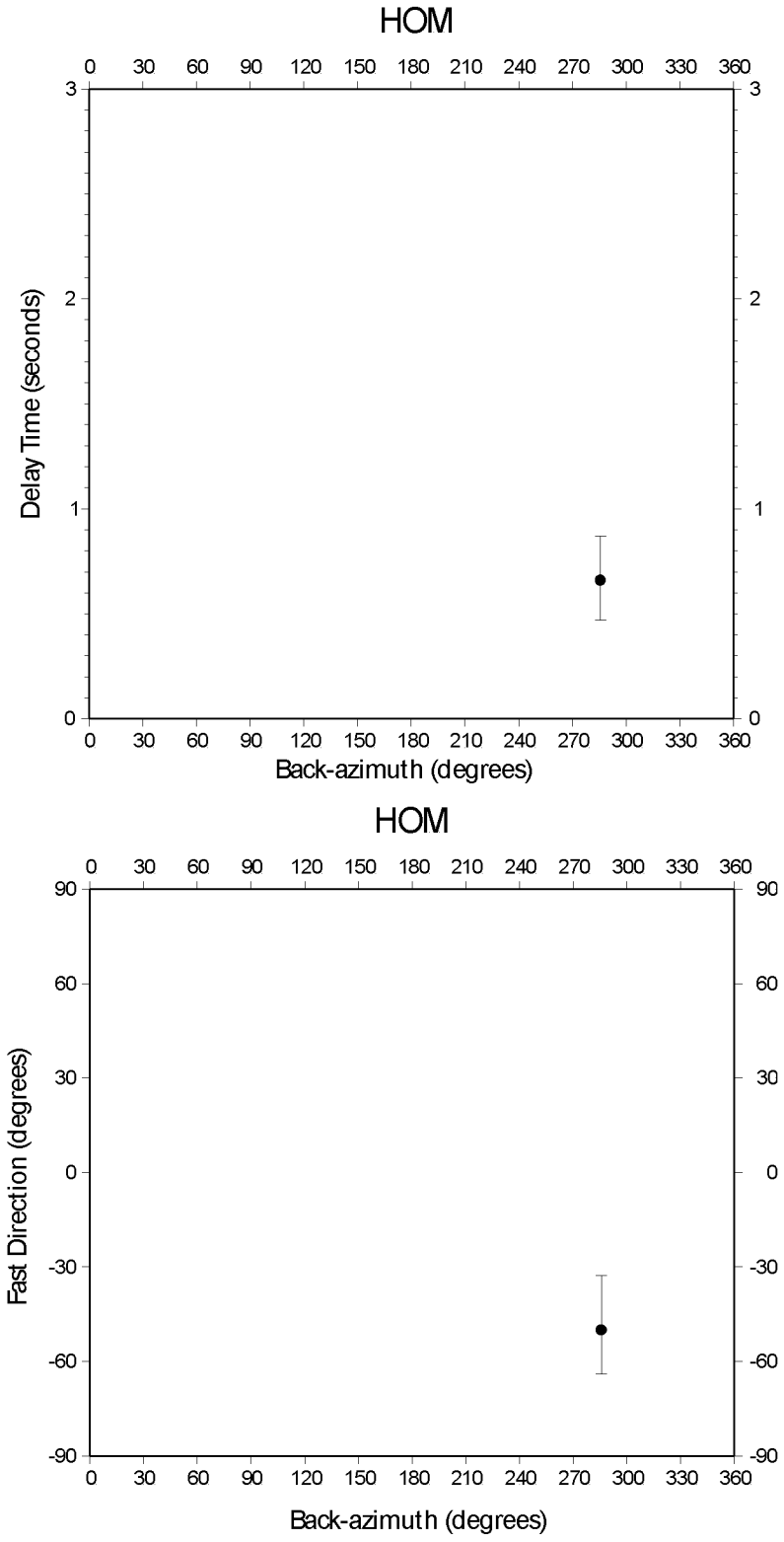

Figure C.16: Station HOM from the AEIC network.
Delay times vs. back-azimuth (top) and fast direction vs. back-azimuth (bottom).

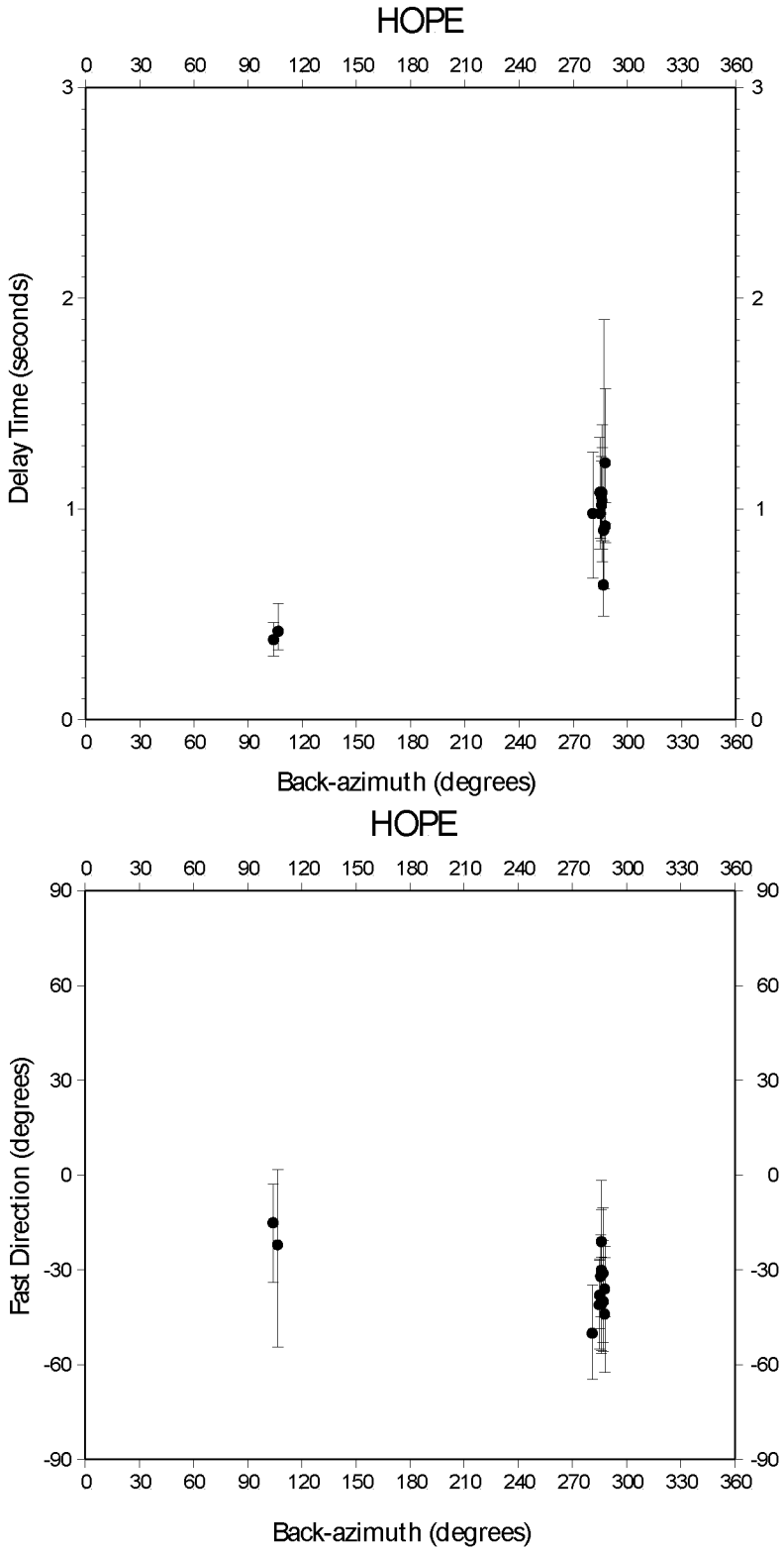

Figure C.17: Station HOPE from the MOOS network.
Delay times vs. back-azimuth (top) and fast direction vs. back-azimuth (bottom).

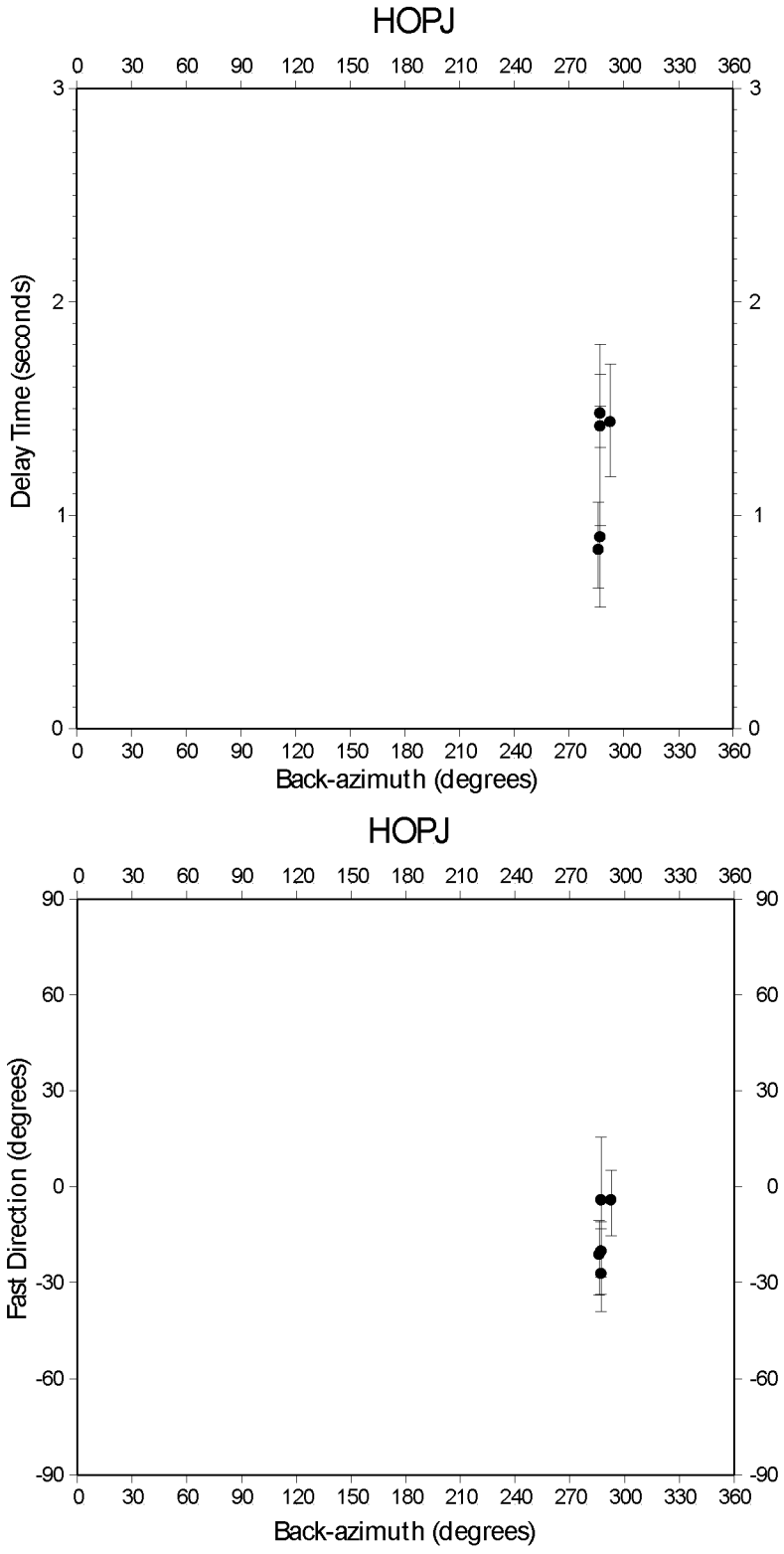

Figure C.18: Station HOPJ from the MOOS network.
Delay times vs. back-azimuth (top) and fast direction vs. back-azimuth (bottom).

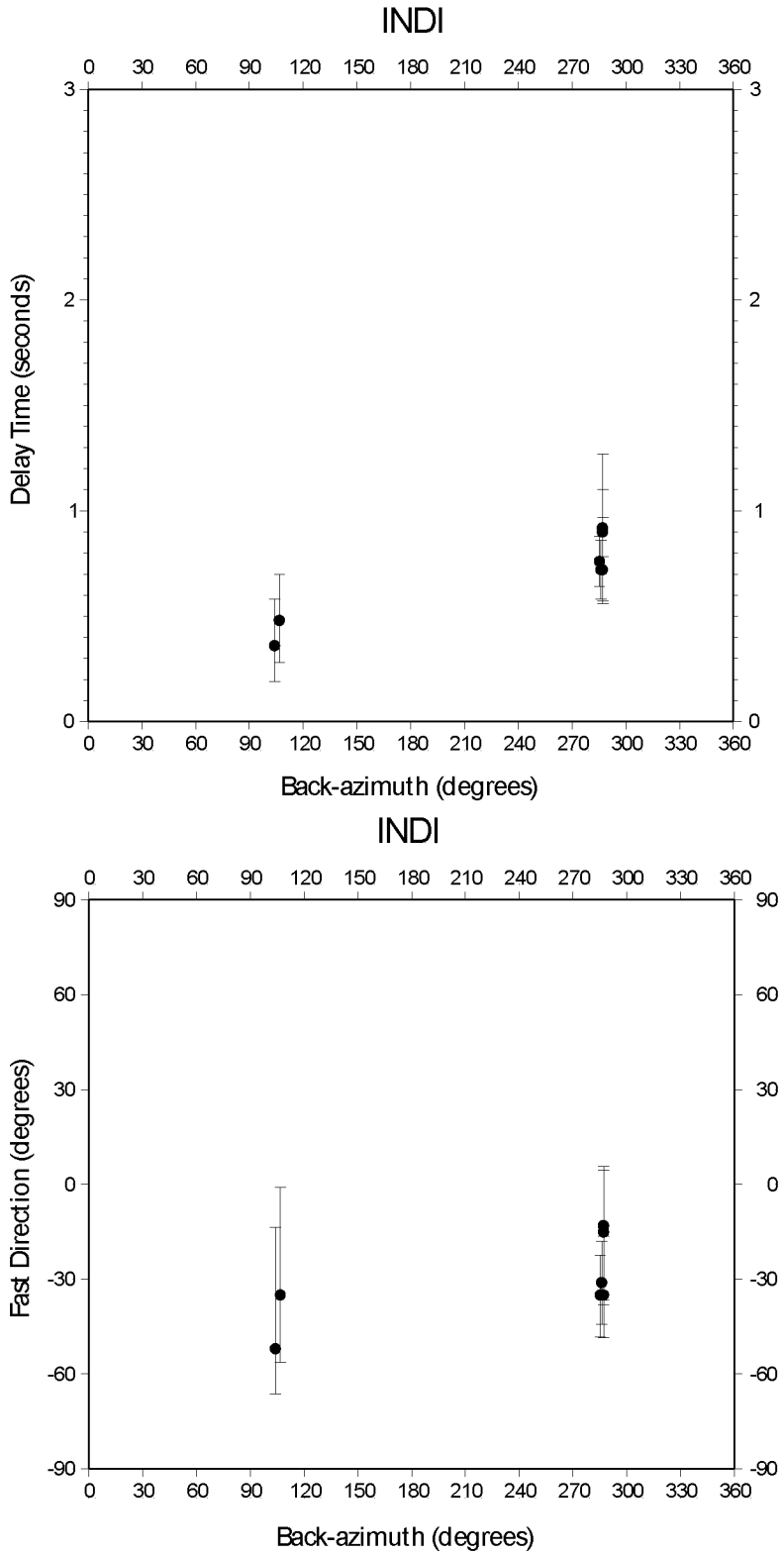

Figure C.19: Station INDI from the MOOS network.
Delay times vs. back-azimuth (top) and fast direction vs. back-azimuth (bottom).

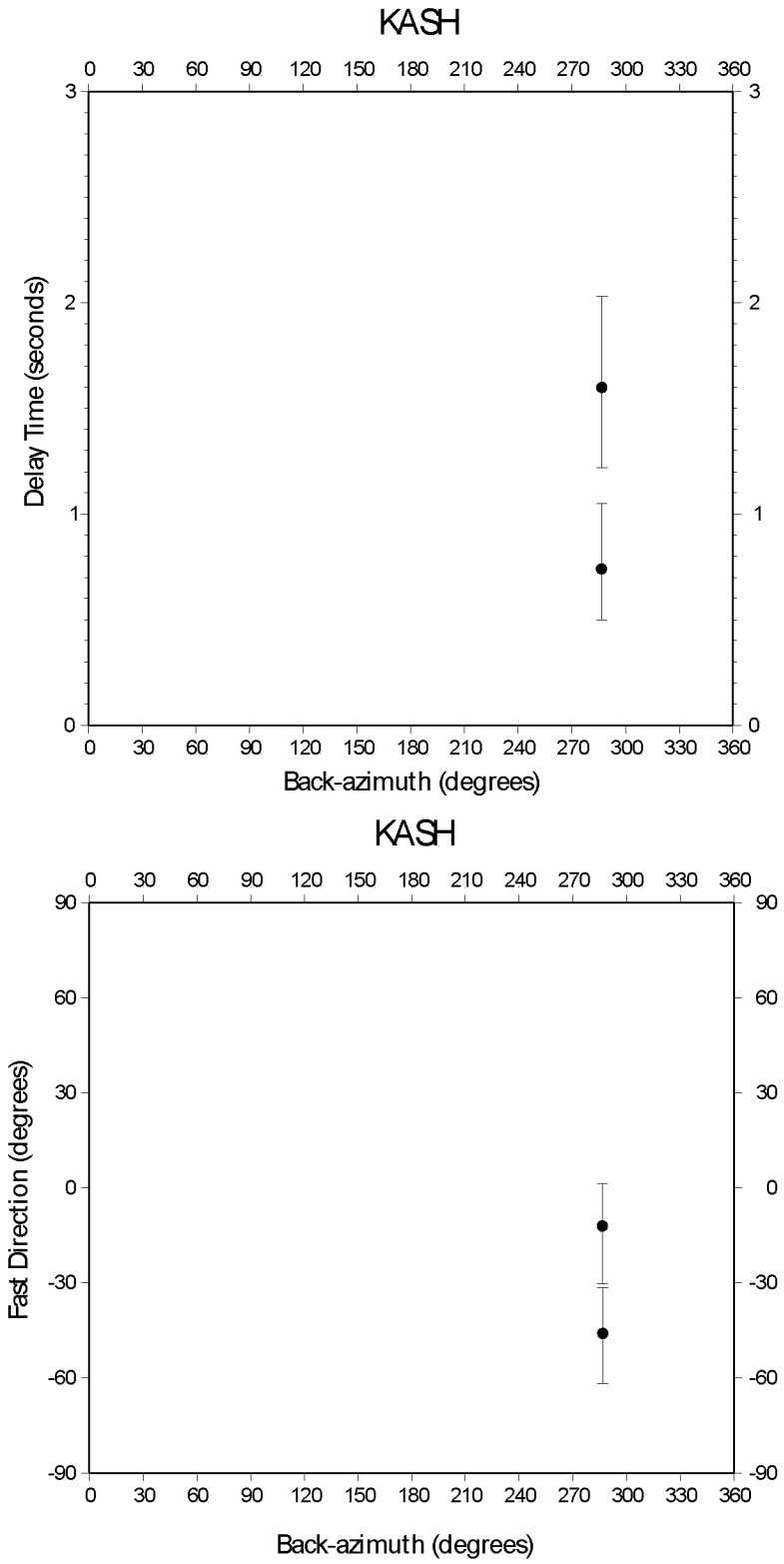

Figure C.20: Station KASH from the MOOS network.
Delay times vs. back-azimuth (top) and fast direction vs. back-azimuth (bottom).

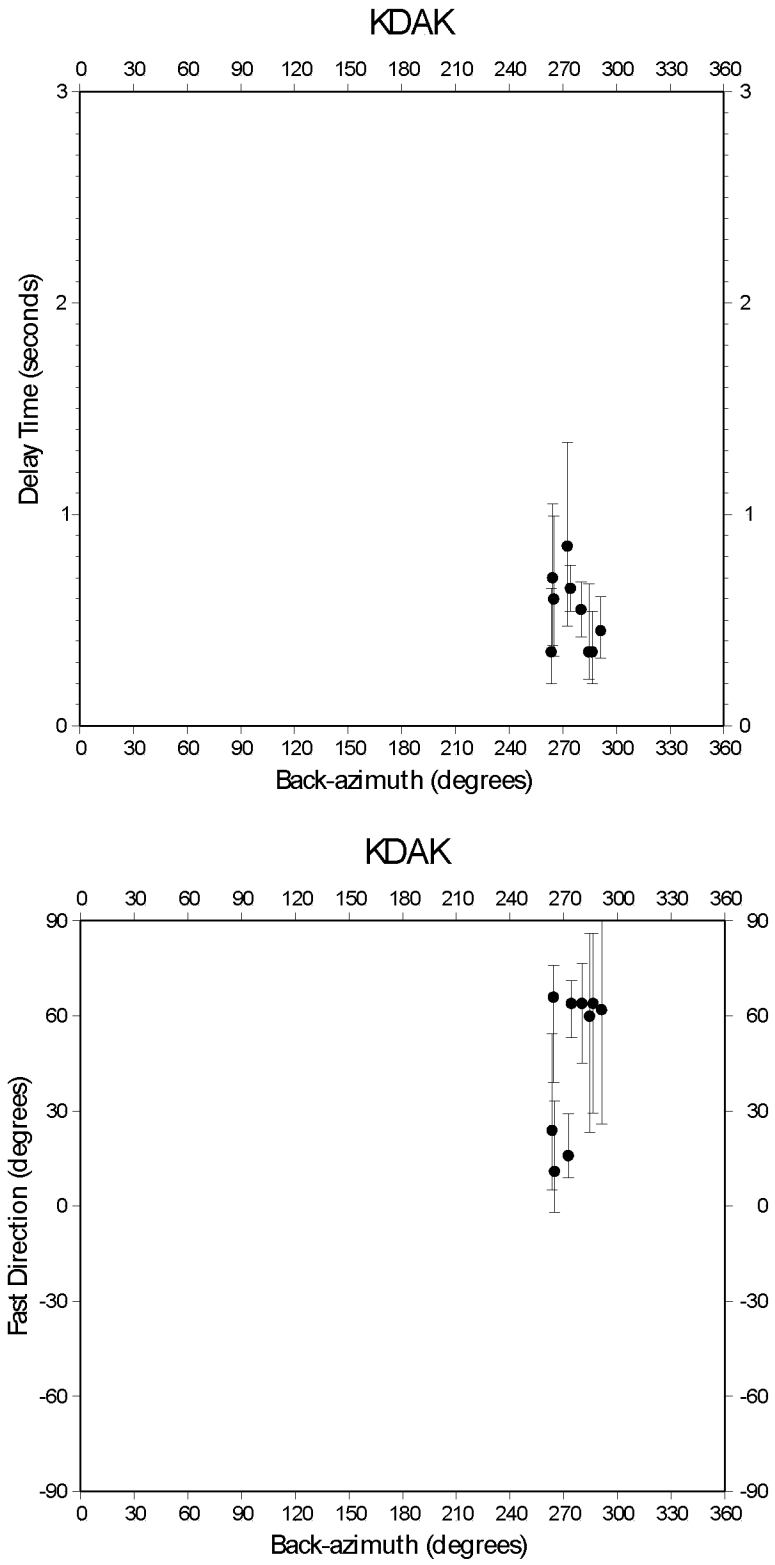

Figure C.21: Station KDAK from the AEIC network.
Delay times vs. back-azimuth (top) and fast direction vs. back-azimuth (bottom).

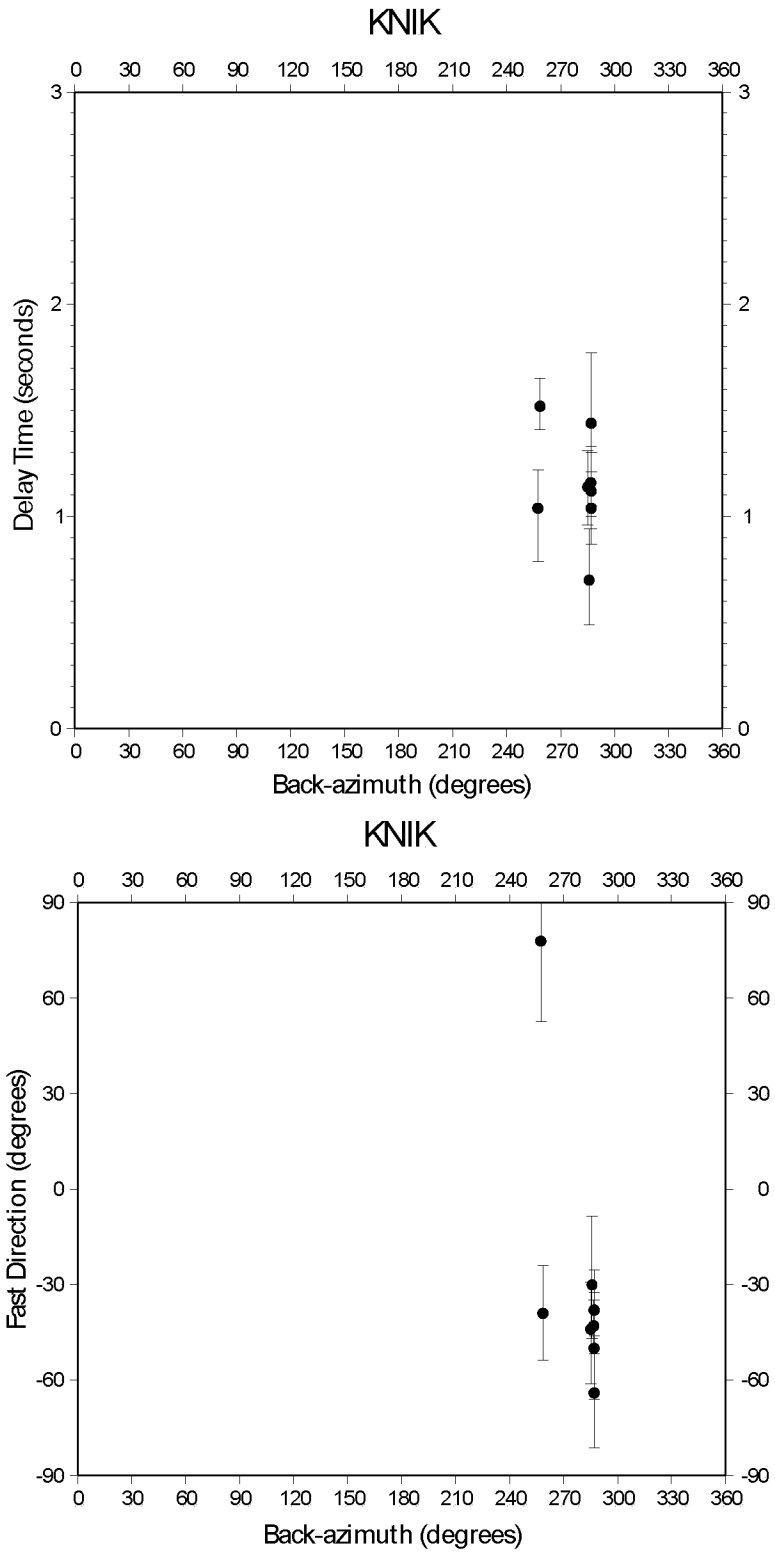

Figure C.22: Station KNIK from the MOOS network.
Delay times vs. back-azimuth (top) and fast direction vs. back-azimuth (bottom).

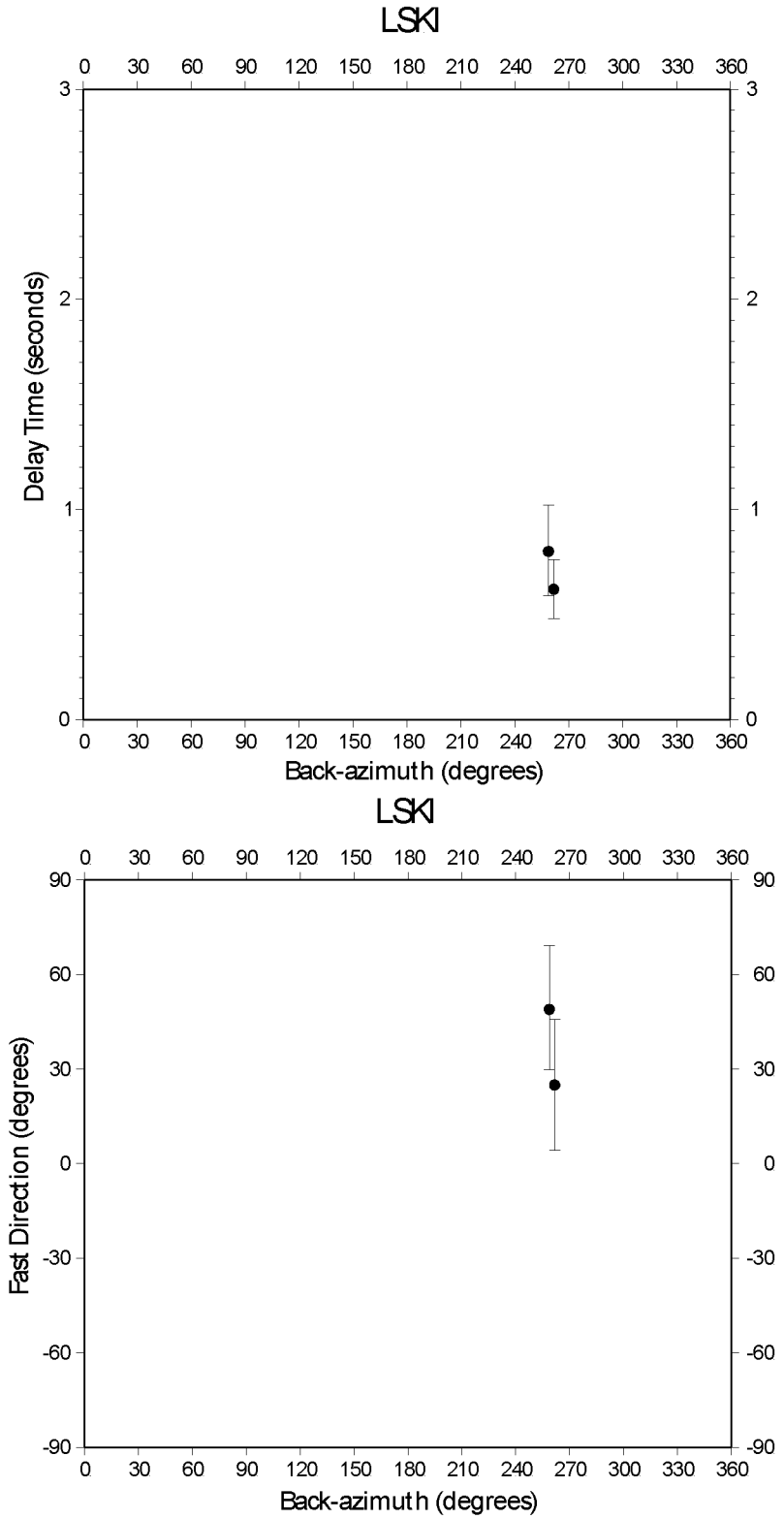

Figure C.23: Station LSKI from the MOOS network.
Delay times vs. back-azimuth (top) and fast direction vs. back-azimuth (bottom).

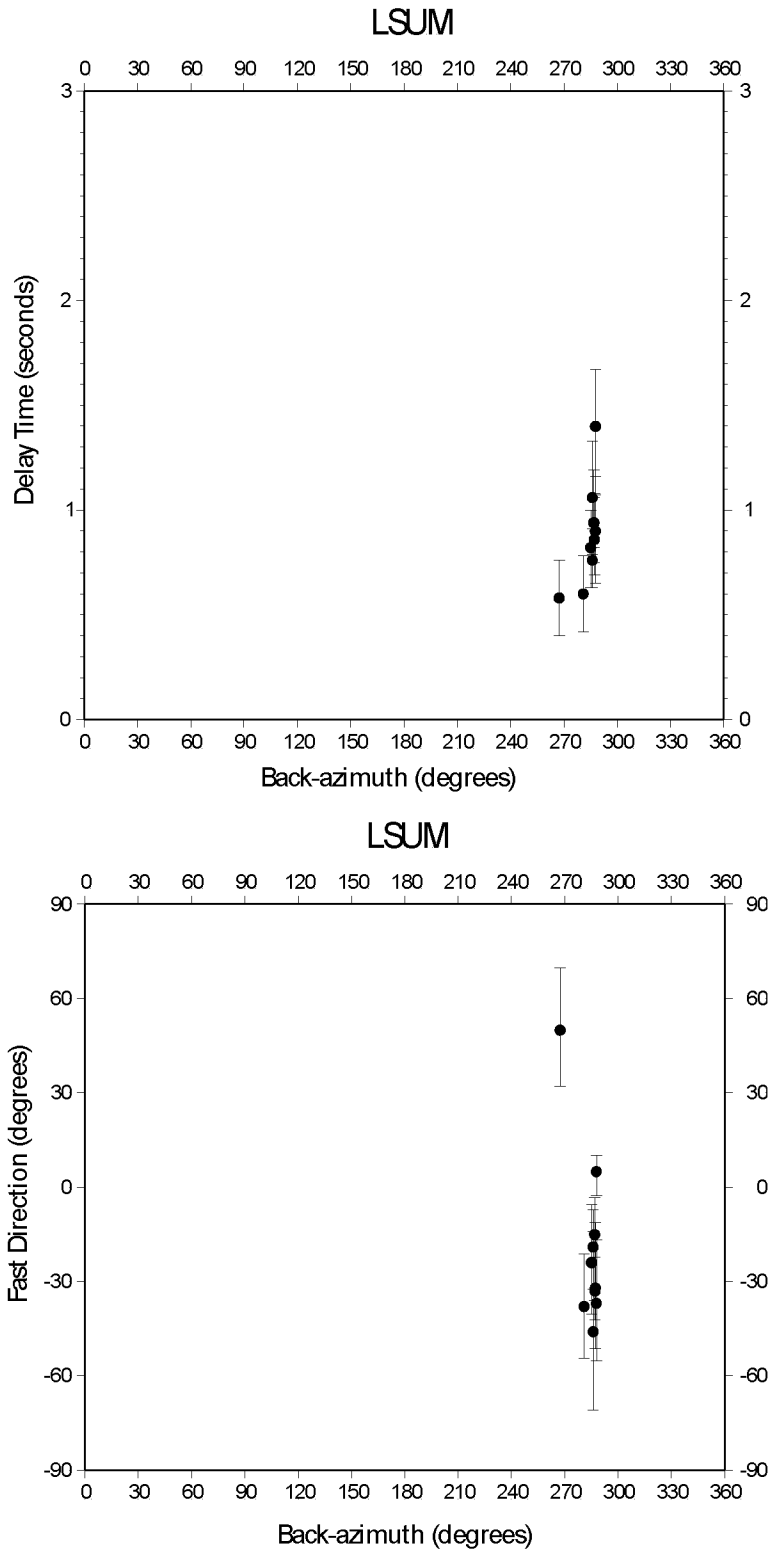

Figure C.24: Station LSUM from the MOOS network.
Delay times vs. back-azimuth (top) and fast direction vs. back-azimuth (bottom).

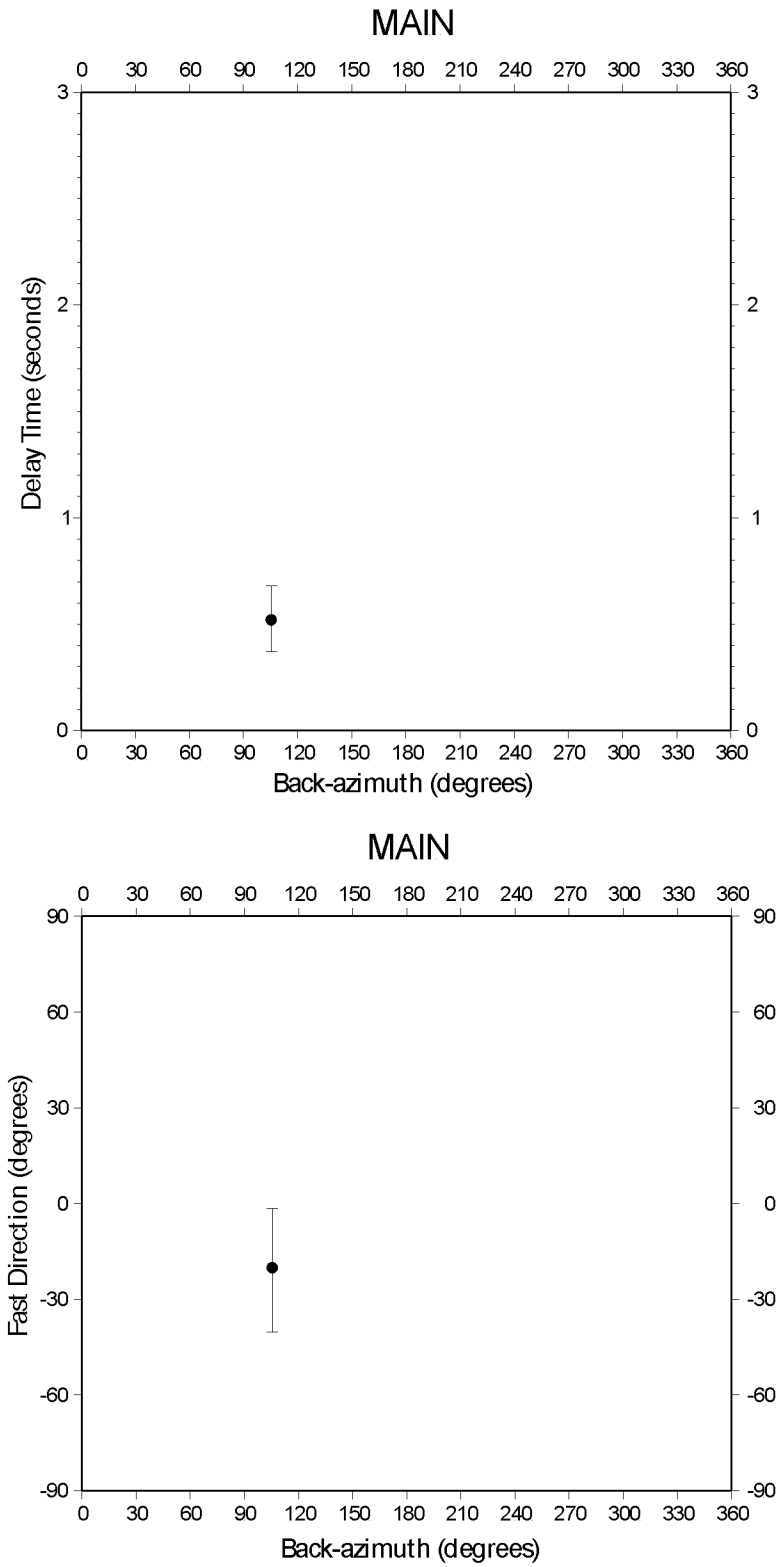

Figure C.25: Station MAIN from the MOOS network.
Delay times vs. back-azimuth (top) and fast direction vs. back-azimuth (bottom).

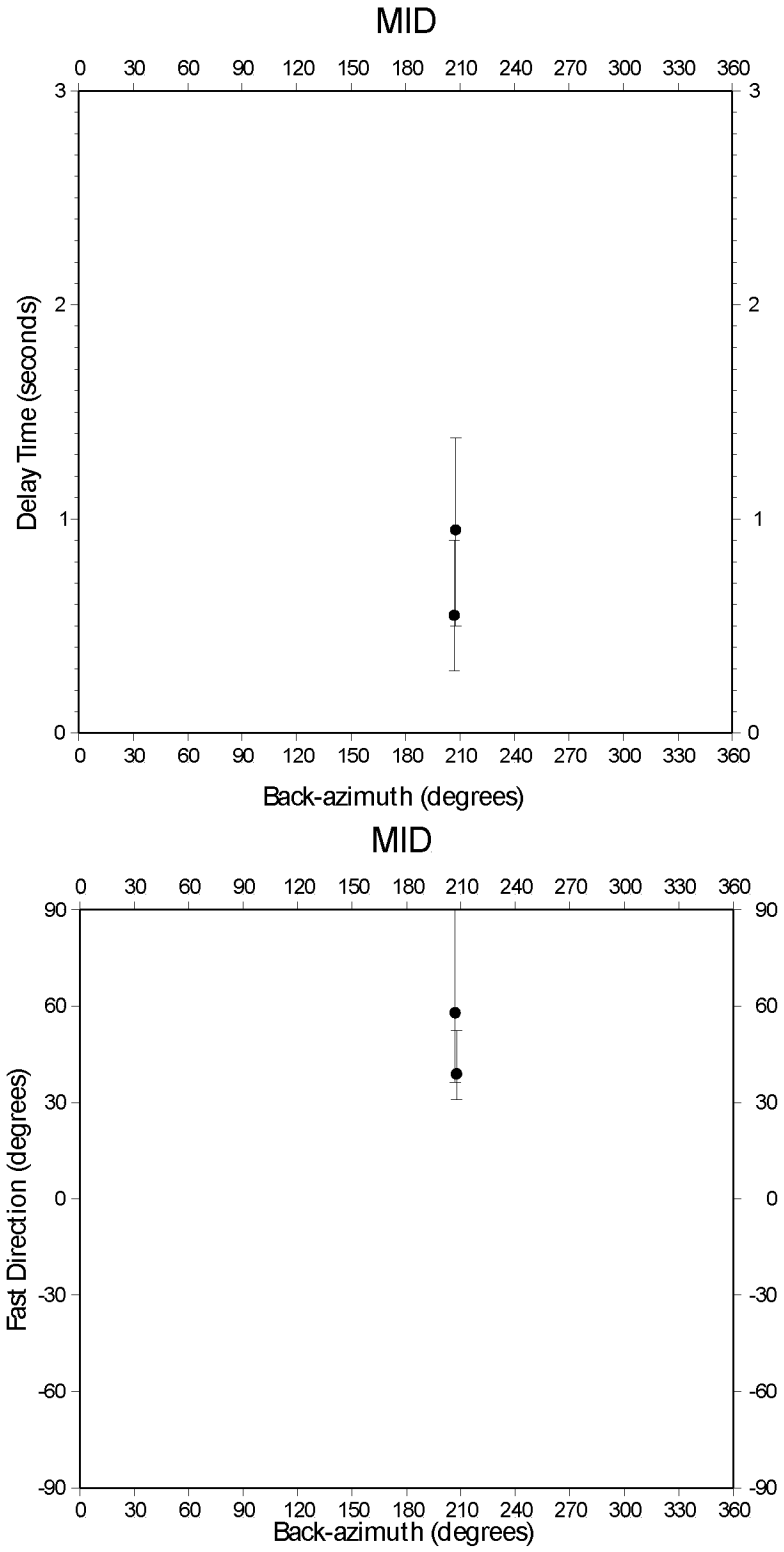

Figure C.26: Station MID from the AEIC network.
Delay times vs. back-azimuth (top) and fast direction vs. back-azimuth (bottom).

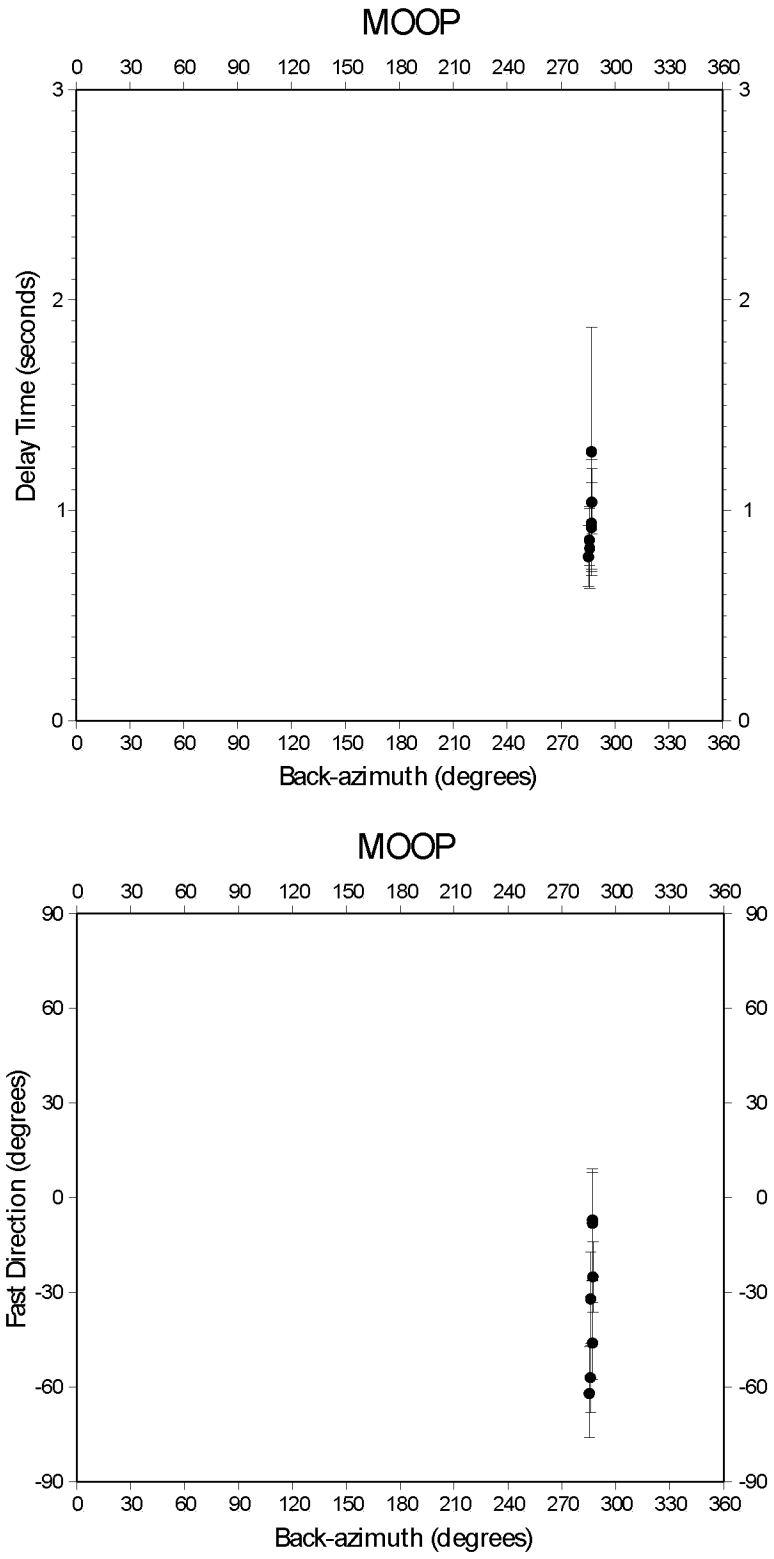

Figure C.27: Station MOOP from the MOOS network.
Delay times vs. back-azimuth (top) and fast direction vs. back-azimuth (bottom).

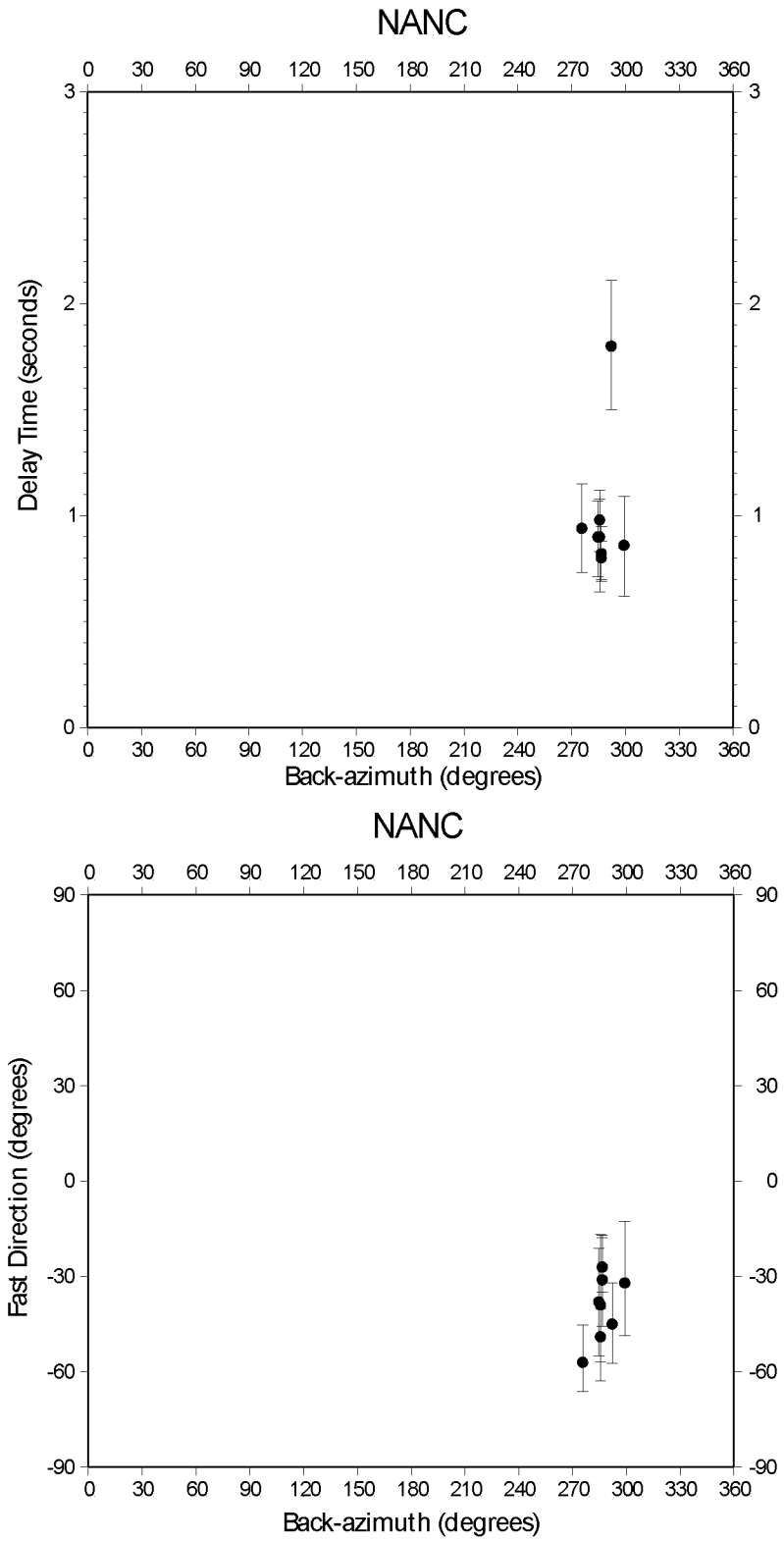

Figure C.28: Station NANC from the MOOS network.
Delay times vs. back-azimuth (top) and fast direction vs. back-azimuth (bottom).

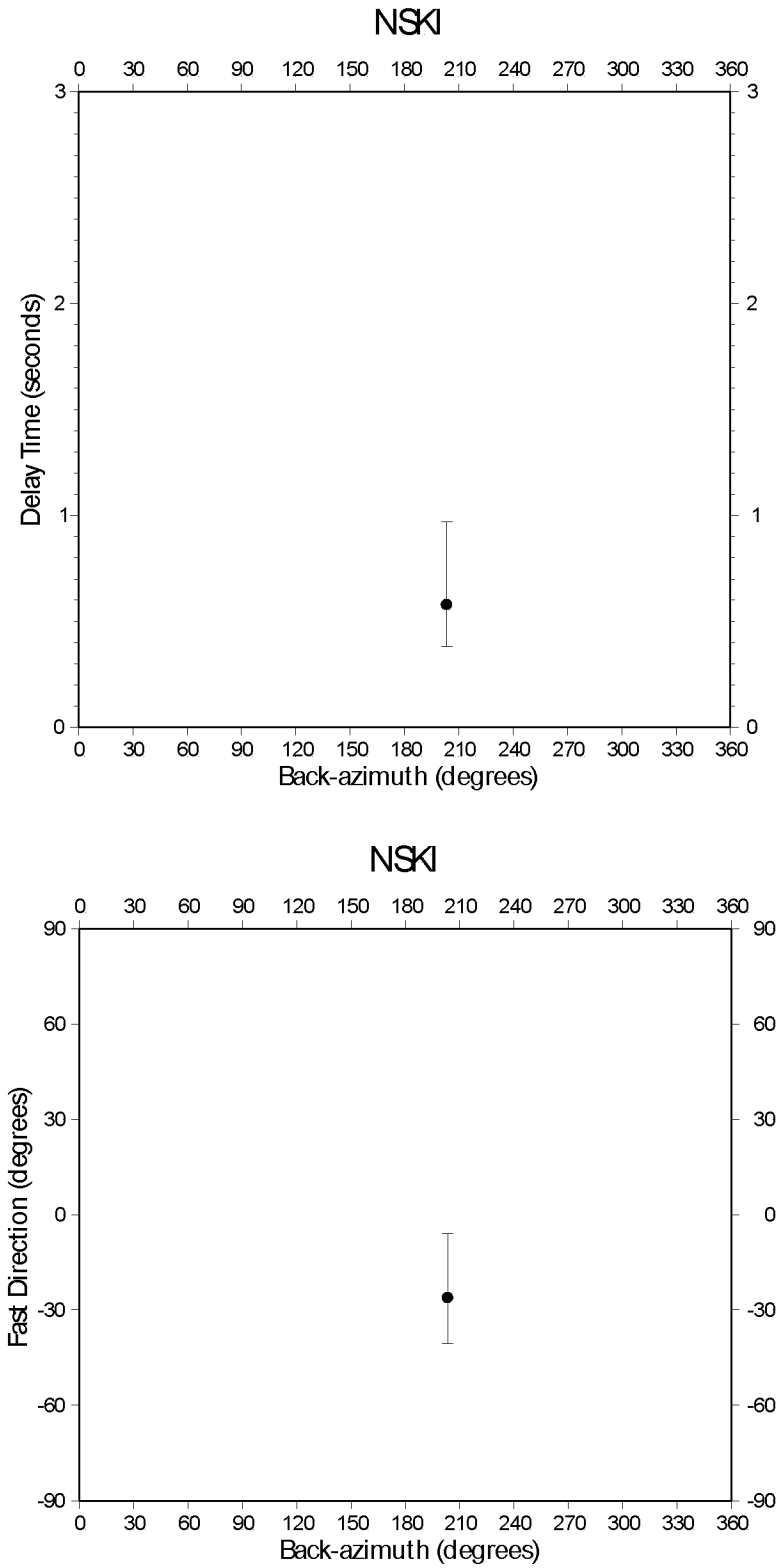

Figure C.29: Station NSKI from the MOOS network.
Delay times vs. back-azimuth (top) and fast direction vs. back-azimuth (bottom).

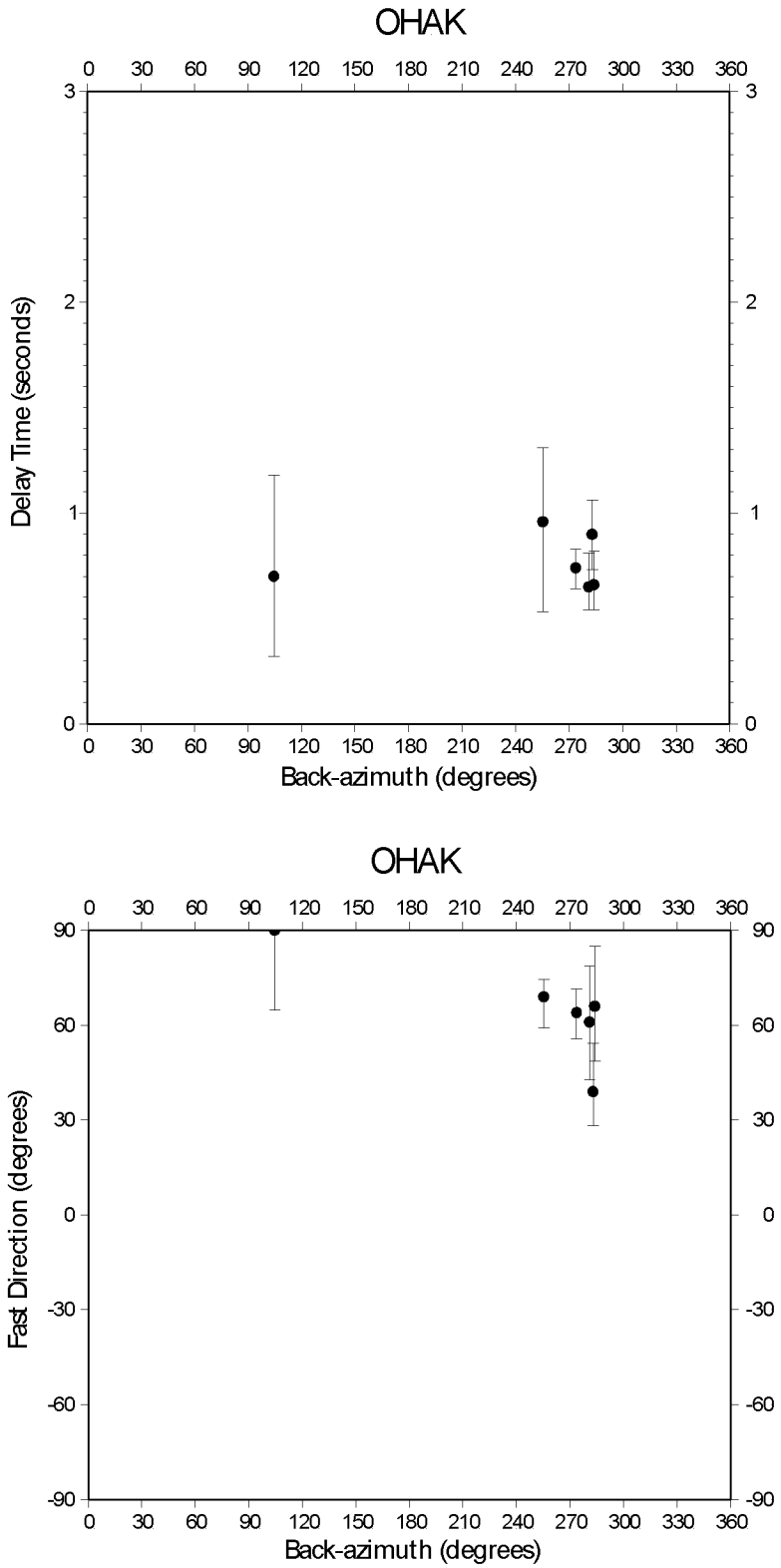

Figure C.30: Station OHAK from the AEIC network.
Delay times vs. back-azimuth (top) and fast direction vs. back-azimuth (bottom).

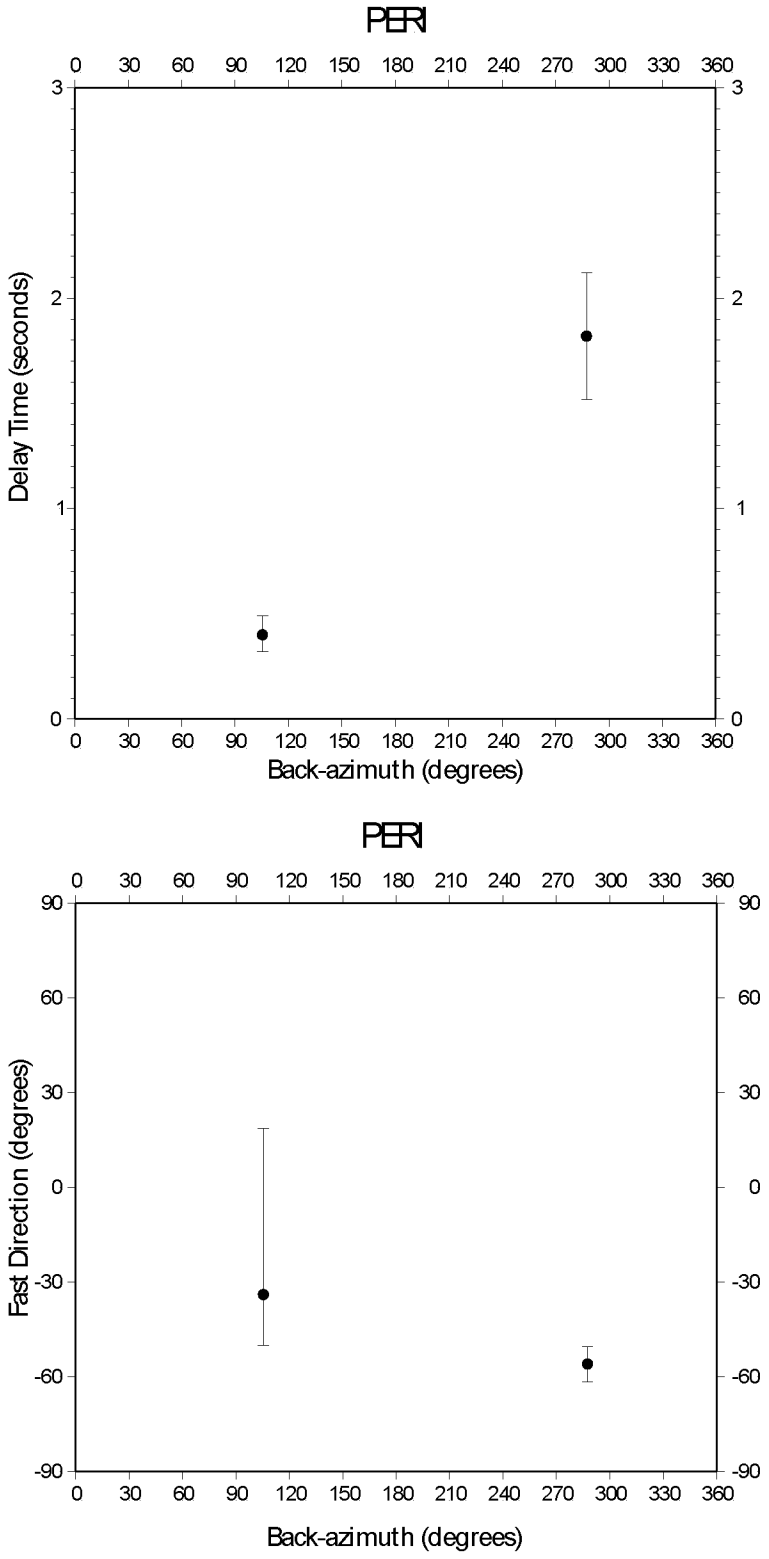

Figure C.31: Station PERI from the MOOS network.
Delay times vs. back-azimuth (top) and fast direction vs. back-azimuth (bottom).

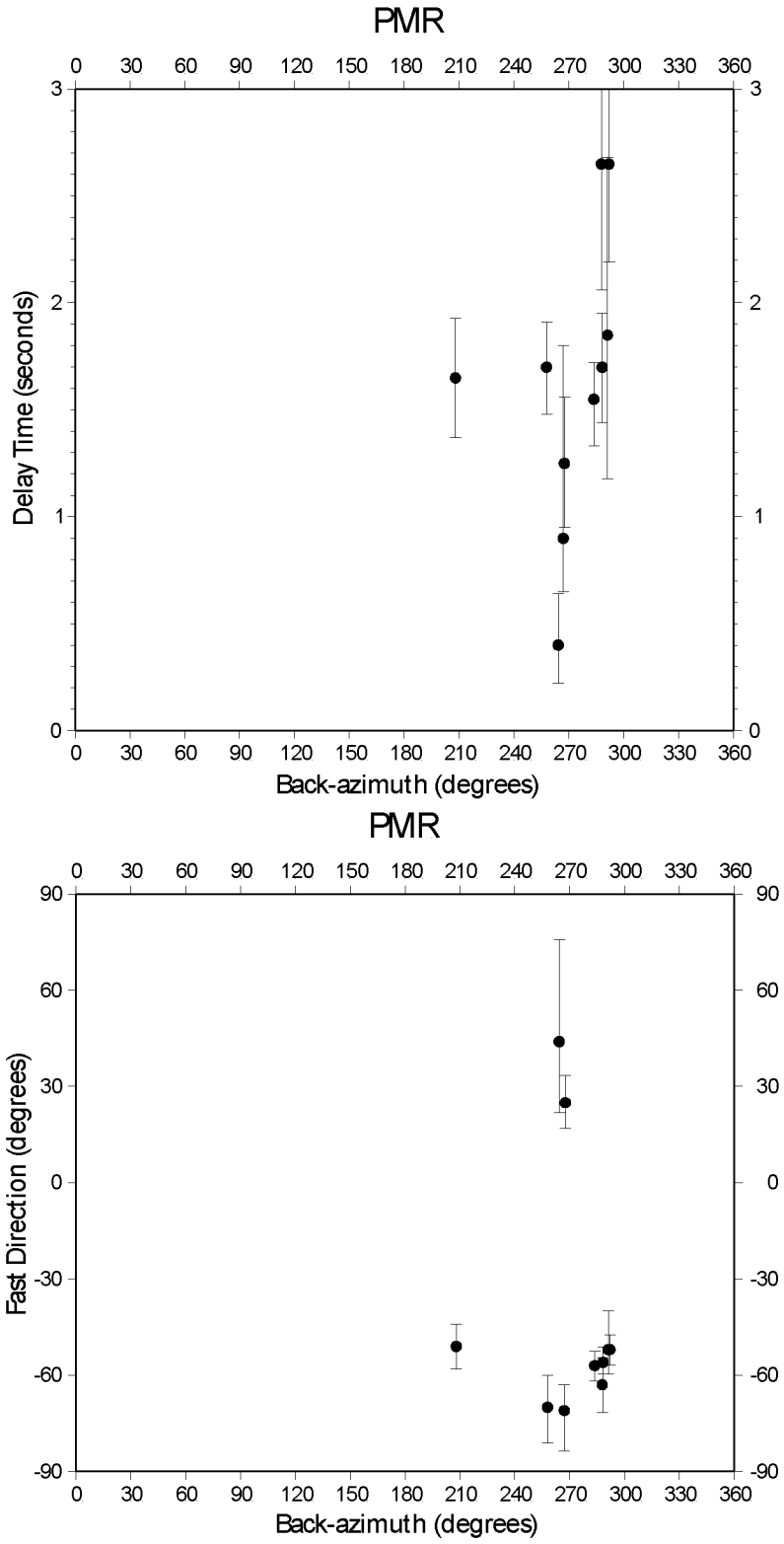

Figure C.32: Station PMR from the AEIC network.
Delay times vs. back-azimuth (top) and fast direction vs. back-azimuth (bottom).

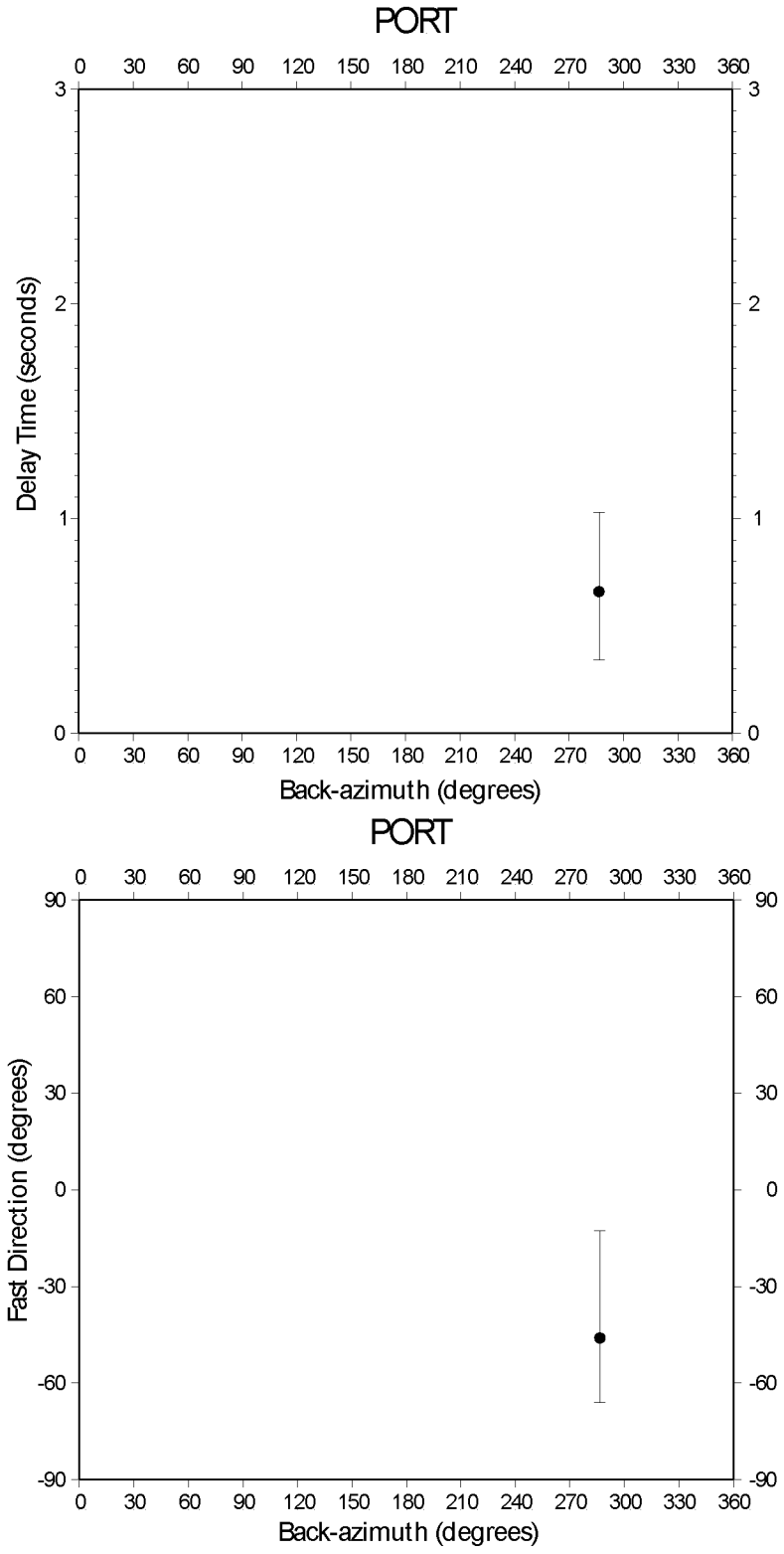

Figure C.33: Station PORT from the MOOS network.
Delay times vs. back-azimuth (top) and fast direction vs. back-azimuth (bottom).

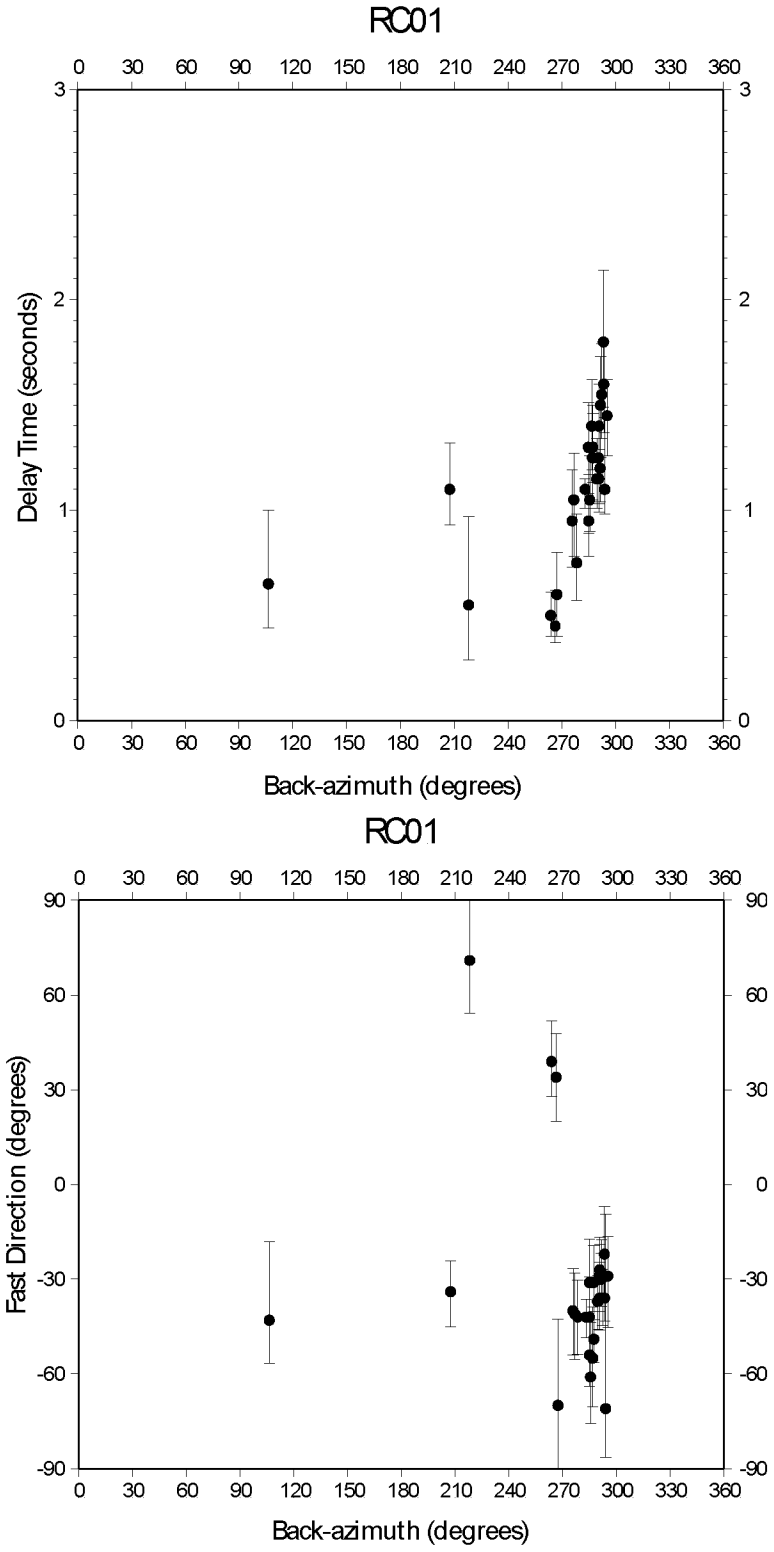

Figure C.34: Station RC01 from the AEIC network.
Delay times vs. back-azimuth (top) and fast direction vs. back-azimuth (bottom).

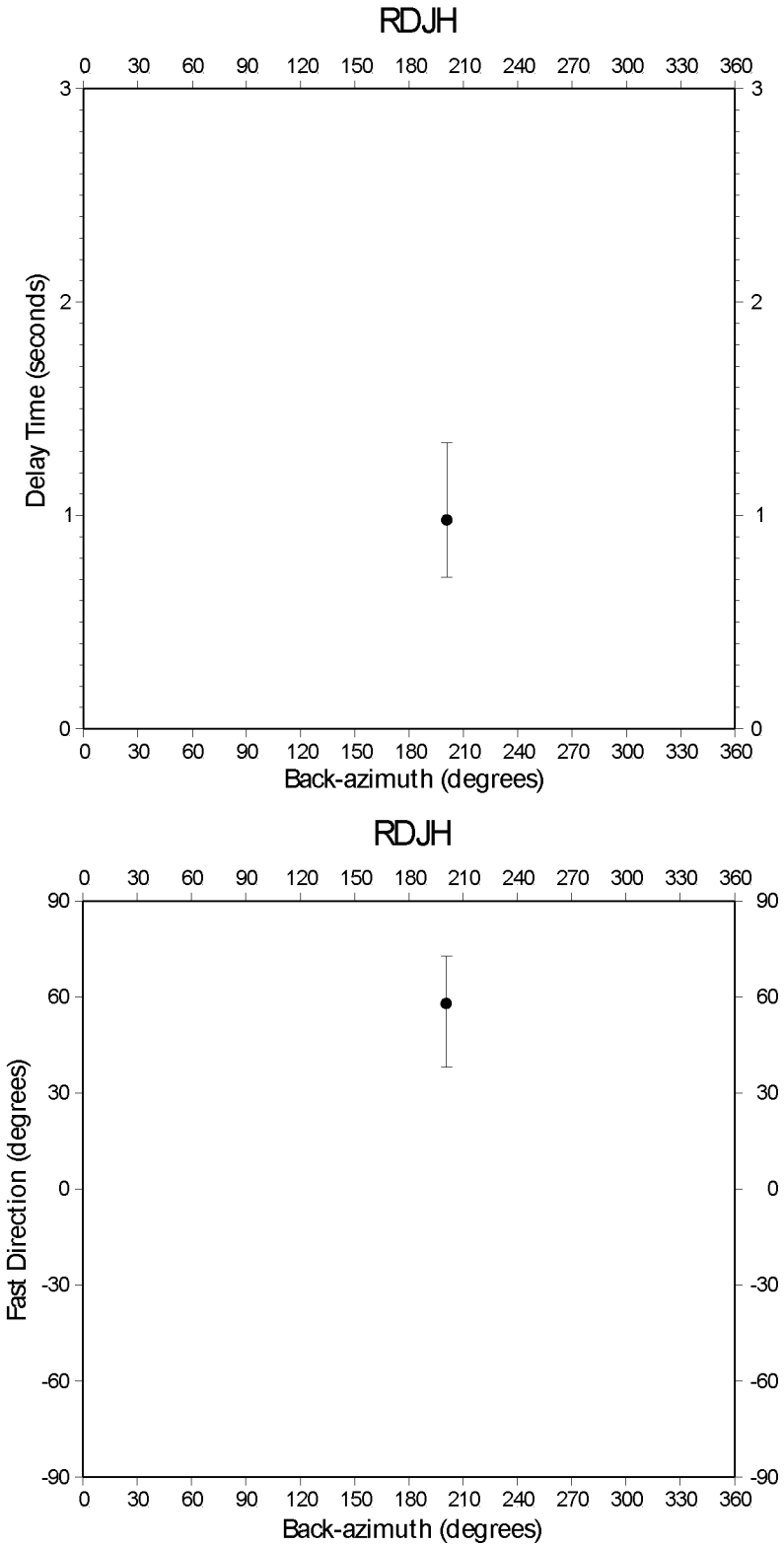

Figure C.35: Station RDJH from the AVO network.
Delay times vs. back-azimuth (top) and fast direction vs. back-azimuth (bottom).

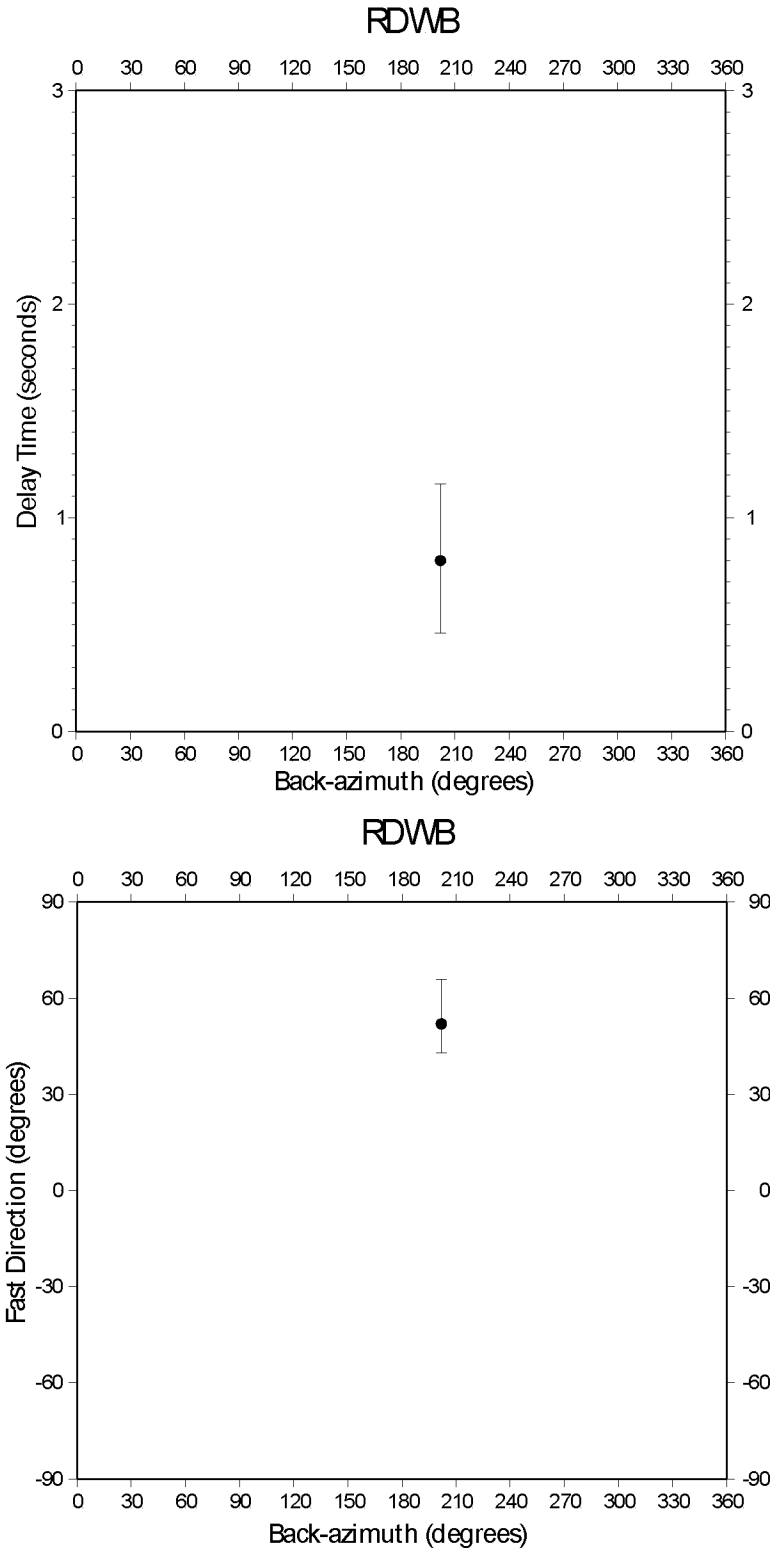

Figure C.36: Station RDWB from the AVO network.
Delay times vs. back-azimuth (top) and fast direction vs. back-azimuth (bottom).

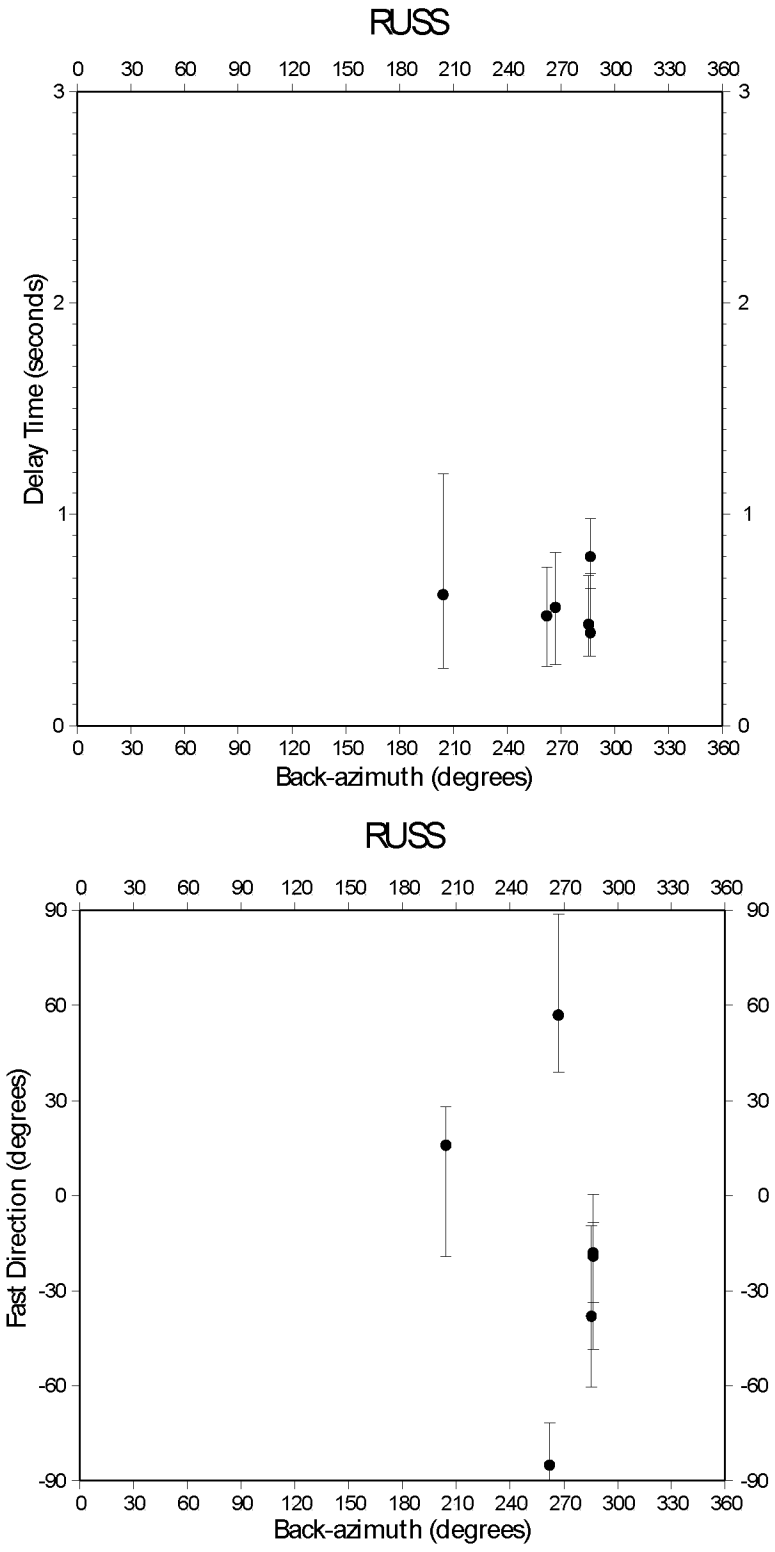

Figure C.37: Station RUSS from the MOOS network.
Delay times vs. back-azimuth (top) and fast direction vs. back-azimuth (bottom).

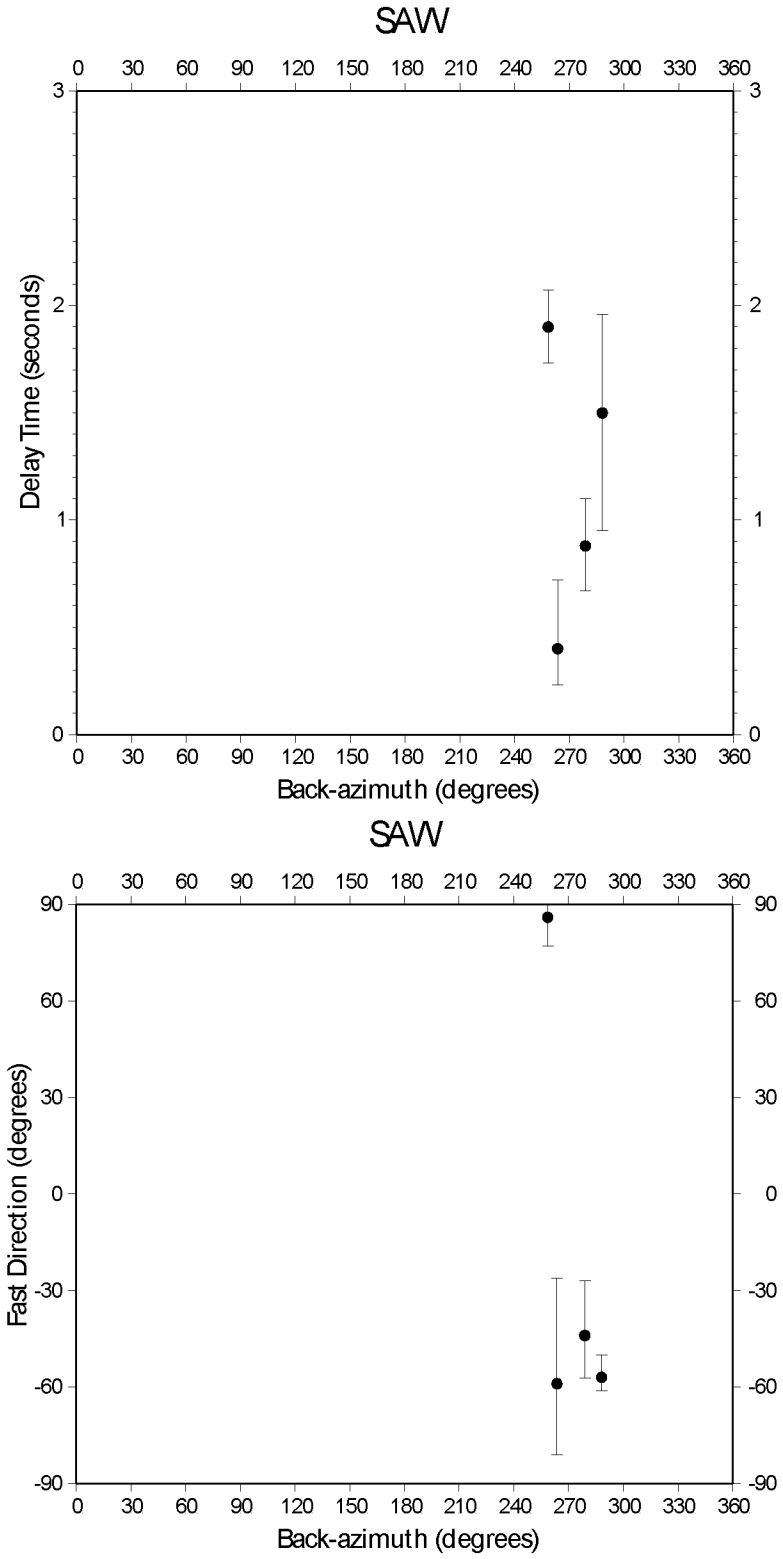

Figure C.38: Station SAW from the AEIC network.
Delay times vs. back-azimuth (top) and fast direction vs. back-azimuth (bottom).

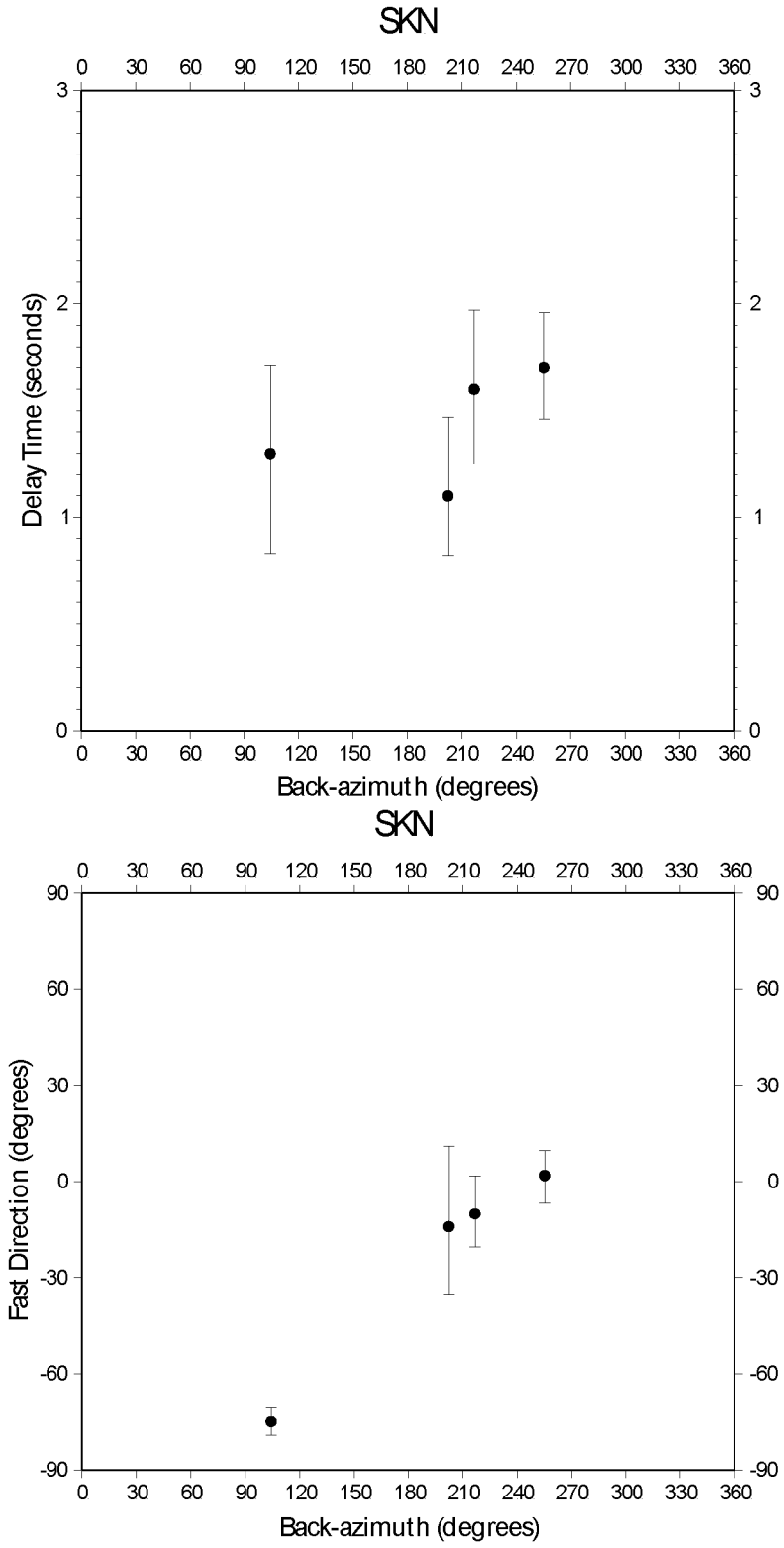

Figure C.39: Station SKN from the AEIC network.
Delay times vs. back-azimuth (top) and fast direction vs. back-azimuth (bottom).

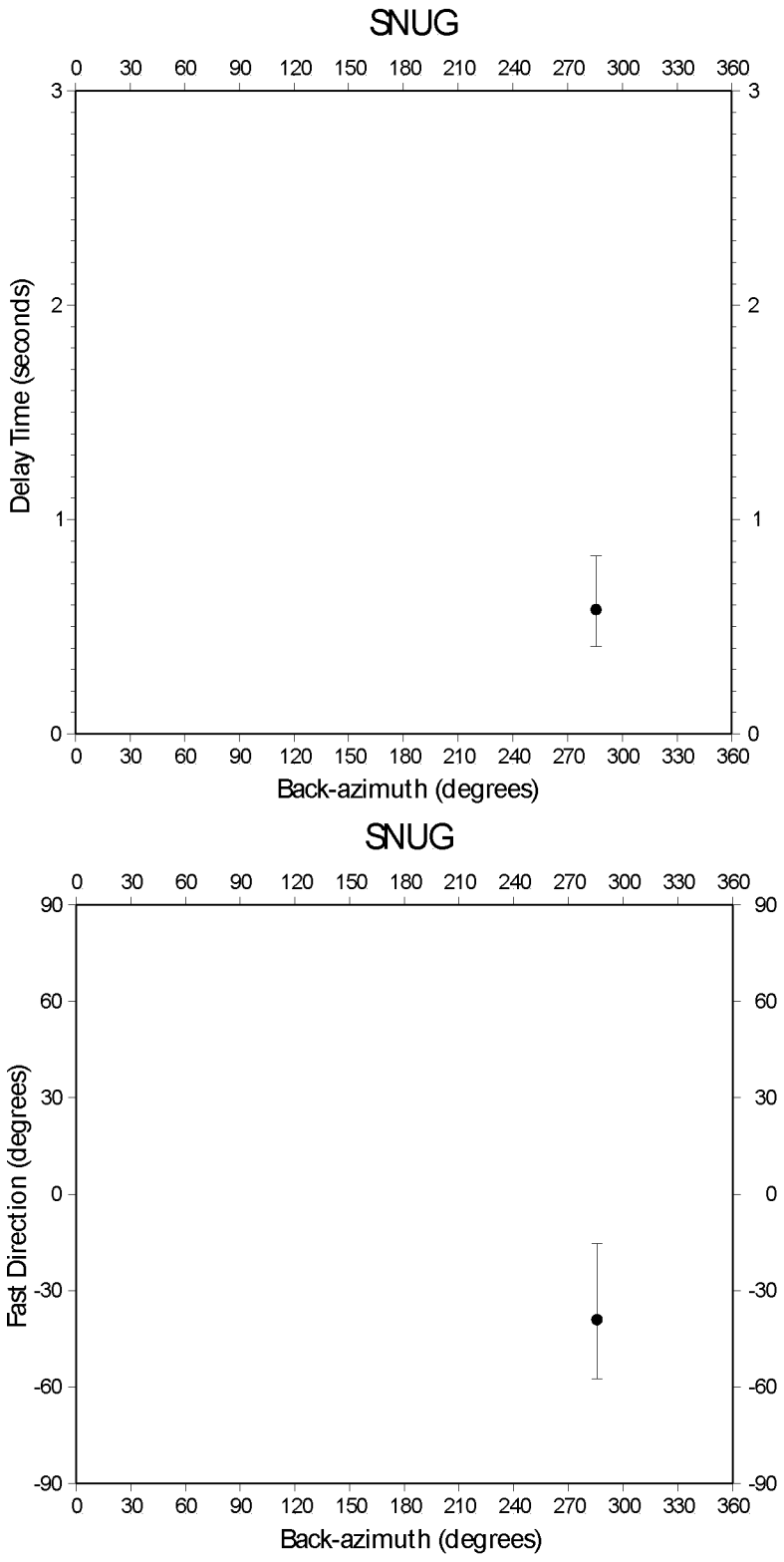

Figure C.40: Station SNUG from the MOOS network.
Delay times vs. back-azimuth (top) and fast direction vs. back-azimuth (bottom).

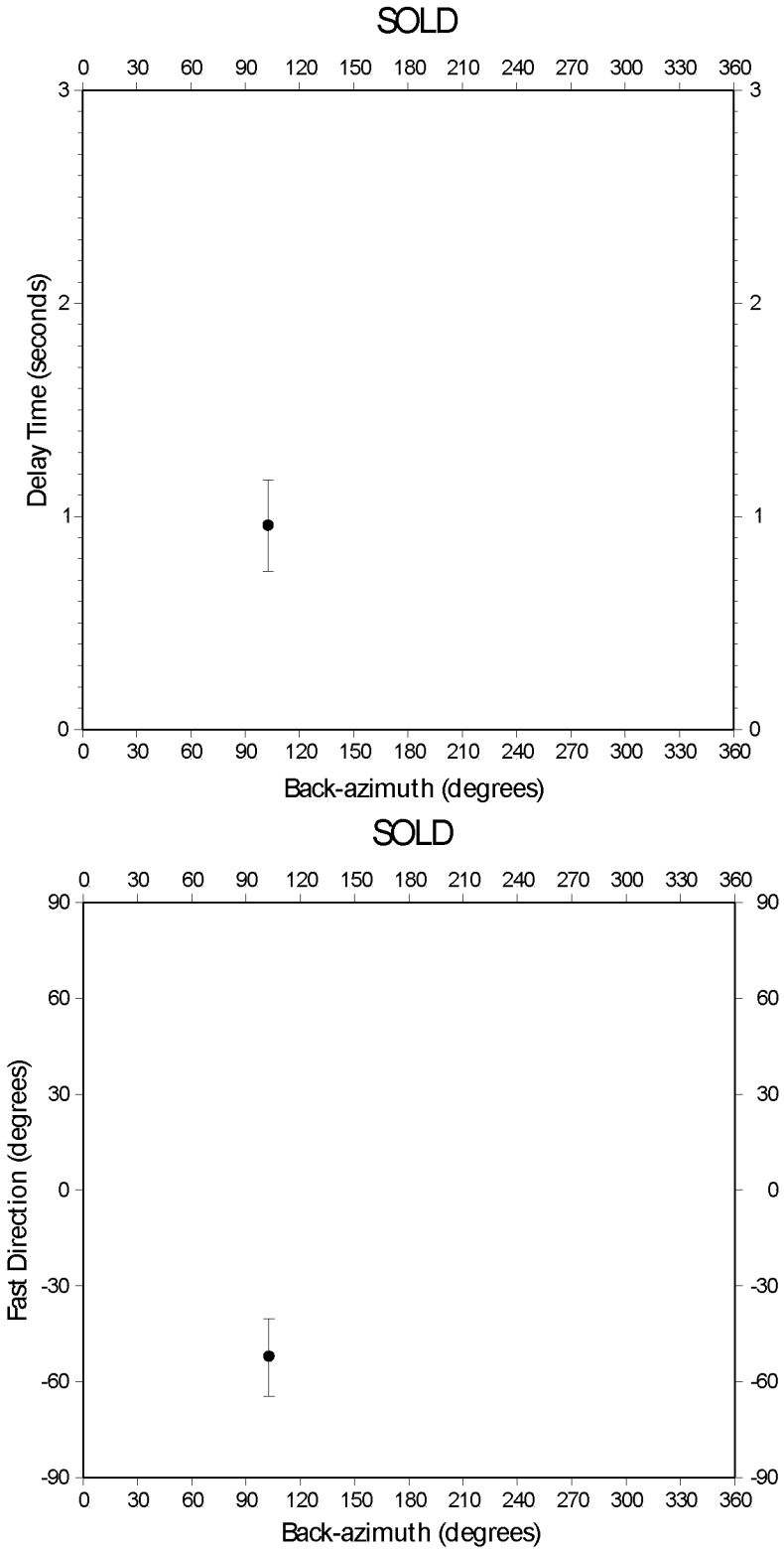

Figure C.41: Station SOLD from the MOOS network.
Delay times vs. back-azimuth (top) and fast direction vs. back-azimuth (bottom).

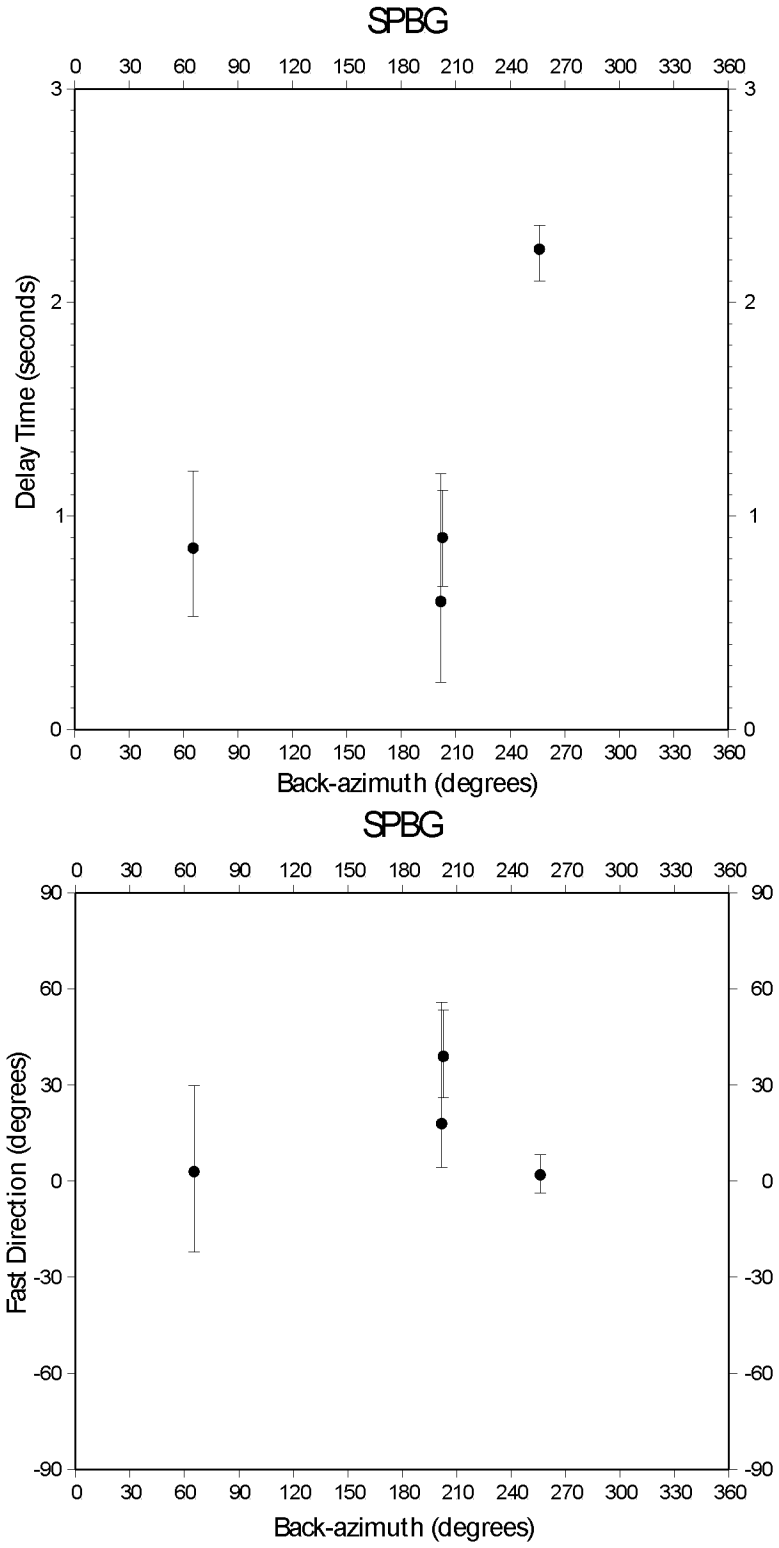

Figure C.42: Station SPBG from the AVO network.
Delay times vs. back-azimuth (top) and fast direction vs. back-azimuth (bottom).

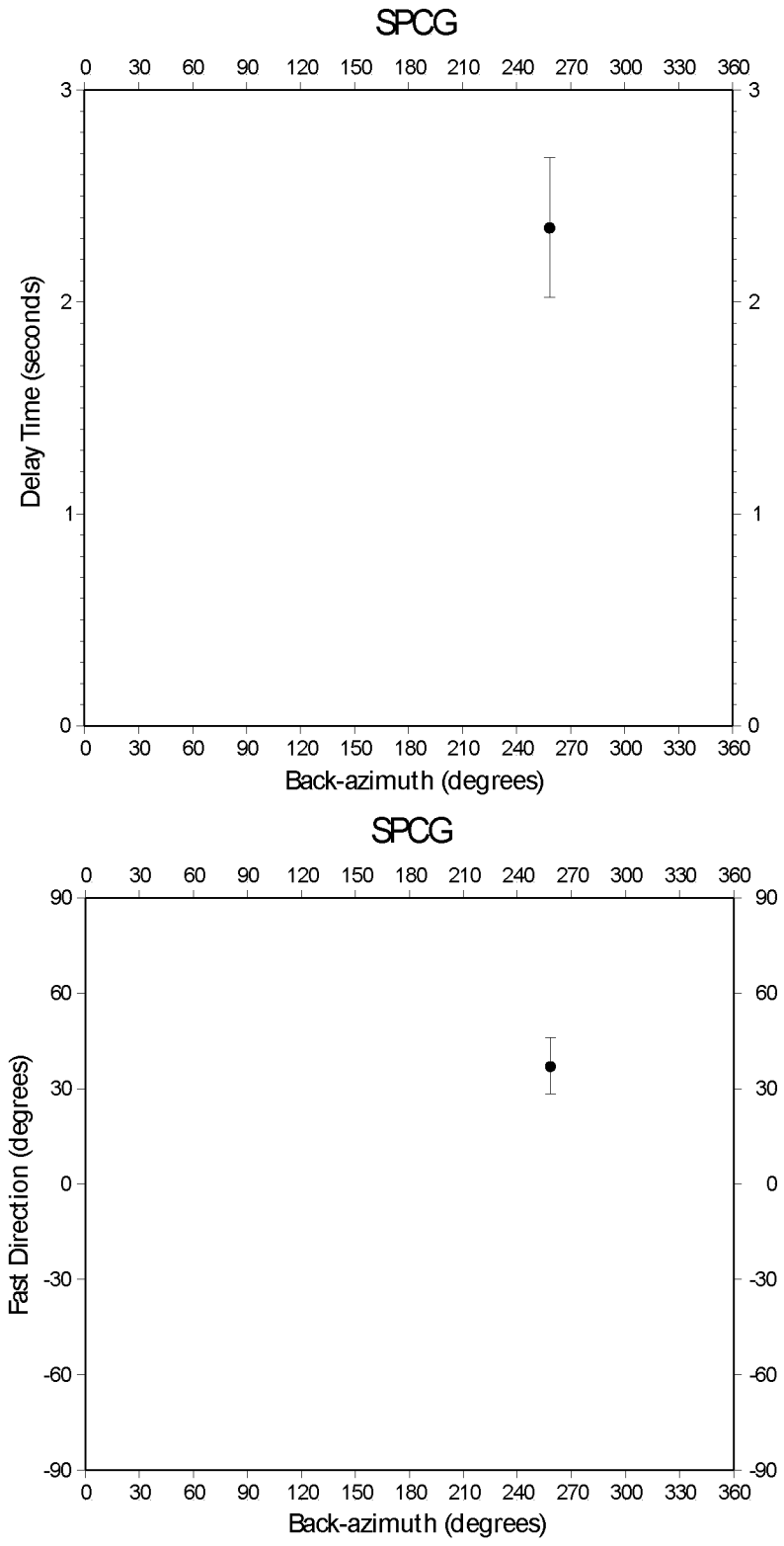

Figure C.43: Station SPCG from the AVO network.
Delay times vs. back-azimuth (top) and fast direction vs. back-azimuth (bottom).

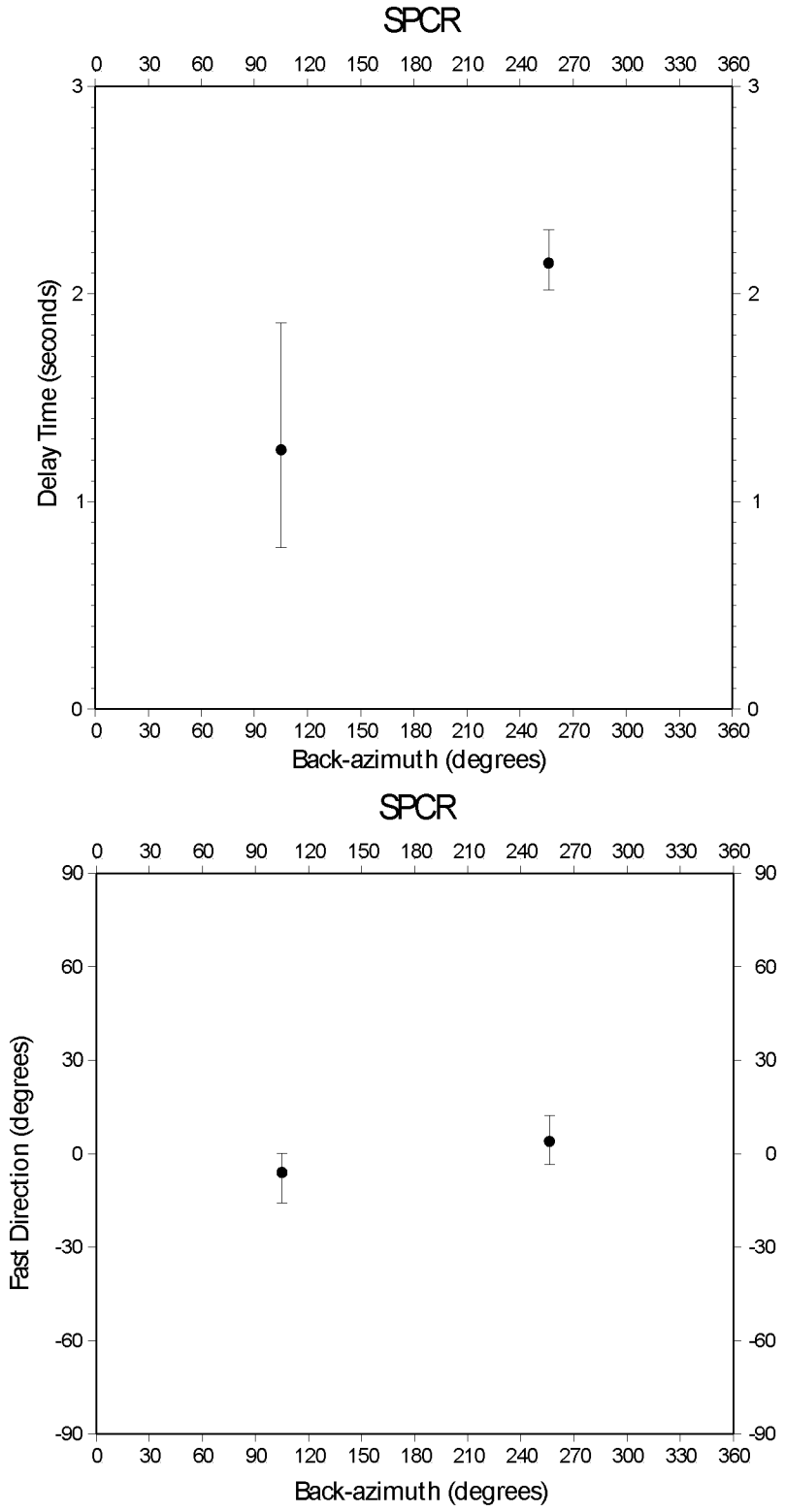

Figure C.44: Station SPCR from the AVO network.
Delay times vs. back-azimuth (top) and fast direction vs. back-azimuth (bottom).

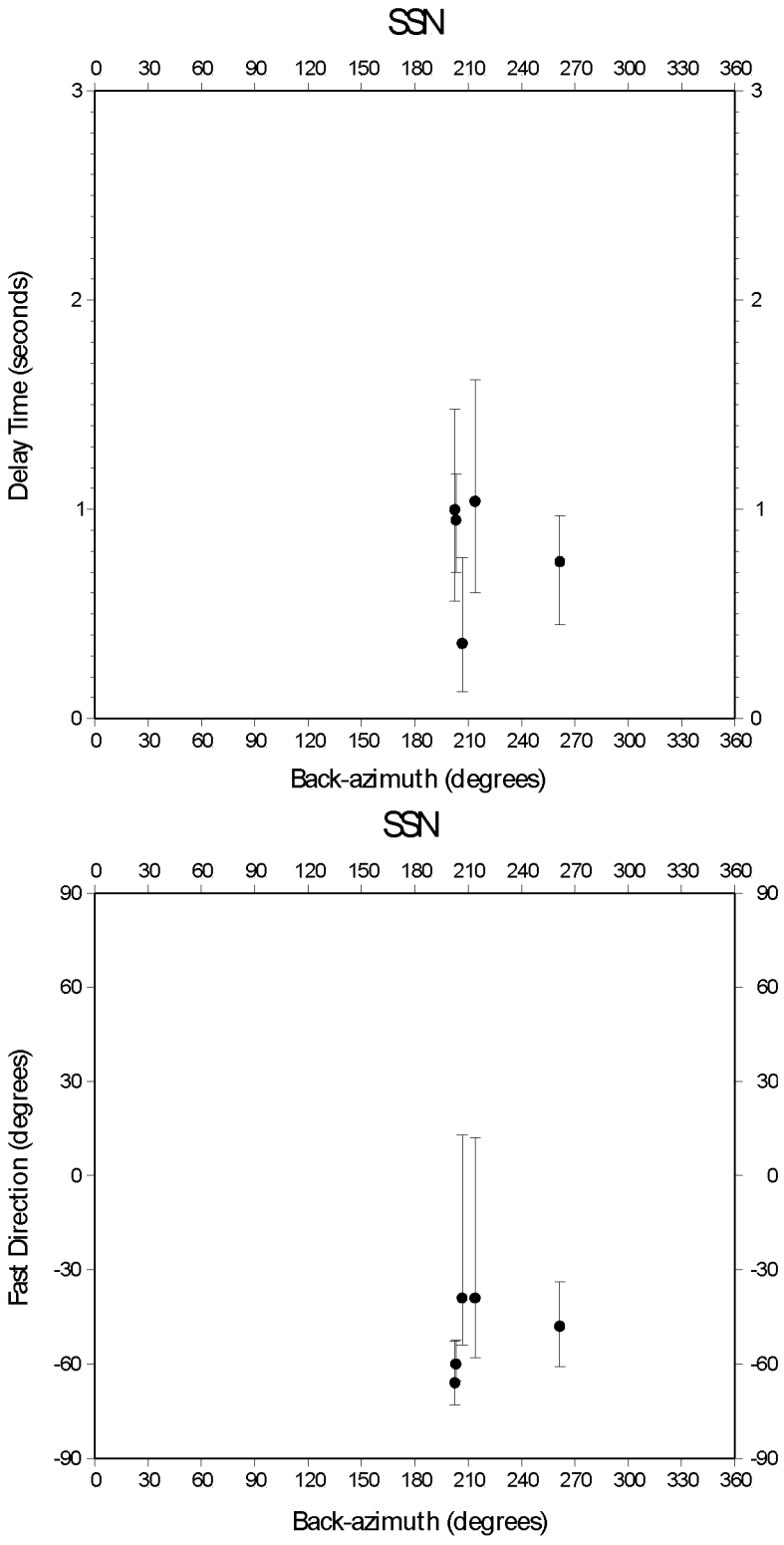

Figure C.45: Station SSN from the AEIC network.
Delay times vs. back-azimuth (top) and fast direction vs. back-azimuth (bottom).

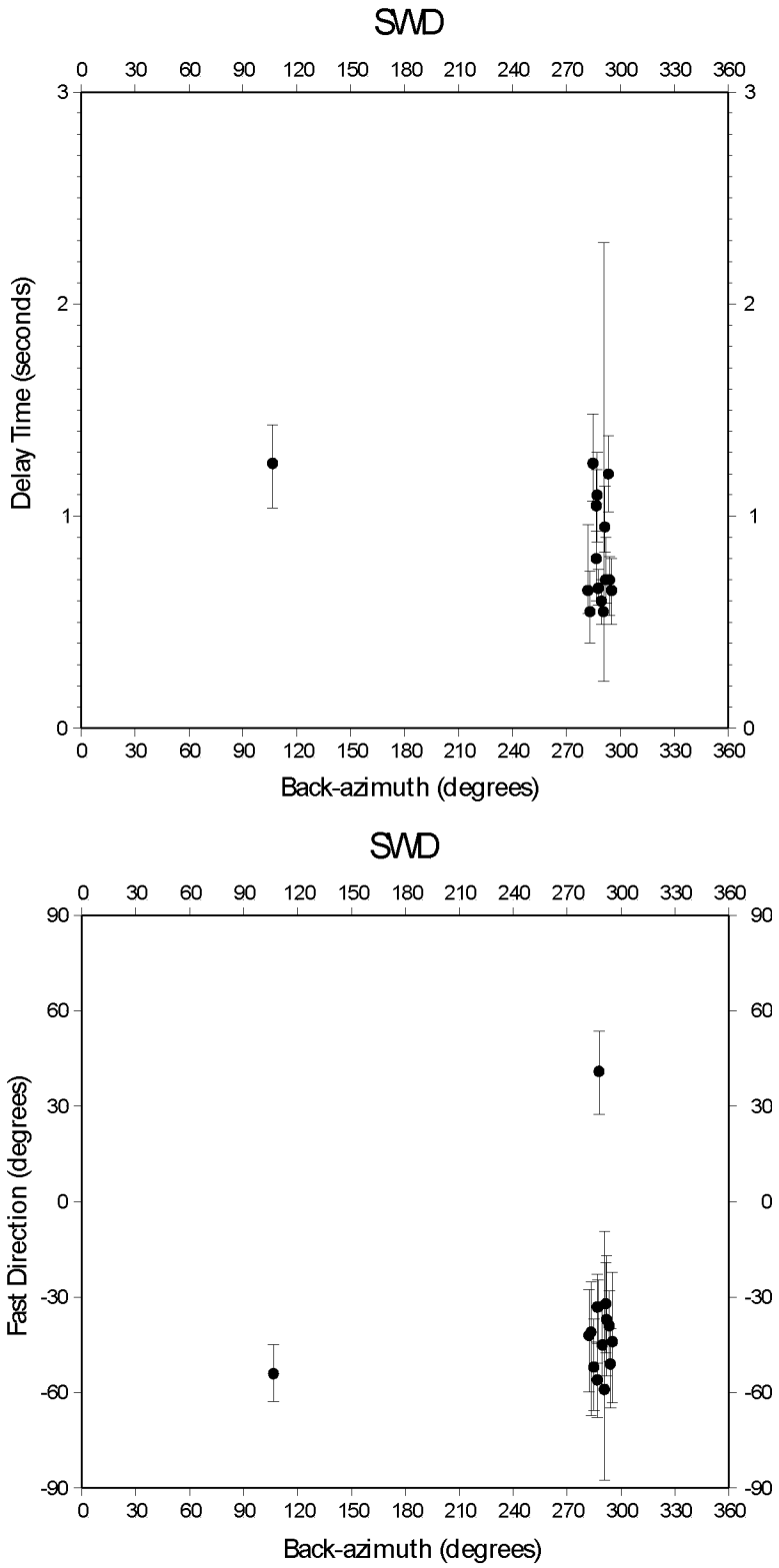

Figure C.46: Station SWD from the AEIC network.
Delay times vs. back-azimuth (top) and fast direction vs. back-azimuth (bottom).

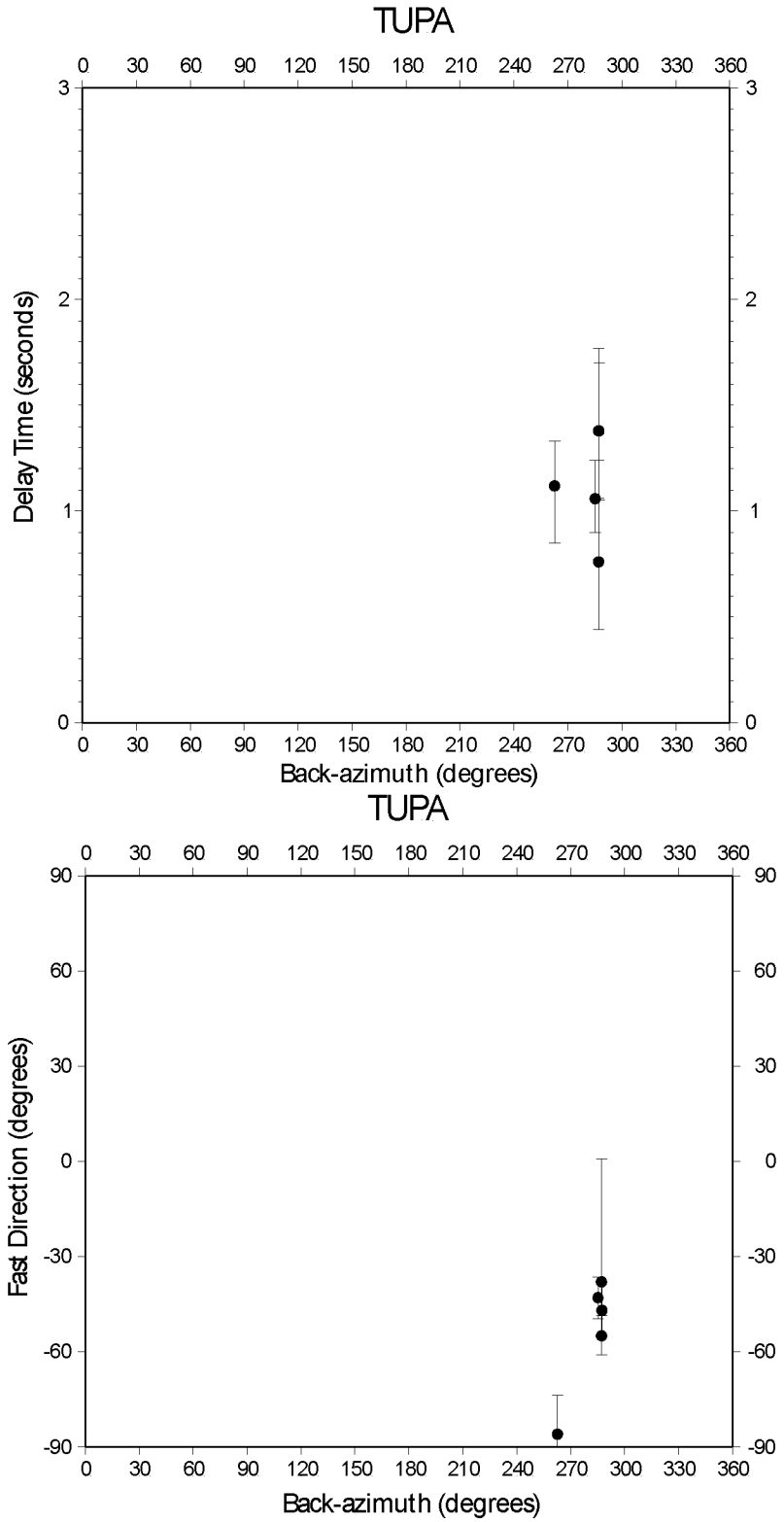

Figure C.47: Station TUPA from the MOOS network.
Delay times vs. back-azimuth (top) and fast direction vs. back-azimuth (bottom).

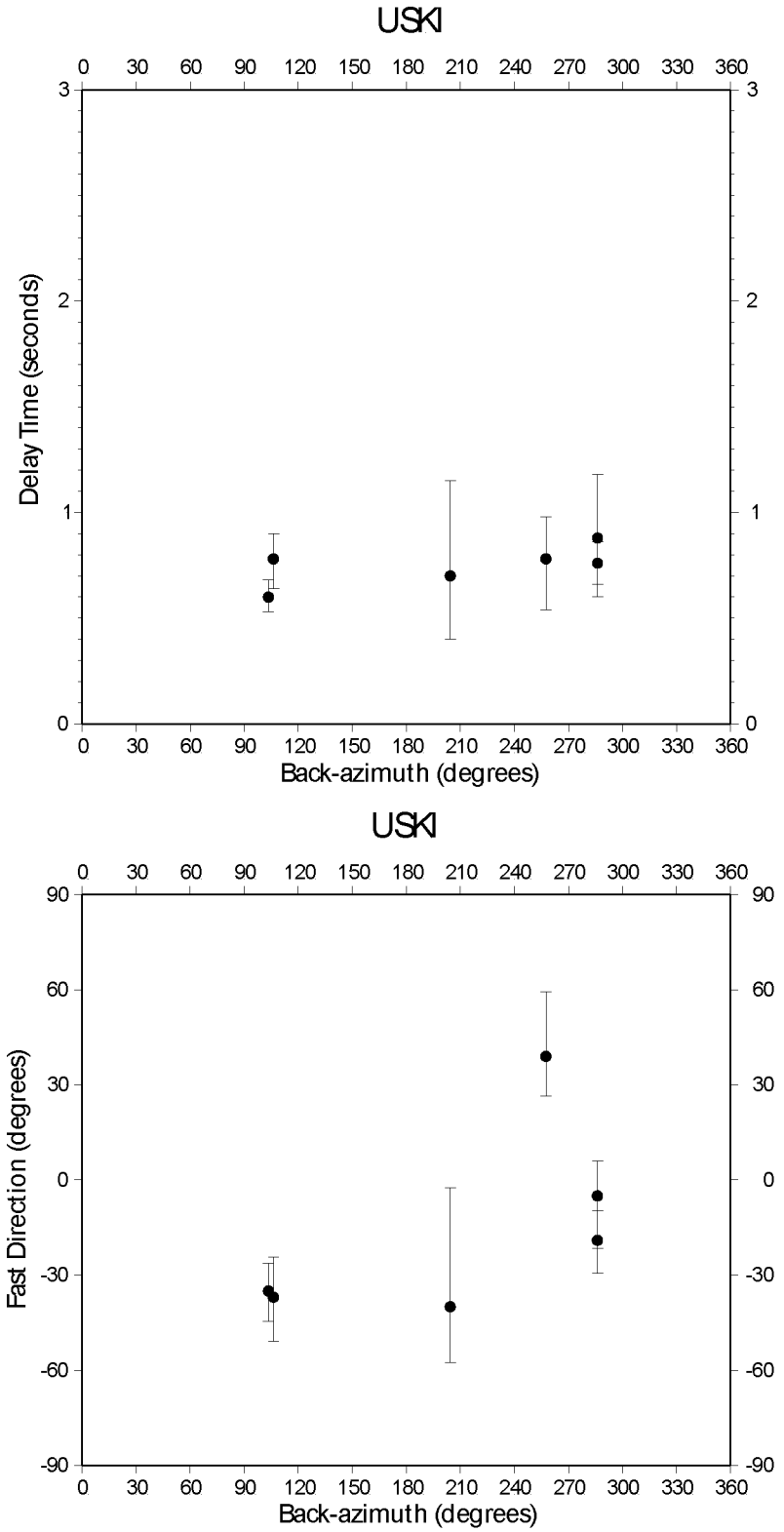

Figure C.48: Station USKI from the MOOS network.
Delay times vs. back-azimuth (top) and fast direction vs. back-azimuth (bottom).

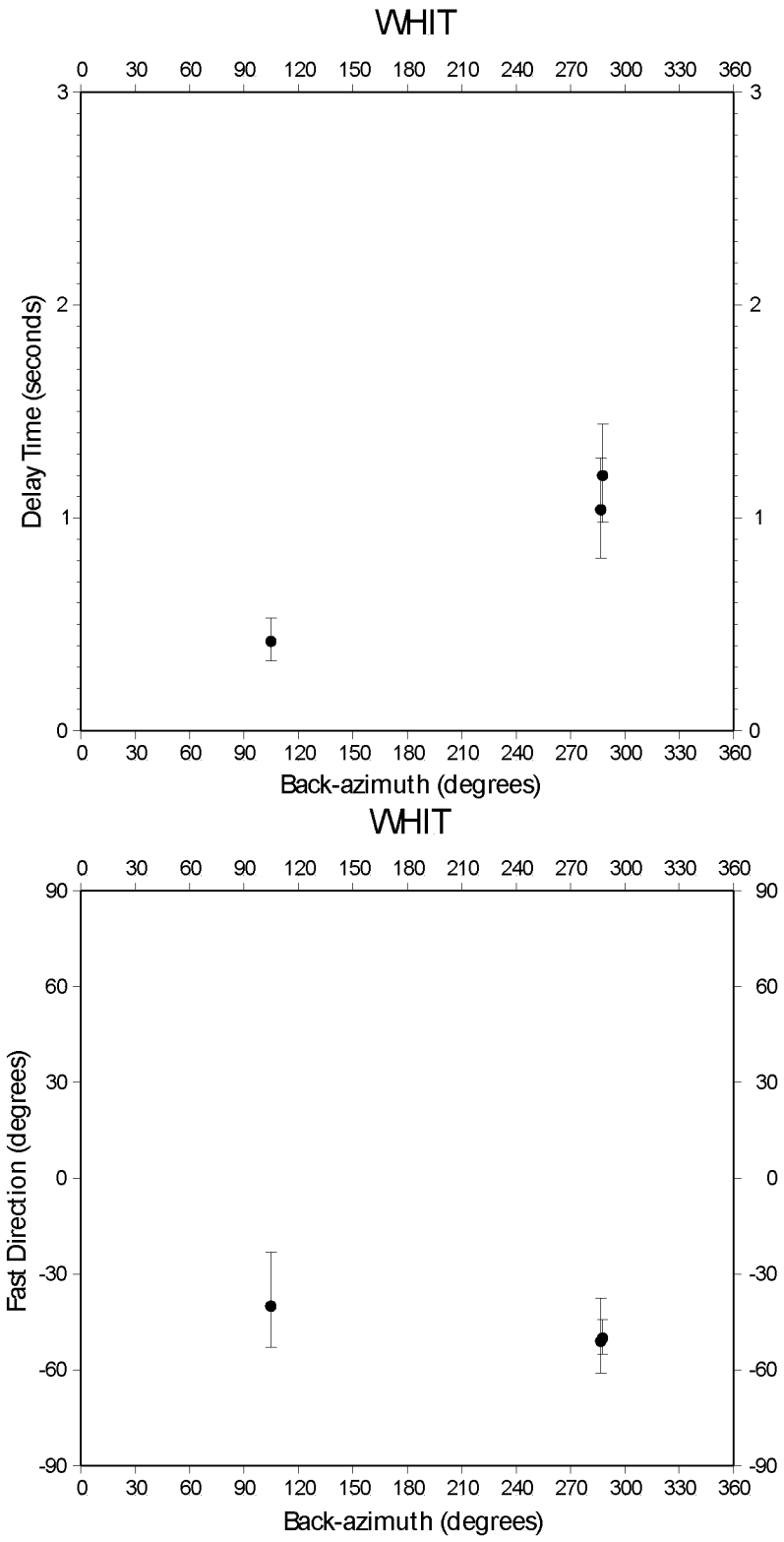

Figure C.49: Station WHIT from the MOOS network.
Delay times vs. back-azimuth (top) and fast direction vs. back-azimuth (bottom).